Bio-inspired iron and manganese complexes derived from mixed N,O ligands for the oxidation of olefins

Bio-geinspireerde ijzer- en mangaancomplexen gebaseerd op samengestelde N,O liganden voor de oxidatie van olefines

(met een samenvatting in het Nederlands)

Proefschrift

ter verkrijging van de graad van doctor aan de Universiteit Utrecht op gezag van de rector magnificus, prof.dr. G.J. van der Zwaan, ingevolge het besluit van het college voor promoties in het openbaar te verdedigen op woensdag 22 januari 2014 des middags te 12.45 uur

door

Marcel Antonius Henricus Moelands

geboren op 27 maart 1981
te *Uden*

Promotor: Prof. dr. R.J.M. Klein Gebbink

Bio-inspired iron and manganese complexes derived from mixed N,O ligands for the oxidation of olefins

Moelands, Marcel Antonius Henricus

Title: Bio-inspired iron and manganese complexes derived from mixed N,O ligands for the oxidation of olefins
Utrecht, Utrecht University, Faculty of Science
Thesis Utrecht University – with ref. – with summary in Dutch
ISBN: 978-94-6259-021-2

The work described in this thesis was carried out at:
Faculty of Science, Debye Institute for Nanomaterial Research
Organic Chemistry and Catalysis
Utrecht University
Utrecht, The Netherlands

This investigation was financially supported by the National Research School Combination-Catalysis (NRSC-C)

Contents

Preface

The selective oxidation of alkanes and alkenes using environmentally friendly oxidants such as O_2 and H_2O_2 is an important research topic in synthetic chemistry.[1,2] In the search for new catalysts for these transformations, biological systems play an important role in the design.[3] Many catalyst are models of the actives sites of metallo-enzymes that are capable of the activation of dioxygen to oxidize substrates.[4]
Modeling the chemistry of metallo-enzymes is quite a challenging task. The active site of the enzymes is often buried in a cavity surrounded by a hydrophobic shield. This means that the synthesis of small molecules capable of performing the same chemical transformation is difficult. In the synthesis of models systems of these enzymes there are two main goals. The first one is to synthesize metal complexes that mimic the function of the enzyme, i.e. in catalyzing a particular chemical transformation (functional models). The other is to gain insight into the biological system, e.g. through the synthesis of putative intermediates or to establish structure-activity relationships (structural models).

The aim of the work described in this thesis is the synthesis of (chiral) metal complexes for the oxidation of alkenes. The metal complexes are based on iron(II) or manganese(II). The prepared complexes are inspired by a class of mono-nuclear non-heme iron enzymes that feature a so-called 2-His-1-carboxylate facial triad in their active site (Figure 1). In the active site of these enzymes the iron center is facially bound to two histidine residues and one aspartate or glutamate residue. Efforts to model the structural and reactivity aspects of the facial triad enzymes have mainly focused on the use of all-nitrogen ligands and have to a much lesser extent made use of mixed N,O ligand donor sets.

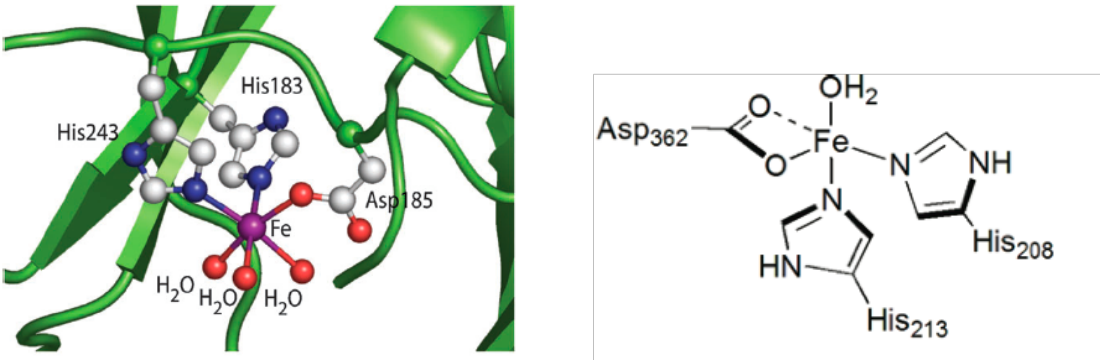

Figure 1. Representation of the 2-His-1-carboxylate facial triad.

The first part of this thesis is dedicated to a study on manganese complexes derived from mixed N,O ligands, while the second part focuses on iron complexes based on related, yet different mixed N,O ligands.
The chiral manganese complexes described in the first part of this thesis are based on a pyridine backbone substituted with two proline-derived molecules. These chiral proline moieties are readily available from the chiral pool. The side chain on the stereogenic center in the pyrrolidine ring can be easily modified through the presence of the carboxylic group with the full retention of the original configuration. See Figure 2 (left) for a representation of the double substituted pyridine ligand used in the first part of this thesis.

In **Chapter 1** an overview is given of typical bio-inspired ligands and the corresponding iron and manganese complexes developed nowadays for the oxidation of alkenes.

Chapter 2 describes the synthesis of two manganese(II)triflate complexes based on the bis(proline) appended pyridine ligand scaffold, bearing, either an methyl ester group or a prolinol group ($Py(ProR)_2$). The structure of both complexes is examined with X-ray diffraction and showed for both the formation of a seven-coordinated Mn-complex with distorted pentagonal bipyramidal geometries. Furthermore the catalytic potential of these two complexes is investigated, together with the suitable catalytic conditions.

Chapter 3 takes a closer look at the reaction conditions applied during the catalytic screenings reported in chapter 2. During these catalytic reactions 4-methylimidazole has been used as additive to increase the catalytic activity. The effect of this additive is investigated through a combination of spectroscopic techniques (^{19}F-NMR, IR, EPR, and ESI-MS).

In **Chapter 4** the potential of the double substituted manganese complexes described in chapter 2 is further investigated through the synthesis of a small library of ONN'NO ligands, in which the proline moieties are systematically varied. Next to the five-membered pyrrolidine ring also ligands are prepared with either a four-membered azetidine ring or a six-membered piperidine ring. The catalytic potential of the manganese complexes derived from these ligands is investigated.

The second part of this thesis deals with the synthesis of two different kinds of ligand systems and the corresponding iron(II) complexes (Figure 2, middle and right). The iron coordination chemistry of such ligands has been studied to address their potential to mimic the active site structure in non-heme iron enzymes with a 2-His-1-carboxylate facial triad.

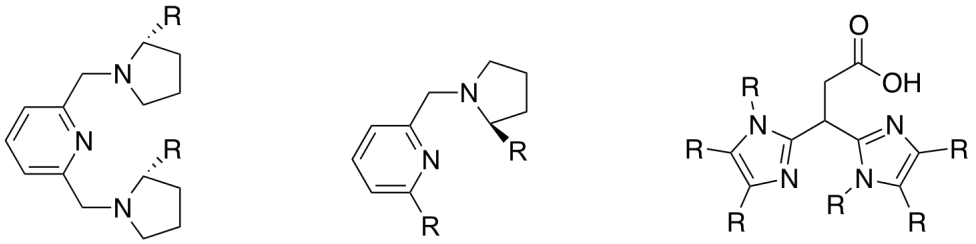

Figure 2. General structure of the di-substituted pyridine ligand used in chapters 2-4 (right) and the general structure of the ligands used in chapters 5 and 6 (middle and left).

Chapter 5 describes how the omission of one of the proline moieties from the ligands studied in chapters 2-4 provides access to ligands with an NN'O binding motif. From these ligands both iron triflate and iron chloride complexes are prepared. These complexes are studied both in terms of their structure and their reactivity.

Chapter 6 reports on the synthesis of a library of ligands based on the 3,3-bis(1-alkylimidazole-2-yl)propionate ligand system. Different variations are made in the propionate side chain and the size of the imidazole backbone. The structures of the complexes are examined with X-ray diffraction and the catalytic potential of these iron complexes is investigated in the oxidation of olefins.

The **Appendix** consists out of two parts. In the first part two newly prepared iron complexes with different counter ions based on the ligand system reported in chapter 6 are described. One of these complexes showed the formation of a short-lived green intermediate when reacted with an oxidant. The spectral features of this green intermediate seem to point to an iron(IV)-oxo species. The second part of the appendix reports on the crystal structure of a manganese triflate starting material that was obtained during these studies.

References

1. Sheldon, R.A.; Kochi, J.K. *Metal-Catalyzed Oxidations of Organic Compounds*, Academic Press , New York, 1981.
2. Bäckvall, J-E. *Modern Oxidations Methods*, Wiley-VCH, Weinheim, 2004.
3. Meunier, B. *Biomimetic catalyzed by transition metal complexes*, Imperial College Press, London, 1999.
4. Costas, M.; Mehn, M.P.; Jensen, M.P.; Que, L., Jr. *Chem. Rev.* **2004**, *104*, 939-986.

1

Nitrogen and oxygen based ligands in combination with iron(II) and manganese(II) for the oxidation of alkenes

This review describes the development of iron(II) and manganese(II) oxidation catalysts for the oxidation of alkenes towards epoxides and vicinal diols. The review will in particular highlight catalysts that are based on mixed N,O ligand systems. In this overall non-comprehensive review several of the recently developed biomimetic and bio-inspired non-heme iron and manganese catalyst are discussed.

1.1 Introduction

The selective oxidation of alkanes and alkenes using environmentally friendly oxidants such as O_2 and H_2O_2 is an important research topic in synthetic chemistry.[1,2] In the design of new catalysts for these transformations, biological systems play an important inspirational role.[3] Nature has evolved numerous iron enzymes that carry out oxidation reactions, for example alkane hydroxylation and olefin cis-dihydroxylations. The first transformation is carried out by enzymes with either heme (cytochrome P450) or non-heme iron centers (bleomycin and methane monooxygenase). The second transformation, cis-dihydroxylation, is a unique activity of non-heme iron containing Rieske dioxygenase, which attack arene double bonds in the first step of the biodegradation of arenes by soil bacteria. As already mentioned the iron containing enzymes can be divided into two groups based on the active site structures, heme and non-heme containing enzymes. The heme-enzymes have been extensively studied with cytochrome P450 as the prototypical example.[4] The class of non-heme containing enzymes can be divided into mononuclear and dinuclear iron enzymes.[5-7]

Modeling the chemistry of non-heme iron proteins is quite a challenging task. In a typical enzyme, the active site is buried in a cavity surrounded by a hydrophobic shield. This means that the synthesis of small molecules capable of performing the same chemical transformation is difficult. The purpose of synthetic model chemistry is twofold. One goal is to mimic the function of the enzyme that catalyzes important chemical transformations. The other is to gain insight into the biological system, e.g. through the synthesis of putative intermediates or to establish structure-activity relationships.

This review describes the development of iron(II) and manganese(II) oxidation catalysts for the oxidation of alkenes towards epoxides and vicinal diols. The review will in particular highlight catalysts that are based on mixed N,O ligand systems. In this overall non-comprehensive review several of the recently developed biomimetic and bio-inspired non-heme iron and manganese catalyst are discussed. The chemistry of these man-made catalysts is furthermore discussed in relation to their structural and functional similarities to natural non-heme enzymes.

Mononuclear non-heme iron oxygenases have received a lot of attention lately, primarily because of the recent availability of crystal structures of a particular and large subgroup of these non-heme enzymes. These structures have established a new common structural motif for the activation of dioxygen to catalyze a variety of oxidative transformations.[8] This structural motif is based on a mononuclear iron(II) center surrounded in a facial fashion by two histidine residues and one carboxylato ligand, either from a glutamate or aspartate residue (Figure 1). This structural motif is called the 2-His-1-carboxylate facial triad.[9,10] The three other sides of the octahedron around iron are left to bind substrate, dioxygen and/or cofactor. When none of these

are bound, the sites are either occupied by weakly bounded solvent molecules or are just vacant.

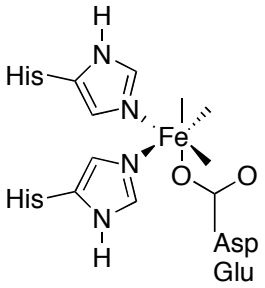

Figure 1. The 2-His-1-carboxylate facial triad.

Enzymes with this facial triad can be classified into five different groups based on their specific requirements for catalysis. The five different groups are 1) Extradiol cleaving catechol dioxygenase, 2) Rieske oxygenase, 3) α-ketoglutarate dependent enzymes, 4) Pterin dependent hydroxylases and the last 5) a miscellaneous group.[11] Many of the oxidation catalysts and enzyme models discussed in this review are based on the second groups of enzymes, the Rieske oxygenases, which are capable of the *cis*-dihydroxylation of arene double bonds.
This above-mentioned 2-His-1-carboxylate facial triad has been an important structural and functional target in synthetic bioinorganic chemistry and forms an imported inspiration source for the design of new oxidation catalysts based on iron as well as on manganese.

Initial research efforts aimed at mimicking the 2-His-1-carboxylate facial triad have focused on the development of functional models of the enzyme systems. These model compounds were mostly based on polydentate all-nitrogen ligands. At a later stage, studies focused on the development of structural models of the facial triad. These model compounds are based on a mixed N,O donor set of ligands in order to more accurately mimic the facial coordination of the two imidazole groups and a mono- or bidentate carboxylato group in the facial triad active site.
The first and largest part of this review describes studies on iron-based functional models, followed by a description of structural models based on iron. The last part of the review discusses synthetic manganese complexes along a similar vein. The main focus in the description of the catalytic properties of these model systems is on the use of the benign oxidant hydrogen peroxide and on its possible combined used together with acetic acid. The acetic acid additive may act as a ligand to the central metal ion, by which it may formally establish a mixed N,O coordination environment. In doing so, it may aid the activation of the hydrogen peroxide oxidant and facilitate the formation of the metal-based oxidant. Alternatively, it may lead to the formation of the stronger oxidant peracetic acid.

1.2 Complexes based on iron(II)

1.2.1 Functional models based on iron

The group of Que reported the first functional model of Rieske dioxygenase that was able to catalyze the *cis*-dihydroxylation of olefins.[12] The design of this system was based on the active site of naphthalene 1,2-dioxygenase (NDO).[13] The reported complex comprises a methyl substituted version of the TPA ligand system (TPA = tetradentate tris(2-pyridylmethyl)amine). In the mononuclear non-heme iron complex $[Fe^{II}(6\text{-}Me_3\text{-}TPA)(CH_3CN)_2](ClO_4)_2$ (**1**) the Fe(II) center is coordinated by the tetradentate ligand and two *cis*-coordinated solvent ligands (Figure 2).[14]

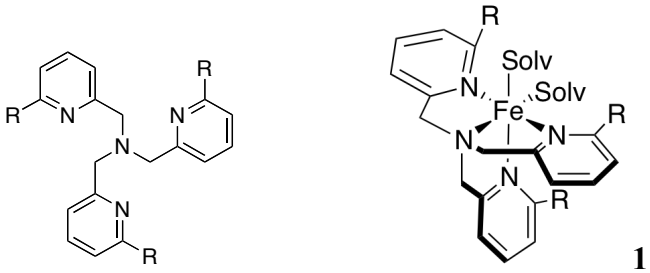

1

Figure 2. Structure of the TPA ligand and the mono-nuclear $[Fe^{II}(6\text{-}Me_3\text{-}TPA)]^{2+}$ complex, where R = Me and Solv = acetonitrile.

Complex **1** was tested as a catalyst in the *cis*-dihydroxylation of cyclooctene, *cis*-2-hexene and *trans*-2-hexene. The results of these reactions are depicted in Table 1 (entries 1-5). Using 10 equiv. of hydrogen peroxide a turnover number of 4.9 of *cis*-cyclooctane-1,2-diol is obtained and a small amount of epoxide is formed (entry 1). When more equivalents of hydrogen peroxide are added the productive consumption of H_2O_2 stays almost the same (50%, entries 2 and 3). The complex is also able to catalyze the oxidation of *cis*- and *trans*-2-hexene to the corresponding *cis*-diol products (entries 4 and 5). When the oxide product was reacted under these reaction conditions no diol product was formed, which suggest that the epoxides are not the precursors for the *cis*-diol products. When the corresponding TPA ligand without the Me groups is applied in catalysis a lower ratio of *cis*-diol is obtained and more epoxide is formed (entry 6).

Table 1. Catalytic oxidation of alkenes by iron TPA complexes in combination with H_2O_2.[a]

Entry	Ligand	Substrate	Equiv. H_2O_2	*cis*-Diol[b]	Epoxide[b]
1	6-Me3-TPA	cyclooctene	10	4.9(6)	0.7(2)
2	6-Me3-TPA		20	10(2)	0.8(1)
3	6-Me3-TPA		40	22(1)	1.6(1)
4	6-Me3-TPA	*cis*-2-hexene	10	5.2(6)	0.3(1)
5	6-Me3-TPA	*trans*-2-hexene	10	4.0(7)	0.3(1)
6	TPA	cyclooctene	10	2.6(3)	2.3(2)

[a] Reaction conditions: 0.7 mM of iron complex, catalyst to substrate ratio 1:1000, MeCN at 25 ºC, H_2O_2 was added via syringe pump over 30 min; [b] Turnover numbers (moles of product per mole of catalyst).

Following this first example of a catalytic *cis*-dihydroxylation carried out by an iron complex, many other studies were initiated to development improved iron-based catalysts for this reaction. Some of the complexes developed during these studies that are actually not able to form *cis*-diols out of olefins are shown in Figure 3. The iron(II) complexes, $[Fe^{II}(BPH)(CH_3CN)_2](ClO_4)_2$ (**2**)[12] (BPH = 1,4-bis(2-pyridinylmethyl)-1,4-diazepane) and $[Fe^{II}(CYCLAM)(CH_3CN)](SO_3CF_3)_2$ (**3**)[15] (CYCLAM = 1,4,8,11-tetraazacyclotetradecane) are able to oxidize olefins to epoxides using H_2O_2 as terminal oxidant, whereas $[Fe^{II}(N4Py)(CH_3CN)](ClO_4)_2$ (**4**)[16,17] (N4Py = tetradentate tris(2-pyridylmethyl)amine) is actually a poor catalyst for olefin oxidation. This difference in reactivity can be explained by the presence of two labile *cis* coordination sites in complex **1**, which are not present in complexes **2**-**4**. In complexes **2**-**3** two *trans* labile sites are present and complex **4** comprises only a single labile site. In the active site of the enzyme NDO also two *cis* labile sites are present. This structural and functional analogy has lead to a focus on the development of iron catalysts bearing two *cis* labile sites for olefin *cis*-dihydroxylation reactions.

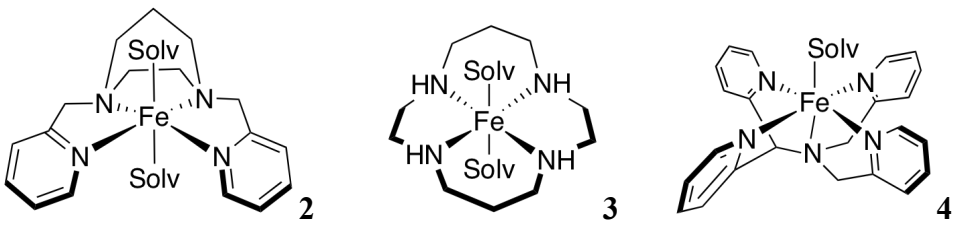

Figure 3. Structures of the synthetic dicationic non-heme iron complexes **2**, **3** and **4**, Solv = acetonitrile.

The groups of Que continued their research towards non-heme iron complexes for *cis*-dihydroxylation and investigated the possibility for enantioselective olefin *cis*-dihydroxylation.[18] In this study the tripodal tetradentate ligand (TPA) was replaced by a linear tetradentate ligand derived from a chiral diamine backbone (Figure 4, ligand **7** and **8**). The use of ligands based on the chiral *trans*-cyclohexane-1,2-diamine backbone is a known strategy for chiral induction in metal-catalyzed oxidations.[19,20]

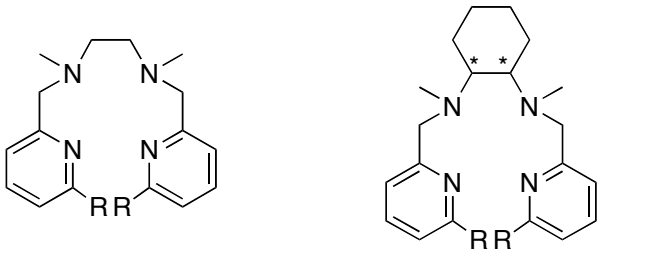

5 R = H, BPMEN
6 R = Me, 6-Me$_2$-BPMEN
7 R = H, BPMCN
8 R = Me, 6-Me$_2$-BPMCN

Figure 4. Tetradentate BPMEN and BPMCN ligands.

Before the reactions were tested with the chiral ligands, the ability of iron complexes derived from the achiral BPMEN ligands (BPMEN = *N,N'*-bis-(2-pyridylmethyl)-*N,N'*-dimethyl-1,2-ethylenediamine) to catalyze olefin *cis*-dihydroxylation was investigated (Figure 4, ligands **5** and **6**). The complexes prepared with these two ligands, [Fe(BPMEN)(MeCN)$_2$](ClO$_4$)$_2$ (**9**) and the 6-methyl substituted analogue [Fe(6-Me$_2$-BPMEN)](CF$_3$SO$_3$)$_2$ (**10**) were tested as catalyst in the oxidation of cyclooctene (Table 2). Both complexes showed a coordination environment around iron with two labile *cis*-coordination sites. Complex **9** afforded cyclooctene oxide and the *cis*-diol in respectively yields of 75 and 9% (relative to the amount of H_2O_2 used; entry 1). Complex **10** however gave under the same conditions epoxide and *cis*-diol in respective yields of 15 and 64% (entry 2). Much like in the case for TPA-type complexes, the introduction of 6-methyl substituents on the pyridine rings changes the ratio between epoxide and *cis*-diol products favoring the *cis*-dihydroxylation pathway. With these good results the complexes [Fe(BPMCN)(CF$_3$SO$_3$)$_2$] (**11**) and [Fe(6-Me$_2$-BPMCN)(CF$_3$SO$_3$)$_2$] (**12**) with the chiral *trans*-cyclohexane-1,2-diamine backbone was prepared. Also these complexes were tested in the oxidation reactions using H_2O_2 as oxidant. The results of the catalytic studies are reported in Table 2.

The chiral complex [Fe(BPMCN)(CF$_3$SO$_3$)$_2$] (**11**) gave predominately the epoxide product (entry 3), while incorporation of Me groups in the 6-position of the pyridine rings as in [Fe(6-Me$_2$-BPMCN)(CF$_3$SO$_3$)$_2$] (**12**) again resulted in a change in product distribution towards the predominant formation of the *cis*-diol product (entry 5). When *trans*-2-heptane was used as prochiral substrate the same trends were observed as for cyclooctene. Complex **11,** without the Me groups, gave 5.4 TON of the epoxide

and 0.3 TON of the diol in 29% *ee*. When complex **12** was used, a TON of 2.4 was obtained for the epoxide and a TON of 7.5 for the *cis*-diol in 79% *ee*. So adding the Me group to the ligand not only has its positive effect on the product distribution but also on the enantioselectivity of the *cis*-dihydroxylation. The use of the opposite enantiomer of the 6-Me_2-BPMCN ligand gave a comparable epoxide/diol ratio and gave the major diol product in the opposite configuration (entry 8). Complexes **11** and **12** were the first synthetic iron complexes capable of catalyzing enantioselective *cis*-dihydroxylation of olefins. With this discovery a start was made for the future development of biomimetic iron catalysts that could replace the more traditional methods for the preparation of enantiopure vicinal diols from olefins.

Table 2. Olefin oxidations with H_2O_2 catalyzed by complexes **9-12**.[a]

Entry	Cat	substrate/equiv. H_2O_2	Epoxide (de)	Diol (de)	ee
1	**9**	cyclooctene/10	7.5(100)	0.9(100)	
2	**10**	cyclooctene/10	1.5(100)	6.4(100)	
3	1*R*,2*R*-**11**	cyclooctene/10	5.8(100)	0.7(100)	
4		*trans*-2-heptane/10	5.4(100)	0.3(100)	29(2)
5	1*S*,2*S*-**12**	cyclooctene/10	3.5(100)	5.8(79)	
6		cyclooctene/20	5.4(100)	11.2(89)	
7		*trans*-2-heptane/20	2.4(100)	7.5(100)	79(2)
8	1*R*,2*R*-**12**	*trans*-2-heptane/20	2.1(100)	8.2(100)	76(2)

[a] Reaction conditions: 0.7 mM catalyst and 700 mM olefin in 3 mL of MeCN at 30 ºC under air to which 10-20 equiv. of H_2O_2 (from 50% aqueous H_2O_2) in MeCN is added via syringe pump over 30 min, Results are given as mmol product/mmol of catalyst.

With the goal to achieving higher *ee* values in *cis*-dihydroxylation reactions, the group of Que replaces the *trans*-1,2-diaminocyclohexane unit of the BPMCN ligand system by a bipyrrolidine unit and obtained ligands **13-15** (Figure 5),[21] following the initial use of these ligands by White *et al.* in catalytic hydroxylation reactions.[22]
The complexes [Fe^{II}(BPBP)$(OTf)_2$] (**16**) (BPBP = Bis(2-pyridylmethyl)-(*R*,*R*)-2,2'bipyrrolidine), [Fe^{II}(BQBP)(OTf)(EtOH)](OTf) (**17**) (BQBP = Bis(2-quinolinylmethyl)-(*R*,*R*)-2,2'bipyrrolidine) and [Fe^{II}(6-Me_2-BPBP)$(OTf)_2$] (**18**) (6-Me_2-BPBP = Bis(6-methyl-2-pyridylmethyl)-(*R*,*R*)-2,2'bipyrrolidine) were prepared in a typical manner using $Fe^{II}(OTf)_2$.2MeCN in CH_2Cl_2 under an N_2 atmosphere. The three ligands coordinate in a *cis*-α topology to the iron centers with two equivalent available sites *trans* to the bipyrrolidine backbone (occupied by triflate or ethanol). The *cis*-α topology is determined by the constrained bipyrrolidine backbone, which is in contrast to the BPMCN ligand that forms both *cis*-α and *cis*-β iron(II) complexes.

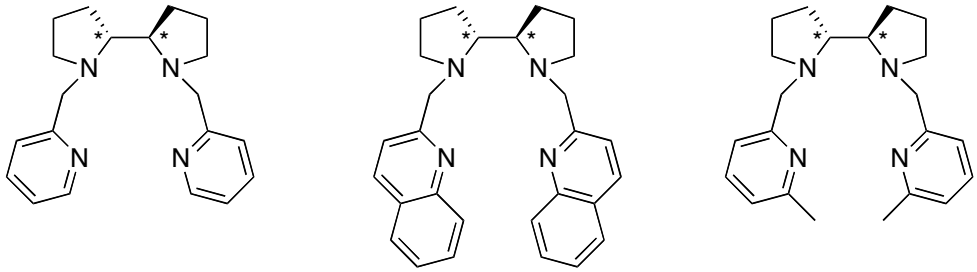

13: BPBP **14**: BQBP **15**: 6-Me_2-BPBP

Figure 5. Structure of the optically active ligands.

The BPBP-derived catalysts were tested in the asymmetric *cis*-dihydroxylation of olefins. For the results of the catalytic screenings see Table 3.

Table 3. Oxidation of olefins with H_2O_2 catalyzed by complexes **16**-**18**.[a]

Catalyst	Substrate	Epoxide TON	Diol TON	*cis*-diol % ee	Diol/Epox.
16	*trans*-2-heptane	5.1	1.1	38	1:4.6
16	1-octene	2.6	1.7	11	1:1.5
16	*tert*-butyl acrylate	3.0	0.1		1:30
17	*trans*-2-heptane	0.9	3.6	78	4:1
17	1-octene	0.5	4.6	29	9:1
17	*tert*-butyl acrylate	<0.1	2.7	23	>27:1
18	*trans-2-heptane*	0.2	5.2	97	26:1
18	*cis*-2-heptane	0.6	3.4	11	5.7:1
18	*trans*-4-octene	0.3	3.9	96	13:1
18	*cyclooctene*	0.7	4.0		5.7:1
18	*1-octene*	0.1	6.4	76	64:1
18	*styrene*	<0.1	6.5	15	>65:1

[a] Reaction conditions: a 70 mM solution of H_2O_2 (10 equiv.) in MeCN was added via syringe pump in 20 min to a degassed solution of catalyst (0.7 mM) and substrate (0.35M) at 25 °C in air for **16** and **17** and under Ar atmosphere for **18**.

When using these complexes in the catalytic oxidation of olefins with H_2O_2, the same trend in product formation was observed as for the BPMCN complexes: the selectivity for the *cis*-diol product increases upon introduction of methyl substituents on the pyridine rings. With increasing steric bulk, the catalyst goes from epoxide selective (**16**), to cis-diol selective in the case of complex **17**, to even more selective in the case of complex **18**. The observed asymmetric induction is the highest with complex **18** and the best for electron-rich, *trans*-disubstituted olefins. The observed *ee*-values are

comparable to values obtained with the benchmark osmium-based Sharpless AD mixes.

The group of Que continues their work on the different ligand systems and has tried to explain the different product profiles observed during the catalytic studies.[23-26] The different outcomes can be explained by the formation of different kind of coordination topologies (*cis*-α or *cis*-β) caused by the different ligands. These topologies give rise to different activated iron species, either low-spin or high-spin Fe^{III}-OOH complexes, which in turn provide the different epoxide/diol product distributions. The activated species that are formed during the catalysis will not be further discussed here, as this is outside the scope of this review.

The group of Feringa and co-workers have reported on a class of functional models for the non-heme iron-based dioxygenases that make use of ligands that are closely related to the TPA ligand.[27] In their approach they redesigned their original N4Py ligand system[16,17] from a pentadentate ligand into a tetradentate ligand. In the new system one of the picolyl groups in N4Py is replaced by a non-coordinating moiety like a methyl or benzyl group (Figure 6).

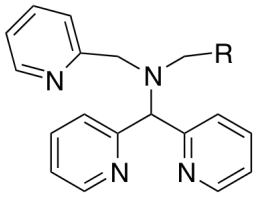

R = pyridine, N4Py
R = H, N3Py-Me
R = phenyl, N3Py-Bn

Figure 6. The N3Py-R ligand system.

In the complexes $[Fe(N3Py\text{-}Me)(MeCN)_2](ClO_4)_2$ (**19**) (N3Py-Me = di(2-pyridyl)methyl]methyl(2-pyridyl)methylamine) and $[Fe(N3Py\text{-}Bn)(MeCN)_2](ClO_4)_2$ (**20**) (N3Py-Bn = di(2-pyridyl)methyl]benzyl(2-pyridyl)methylamine), the ligands show the same coordination behavior as the TPA ligand and give rise to distorted octahedral complexes with a six-coordinated Fe^{II} center. The two labile coordination sites in these complexes are *cis* to each other and are occupied by solvent molecules (MeCN). Where the N4Py-based complexes did not catalyze the oxidation of alkenes, the N3Py-based complexes were shown to oxidize a number of different alkene substrates. Interestingly, the product outcome when using these catalysts was found to depend on the solvent used for the reaction (either acetonitrile or acetone; Table 4).

Table 4. Results of the catalysis of complexes **19** and **20** in acetonitrile and acetone.[a]

cat.	substrate	acetonitrile				acetone			
		cis-epoxide	*trans*-epoxide	*cis*-diol	*trans*-diol	*cis*-epoxide	*trans*-epoxide	*cis*-diol	*trans*-diol
19	cyclooctene	14	-	22	1	17	-	0.2	4
20	cyclooctene	16	-	14	0	19	-	3	10
19	cyclohexene[b]	11	-	13	0.7	0.8	-	0	2.4

[a] Reaction conditions: 50 equiv. of H_2O_2 was added under air via a syringe pump, in 60 min for the reactions in MeCN and in 30 min for the reactions in acetone, yields given in Turnover number = mol product/mol catalyst; [b] Reaction carried out under argon.

In acetonitrile, complexes **19** and **20** predominately give the *cis*-epoxide and the *cis*-diol product (approx. 1:1 ratio) as was also observed for the TPA-complex. In the oxidation of cyclohexene the typical allylic oxidation side products, cyclohexenol and cyclohexenone, were also observed. Reactions carried out in acetone gave a somewhat different product distribution and more side product formation. In this solvent, the *trans*-diol was obtained as the major diol product. In a control experiment the cyclooctene oxide was subjected to the same reaction conditions and no diol formation was observed. This means that the *trans*-diol product is formed via an independent route and is not a decomposition product of the epoxide. The reactions were also tested with other substrates like *cis*- and *trans*-stilbene and cis- and *trans*-4-octene, also these substrates showed the same product distribution. In acetonitrile the *cis*-diol is favored and in acetone the *trans*-diol is favored. This is the first example of a catalyst that can give both *cis*- and *trans*-dihydroxylation depending the reaction solvent.

Costas and co-workers reported on the synthesis of a novel ligand platform with large tunability for the modeling of non-heme oxygenases.[28] The ligand system is based on the triazacyclononane (TACN) backbone to which a pyridine group is appended. This PyTACN ligand (^{R,Y,X}PyTACN=1-[2′-(4-Y-6-X-pyridyl)methyl]-4,7-dialkyl-1,4,7-triazacyclononane) can be substituted on the N-atoms of the triazamacrocycle and on the pyridine ring (Figure 7), which can be used to control product selectivities in the oxidation of alkane and alkene substrates. The complexes Fe(^{iPr,H}PyTACN)$(OTf)_2$] (**21**), Fe(^{iPr,Me}PyTACN)$(OTf)_2$] (**22**), Fe(^{Me,H}PyTACN)$(OTf)_2$] (**23**) and Fe(^{Me,Me}PyTACN)$(OTf)_2$] (**24**) show a distorted octahedral geometry around iron with the two labile triflate groups in *cis*-position (Figure 7).

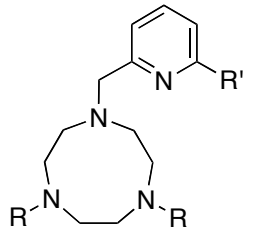

R = iPr, R' = H ($^{iPr, H}$PyTACN)
R = iPr, R' = Me ($^{iPr, Me}$PyTACN)
R = Me, R' = H ($^{Me, H}$PyTACN)
R = Me, R' = Me ($^{Me, Me}$PyTACN)

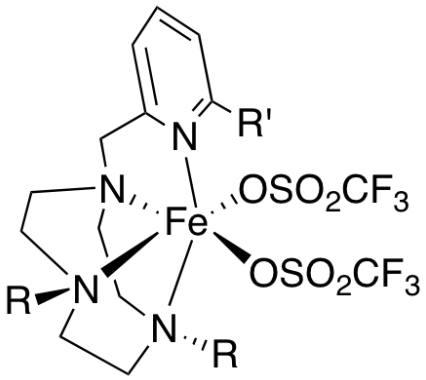

Figure 7. The PyTACN ligand system and the structure of the complexes.

These complexes give high overall product yields in the oxidation of cyclooctene, ranging from 50 to 99% based on the amount of H_2O_2 used in the reaction (Table 5). The ratio between diol and epoxide strongly depends on the substituents on the PyTACN ligand. When complex **23** is used a ratio between diol and epoxide of 1:1 is obtained, while the introduction of a methyl group on the pyridine moiety as in **24** increases the ratio between diol and epoxide to 5.5. The introduction of the isopropyl group instead of the methyl group on the TACN ring resulted in a further selectivity change towards the diol product. Complex **22** gives a diol to epoxide ratio of 9. This is nowadays one of the best epoxide/diol selectivities reported in literature. With the addition of more equivalents of hydrogen peroxide very high activities can be obtained with complexes **21**, **23** and **24**. The PyTACN ligand system reported by Costas represents a very nice, functional model of the Rieske dioxygenase showing good overall activities and selectivities and further opportunities for ligand variation.

Table 5. Results of the oxidation of cyclooctene with complexes **21**-**24**.[a]

Cat.	Equiv. H_2O_2	Diol	Epoxide	Diol/epoxide	Yield (%)
21	10	6.2	1.9	3.3	81
	100	73	12	6.0	85
22	10	4.5	0.5	9.0	50
	100	10	4.0	2.5	14
23	10	4.1	4.0	1.0	81
	100	50	49	1.0	99
	300	123	129	0.8	77
24	10	6.0	1.1	5.5	71
	100	74	12	6.2	86
	300	141	29	4.9	57

[a] Reaction conditions: H_2O_2 was added via syringe pump over 30 min to a solution of substrate (1000 equiv.) in MeCN at 25 °C, under nitrogen, Yield given in Turnover number (mol product/mol catalyst).

Comba *et al.* together with Que have reported on the synthesis of the pentadentate bispidine ligand.[29] The ligand was synthesized with two different substitution patterns, from these ligands the corresponding $[Fe(L^1)E]^{2+}$ (**25**) and $[Fe(L^2)A]^{2+}$ (**26**) iron complexes were prepared (Figure 8).
In **25** the co-ligand X is coordinated trans to N3 (equatorial, E) through a short and strong Fe^{II}-X bond, while in **26** the X ligand is positioned trans to N7 (axial, A) through a long and weak Fe^{II}-X bond, where co-ligand X = MeOH, MeCN.

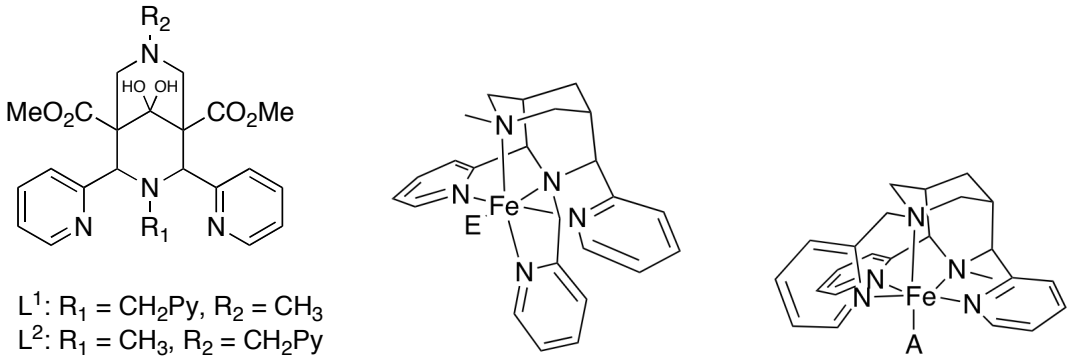

Figure 8. Structure of the prepared ligands and the corresponding complexes **25** and **26**, were X=MeCN, MeOH; A=axial X; E=equatorial X.

Both isomeric Fe(II) complexes are active in the oxidation of cyclooctene with H_2O_2 under different conditions (Table 6). The initial conversion is higher for complex **26** compared to **25**, complex **25** gives only 1.2 TON towards the diol and epoxide product while **26** gives 5 TON of oxidation products (Table 6, entries 1 and 6). After a reaction time of 6 h almost the same conversion is obtained for both complexes (entries 4 and 9). For complex **25** the TON reached a value of 6.8 while complex **26** reached TON of 8.1. When complex **26** was used under argon a decrease in activity was observed (entry 10), but next to the epoxide also some diol (*cis*/*trans* 40/60) was observed. The difference in reactivity is proposed to come from the slightly different structures of the complexes and the formed active intermediates from these complexes.

Table 6. Results of the oxidation of cyclooctene with complexes **25** and **26**.[a]

entry	Ligand	Experimental conditions	Diol + epoxide[b]	Diol/Epoxide
1	L^1	air (0.5 h)	1.2	0.1:1
2	L^1	air (1.5 h)	3.3	0.1:1
3	L^1	air (3.5 h)	6.0	<0.1:1
4	L^1	air (6 h)	6.8	<0.1:1
5	L^1	argon (0.5 h)	1.0	0.2:1
6	L^2	air (0.5 h)	5	0:1
7	L^2	air (1.5 h)	6.3	0:1
8	L^2	air (3.5 h)	7.3	0:1
9	L^2	air (6 h)	8.1	0:1
10	L^2	argon (0.5 h)	2.0	1:1

[a] Reaction conditions: To a solution of 1000 equiv. cyclooctene in MeCN at 25 °C was added by syringe pump in 30 min a solution of 10 equiv. H_2O_2 u.nder air or argon; [b] TON.

The group of Beller has used a different approach in the preparation of biomimetic iron complexes for the epoxidation of olefins. In their approach they do not start with pre-made iron complexes, but instead the active complex is made *in situ* and used directly to perform the epoxidation reaction. All the *in situ* prepared complexes reported by Beller are based on iron(III) instead of iron(II). A full description of iron(III)-based oxidation catalysts is outside the scope of this review, but the use of imidazole ligands in the design of iron-based oxidation catalysts is worthwhile to mention. The system applied by the group of Beller consists out of $FeCl_3.6H_2O$ and an imidazole moiety as ligand. At first 5-chloro-1-methylimidazole (5-Cl-1-MeIm) was selected as the suitable imidazole ligand based on a screening of different imidazoles in the epoxidation of *trans*-stilbene.[30] Unfortunately this system was only able to epoxidize aromatic olefins in moderate to good yields. For the epoxidation of aliphatic olefins a differently substituted imidazole was selected, i.e. 2,6-diisopropyl-N-phenylimidazole (IPrPIm).[31] This imidazole was also effective in the epoxidation of aromatic olefins. A selected overview of the catalytic results obtained with the imidazole IPrPIm is depicted in Table 7.

Table 7. Olefin epoxidation catalyzed by the Fe(III)/IPrPIm system.[a]

Substrate	Conv. (%)	Yield (%)	Selectivity (%)
trans-stilbene	72	66	92
Styrene	100	87	87
4-chloro-styrene	92	88	96
trans-beta-methylstyrene	94	94	>99
cyclooctene	77	65	84
1-octene	24	18	75
2-octene	49	42	86

[a] Reaction conditions: To a solution of alkene (0.5 mmol), $FeCl_3.6H_2O$ (5 mol%), IPrPIm (10.0 mol%) in tert-amyl alcohol in air was added H_2O_2 (1.5 mmol, 3 equiv.) in 1 h via syringe pump at 25 °C.

The *in situ* generated imidazole systems give a high epoxide yield and selectivity for aromatic olefins and a modest yield and good selectivity for aliphatic olefins. The drawback of these systems is that it is difficult to get some insight into the catalytic species present in solution. Beller *et al.* tried to isolate some of the possible complexes and succeeded in the isolation of a complex derived from the IPrPIm ligand, i.e. [(*N*-(2,6-diisopropylphenyl)imidazole)$_4$ClFeOFeCl$_3$] (**27**). This compound turned out to posses some activity towards the epoxidation of olefins, but did not show the characteristics of the *in-situ* prepared complex. Furthermore, they were also able to isolate the complex *trans*-[FeCl$_2$(5-chloro-*N*-methylimidazole)$_4$]Cl (**28**). This complex showed a slightly higher activity for the epoxidation of *trans*-stilbene then the *in-situ* prepared complex. These bio-inspired catalyst based on imidazole are easy to prepare and show good activities towards different olefinic substrates.

Catalysis with H_2O_2/AcOH and AcOOH

Most of the oxidation reactions mentioned above are carried out using a large excess of substrate in order to optimize the productive use of oxidant. From a practical point of view, e.g. when using expensive substrates, these conditions are not practical for synthetic purposes. In order to address this issue, White *et al.* have reported the use of the BPMEN ligand in the epoxidation of alkenes under substrate limiting conditions making the reaction synthetically useful.[32] As follow up the group of Que tested the family of TPA-based catalysts under substrate limiting conditions.[33] For some of the TPA complexes the epoxide and *cis*-diol products were obtained with yields of 69-87%. For their catalytic reaction White *et al.* used H_2O_2 as oxidant in the presence of acetic acid (AcOH). The interest of the group of Que into the development of bio-inspired epoxidation catalyst also led them to investigate the effect of added AcOH on the catalytic reactions with H_2O_2. These studies show that catalysts based on the TPA and BPMEN ligands are able to catalyze the *in situ* formation of AcOOH from H_2O_2

and AcOH.[34] The results obtained for TPA-catalyst complex **29** in the oxidation of cyclooctene are depicted in Table 8.

Table 8. Catalytic oxidation of cyclooctene catalyzed by **29** in the presence and absence of AcOH.[a]

Entry	Equiv. AcOOH	Equiv. H_2O_2	Equiv. AcOH	Epoxide[b]	*cis*-diol[b]	epoxide:diol	total yield(%)[c]
1		14.5		4.3	5.9	0.7:1	70
2		14.5	2	6.5	6.8	1:1	92
3		14.5	17	11.8	2.7	4:1	100
4		14.5	29	12.7	2.1	6:1	102
5		14.5	100	13.1	0.8	16:1	96
6	10	4.5	17	11.7	2.0	6:1	94
7		4.5		1.5	1.9	1:1	76
8		4.5	17	3.1	0.8	4:1	87
9	10	4.5	34	12.0	1.6	8:1	94
10	10	4.5	100	12.7	1.5	8:1	98
11	10	4.5	200	12.8	1.5	8:1	99

[a] Reaction conditions: To a solution of cyclooctene (1.05 mmol) and catalyst (2.1 μmol Fe) in acetonitrile under air at 25 °C was added the H_2O_2 or AcOOH via syringe pump; [b] Amounts expressed as equiv. formed per mol iron catalyst; [c] Total yield of the epoxide and the diol based on the total peroxide content.

Entry 1 shows the reaction without the addition of AcOH, in this reaction 14.5 equiv. (per Fe) H_2O_2 were gradually added to the solution of cyclooctene and **29** in acetonitrile, 4.3 equiv. epoxide and 5.9 equiv. *cis*-diol were formed (entry 1), with overall yield of 70% based on the oxidant. When increasing amounts of AcOH are added to the reaction mixture, the amount of epoxide formed increases and the amount of diol formed decreases (entries 2-5). When some AcOOH is added to replace some of the added H_2O_2, 11.7 equiv. of epoxide were formed and 2.0 equiv. of the *cis*-diol (entry 6). This indicates that complex **29** also is a suitable catalyst with AcOOH as oxidant. The addition of more equivalents of AcOH to the reaction catalyzed by the AcOOH/H_2O_2 mixture further enhances epoxide formation (entries 7-11). Overall, complex **29** seems to catalyze the in situ formation of AcOOH from AcOH and H_2O_2 and seems to become a more selective epoxidation catalyst upon the addition of AcOH. Similar trends as for complex **29** were also observed for the complex based on the BPMEN ligand system. The group of Que further continued their research on the effect of the added acetic acid and reported on the formation of an active intermediate $[(L)Fe^{V}(O)(OOCCH_3)]^{2+}$ which is most likely the oxidizing species in these reactions.[35]

More recently the group of Que reported the first example of the *cis*-dihydroxylation of an aromatic double bond by a synthetic iron catalyst, mimicking the action of the non-heme iron enzyme naphthalene 1,2-dioxygenase (NDO) (Scheme 1).[36]

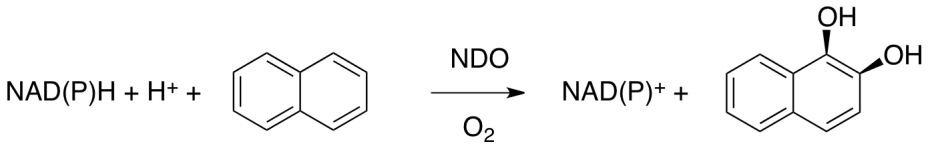

Scheme 1. Naphthalene oxidation by naphthalene 1,2-dioxygenase (NDO).

This reaction makes use of the complex $[(TPA)Fe^{II}(MeCN)_2](OTf)_2$ (**29**) as the catalyst. This complex has earlier been used in the olefin epoxidation and *cis*-dihydroxylation with H_2O_2 as oxidant.[24] For the catalytic reaction a 10 mM solution of H_2O_2 was pumped slowly with a syringe pump (2 equiv. min^{-1}) to a solution of 1 mM catalyst and 0.5 M naphthalene in MeCN at 25 °C. After the addition, the reaction was stirred for an additional 20 minutes. Four different products were identified after the reaction. The major product was the *cis*-1,2-dihydro-1,2-naphthalenediol (30% conversion based on the 10 equiv. of H_2O_2 added). The other products identified were 1-naphthol (5%), 2-naphtol (2%) and 1,4-naphthoquinone (3%). These results represent the first example of an iron-catalyzed arene *cis*-dihydroxylation.

The group of Klein Gebbink reported on the synthesis of chiral ligands **30**-**32** that may either act as tridentate N,N',N or as pentadentate O,N,N',N,O meridionally coordinating ligands (Figure 9).[37,38] These ligands are easily obtained starting from L-proline from the natural chiral pool.

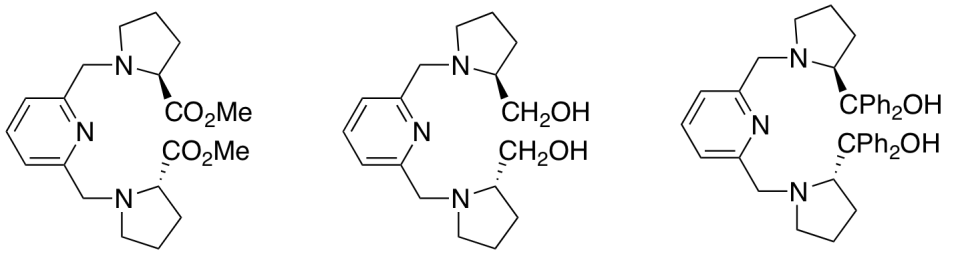

30: $Py(ProMe)_2$ **31**: $Py(ProOH)_2$ **32**: $Py(ProPh_2OH)_2$

Figure 9. Chiral $Py(ProMe)_2$, $Py(ProOH)_2$, and $Py(ProPh_2OH)_2$ ligands.

Depending on the counter anions, the structure of the iron complexes derived from these ligands show different coordination geometries. Complex $[FeCl_2(PyProMe)_2)]$ (**33**) ($Py(ProMe)_2$ = 2,6-bis[[(S)-2-(methyloxycarbonyl)-1-pyrrolidinyl]methyl]-pyridine) features a 5-coordinated iron center with a meridional N,N',N coordination mode of the ligand and the additional coordination of the two chloride atoms. In

contrast, the ligand coordination mode in [Fe(OTf)$_2$(PyProMe)$_2$)] (**34**) has changed to meridional O,N,N',N,O pentadentate through coordination of the carbonyl oxygen donors to iron and yields a 7-coordinated iron center (Figure 10, left). Complex **34** catalyzed the oxidation of hydrocarbons in the presence of TBHP.

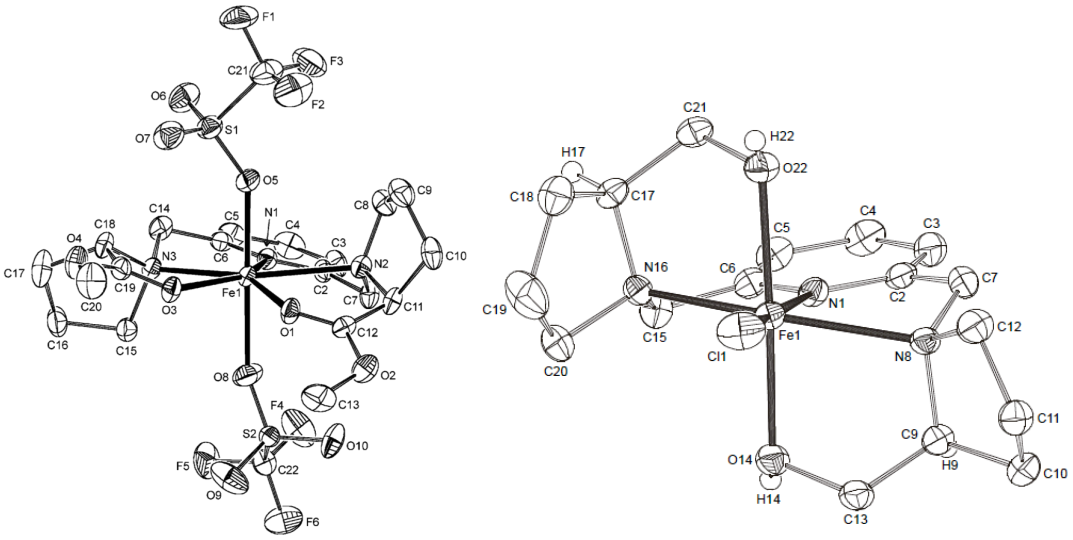

Figure 10. Structure of the seven-coordinated complex **34** and that of complex [FeX(Py(ProOH)$_2$]X were X= Cl.

The coordination behavior of the proline alcohol ligands **31** and **32** differs from that of **30** in the sense that six-coordinated complexes are obtained comprising a meridional N,N',N ligation complemented by axial alcohol ligation and the coordination of one counter ion, to yield cationic octahedral complexes of the type [FeX(L)]X (L = Py(ProOH)$_2$, Py(ProPh$_2$OH)$_2$, X = Cl, OTf). Of these complexes, [FeX(Py(ProOH)$_2$]X complexes were found to be inactive in the oxidation of alkanes and alkenes (Figure 10, right).

Complexes [FeCl(Py(ProPh$_2$OH)$_2$]Cl (**35**) and [Fe(OTf)(Py(ProPh$_2$OH)$_2$](OTf) (**36**) do show some activity in the oxidation of alkenes, yet the overall activity is rather low. Nonetheless, in the case of cyclooctene a small amount of *cis*-diol is formed in a ½ epoxide/diol ratio when using complex **36**.

1.2.2 Structural models based on iron

Next to the extensive development of functional models for the 2-His-1-carboxylate facial triad, the attempts to model this particular enzyme active site in a structural sense are less widespread. This section describes research efforts that endeavor to mimic the coordination environment of iron center in the triad as accurately as possible. Unlike the functional models discussed in the previous section, these

structural models typically make use of ligands that provide a mixed N,O donor set to the metal.

Burzlaff and co-workers reported the use of heteroscorpionate ligands as structural model for the active site of non-heme iron oxidases and zinc enzymes with the 2-His-1-carboxylate facial triad.[39,40] They reported on the use of two scorpionate ligands, bis(3,5-dimethylpyrazol-1-yl) acetic acid (BDMPZA, **37**) and the more sterically hindered ligand bis(3,5-di-*tert*-butylpyrazol-1-yl) acetic acid (BDTBPZA, **38**) which could function as suitable mimic for the facial triad (Figure 11).

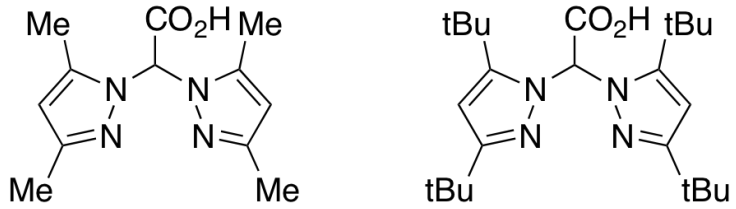

37: bdmpza **38**: bdtbpza

Figure 11. Ligands BDMPZA (**37**) and BDTBPZA (**38**).

The iron coordination chemistry of these two ligand iron complexes was initially studied with $FeCl_2$. The first complex prepared with the BDMPZA ligand afforded the homoleptic 2:1 ligand to metal complex [Fe(BDMPZA)$_2$] (**39**; Figure 12). In an attempt to prevent the coordination of two ligands to iron, sterically demanding *tert*-butyl groups were added to the BDMPZA ligand, giving rise to the BDTBPZA ligand system. While this strategy was successful in achieving a ligand to metal ratio of 1:1, the complex isolated from this ligand turned out to be the dimeric complex [Fe(BDTBPZA)Cl]$_2$ (**40**).

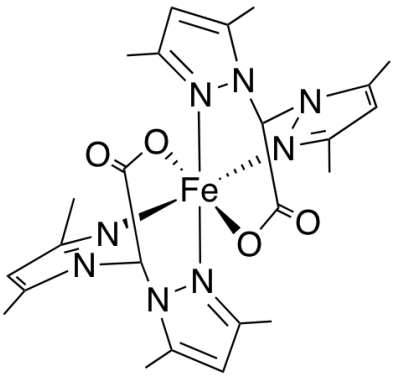

Figure 12. Structure of complex **39**.

While these heteroscorpionate ligands provide access to interesting structural mimics of the facial coordination mode of the 2-His-1-carboxylate facial triad, these systems do unfortunately not act as functional models of the facial triad enzymes.

In a effort to obtain a ligand environment that more closely mimics the facial *N*,*N*,*O* site of the mononuclear iron center in Rieske dioxygenases, the group of Que designed the tridentate (di-(2-pyridyl)methyl)benzamide (Ph-DPAH, **41**) ligand.[41] This ligand can coordinate in a facial manner with the two-pyridine ligands and a carboxyl oxygen analogous to the 2-His-1-carboxylate facial triad. Much like the heteroscorpionate complexes studied by Burzlaff, two of these ligands coordinate in a facial fashion around iron center to form the complex $[Fe^{II}(Ph\text{-}DPAH)_2](OTf)_2$ (**42**; see Figure 13).

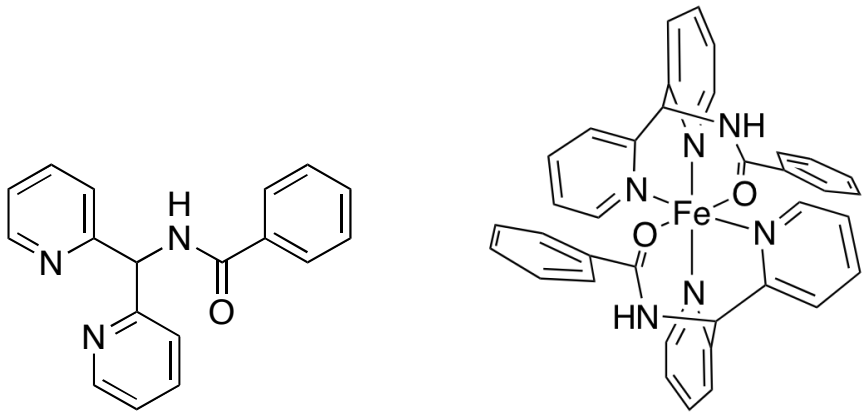

Figure 13. The Ph-DPAH ligand (**41**) and the structure of the corresponding complex $[Fe^{II}(Ph\text{-}DPAH)_2]^{2+}$ (**42**).

Unlike the systems developed by Burzlaff, complex **42** turned out to be an excellent catalyst for the *cis*-dihydroxylation of olefins with H_2O_2 as the oxidant (Table 9). Conversions of 50-80% based on the added amount of H_2O_2 were obtained with this cationic system.

Based on the crystal structure, complex **42** has a coordinatively saturated iron center devoid of open coordination sites for substrate or oxidant. For *cis*-dihydroxylation to take place at least two vacant sites in a *cis*-position are required and it was therefore assumed likely that ligand dissociation would precede catalytic activity. ESI-MS analysis indeed shows the presence of free ligand and of the 1:1 complex $[Fe^{II}(Ph\text{-}DPAH)]^{2+}$ in solutions of **42**. This mono-ligand complex now has three free facial sites and is able to perform the *cis*-dihydroxylation reaction. Complex **42** represents the first iron complex for olefin *cis*-dihydroxylation featuring a biomimetic facial *N*,*N*,*O*-ligand arrangement, i.e. it is the first system to unite structural and functional mimicry of the Rieske dioxygenases.

Table 9. Results of the catalysis with complex **42**.[a]

substrate	diol[%RC]	epoxide[%RC]	diol:epoxide
Styrene[b]	8.0(5)	0.1(1)	80:1
cyclooctene	7.0(6)	0.5(1)	14:1
1-octene			
H_2O_2 (5 equiv.)	3.6(3)	0.04(1)	90:1
H_2O_2 (10 equiv.)	7.6(3)	0.1(1)	76:1
H_2O_2 (20 equiv.)	10.3(7)	0.2(1)	52:1
Cyclohexane[b]	6.2(2)	0.7(1)	9:1
cis-2-heptane	4.9(4)[99]	0.7(1)[57]	7:1
trans-2-heptane	4.9(3)[>99]	0.5(1)[>99]	10:1

[a] Reaction conditions: To a solution of substrate (0.35 M) and catalyst (0.35 mM) in MeCN was added at 25 °C under air the H_2O_2 (10 equiv., except were indicated) by syringe pump in 5 min, Yields expressed as turnover numbers, TON, (μmol product/μmol catalyst); [b] under an argon atmosphere.

Tolman together with Que reported on a different approach to obtain structural models of the 2-His-1-carboxylate facial triad. Instead of using preorganized tridentate chelates, Tolman combined a sterically hindered carboxylate with N-donor ligands in the presence of an Fe^{II} source.[42] Structural data show that the obtained structures replicate the geometry and ligand donor set of the 2-His-1-carboxylate facial triad. A representation of the complex (**43**) synthesis is depicted in Scheme 2. These authors did not report the reactivity of the prepared complex in the oxidation of olefins.

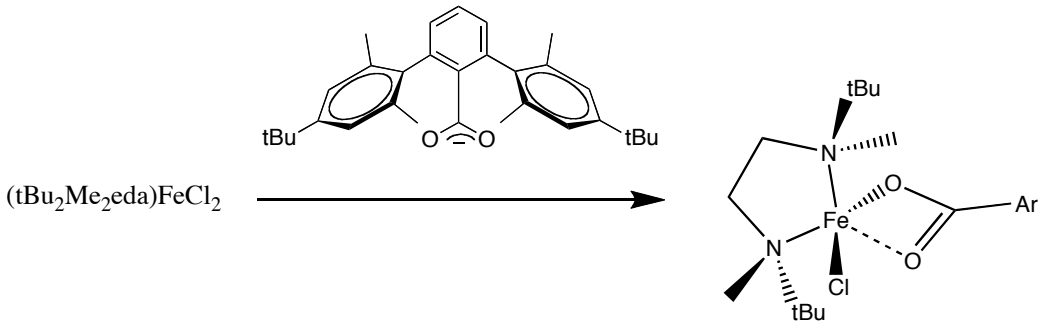

Scheme 2. Mixed ligand complex **43** synthesized by Tolman.

In the ongoing search for structural and functional models Que reported the synthesis of a new polydentate ligand (3-(dipyridine-2-yl-methyl)-1,5,7-trimethyl-2,4-dioxo-3-azabicyclo[3.3.1]nonane-7-carboxylic acid (HL1; **44**) that has two coordinating pyridines and one bidentate coordinating carboxylate group (Figure 14).[43]

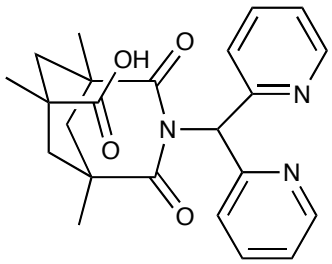

Figure 14. Structure of ligand HL1 (**44**).

The iron(II) complexes made from this ligands perform the epoxidation and *cis*-dihydroxylation of olefins with H_2O_2 as oxidant. This means that the complex is both a structural and functional model of the active site of the Rieske dioxygenases. The complex prepared from this ligand in combination with $FeCl_2$, ([Fe^{II}(L1)Cl] (**45**)), shows a square pyramidal iron center with a apical chloride ligand and the tetradentate ligand in the basal plane (Figure 15). This structure resembles the iron center found in the substrate-bound complex of naphthalene 1,2-dioxygenase (NDO).

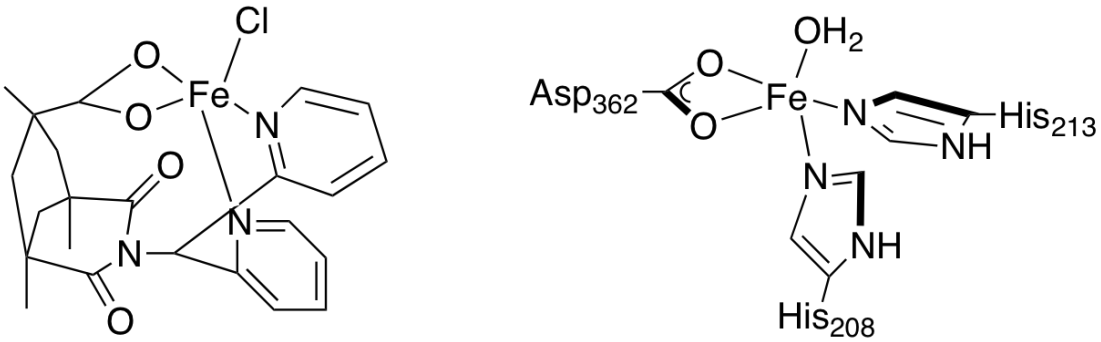

Figure 15. Structure of complex **45** and substrate-bound form of NDO.

Reaction of complex **45** with AgOTf yielded the corresponding triflate complex [Fe^{II}(L1)OTf] (**46**). Both complexes were tested in the oxidation of different olefin substrates (Table 10). Both complexes were found active in the oxidation of olefins, but while chloride complex **45** yields the epoxide in equal or excess amounts to the diol product, triflate complex **46** gives the *cis*-diol product. This difference can be explained by the fact that for *cis*-dihydroxylation to take place two labile *cis* sites are required. The triflate group is much more labile then the chloride group and because of that will be easier split of to create two vacant *cis* sites. The overall activity of both complexes is low and less then one turnover of product is formed. This indicates that the active catalytic species cannot be regenerated; mass analysis at the end of the reaction shows the presence of the free ligand, which indicates the decomposition of the catalyst. Iron complexes based on the HL1 ligand therefore combine structural and functional mimicry, but they are not engaged in catalytic reactivity.

Table 10. Catalytic results of complexes **45** and **46**.[a]

	45		**46**	
substrate	epoxide	diol	epoxide	diol
cis-2-heptane	0.32(4)[47]	<0.05	0.37(10)[51]	0.47(5)[96]
1-octene	0.26(6)	<0.05	0.11(1)	0.67(2)
tert-butyl acrylate	<0.05	0.08(1)		0.58(4)
dimethyl fumarate	<0.05	<0.05[99]		0.42(4)[99]

[a] Reaction conditions: H_2O_2 (10 equiv.) was added by syringe pump in 25 min to a solution of the catalyst (0.7 mM) and substrate (0.35 M) in MeCN under argon. Yields are expressed as mmol product per mmol iron complex with standard deviation values shown in parentheses. Numbers in square brackets represent %RC values; %RC=100L(A_B)/(A + B), where A is the yield of cis-diol or epoxide with retention of configuration and B is the yield of epimer.

The nitrogen donor groups in the structural models presented so far all are different from the histidyl imidazole groups found in the biological systems. For instance, the pyrazole rings used in the heteroscorpionate bispyrazolylacetates differ significantly in their chemical and electronic properties from the histidine prototype. In an attempt to resemble the electronic properties of the facial triad more precisely a new tripodal ligand system was developed by the group of Klein Gebbink[44] and that of Burzlaff at approximately the same time.[45] This new family of substituted 3,3-bis(1-alkylimidazol-2-yl)propionates (RIm_2Pr) is based on the more biologically relevant bis-imidazol-2-yl methane framework with a additional coordinating carboxylate donor group (Figure 16). The ability of this ligand to bind in a facial manner to metal centers was at first illustrated by the coordination of the ligand to different metals, i.e. copper,[44] rhenium and manganese.[45] The two complexes [$Re(MIm_2Pr)(CO)_3$] (**47**) and [$Mn(MIm_2Pr)(CO)_3$] (**48**) synthesized by Burzlaff and co-workers show a facial coordination of the ligand with the additional coordination of three carbon monoxide ligands. The group of Klein Gebbink reported the synthesis of copper complexes based on Mim_2Pr (**49**) and its benzimidazole analogue ($BenzMim_2Pr$ (**50**; Figure 16).

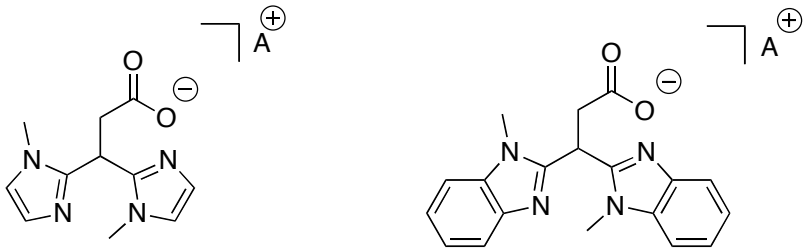

Figure 16. *N,N,O* ligands A[MIm_2Pr] (**49**) and A[$BenzMIm_2Pr$] (**50**).

In these copper complexes, [$Cu(MIm_2Pr)_2$] (**51**) and [$Cu(BenzMIm_2Pr)_2$] (**52**), two of the monoanionic ligands are coordinated to the copper center. This gives rise to

complexes with an octahedral coordination geometry and a trans coordination of the ligands (Figure 17).

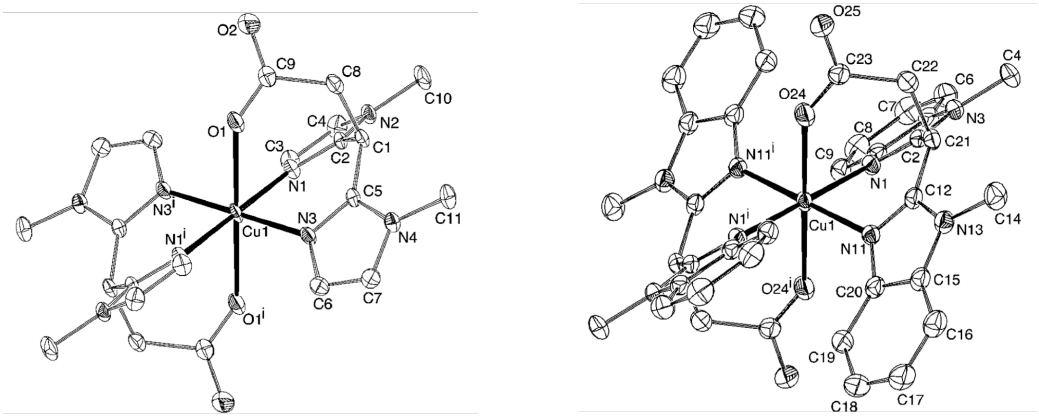

Figure 17. Crystal structures of complexes **51** and **52**.

Although these complexes show the facial coordination mode of these imidazole ligands, in order to mimic the coordination environment around the metal in 2-his-1-carboxylate type enzymes only one of these ligands should coordinate to the metal to leave the coordination sides open for further chemistry.

The group of Klein Gebbink continued the work based on these ligands systems and reported on the synthesis of iron complexes based on these ligands and on the corresponding ester ligands.[46] Starting with the parent ligand **49** or its the neutral propyl ester analogue propyl 3,3-bis(1-methylimidazol-2-yl)-propionate (PrL1, **53**) gave the structurally related homoleptic bis-ligand complexes $[Fe^{II}(MIm_2Pr)_2]$ (**54**) and $[Fe^{II}(PrL1)_2]$ (**55**) (Figure 18).

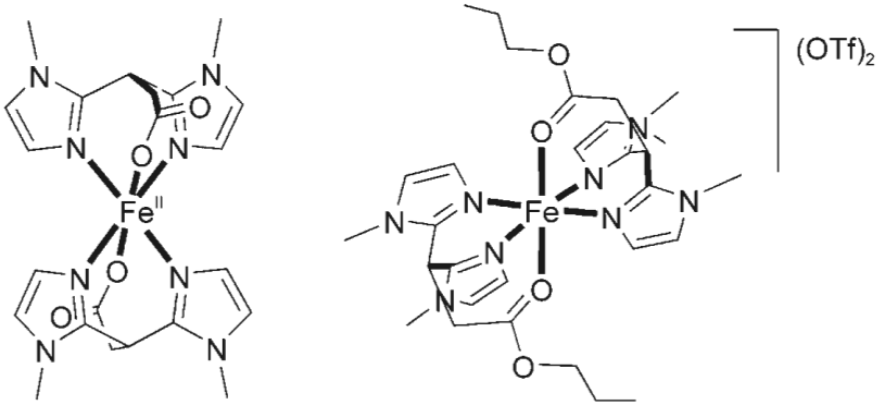

Figure 18. Structure of iron(II) complexes $[Fe^{II}(MIm_2Pr)_2]$ (**54**) and $Fe^{II}(PrL1)_2](OTf)_2$ (**55**).

In both structures the facial coordination of the two ligands around the iron center features the anticipated N,N,O binding motif. The structure of complex **54** is

isostructural with the previously obtained copper complex **51**. For complex **55** unfortunately no crystal structure was obtained but its structure is based on the crystal structure obtained for the complex $[Fe^{II}(PrL1)_2](BPh_4)_2$ (**56)** with BPh_4 counter ions instead of triflate. In this structure it are the two nitrogen atoms from the two imidazole rings that coordinate to the metal center and the carbonyl oxygen from the ester groups. The structure of complex **56** is similar to the iron(II) complex $[Fe^{II}(Ph\text{-}daph)_2](OTf)_2$ (**42**) as reported by Que.[41] The prepared complexes were tested as catalyst in the oxidation of different olefins. Complex **54** turned out not to be active in the catalytic reaction, probably due to the slow ligand exchange, cased by the monoanionic ligands. The results obtained with complexes **55** and **56** are summarized in Table 11.

Table 11. Oxidation of alkenes by complexes **55** and **56**.[a]

		Epoxide [RC]		Diol [RC]		Conversion		ratio epox/diol
Substrate	H_2O_2 (eq)	**55**	**56**	**55**	**56**	**55**	**56**	**55**
Cyclooctene	10	2.8	0.8	1.1	0	39	8	2.5:1
	20	3.8	1.5	1.5	0	27	8	2.5:1
Styrene	10	2.3	1.2	1.7	0	40	12	1.4:1
	20	4.9	2.2	3.4	0	41	11	1.4:1
1-octene	10	1.6		2.7		43		1:1.7
	20	2.4		2.5		35		1:1.9
	40	3.3		7.0		26		1:2.1
trans-2-heptane	20	3.2[93]		2.3[91]		28		1.4:1
cis-2-heptane	20	6.2[84]		6.3[92]		63		1:1

[a] Reaction conditions: To a solution of the substrate (1000 equiv., 3 mmol) and catalyst (3 µmol) in MeCN at 25 °C was added drop wise in 20 min a solution of H_2O_2.

Complex **55** is active in the formation of epoxide as well as *cis*-diol products. For 1-octene a slight preference for the diol product was observed, the other substrates gave the epoxide as major product. Also the stereoselectivity of the *cis*-dihydroxylation reaction was examined by the reaction with *trans* and *cis*-2-heptane. For both substrates high stereoselectivity was observed with the retention of substrate configuration between 84 and 93%. Complex **56** on the other hand showed hardly any activity in the oxidation reactions, which points to the importance of the type of counter anion in these reactivity studies. Overall, complex **55** adds a new structural and functional facial triad model to the class of non-heme iron catalyst capable of the epoxidation and *cis*-dihydroxylation of olefins.

1.3 Manganese-based systems

In the first part of this review the developments of iron based complexes that functionally and/or structurally mimic the 2-His-1-carboxylate facial triad were described. Next to the iron complexes discussed above also manganese complexes are developed for the epoxidation of alkenes. These manganese complexes are often based on the ligands that where used in combination with iron. The best-known manganese-based system for the catalytic epoxidation of olefins is the system reported by Jacobsen using manganese salen complexes. This system from Jacobsen will be shortly discussed. The main part of this chapter will be devoted to the manganese analogue of the iron complexes previously discussed, which are functional or structural models of the active site of enzymes.

The group of Kochi *et al.*[47] was the first to report on manganese salen complexes for epoxidation reactions. After this report the groups of Jacobsen[48] and Katsuki[49] reported around the same time their first papers about the use of manganese salen complexes for the asymmetric epoxidation of olefins. The salen catalyst are based on a Mn(III) center and mixed N,O bis-phenol-imine type ligand that offers different sides for the introduction of substituents. Via these variations the steric and electronic properties of the salen ligand can be varied. One of the most famous salen-based systems is the so-called Jacobsen catalyst (Figure 19). This catalyst shows high activities and high enantioselectivities in the epoxidation of prochiral olefins.[50-52] The catalyst is nowadays commercially available in both enantiomeric forms.[53]

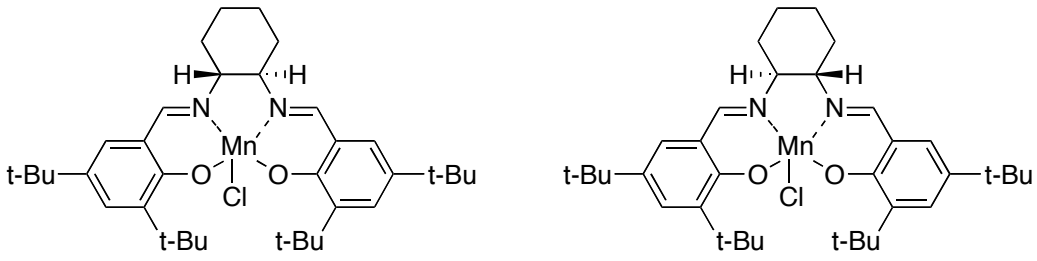

Figure 19. Both enantiomers of the Jacobsen catalyst.

An example of the reactivity of the complex is depicted in Table 12 using the *S*,*S* form of the catalyst shown in Figure 19.[51] For the catalytic reaction with the salen type complexes bleach (NaOCl) or iodosylbenzene are commonly used as the oxidant.

Table 12. Examples of enantioselective olefin epoxidation by the *S*,*S*-Jacobsen catalyst.[a]

Substrate	yield %	ee %
cis-*beta*-methylstyrene	84	92
4-chloro-*cis*-*beta*-methylstyrene	67	92
2,2-dimethylchromene	72	98
6-cyano-2,2-dimethylchromene	96	97
epoxy ketals	63	94
cis-methyl-cinnamate	65	89

[a] Reaction conditions: To a 0.55 M solution in NaOCl at pH 11.3 (made from household bleach) was added the catalyst (0.25 mmol) and the substrate (12.5 mmol) in CH_2Cl_2 the two-phase mixture was stirred at 4 °C under air.

This catalyst performs well for conjugated *cis*-disubstituted and trisubstituted olefins, where it gives *ee* values >90%. On the other hand, the catalyst is less suitable for *trans*-substituted olefins. The drawback of this system is the use of bleach or iodosylbenzene as oxidant and that is requires high catalyst loadings (usually 2-5%). To obtain a more environmentally friendly system the use of hydrogen peroxide as oxidant was investigated with the salen systems. Berkessel reported on the use of hydrogen peroxide as terminal oxidant through the use of a modified salen 'biomimetic' salen ligand.[54-56] For these reactions the salen ligand was adapted with a covalently attached axial imidazole donor group. Complexes based on this ligand give rise to an enantioselectivity of 64% in the epoxidation of 1,2-dihydronaphtalene as substrate at 10 mol% catalyst loading. Pietikäinen *et al.* also reported on the use of hydrogen peroxide in the epoxidation with manganese salen complexes. In this case epoxidations were carried out with the use of the additives imidazole and N-methyl imidazole as axial ligand[57] or carboxylate salts as cocatalyst.[58]

Next to the mixed N,O salen ligand system used in the Jacobsen catalyst, many of the all-nitrogen ligands that have been used to develop olefin oxidation catalysts based on iron have also been used to develop similar catalysts based on manganese. Also in the development of these manganese catalysts the focus is on the use of hydrogen peroxide as the terminal oxidant, and again the combination of hydrogen peroxide and acetic acid or of peracetic acid is explored as well.
Stack *et al.* have reported the use of the previously used ligands BPMEN (MEP) (**5**) and BPMCN (R,R-MCP) (**7**) in combination with manganese.[57] These authors reported the synthesis of the complexes $[Mn^{II}(BPMEN)(OTf)_2]$ (**57**) and $[Mn^{II}(BPMCN)(OTf)_2]$ (**58**), which are isostructural to the iron analogues with an octahedral geometry and two *cis*-bound triflate anions (Figure 20).

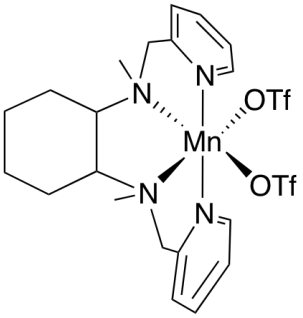

Figure 20. Structure of manganese complex **58**.

The presence of two labile *cis*-sites allows the formation of dimeric Mn^{II} and Mn^{III} complexes under aqueous conditions. These dimeric complexes are good H_2O_2 disproportionation catalysts. Complexes **57** and **58** indeed showed the disproportionation of H_2O_2 to the extent that H_2O_2 is not a suitable oxidant for catalytic olefin oxidation with these complexes. For that reason other oxidants such as peracids, alkylperoxides or iodosylbenzene need to be used. Using peracetic acid as the oxidant, it turned out that catalyst **58** is the kinetically and thermodynamically more stable catalyst in the oxidation of different olefins (Table 13).
Complex **58** shows high reactivities and with different kind of substrates reactions go to completion within a few minutes. In follow-up studies, the group of Stack investigated a library of manganese triflate complexes in olefin oxidation reactions with per acetic acid as oxidant at high and low pH conditions.[60,61]

Table 13. Catalytic results obtained with complex **58**.[a]

Substrate	mol % **58**	oxidant (equiv.)	yield (GC)
cyclooctene	0.1	1.2	99
cyclohexene	0.1	1.2	98
1-methyl-cyclohexene	0.1	2	92
cis-2-heptene	0.1	1.2	99
trans-2-heptene	0.1	1.2	99
1-heptene	0.1	1.2	95
cis-beta-methylstyrene	0.1	1.2	90
trans-beta-methylstyrene	0.1	1.2	97

[a] Reaction conditions: Olefin (0.5 M in MeCN), 32% CH_3CO_3H in acetic acid/water at 25 °C in 5 min.

The group of Costas continued on the work by Stack through the introduction of pinene rings at the 4 and 5 position of the two pyridine groups of the BPMCN (R,R-MCP, **7**) ligand (Figure 21).[62] By the introduction of these groups the two labile

binding sites of the manganese ion are confined in a better-defined chiral pocket compared to in the BPMCN ligand system.

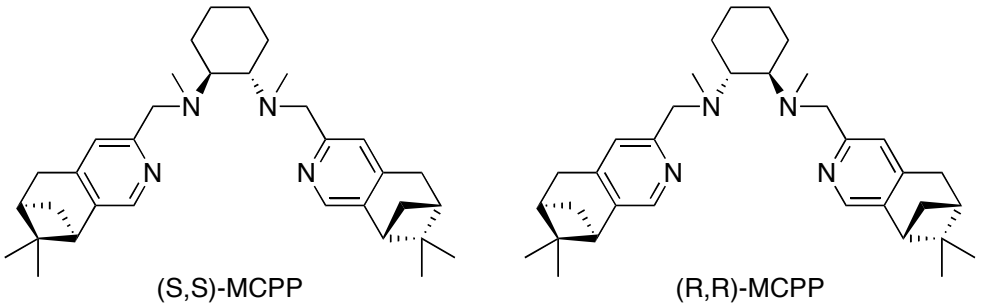

Figure 21. MCPP ligands developed by Costas *et al*..

With these MCPP ligands (MCPP = N,N'-dimethyl-N,N'-bis((R)-4,5-pinenepyridin-2-yl)methyl)cyclohexane-1,2-diamine) the complexes [$Mn^{II}(OTf)_2$((*S*,*S*)-MCPP)] (**59**) and [$Mn^{II}(OTf)_2$((*R*,*R*)-MCPP)] (**60**) were prepared, which adopt a distorted octahedral geometry with the ligand in a *cis*-α topology. Crystallographic studies indeed showed that the two triflate groups are located in a cavity formed by the two pinene moieties. In initial screenings it turned out that complex **59** is the better catalysts of the two prepared complexes and further studies focused on the use of this complex. Complex **59** was tested in the oxidation of different olefins under optimized conditions with per acetic acid as oxidant (Table 14).

Table 14. Results of the catalytic oxidations with complex **59**.[a]

Substrate	conversion (%)	yield (%)	selectivity (%)	ee (%)
trans-beta-methylstyrene	100	93	93	36
Styrene[b]	99	78	79	46
4-chlorostyrene	76	60	79	43
4-methylstyrene	81	49	61	34
3-nitrostyrene	85	85	100	27
1-octene	76	60	79	
cyclooctene	89	81	91	

[a] Reaction conditions: To a solution of catalyst (1 equiv.) and olefin (0.5 M in MeCN, 200 equiv.) at 0 °C is added in 3 min a solution of 32% ACOOH in acetic acid/water (200 equiv.); [b] Reaction at -40 °C with 220 equiv. of AcOOH.

It is apparent that the introduction of the pinene groups has a positive influence on the enantioselectivity of the epoxidation reactions, with *ee* values up to 46%, while the corresponding complex without the pinene groups gives only marginal stereoselectivities (≤10%). These pinene-appended ligands are a step forward towards the development of efficient chiral epoxidation catalyst.

In ongoing research to develop better and more enantioselective catalysts, Sun *et al.*[63] have reported on a novel series of chiral tetradentate N_4 ligands derived from the R,R-MCP (**7**) (MCP = (*R*,*R*)-*N*,*N*′-dimethyl-*N*,*N*′-bis(2-pyridylmethyl)cyclohexane-1,2-diamine) ligand system reported by Stack.[59] The reported ligands have aromatic groups introduced at both of the 2-pyridylmethyl positions C7 and C7' of the original R,R-MCP ligand (Figure 22).

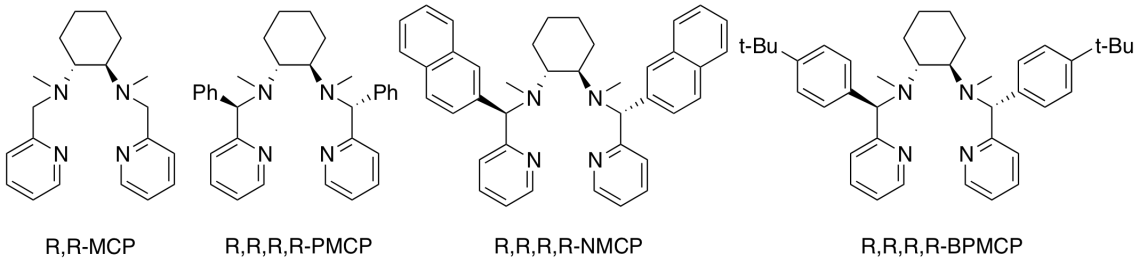

Figure 22. Three new chiral ligands prepared by Sun based on the R,R-MCP ligand system.

With these new ligands the following manganese(II) complexes were prepared, $[Mn^{II}(PMCP)(OTf)_2]$ (**61**) (PMCP = N,N'-dimethyl-N,N'-bis[*R*-phenyl(2-pyridinylmethyl)] cyclohexane-1*R*,2*R*-diamine), $[Mn^{II}(NMCP)(OTf)_2]$ (**62**) (NMCP = N,N'-dimethyl-N,N'-bis[*R*-naphthalen-2-yl-(2-pyridinylmethyl)] cyclohexane-1*R*,2*R*diamine) and $[Mn^{II}(BPMCP)(OTf)_2]$ (**63**) (BPMCP = N,N'-dimethyl-N,N'-bis[*R*-4-*tert*-butylphenyl(2-pyridinylmethyl)] cyclohexane-1*R*,2*R*diamine). From the first two complexes a crystal structure was obtained showing that the ligands coordinate in a *cis*-α topology with the *cis* coordination of both triflate groups. The obtained complexes were at first tested in the epoxidation of styrene with the H_2O_2 as oxidant in the presence of acetic acid. The results of this first screening are depicted in Table 15.

As can be seen in Table 15 the prepared complexes show good activities and higher enantioselectivities as reported for the R,R-MCP ligand system. Complex **63** was also tested in the epoxidation of a variety of α,β-unsaturated ketones. The epoxides were obtained in good yields >80% and moderate to excellent enantioselectivities for most cases (70-89%). This work shows that the introduction of the proper groups in the right position can have a beneficial result on the activity and the selectivity of the catalyst.

Table 15. Epoxidation with complexes **61**-**63**.[a]

Substrate	Complex	Yield %	ee %
styrene	**61**	89	46
styrene	**62**	78	46
styrene	**63**	85	43
4-chloro-styrene	**63**	85	43
4-bromo-styrene	**63**	89	43
styrene	**58**	30	26
chalcone	**61**	90	77
chalcone	**62**	87	71
chalcone	**63**	91	78

[a] Reaction conditions: Reaction were carried out in MeCN at 25 °C with 0.25 mmol of substrate, 1 mol% of complex, 6 equiv. of H_2O_2 and 5 equiv. of AcOH.

The group of Talsi recently also reported on the BPMCN ligand system in their search for a chiral non-heme aminopyridine manganese complex.[64] In their work they used complex **58** previously reported by Stack and co-workers[59] but they also reported on the use of the PDP (BPBP) ligand system with manganese already reported by White and Chen[65] in combination with iron (Figure 23). The manganese complex [Mn(II)[(S,S)-PDP](CF$_3$SO$_3$)$_2$] (**64**) possesses the same *cis*-α topology as the related BPMCN manganese complex ([Mn(II)[(R,R)-BPMCN](CF$_3$SO$_3$)$_2$ and [Mn(II)[(S,S)-BPMCN](CF$_3$SO$_3$)$_2$]).

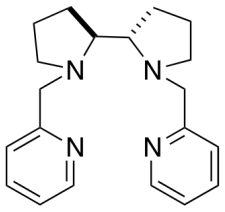

S,S-pdp

Figure 23. The S,S-pdp ligand.

In catalysis both three complexes shows good results and high chemo- and enantioselectivities, different kind of olefins (chalcone and its heterocyclic counterparts) were reacted with peracetic acid or hydrogen peroxide and gave moderate to high yields and ee values up to 89% (peracetic acid, AcOOH) and 84% (hydrogen peroxide, H_2O_2), performing as many as 1000 turnovers. These results are close to those demonstrated by the Katsuki-Jacobsen salen manganese catalyst. Using peracetic acid as the oxidant, *ee* values up to 89% are reached and with hydrogen peroxide *ee* values up to 84%.

Talsi continued his studies on bipyrrolidine complex **64** and investigated the effect of carboxylic acids as additive during the catalytic reaction with hydrogen peroxide.[66] Next to acetic acid he investigated other more bulky carboxylic acids and also compared the catalytic performance of manganese complex **64** to that of the corresponding iron complex **16**. This study showed that the more bulky acids give higher product *ee's*. Furthermore, the manganese complex showed a higher efficiency and a higher enantioselectivity compared to the iron complex. With manganese complex **64** *ee* values up to 93% were reported in the epoxidation of manly styrene type of substrates and chalcone.

More recently the group of Costas reported on an extension of the bis-pyrrolidine-based ligand scaffold by the introduction of 4,5-pinene appended pyridine rings, in similar way as they earlier reported for the MCPP ligand (Figure 24).[67]

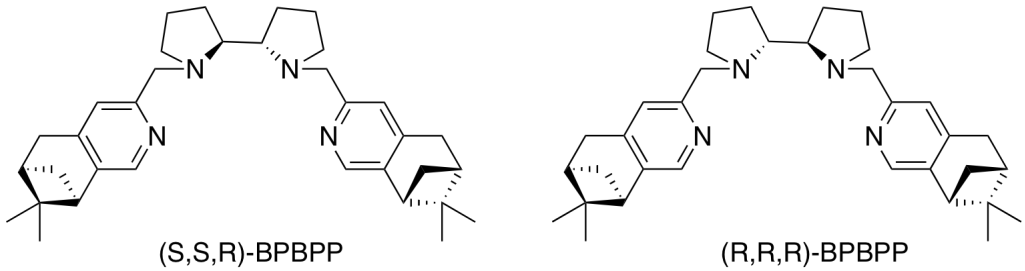

Figure 24. The two BPBPP ligands.

Mn(II) complexes derived from these ligands have a distorted octahedral geometry with the ligand in a C_2-symmetrical *cis*-α topology, in analogy with the Mn-MCP complexes. The two triflate groups again coordinate at the two remaining positions *cis* with respect to each other. In catalytic screenings these complexes were found to catalyze the epoxidation of a wide range of olefins (manly styrene based substrates, and chalcone) using low catalyst loadings (0.1%) and hydrogen peroxide as oxidant. The complexes gave good yields (60-100%) and moderate to good enantioselectivities (40-73%).

Sun *et al.* continued the research towards biologically inspired tetradentate nitrogen (N_4)-based ligands for the asymmetric oxidation of olefins.[68] In analogy to the bispyrrolidine scaffold, they reported on a N_4 ligand system based on a rigid chiral diamine derived from proline and two benzimidazoles (Figure 25).

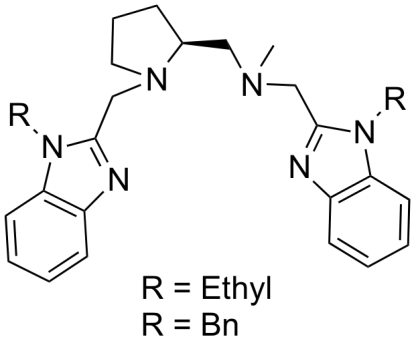

Figure 25. Bis-benzimidazole ligands reported by Sun *et al.*.

Manganese complexes derived from these ligands efficiently catalyze the asymmetric epoxidation of different α,β unsaturated ketones (like chalcone) with 60-99% isolated yield and up to 95% ee with 0.01-0.2 mol% catalyst loadings. This catalyst system was also suitable for gram-scale production without any loss in enantioselectivity.

The group of Feringa has reported on dinuclear manganese catalyst based on the TMTACN (Me_3TACN) ligand system (TMTACN = *N,N',N''*-trimethyl-1,4,7-triazacyclononane).[69-72] These complexes display a very high activity in the epoxidation and *cis*-dihydroxylation of olefins. Other groups have also reported on the use of this dinuclear manganese system in oxidation catalysis. These studies included the development of chiral TACN ligand systems, but these systems were not very successful, as these suffer from low activities and modest stereoselectivities.[73-75] A detailed description of these dinuclear systems is outside of the scope of this introduction chapter.
Next to dinuclear TMTACN manganese systems,[76,77] De Vos *et al.* also reported on the formation of mononuclear species using tris(methyl)-l,4,7-triazacyclononane (**L1**), tris(2-hydroxybutyl)-l,4,7-triazacyclononane (**L2**) and 1,4,7-tris(acetato)-1,4,7-triazacyclononane (**L3**) ligands.[78] Ligands **L2** and **L3** can coordinate in a hexadentate manner to the manganese center forming a monomeric complex. All three ligands were tested in catalysis using different solvents and temperature. See Table 16 for the obtained catalytic results with cyclohexene and styrene as substrates.

Table 16. Effects of temperature and solvent in the epoxidation of cyclohexene and styrene using manganese complexes with ligands **L1-L3**.[a]

Solvent	T (K)	Cyclohexene epoxide yield (%)			Styrene epoxide yield (%)		
		Mn-L1	**Mn-L2**	**Mn-L3**	**Mn-L1**	**Mn-L2**	**Mn-L3**
THF	298	2.0	4.9	1.0	1.4	12.8	n.d.
	273	0.9	2.0	1.3	0.5	5.7	n.d.
Acetonitrile	298	6.2	18.8	3.4	5.4	16.0	1.3
	273	1.8	10.6	2.2	1.4	10.2	1.5
Acetone	298	25.2	13.5	9.6	32.7	29.6	14.7
	273	79.2	38.5	18.0	98.0	53.4	32.9
Methanol	298	6.1	34.2	32.3	4.5	48.1	14.0
	273	3.4	40.8	29.3	3.4	60.0	15.2

[a] Reaction conditions: 1 mmol olefin, 2 mmol H_2O_2, 1.1 g of solvent, 7.5 μmol of **L2** or **L3** and 5 μmol Mn, 10h (or 1.5 μmol of **L1**, 1 μmol Mn, 3h).

With **Mn-L1** considerable amount of epoxide are formed in acetone as solvent, cyclohexene 79.2% and styrene 98.0% at 273 K. The other solvents were not suitable for this complex. With the other two complexes different reaction result were seen. The reactions with Ligands **Mn-L2** and **Mn-L3** were slower compared to **Mn-L1**. Furthermore **Mn-L2** was especially active in methanol as solvent while complex **Mn-L3** gave the highest yield in acetone.

The group of Costas reported on the synthesis of the highly tunable PyTACN ligand system, in which one of the nitrogen atom in the TACN ring is substituted with a pyridyl moieties, as ligand in the modeling of non-heme iron oxygenases.[28] They have also used the same ligand system in their research on suitable manganese oxidation systems.[79] With the previously reported PyTACN ligands, four manganese complexes were synthesized (Scheme 3).

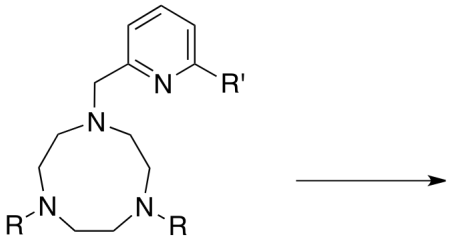

65 = $[Mn(OTf)_2(^{iPr,\ H}PyTACN)]$
66 = $[Mn(OTf)_2(^{iPr,\ Me}PyTACN)]$
67 = $[Mn(OTf)_2(^{Me,\ H}PyTACN)]$
68 = $[Mn(OTf)_2(^{Me,\ Me}PyTACN)]$

R = iPr, R' = H ($^{iPr,\ H}$PyTACN)
R = iPr, R' = Me ($^{iPr,\ Me}$PyTACN)
R = Me, R' = H ($^{Me,\ H}$PyTACN)
R = Me, R' = Me ($^{Me,\ Me}$PyTACN)

Scheme 3. Synthesis of four PyTACN-based manganese complexes.

In the first screening of these complexes with 1-octene as substrate a remarkable dependence of the catalytic activity on the structure of the complexes was observed. Both complexes **65** and **66** hardly showed any activity (1% epoxide yield), complex **68** showed a moderate activity (27%) and complex **67** was the most active one and gave the epoxide in a yield of 97%. The crystal structure of complex **67** shows the manganese center in a distorted octahedral geometry, in which the four nitrogen atoms of the tetradentate ligand coordinate towards manganese and the two triflate groups are coordinated in a *cis*-position to each other. Further catalytic studies with complex **67** used peracetic acid as the oxidant, instead of H_2O_2, which was used in the study of the corresponding iron complexes (Table 17). The catalyst shows a good activity for a wide range of different types of olefins with an excellent product selectivity. Perhaps only drawback of the system is the laborious preparation of the ligand.

Table 17. Epoxidation of different olefins with catalyst **67**.[a]

substrate	cat.(%)/t (h)	Conv.% (yield %)	TON
Styrene	0.1/1	100(91)	910
4-chlorostyrene	0.1/1	100(>99)	1000
4-nitrostyrene	0.1/6	100(>99)	1000
trans-beta-methylstyrene	0.15/6	96(92)	615
cis-beta-methylstyrene	0.1/2	98(93)	970
trans-stilbene	0.1/1	86(58)	580
cis-stilbene	0.1/1	26(24)	240
cyclooctene	0.1/1	100(>99)	1000
cyclohexene	0.1/1	100(>99)	1000
1-octene	0.15/6	100(96)	640

[a] Reaction conditions: To a solution of olefin (0.12 M), and catalyst (0.1-0.15 mol%) is added a solution of 1.4 equiv. of CH_3CO_3H (32% dissolved in MeCN (1:1)) in 30 min at 0 °C.

The use of peracetic acid as oxidant also has some important drawbacks such as a poorer atom economy then H_2O_2, the higher price and the acidity of commercially available peracetic acid solutions. Because of the acidity the use of **67** in the epoxidation of acid-sensitive substrates is limited. However, the use of H_2O_2 in catalytic systems based on manganese generally leads to the loss of a major part of the peroxide through manganese-catalyzed disproportionation. To overcome this problem the group of Costas reported a procedure in which H_2O_2 is used in combination with 14 equivalents of acetic acid.[80] In reactions only employing H_2O_2 the immediate evolution of O_2 arising from peroxide disproportionation was indeed observed. The addition of small amounts of acetic acid to these reactions resulted in increased epoxide yields, reaching a maximum at 14 equiv. of acetic acid. It has been proposed that per acetic acid may be formed under these conditions in situ.[34] The scope of these

conditions was tested on a broad range of substrates. In comparison the complex $[Mn^{II}(BPMCN)(OTf)_2]$ (**58**)[59] was also tested under these conditions. This complex showed a very high epoxidation activity in combination with peracetic acid. Furthermore, this complex is easier to prepare than complex **67**. The catalytic results for both complexes in the oxidation of a series of olefin substrates with the H_2O_2/acetic acid mixture are represented in Table 18.

Table 18. Epoxidation with catalyst **67** and **58** with H_2O_2/acetic acid.[a]

substrate	cat (mol%)/H_2O_2 (equiv.)	conv. (yield)	
		67	**58**
styrene	0.1/1.2	100(94)	89(77)
	0.02/1.2	90(90)	
trans-beta-methylstyrene	0.1/1.2	91(91)	31(31)
cis-beta-methylstyrene	0.1/1.2	100(94)	83(87)
trans-stilbene	0.1/1.2	100(95)	26(26)
cis-stilbene	0.1/1.2	100(88)	36(28)
cyclooctene	0.1/1.1	100(95)	100(97)
1-octene	0.1/1.1	90(90)	89(89)

[a] Reaction conditions: To a solution of olefin (1.66 mmol), catalyst (1.66 μmol, 0.1 mol%), and AcOH (23.3 mmol, 14 equiv.) in MeCN at 0 °C was added the H_2O_2 (1.1-1.2 equiv.) by syringe pump in 30 min.

Complex **67** showed to be active over the whole range of substrates and the overall efficiency and selectivity of these reactions resemble those when peracetic acid is used as the sacrificial oxidant. Complex **58** also showed to be active under these conditions and in particular with aliphatic olefins. Overall, this new method for the epoxidation of a wide range of olefins uses milder reaction conditions than when using commercially available peracetic acid.

1.4 Concluding Remarks

The last years have shown the development of many different ligands systems for the construction of model systems for the active sites of non-hem iron enzymes and of biomimetic oxidation catalysts. In the beginning these ligands were predominately nitrogen-based and the corresponding catalytically active iron complexes could be considered as functional mimics of the enzymes. Later, research efforts also shifted towards the preparation of structural models of these enzymes, in an attempt to mimic the active site as close as possible. These efforts made use of ligands systems based on a mixed N,O donor set. In parallel to the development of these iron-based

biomimetic oxidation catalysts the same types of ligands have also been used to construct manganese-based catalysts.

Each of the catalysts presented in this review has its own drawbacks, ranging from a limited substrate scope, to the use of non-green oxidants, a difficult ligand synthesis, or to low catalyst activity or enantioselectivity. This means that there are still a lot of possibilities to optimize these different catalyst systems either by the synthesis of new ligand classes or by amending the existing systems. The ideal catalyst system would be easy to prepare, uses H_2O_2 or O_2 as the oxidant, has a wide substrate scope with high selectivities and enantioselectivities, and is applicable at a synthetic scale.

References

1. Sheldon, R.A.; Kochi, J.K. *Metal-catalyzed Oxidations of Organic Compounds*, Academic Press, New York, 1981.
2. Bäckvall, J-E. *Modern Oxidation Methods*, Wiley-VCH, Weinheim, 2004.
3. Meunier, B. *Biomimetic catalyzed by transition metal complexes*, Imperial College Press, London, 1999.
4. Denisov, I.G.; Makris, T.M.; Sligar, S.G.; Schlichting, I. *Chem. Rev.* **2005**, *105*, 2253.
5. Solomon, E.I.; Brunold, T.C.; Davis, M.I.; Kernsley, J.N.; Lee, S.-K.; Lehnert, N.; Neese, F.; Skulan, A.J.; Yang, Y.-S.; Zhou, J. *Chem. Rev*. **2000**, *100*, 235.
6. Costas, M.; Mehn, M.P.; Jensen, M.P.; Que, L. Jr. *Chem. Rev.* **2004**, *104*, 939.
7. Tshuva, E.Y.; Lippard, S.J. *Chem. Rev.* **2004**, *104*, 987.
8. Koehntop, K.D.; Emerson, J.P.; Que, L. Jr. *J. Biol. Inorg. Chem.* **2005**, *10*, 87.
9. Hegg, E.L.; Que, L. Jr. *Eur. J. Biochem.* **1997**, *250*, 625.
10. Que, L. Jr. *Nat. Struct. Biol.* **2000**, *7*, 182.
11. Bruijnincx, P.C.A.; van Koten, G.; Klein Gebbink, R.J.M. *Chem. Soc. Rev*. **2008**, *37*, 2716-2744.
12. Chen. K.; Que, L. Jr. *Angew. Chem. Int. Ed.* **1999**, *38*, 2227-2229.
13. Kauppi, B.; Lee, K.; Carredano, E.; Parales, R.E.; Gibson, D.T.; Eklund, H.; Ramaswamy, S. *Structure*, **1998**, *6*, 571-586.
14. Zang, Y.; Kim, J.; Dong, Y.; Wilkinson, E.Z.; Appelman, E.H.; Que, L. Jr. *J. Am. Chem. Soc*. **1997**, *119*, 4197-4205.
15. Nam, W.; Ho, R.Y.N.; Valentine, J.S. *J. Am. Chem. Soc.* **1991**, *113*, 7052-7054.
16. Lubben, M.; Meetsma, A.; Wilkinson, E.C.; Feringa, B.; Que, L. Jr. *Angew. Chem. Int. Ed.* **1995**, *34*, 1512-1514.
17. Roelfes, G.; Lubben, M. Hage, R.; Que, L. Jr.; Feringa, B.L. *Chem. Eur. J*. **2000**, *6*, 12, 2152-2159.
18. Costas, M.; Tipton, A.K.; Chen, K.; Jo. D-H.; Que, L. Jr. *J. Am. Chem. Soc.* **2001**, *123*, 6722-6723.
19. Jacobsen, E.N. in *Catalytic Asymmetric Synthesis*; Ojima, I., Ed.; Wiley-VCH: New York, 1993, pp. 159-202.
20. Katsuki, T. In *Catalytic Asymmetric Synthesis*, 2nd ed.; Ojima, I., Ed.; Wiley-VCH: New York, 2000, pp. 287-325.
21. Suzuki, K.; Oldenburg, P.D.; Que, L. Jr. *Angew. Chem. Int. Ed.* **2008**, *47*, 1887-1889.
22. Bigi, M.A.; Liu, P.; Zou, L.; Houk, K.N.; White, M.C. *Synlett* **2012**, *23*, 2768-2772.
23. Chen, K.; Costas, M.; Que, L. Jr. *J. Chem. Soc., Dalton Trans.* **2002**, 672-679.
24. Chen, K.; Costas, M.; Kim, J.; Tipton, A.K.; Que, L. Jr. *J. Am. Chem. Soc.* **2002**, *124*, 3026-3035.
25. Costas, M.; Que, L. Jr. *Angew. Chem. Int. Ed*. **2002**, *41*, 2179-2181.
26. Mas-Ballesté, R.; Costas, M.; van den Berg. T.; Que, L. Jr. *Chem. Eur. J.* **2006**, *12*, 7489-7500.

27. Klopstra, M.; Roelfes, G.; Hage, R.; Kellogg, R.M.; Feringa, B.L. *Eur. J. Inorg. Chem.* **2004**, 846-856.
28. Company, A.; Gómez, L.; Fontrodona, X.; Ribas, X.; Costas, M. *Chem. Eur. J.* **2008**, *14*, 5727-5731.
29. Bukowski, M.R.; Comba, P.; Lienke, A.; Limberg, C.; Lopez de Laorden, C.; Mas-Ballesté, R.; Merz, M.; Que, L. Jr. *Angew. Chem. Int. Ed*. **2006**, *45*, 3446, 3449.
30. Schröder, K.; Tong, X.; Bitterlich, B.; Tse, M.K.; Gelalcha, F.G.; Brückner, A.; Beller, M. *Tetrahedron Letters* **2007**, *48*, 6339-6342.
31. Schröder, K.; Enthaler, S.; Bitterlich, B.; Schulz, T.; Spannenberg, A.; Tse, M.K.; Junge, K.; Beller, M. *Chem. Eur. J.* **2009**, *15*, 5471-5481.
32. White, M.C.; Doyle, A.G.; Jacobsen, E.N. *J. Am. Chem. Soc.* **2001**, *123*, 7194-7195.
33. Ryu, J.Y.; Kim, J.; Costas, M.; Chen, K.; Nam, W.; Que, L. Jr. *Chem. Commun.* **2002**, 1288-1289.
34. Fujita, M.; Que, L. Jr. *Adv. Synth. Catal.* **2004**, *346*, 190-194.
35. Mas-Ballesté, R.; Que, L. Jr. *J. Am. Chem. Soc.* **2007**, *129*, 15964-15972.
36. Feng, Y.; Ke, C-Y.; Xue, G.; Que, L. Jr. *Chem. Commun.* **2009**, 50-52.
37. Gosiewska, S.; Cornelissen, J.J.L.M.; Lutz, M.; Spek, A.L.; van Koten, G.; Klein Gebbink, R.J.M. *Inorg. Chem.* **2006**, *45*, 4214-4227.
38. Gosiewska, S.; Lutz, M.; Spek, A.L.; Klein Gebbink, R.J.M. *Inorg. Chim. Acta* **2007**, *360*, 406-417.
39. Beck, A.; Weibert, B.; Burzlaff, N. *Eur. J. Inorg. Chem.* **2001**, 521-527.
40. Beck, A.; Barth, A.; Hübner, E. Burzlaff, N. *Inorg. Chem*. **2003**, *42*, 7182-7188.
41. Oldenburg, P.D.; Shteinman, A.S.; Que, L. Jr. *J. Am. Chem. Soc.* **2005**, *127*, 15672-15673.
42. Friese, S.J.; Kucera, B.E.; Que, L. Jr.; Tolman, W.B. *Inorg. Chem.* **2006**, *45*, 8003-8005.
43. Oldenburg, P.D.; Ke, C.Y.; Tipton, A.A.; Shteinman, A.A.; Que, L. Jr. *Angew. Chem. Int. Ed.* **2006**, *45*, 7975-7978.
44. Bruijnincx, P.C.A.; Lutz, M.; Spek, A.L.; van Faassen, E.E.; Weckhuysen, B.M.; van Koten, G.; Klein Gebbink, R.J.M. *Eur. J. Inorg. Chem*. **2005**, 779-787.
45. Peters, L.; Hübner, E.; Burzlaff, N. *J. Organometallic Chem.* **2005**, *690*, 2009-2016.
46. Bruijnincx, P.C.A.; Buurmans, I.L.C.; Gosiewska, S.; Moelands, M.A.H.; Lutz, M.; Spek, A.L.; van Koten, G.; Klein Gebbink, R.J.M. *Chem. Eur. J.* **2008**, *14*, 1228-1237.
47. Srinivasan, K.; Michaud, P.; Kochi, J.K. *J. Am. Chem. Soc.* **1986**, *108*, 2309-2320.
48. Zhang, W.; Loebach, J.L.; Wilson, S.R.; Jacobsen, E.N. *J. Am. Chem. Soc.* **1990**, *112*, 2801-2803.
49. Irie, R.; Noda, K.; Ito, Y.; Matsumoto, N.; Katsuki, T. *Tetrahedron Lett.* **1990**, *31*, 7345-7348.
50. Zang, W.; Jacobsen, E.N. *J. Org. Chem*. **1991**, *56*, 2296-2298.
51. Jacobsen, E.N.; Zhang, W.; Muci, A.R.; Ecker, J.R.; Deng, L. *J. Am. Chem. Soc*. **1991**, *113*, 7063-7064.
52. Brandes, B.D.; Jacobsen, E.N. *J. Org. Chem*. **1994**, *59*, 4378-4380.
53. Available at Sigma Aldrich, **(*R,R*)-Jacobsen's catalyst,** CAS Number 138124-32-0, **(*S,S*)-Jacobsen's catalyst,** CAS Number 135620-04-1.
54. Schwenkreis, T.; Berkessel, A. *Tetrahedron Letters* **1993**, *34*, 4785-4788.
55. Berkessel, A.; Frauenkron, M.; Schwenkreis, T.; Steinmetz, A.; Baum, G.; Fenske, D. *Journal of Molecular Catalysis A: Chemical* **1996**, *113*, 321-342.
56. Berkessel, A.; Frauenkron, M.; Schwenkreis, T.; Steinmetz, A. *Journal of Molecular Catalysis A: Chemical* **1997**, *117*, 339-346.
57. Pietikäinen, P. Tetrahedron Letters, 1994, 35, 941-944.
58. Pietikäinen, P. Tetrahedron 1998, 54, 4319-4326.
59. Murphy, A.; Dubois, G.; Stack, T.D.P *J. Am. Chem. Soc.* **2003**, *125*, 5250-5251.
60. Murphy, A.; Pace, A.; Stack, T.D.P. *Organic Letters*, **2004**, *6*, 3119-3122.

61. Murphy, A.; Stack, T.D.P. *Journal of molecular Catalysis A: Chemical* **2006**. *251*, 78-88.
62. Gómez, L.; Garcia-Bosch, I.; Company, A.; Sala, X.; Fontrodona,X.; Ribas, X.; Costas, M. *Dalton Trans.* **2007**, 5539-5545.
63. Wu, M.; Wang, B.; Wang, S.; Xia, C.; Sun, W. *Organic Letters* **2009**, *11*, 3622-3625.
64. Ottenbacher, R.V.; Bryliakov, K.P.; Talsi, E.P. *Adv. Synth. Catal*. **2011**, *353*, 885-889.
65. a) Chen, M.S.; White, M.C. *Science* **2007**, *318*, 783-787; b) Chen, M.S.; White, M.C. *Science* **2010**, *327*, 566-571.
66. Lyakin, O.Y.; Ottenbacher, R.V.; Bryliakov, K.P.; Talsi, E.P. *ACS Catal.* **2012**, *2*, 1196-1202.
67. Garcia-Bosch, I.; Gómez, L.; Polo, A.; Ribas, X.; Costas, M. *Adv. Synth. Catal.* **2012**. *354*, 65-70.
68. Wang, B.; Miao, C.; Wang, S.; Xia, C.; Sun, W. *Chem. Eur. J.* **2012**, *18*, 6750-6753.
69. Brinksma, J.; Schmieder, L.; van Vliet, G.; Boaron, R.; Hage, R.; de Vos, D.E.; Alsters, P.L.; Feringa, B.L. *Tetrahedron Letters* **2002**, *43*, 2619-2622.
70. de Boer, J.W.; Brinksma, J.; Browne, W.R.; Meetsma, A.; Alsters, P.L.; Hage, R.; Feringa, B.L. *J. Am. Chem. Soc.* **2005,** *127*, 7990-7991.
71. de Boer, J.W.; Browne, W.R.; Brinksma, J.; Alsters, P.L.; Hage, R.; Feringa, B.L. *Inorg. Chem*. **2007**, *46*, 6353-6372.
72. de Boer, J.W.; Browne, W.R.; Harutyunyan, S.R.; Bini, L.; Tiemersma-Wegman, T.D.; Alsters, P.L.; Hage, R.; Feringa, B.L. *Chem. Commun*. **2008**, 3747-3749.
73. Bolm. C.; Kadereit, D. Valacchi, M. *Synlett* **1997**, 687-689.
74. Bolm, C.; Meyer, N.; Raabe, G.; Weyhermüller, T.; Bothe, E. *Chem. Commun*. **2000**, 2435-2436.
75. Romakh, V.B.; Therrien, B.; Süss-Fink, G.; Shul'pin, G.B. *Inorg. Chem.* **2007**, *46*, 1315-1331.
76. De Vos. D.E.; Bein, T. *Chem. Commun*. **1996**, 917-918.
77. De Vos. D.E.; Sels, B.F.; Reynaers, M.; Rao, Y.V.S.; Jacobs, P.A. *Tetrahedron Letters* **1998**, *39*, 3221-3224.
78. De Vos. D.E.; Bein, T. *J. Organometallic Chem.* **1996**, *520*, 195-200.
79. Garcia-Bosch, I.; Company, A.; Fontrodona, X.; Ribas, X.; Costas, M. *Organic Letters* **2008**, *10*, 2095-2098.
80. Garcia-Bosch, I.; Ribas, A.; Costas, M. *Adv. Synth. Catal.* **2009**, *351*, 348-352.

2

Proline-based Mn(II)-complexes derived from the Py(ProMe)$_2$ and Py(ProOH)$_2$ ligands as alkene epoxidation catalyst with H_2O_2

The synthesis and analysis of two chiral manganese(II) triflate complexes, [Mn(OTf)$_2$(**Py(ProMe)$_2$**)] (**4**) and [Mn(OTf)$_2$(**Py(ProOH)$_2$**)] (**5**), derived from the earlier reported **Py(ProMe)$_2$** (**1**) and **Py(ProOH)$_2$** (**2**) ligands, that combine a pyridine backbone with two proline-derived substituents, is described. From the X-ray crystal structures, the two manganese complexes were found to contain seven coordinated Mn-centers, respectively, with distorted pentagonal bipyramidal geometries. The organic ligands coordinate in the meridional plane around Mn via the pyridine group, the proline nitrogen atoms, and furthermore via the additional coordination of the oxygen atoms of the proline side chains. The two triflate counter ions coordinate in the axial positions around the manganese center. The complexes were tested as oxidation catalysts in the epoxidation of different (pro-chiral) alkene substrates. Optimized reaction conditions for these complexes are: acetone as the solvent, hydrogen peroxide as oxidant, and the addition of several equivalents of 4-methylimidazole as an additive. The complexes are active in the epoxidation of various substrates. In the epoxidation of cyclooctene TON's up to 94 and substrate conversions up to 45% were obtained. The complexes were less suitable for linear terminal alkenes like 1-octene or 1-decene. Furthermore, these manganese complexes are part of a small number of manganese(II) compounds able to perform the enantioselective epoxidation of alkenes using hydrogen peroxide as the oxidant. With the pro-chiral substrate trans-beta-methylstyrene, ee's up to 35% were reached in the first screenings.

2.1 Introduction

The selective oxidation of alkanes and alkenes using environmentally friendly oxidants such as O_2 and H_2O_2 is an important research topic in synthetic chemistry.[1,2] In the search for new catalysts for these transformations, biological systems play an important inspirational role.[3] Many synthetic complexes under investigation as oxidation catalyst are at the same time models of the actives sites of metallo-enzymes that are capable of the activation of dioxygen to oxidize organic substrates.[4]

In literature manganese-based complexes derived from polydentate nitrogen and oxygen ligands have been reported to be capable of (enantioselective) oxidizing olefins to epoxides (Figure 1). For the epoxidation different kinds of oxidants are used and reported in the literature, for instance peracetic acid, iodosylbenzene, bleach and hydrogen peroxide. For now I will manly focus on the more environmentally friendly oxidant hydrogen peroxide, which is also the oxidant of choose for the catalytic studies. One of the best-known epoxidation catalyst is the Mn-salen system reported by Jacobsen and co-workers.[5] This system is able to epoxidize a wide variety of substrates in an enantioselective manner with excellent ee values above 90%. Both Pietikainen[6-8] and Katsuki[9] reported on the use of Mn-salen ligand in combination with hydrogen peroxide for the epoxidation of alkenes. They both reported on the use of additives during the catalytic reactions. The groups of Berkessel[10-12] and Katzuki[13] both reported on the synthesis and epoxidation of mixed salen-imidazole based ligand systems. In these systems the required additive (imidazole) was already covalently bound to the ligand. The salen ligands were mixed N,O donor ligands, nowadays much of the developed ligands systems are all N-based donors.

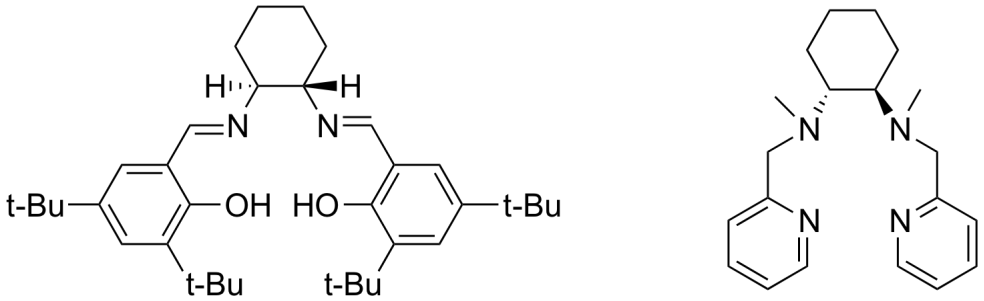

Figure 1. Structures of the salen (left) and BPMCB (right) ligands used in enantioselective Mn-catalyzed olefin epoxidations.

The group of Costas reported on two all N-based ligands which use hydrogen peroxide as oxidant in combination with acetic acid as additive.[14] Both [Mn^{II}(^{H,me}PyTACN)$(OTf)_2$] and [Mn^{II}(BPMCN)$(OTf)_2$] showed good reactivities for a wide range of substrates and high epoxide yields up to 97% were obtained. Bolm and co-workers prepared chiral derived TACN ligands and obtained low to moderate

enantioselectivities in the epoxidation reactions with hydrogen peroxide.[15,16] Costas *et al.* reported on the use of a new ligand MCPP derived from the BPMCN ligand (MCPP = *N*,*N*'-dimethyl-*N*,*N*'-bis(4,5-pineno-2-picolyl)cyclohexane-1,2-diamine), in which a pinene ring is attached to the 4 and 5 position of the pyridine group of the BPMCN ligand.[17] The corresponding Mn-complex showed to be active in the enantioselective epoxidation of various substrates (*e.g. trans*-beta-methylstyrene and styrene) with ee values up to 46%, but again the drawback of this system is the use of peracetic acid as oxidant. Sun *et al.* reported on a series of Mn-complexes that use hydrogen peroxide in combination with acetic acid for the enantioselective epoxidation of alkenes.[18] These complexes were shown to be active in the epoxidation of styrene and enantioselectivities up to 46% were obtained. The employed ligands are derived from the MCP ligand system reported by Stack (MCP = *N*,*N*'-dimethyl-*N*,*N*'-bis(2-pyridylmethyl)cyclohexane-*trans*-1,2-diamine).[19] Stack also used peracetic acid for his catalytic reactions. More recently, Sun *et al.* reported on the use of C_1-symmetric ligands in the epoxidation of chalcones, where they reached an enantioselectivity of up to 95%.[20] Bryliakov *et al.* reported on a manganese aminopyridine complex that catalyzes the enantioselective epoxidation of alkenes with a nearly stoichiometric amount of hydrogen peroxide in combination with an acid as additive.[21] These aminopyridine complexes turned out to be active in the epoxidation of certain pro-chiral substrates and high ee's up to 84% were obtained for electron-deficient substrates, but more moderate ee's were obtained with other substrates such as styrene (39% ee). The catalytic reactions were performed at –30 °C, using 1.3 equivalents of hydrogen peroxide. The group of Costas also reported recently on Mn-catalyst derived from a new bipyrrolidine type ligand which had a high efficiency (up to 1000 turnovers) but moderate enantioselectivities for the epoxidation of various olefins (between 30-60% ee for most substrates).[22] Reviews by Burgess,[23] Watkinson[24] and the more recent one from Bryliakov and Talsi[25] summarize the advances in manganese-based epoxidation catalysis using hydrogen peroxide as oxidant. As summarized above the amount of good enantioselective epoxidation catalyst with manganese is still limited, so this means that there is room for further development of new type of ligand systems.

Our efforts in the field of non-heme oxidation catalyst have focused on the development of non-heme iron oxidation catalysts.[26-30] Amongst other approaches, substituted pyridine-based ligand systems were used in the search for new chiral ligands. Previously, we have reported on the synthesis of iron(II) complexes derived from the chiral ligands **Py(ProMe)$_2$** (**1**, 2,6-bis[[(S)-2-(methyloxycarbonyl)-1-pyrrolidinyl]methyl]pyridine), **Py(ProOH)$_2$** (**2**, 2,6-bis[[(S)-2-(hydroxymethyl)-1-pyrrolidinyl]methyl]pyridine), and **Py(ProPh$_2$OH)$_2$** (**3**, 2,6-bis[[(S)-2-(diphenylhydroxymethyl)-1-pyrrolidinyl]methyl]pyridine) based on pyridyl and proline building blocks (Figure 2). The **Py(ProMe)$_2$** ligand was found to coordinate in

a κ^3-meridonal *NN'N* fashion towards $FeCl_2$.[26] In the presence of a weakly coordinating anion this same ligand acts as a pentadentate ligand with the additional coordination of the two oxygen atoms of the proline-based substituents, forming iron(II) complexes with a seven coordinated, pentagonal bipyramidal geometry. Ligands **2** and **3** form cationic octahedral complexes with $FeCl_2$ and $Fe(OTf)_2 \cdot 2MeCN$ and adopt a pentadentate coordination mode.[27] These complexes were tested in the oxidation of both alkanes and alkenes. The iron(II) triflate complex derived from **1** showed 4.2-9.4 turnovers within 1 hour and a high productive consumption of TBHP (42-94%) in the oxidation of non-activated alkanes to yield alcohols and ketones. The iron(II) complexes derived from ligands **2** and **3** were tested in the epoxidation of alkene substrates using hydrogen peroxide. The iron chloride and triflate complexes derived from **3** proved to be the most active, although rather low conversions into epoxides were obtained (7-25%). The latter complexes were also tested in the oxidation of sulfides, where especially the chloride complex showed to be highly active; yields up to 90% were obtained, albeit with rather low ee value's (up to 27%).[27]

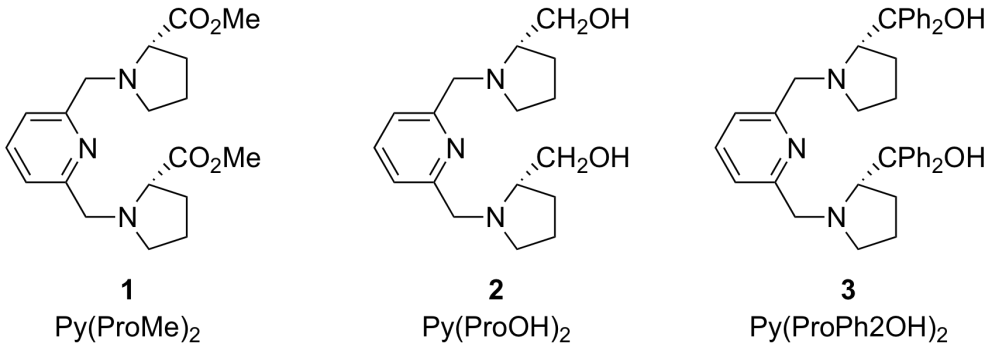

Figure 2. Proline based ligands 1-3.

Here, we report on an extension of this work through a study of the manganese chemistry of ligands **1** and **2**. The synthesis and characterization of $Mn(OTf)_2$ complexes is reported and the catalytic potential of the complexes was investigated in the epoxidation of various (pro-chiral) alkenes with H_2O_2 as oxidant.

2.2 Results

2.2.1 Synthesis

The manganese complexes **4** and **5** were synthesized by mixing equimolar amounts of the ligands **1** or **2** and $Mn(OTf)_2 \cdot 2MeCN$ in acetonitrile (Scheme 1). The resulting complexes were isolated as white and light brown powders in 74 and 72% yield, respectively, by precipitation with Et_2O. The paramagnetic complexes **4** and **5** appeared to be relatively stable towards O_2 and moisture, but were kept under an inert nitrogen atmosphere when stored for longer periods. These complexes were

characterized by a variety of techniques including single crystal X-ray structure determination, IR spectroscopy and elemental analysis. Crystals of complexes **4** and **5** suitable for X-ray diffraction were obtained by slow vapor diffusion of diethyl ether into a solution of the corresponding complex in acetonitrile.

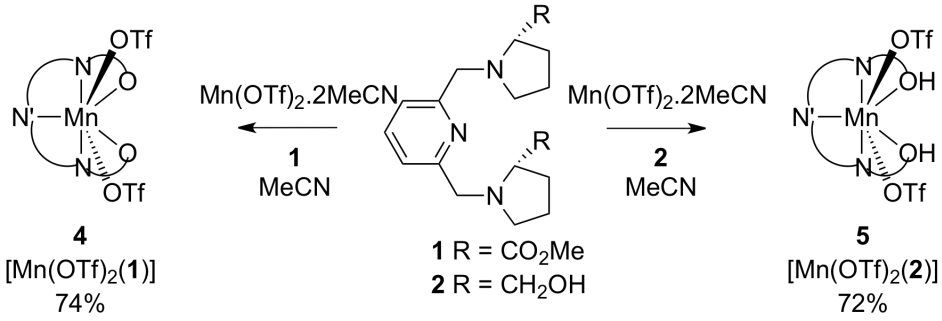

Scheme 1. Synthesis of manganese(II) complexes **4** and **5**.

2.2.2 Structural features of complexes 4 and 5 in the solid state

[Mn(OTf)$_2$(Py(ProMe)$_2$)] (4) The reaction between **1** and Mn(OTf)$_2$·2MeCN gave complex **4** with a sevenfold-coordination geometry around the manganese(II) ion, which can be best described as distorted pentagonal bipyramidal (pbp, Figure 3). The manganese center is in the equatorial plain surrounded by the three nitrogen atoms of the ligand as well as the two oxygen atoms of the carbonyl groups from the ester moieties. The two axial positions are occupied by two monodentate, κ^1-O bound triflate counter anions. Selected bond lengths and angles are listed in Table 1.

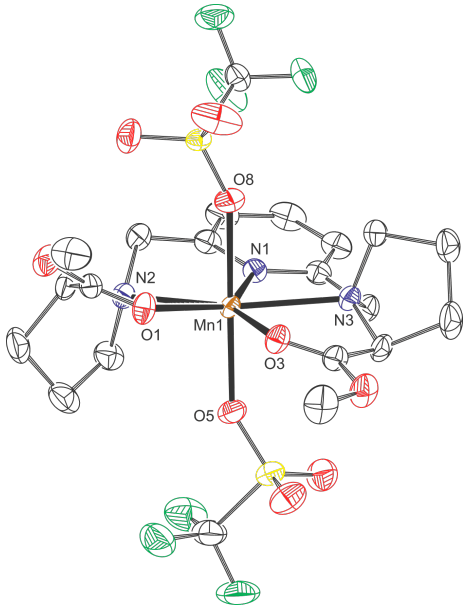

Figure 3. Molecular structure of complex **4** in the crystal. Displacement ellipsoid plot (50% probability); hydrogen atoms are omitted for clarity.

Table 1. Selected bond lengths (Å) and angles (°) for [Mn)OTf)$_2$(**1**)] (**4**).

	Bond length		Angle
Mn1-N1	2.2124(14)	N1-Mn1-N2	70.60(5)
Mn1-N2	2.5335(15)	N1-Mn1-N3	72.52(5)
Mn1-N3	2.3974(13)	N2-Mn1-N3	142.99(5)
Mn1-O1	2.1760(12)	N2-Mn1-O1	70.24(5)
Mn1-O3	2.2636(12)	N3-Mn1-O3	69.89(5)
Mn1-O5	2.1750(12)	O1-Mn1-O3	78.50(5)
Mn1-O8	2.2238(14)	O5-Mn1-O8	178.36(6)

The crystal structure of **4** is isostructural with the corresponding iron complex [Fe(OTf)$_2$(**Py(ProMe)$_2$**)], leading to very similar geometries.[26] The metal ion is on a general crystallographic position and the overall complex has consequently only C_1 symmetry. The equatorial plane is essentially planar with a maximum deviation of 0.2495(14) Å from the least-squares plane. The *cis*-angles at the Mn center vary between 69.89(5) and 78.50(5)º. The *trans*-angle of the triflate oxygen atoms of 178.36(6)º is almost ideal. The geometry of the complex is best described as slightly distorted pentagonal bipyramid. The Mn-N(Pyr) distance is significantly shorter then the Mn-N(Pro) distance, Mn-N(Pyr) = 2.2124(14) Å compared to Mn-N(Pro) = 2.5335(15) Å and 2.3974(13) Å. The Mn-N(2) distance is considerably longer then the Mn-N(3) distance, which is accompanied by the shorter Mn-O(1) bond compared to Mn-O(3).

[Mn(OTf)$_2$(Py(ProOH)$_2$)] (5) The reaction between **2** and Mn(OTf)$_2$·2MeCN gives complex **5** with the same seven coordinated geometry around manganese as complex **4**, a distorted pentagonal bipyramid (pbp, Figure 4). Selected bond lengths and angles in **5** are listed in Table 2. According to these values there is a slight distortion from a pentagonal bipyramidal geometry: the distortion is even smaller than in the case of complex **4**. Accordingly, the coordination polyhedron of **5** is nearly ideal with an r.m.s. deviation of 0.062 Å from C_2 symmetry.[31]

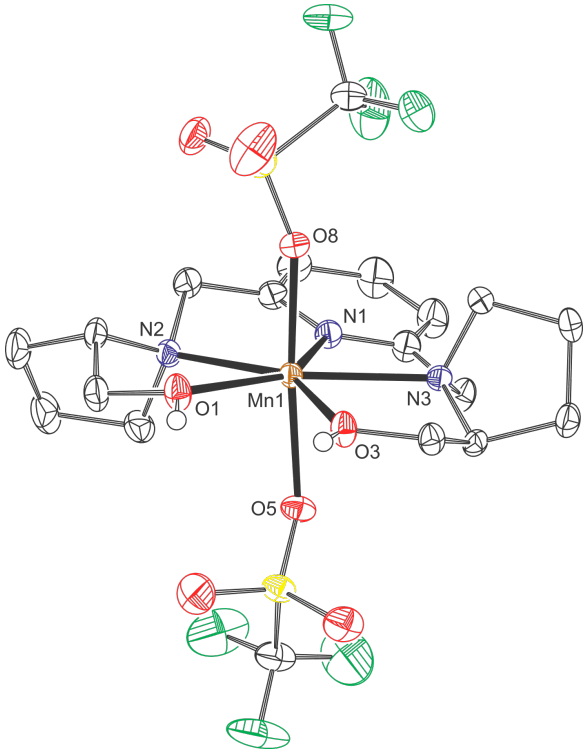

Figure 4. Molecular structure of complex **5** in the crystal. Displacement ellipsoid plot (50% probability); C-H hydrogen atoms are omitted for clarity.

Table 2. Selected bond lengths (Å) and angles (°) for [Mn(OTf)$_2$(**2**)] (**5**).

	Bond length		Angle
Mn1-N1	2.2430(13)	N1-Mn1-N2	70.63(5)
Mn1-N2	2.3835(14)	N1-Mn1-N3	71.39(5)
Mn1-N3	2.3753(14)	N2-Mn1-N3	141.82(5)
Mn1-O1	2.2517(12)	N2-Mn1-O1	71.34(5)
Mn1-O3	2.2431(12)	N3-Mn1-O3	70.86(5)
Mn1-O5	2.2563(12)	O1-Mn1-O3	76.33(5)
Mn1-O8	2.1846(12)	O5-Mn1-O8	175.53(5)

The Mn-N(2) and Mn-N(3) bond lengths are almost equal (2.3835(14) Å and 2.3753(14) Å) and the same accounts for bond lengths Mn-O(1) and Mn-O(3) (2.2517(12) Å and 2.2431(12) Å). The angles around manganese of the five equatorial donor atoms deviate from the ideal value of 72°, having a slightly smaller (70.63(5)°, 71.39(5)°, 71.34(5)° and 70.86(5)°) or higher value (76.33(5)°). The sum of all *cis*-angles around manganese in this complex is 360.55(11)°, which is approximately planar. The *trans*-angle O(3)-Mn-O(6) of 175.53(5)° is again very close to linear.

In the crystal, the molecules of **5** form hydrogen bonded dimers. The coordinated hydroxyl groups act as hydrogen bond donors and the non-coordinated triflate oxygen atoms as acceptors (Figure 5). The dimer is located on a twofold axis (*a,b*-diagonal).

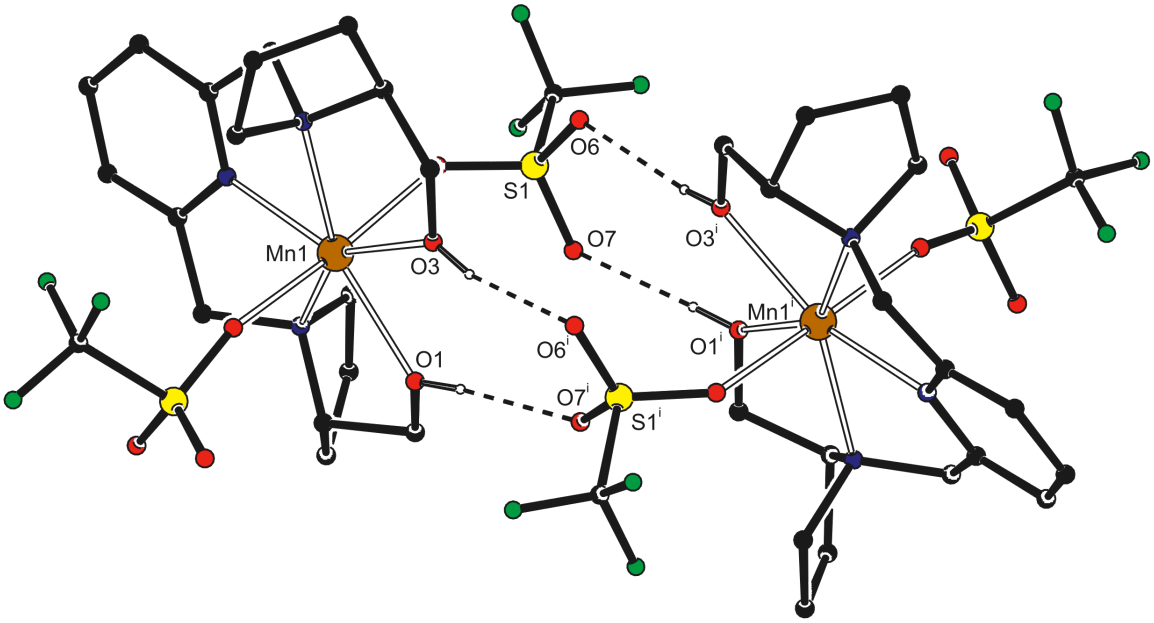

Figure 5. Hydrogen bonded dimer in the crystal structure of **5**. View along the *a*-axis. C-H hydrogen atoms are omitted for clarity. Symmetry operation *i*: y, x, -z.

2.2.3 Solid state and solution IR

For paramagnetic complexes IR spectroscopy is a suitable technique to study the coordination of the ligands around the metal center. Typically the vibration bands of the triflate groups and the carbonyl groups allow for an assignment of these groupings being coordinated or not to the metal. IR spectra of complex [Mn(OTf)$_2$(**1**)] (**4**) were recorded both in the solid state and in solution. The solid-state spectrum shows a clear vibration band of a coordinated carbonyl group at 1686 cm^{-1} (Figure 6a). The frequency of the carbonyl vibration in the free ligand is 1731 cm^{-1}. The symmetric and asymmetric vibrations of the triflate CF_3 and SO_3 groups in **4** are found at 1303 and 1234 (ν_{as} SO_3), 1221 (ν_s CF_3), 1159 (ν_{as} CF_3) and 1031 (ν_s SO_3) cm^{-1}. The double degenerated asymmetric SO_3 mode can be assigned to two components resulting from triflate anion coordination.[32]

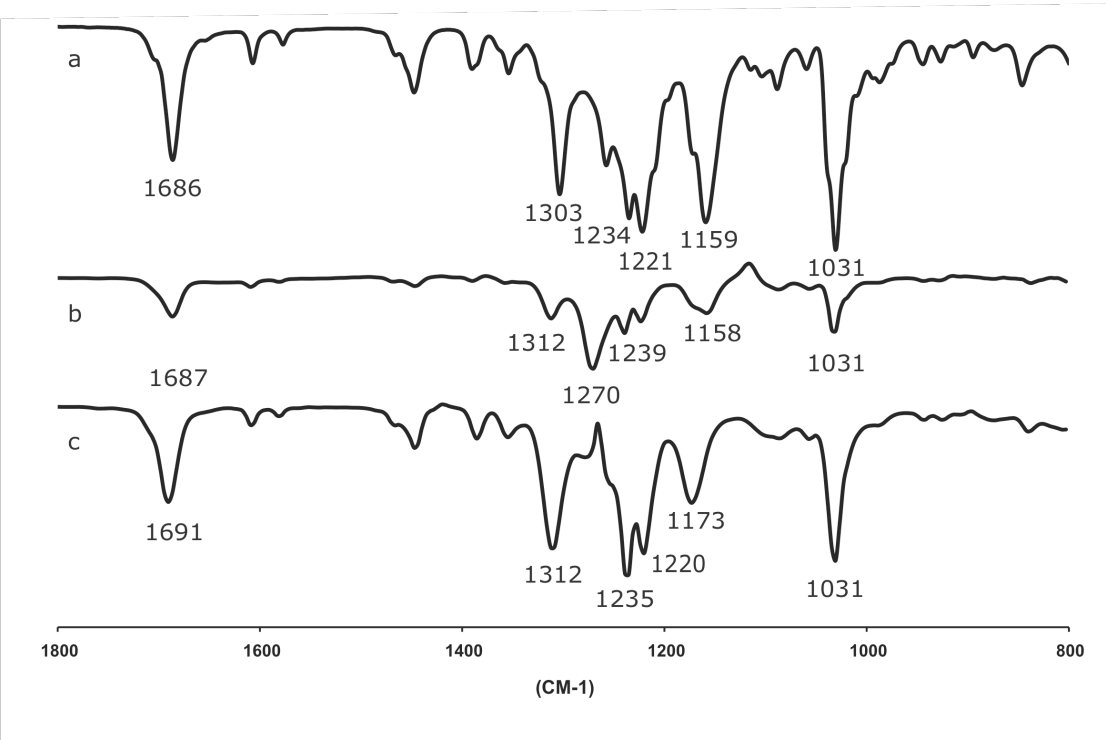

Figure 6. Solid state and solution IR spectra of complex **4**; a) solid, b) MeCN and c) CH_2Cl_2.

The solution IR spectra of complex **4** in MeCN (a coordinating solvent) or CH_2Cl_2 (a non-coordinating solvent) show clear differences with respect to the solid-state spectrum (Figure 6). It was known from earlier studies on the corresponding iron complexes, that depending on the solvent some donor groups of the complex stay coordinated to the metal, while other groups are displaced by coordinating solvent molecules.[19] The carbonyl regions of the solution spectra (MeCN 1687 cm^{-1} and CH_2Cl_2 1691 cm^{-1}) are similar to this region in the solid state spectrum (1686 cm^{-1}). The triflate region on the other hand shows clear differences. In MeCN, the double degenerated signal of the asymmetric SO_3 mode is replaced by a single signal at 1270 cm^{-1}, which indicates the presence of non-coordinated triflate anions[33] (Figure 6b). In CH_2Cl_2, the vibrations are comparable to those in the solid state (1312 and 1235 (ν_{as} SO_3), 1220 (ν_s CF_3), 1173 (ν_{as} CF_3) and 1031 (ν_s SO_3) cm^{-1}), which corresponds to coordinated triflate anions (Figure 6c).

Based on these IR spectra, the coordination of the carbonyl groups in **4** as observed in the solid state is retained in both solvents. However, upon dissolution of **4** in MeCN the triflate groups are no longer coordinated to the metal and are most likely replaced by solvent molecules. In a non-coordinating solvent like CH_2Cl_2 the triflate groups remain coordinated to manganese. A summary of the structures in the solid state and solution is depicted in Scheme 2.

Complex **5** showed a comparable solid-state spectrum as complex **4**, with the coordination of the triflate anions. The corresponding iron complex prepared from ligand (**Py(ProOH)$_2$**), showed in previous studies the same coordination behavior in solution as observed for complex **4**.[27] The coordination of the triflate anions groups in a non-coordinating solvent and the replacement of the triflate groups in a coordinating solvent. Based on these data it is assumed that complex **5** also gives the same coordination behavior in solution as observed for complex **4**.

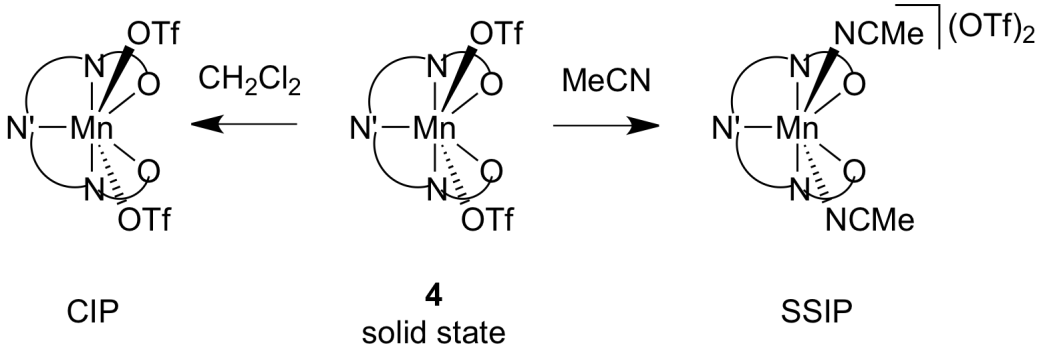

Scheme 2. Summary of the structures in solution of complex **4**, CIP = contact ion pair and SSIP = solvent separated ion pair.

2.2.4 Magnetic susceptibility measurements

The magnetic moments of the manganese(II) bis(triflate) complexes **4** and **5** were determined in acetone at 298 K using Evans' NMR method.[34,35] As expected from the weak ligand field exerted by the triflate anions and by possible axially ligated acetone molecules, acetone solutions of both complexes **4** and **5** showed magnetic moments consistent with high spin manganese(II) (S = 5/2) centers. The obtained μ_{eff} values for complexes **4** and **5** are 5.55 μ_β and 5.71 μ_β, respectively.

2.2.5 ^{19}F NMR Spectroscopy

The ^{19}F chemical shift of the fluorine atoms in triflate anions is dependent on the type of metal center these are associated with. For diamagnetic metal centers there is no difference whether the triflate groups are bound to the metal center or whether they exist as non-coordinating anions.[36] On the other hand triflate coordination to a paramagnetic metal center results in a large change of the resonance frequency of the ^{19}F nucleus.[36] As a result, the ^{19}F NMR spectra of paramagnetic complexes provide a good indication whether the triflate anions function as bridging ligands (ca. +60 ppm), as terminal ligands (ca. –10 ppm) or as counter ions (ca. –80 ppm).[37,38] ^{19}F NMR spectra of complexes **4** and **5** were recorded in acetone and MeCN at RT. The results obtained from these measurements are summarized in Table 3. At ambient temperature, a MeCN solution of complex **4** did not show a ^{19}F-NMR signal. For complex **5** on the other hand a single broad resonance was observed around –70.8

ppm, which corresponds to non-coordinated triflate counter ions. As observed by IR for complex **4**, acetonitrile molecules displace the axial triflates in solution. Lowering the temperature to –40 °C did not result in an observable signal in the case of **4**. However, when 4-methylimidazole (used during catalysis as additive, *vide infra*) was added to the solution of **4**, a fluorine signal was observed at –78.7 ppm, corresponding to non-coordinated triflate ions. When 4-methylimidazole was added to the solution of complex **5** in MeCN a sharp peak was observed at –79.1 ppm. No fluorine signals were detected for acetone solutions of either complex. When 4-methylimidazole was added a fluorine signal was observed at –78.2 ppm for both complexes.

Table 3. Result of ^{19}F NMR measurements of complexes **4** and **5**.

Solvent	**4** (ppm)	**5** (ppm)
MeCN	-	–70.8
MeCN with 4-methylimidazole	–78.7	–79.1
Acetone	-	-
Acetone with 4-methylimidazole	–78.2	–78.2

2.3 Olefin epoxidation

Manganese(II) complexes **4** and **5** were investigated as catalyst for the epoxidation of alkenes. In the catalytic studies, the ratio between catalyst, oxidant, and substrate was varied between substrate and oxidant limiting conditions. Reactions were carried out at ambient temperature in either acetonitrile or acetone. In all cases H_2O_2 was added over the first 30 minutes of reaction, after which the reaction was allowed to proceed for 3 to 24 hours (Scheme 3).

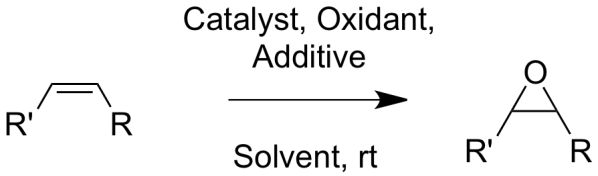

Scheme 3. General scheme of epoxidation catalysis.

In an initial reaction screening in which cyclooctene was used as the benchmark alkene substrate in combination with complex **5**, the conditions applied earlier for the corresponding iron complexes,[27] *i.e.* a ratio between catalyst, oxidant, and substrate of 1:10:500 was used in acetonitrile. This showed that H_2O_2 was not effective as oxidant under these conditions.[39] Using a different catalyst/oxidant/substrate ratio of 1:500:1000 and H_2O_2 as oxidant in acetonitrile gave a disappointing turnover number (TON) of 4 per Mn-center after 3 h. In an attempt to increase the catalytic activity of complex **5**, the effect of different additives was investigated. The addition of

imidazoles to Mn-catalyst based on porphyrin[40-43] and salen[10,44] type ligands have been reported to result in an increased activity of the catalyst. In these cases, the imidazoles coordinate to the manganese center and act as an axial ligand. The effect of a series of imidazoles on the epoxidation activity of **5** towards cyclooctene using H_2O_2 in acetonitrile indeed turned out to be positive. The best imidazole of this series was also tested in reactions carried out in acetone; this turned out to be very beneficial and higher activities were obtained. The results of these initial screenings are detailed in Table 4.

Table 4. Initial screening of the epoxidation properties of complex **5** using different conditions and additives.[a]

	Ratio		TON Epoxide	
Entry	Cat./Oxi./Sub.	Additive (10 equiv.)	1 h	3 h
1	1:500:1000		1.1	4.0
2	1:500:400		1.9	3.0
3	1:500:1000	imidazole	4.5	9.9
4	1:500:1000	2-methylimidazole	1.7	3.0
5	1:500:1000	2-phenylimidazole	4.0	5.5
6	1:500:1000	4-phenylimidazole	8.6	10.1
7	1:500:1000	1-methylimidazole	8.8	9.8
8[b]	1:500:1000	4-methylimidazole	8.2	25.8
9[b]	1.:500:400	4-methylimidazole	12.2	36.9
10[b,c]	1:500:1000	4-methylimidazole	35.9	115.7
11[b,c]	1:500:400	4-methylimidazole	56.8	83.7

[a] Reaction conditions: 0.5 mL of 3.5 M H_2O_2 solution in acetonitrile (1.75 mmol, 500 equiv., diluted from 35% aqueous H_2O_2) was slowly added over 30 min to a stirred solution of 2.8 mL acetonitrile containing **5** (3.5 μmol), additive and cyclooctene at ambient temperature, stirring was continued for another 30 min; [b] some amount of cis-diol product was also observed; [c] reaction carried out in acetone.

Under oxidant limiting conditions and using 0.2 mol% **5** with respect to oxidant, 10 equivalents of 2-methylimidazole or 2-phenylimidazole showed hardly any effect on the catalytic activity of **5** (Table 4, entries 4 and 5). This may be the result of a diminished coordination strength of 2-substituted imidazoles. On the other hand, imidazole, 4-phenylimidazole and 1-methylimidazole did show some increase in activity of **5** (entries 3, 6 and 7). In particular the addition of 10 equiv. of 4-methylimidazole resulted in a considerable increase in activity: TON = 25.8 after 3 h (entry 8). Taking this observation as a lead, several other experiments were carried out with 4-methylimidazole. Changing to substrate limiting conditions (entry 9) resulted in a further activity increase, even though a mediocre TON of 36.9 was achieved after

3 h. Using acetone as the reaction solvent instead of acetonitrile resulted in a further considerable activity increase under both oxidant and substrate limiting conditions (entries 10 and 11). The TON went up to over 100 per Mn under oxidant limiting conditions.

In the reactions were 4-methylimidazole was used as additive the formation of small amounts of *cis*-cyclooctene diol was observed beside the formation of the cyclooctene oxide. The amounts of *cis*-diol product formed in acetonitrile accounted for 1.3 TON after 3 h. For reactions carried out in acetone higher amounts of *cis*-diol were formed. Under oxidant limiting conditions a TON of 7.6 towards the diol product was observed (entry 10), while under substrate limiting conditions a TON of 4.5 was obtained for the *cis*-diol (entry 11).

After these initial screening a series of catalytic experiments were carried out using other olefin substrates and applying both complex **5** as well as complex **4** (Table 5). The reactions were carried out in acetone with three different ratios between catalyst, oxidant and substrate, varying from oxidant limiting (ratio 1:500:1000) to substrate limiting (ratio 1:500:400 and 1:500:100). The oxidant, H_2O_2, was added drop wise over 30 minutes to minimize the chance of disproportionation. In these reactions, 5 equivalents of the 4-methylimidazole were added. The lower amount of imidazole additive then during the initial screening (10 equiv.) was used to prevent the possible formation of a manganese hexakis imidazole complex (*vide infra*).[45]

Complex **4** was tested in the oxidation of cyclooctene and styrene, while complex **5** was also tested in the epoxidation of the terminal linear alkenes 1-octene and 1-decene. The product formation during these reactions was determined after 1 and 3 hours from the start of the reaction and also after 1 night. With cyclooctene as a substrate complex **4** gave the highest initial conversions but after 1 night the highest TON are obtained with complex **5**. This reactivity trend was found not to change when changing the substrate loadings. The highest overall TON's were obtained with the highest substrate loading with both complexes (TON = 94 for **5**). The highest percentage of epoxide product formation was found with the lowest substrate loading, i.e. 45% for **5**.

Table 5. The epoxidation of different alkene substrates with complexes **4** and **5**.[a]

		TON[b]					
	Conditions	1 h		3 h		1 night	
Substrate	Cat./Oxi./Sub.	**4**	**5**	**4**	**5**	**4**	**5**
Cyclooctene[c]	1:500:1000	9.3	7.5	45.9	36.0	61.5	94.0
	1:500:400	12.9	7.6	42.5	30.7	68.3	80.9
	1:500:100	7.6	6.9	22.2	24.7	38.8	44.9
Styrene[d]	1:500:1000	14.5	12.1	34.8	34.8	55.5	58.8
	1:500:400	22.3	18.2	32.1	37.5	57.3	57.5
	1:500:100	12.1	14.3	15.3	31.1	37.0	54.3
1-octene	1:500:400		5.9		17.4		27.0
	1:500:100		3.0		6.6		12.5
1-decene	1:500:1000		4.2		10.9		16.3
	1:500:400		2.6		7.0		11.6
	1:500:100		1.2		2.7		4.6

[a] For reaction conditions see Table 4, all reactions carried out in acetone with the addition of 5 equiv. of 4-methylimidazole as additive; [b] moles of product/moles of catalyst; [c]small amount of *cis*-diol product formed; [d] some benzaldehyde formed.

In the case of styrene as a substrate the activity differences between the two complexes are much smaller. The highest epoxide product formation of 55% was again obtained with complex **5** using the lowest substrate loading. The highest TON for styrene is almost similar to this value, i.e. TON = 59 for **5** at high substrate loading. The ability of complex **5** to epoxidize longer linear alkene substrates is much lower compared to the other substrates, *i.e.* in the best case a TON of 27 was obtained with 1-octene after 1 night.

The formation of a small amount of *cis*-cyclooctene diol was also observed for both complexes in the case cyclooctene was used as a substrate. The highest amount of *cis*-diol was formed with the highest substrate loading, while at the lowest substrate loading almost no *cis*-diol was formed (not shown). The amount of diol varied between a TON of 0 to 5 depending on the complex and the amount of substrate used. In a separate reaction no diol products did form upon replacing the alkene substrate by the epoxide, which shows the stability of the epoxide under the applied reaction conditions and excludes a possible intermediate role of the epoxide in diol formation. When styrene was used as a substrate, minor amounts of benzaldehyde were formed in addition to the desired epoxide during the reaction. The amount of benzaldehyde formed amounted to 3.7 TON with complex **5** under the highest substrate loading.

The ability of complexes **4** and **5** to induce enantioselectivity in olefin epoxidation using hydrogen peroxide as oxidant was tested on *trans*-beta-methylstyrene (Scheme 4 and Table 6). The overall activity in *trans*-beta-methylstyrene epoxidation is somewhat lower than in the styrene epoxidation for both complexes **4** and **5**. The activities of these complexes are comparable after 1 night, while in this case complex **5** showed a higher initial product formation. The trend and magnitude in product enantioselectivity are very similar for **4** and **5**. In the best case, complex **4** gave an ee around 35-37%, with an epoxide product formation of almost 30%. These results were obtained with the lowest substrate loading. The obtained ee increases going from oxidant limiting conditions towards substrate limiting conditions. Ee's obtained after 1 hour are the same as those after 1 night, which indicates that most likely only one mechanism for epoxide formation is operative during the course of reaction. In these reactions small amounts of benzaldehyde were observed. These amounts hardly extended the amounts of benzaldehyde in blank reactions in the absence of complex **4** or **5**.

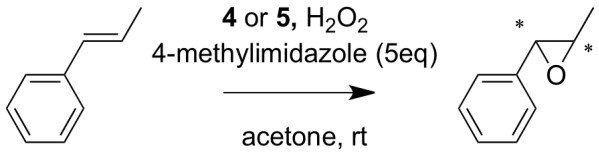

Scheme 4. The chiral epoxidation of *trans*-beta-methylstyrene with catalyst **4** and **5**.

Table 6. Result on the chiral epoxidation of *trans*-beta-methylstyrene with catalyst **4** and **5**.[a]

	Conditions	1 h		3 h		1 night	
	Cat./Oxi./Sub.	TON	ee (%)	TON	ee (%)	TON	ee (%)
4	1:500:1000	9.1	19	16.7	20	40.2	21
	1:500:400	12.7	23	15.8	29	37.3	28
	1:500:100	5.0	31	9.2	37	28.8	35
5	1:500:1000	24.9	18	31.6	18	39.8	18
	1:500:400	24.1	19	28.6	19	40.5	22
	1:500:100	15.2	27	15.1	31	31.4	28

[a] For reaction conditions see Table 4, all reactions carried out in acetone with the addition of 5 equiv. of 4-methylimidazole as additive.

2.4 Discussion

Two manganese complexes **4** and **5** were synthesized with a pentagonal bipyramidal geometry. Ligands **1** and **2** in these complexes coordinate in a meridional fashion around the manganese center and the two axial positions are occupied by two triflate counter ions. The same coordination behavior was observed earlier for the

corresponding iron complex [Fe(**Py(ProMe)$_2$**)(OTf)$_2$].[26] The two coordinating triflate groups in the axial positions turned out to be labile, depending on the solvent in which the complexes are dissolved in. With solution IR spectroscopy it turned out that a coordinating solvent like acetonitrile is able to displace the triflate groups, whereas the triflates stay in place in a non-coordinating solvent like dichloromethane. The presence of two labile sites is beneficially for the use of these complexes in catalysis as these give rise to two possible free coordination sites on the metal for oxidant, additive or substrate binding.

For the synthesis of the complexes manganese triflate was used as the manganese source. According to the literature report that describes the preparation of this versatile manganese salt, it is isolated as Mn(OTf)$_2$·MeCN[46] and it was indeed used like that. At a later stage it was possible to obtain the crystal structure of the as isolated manganese salt and found that it has a polymeric structure in the solid state with a repeating unit of Mn(OTf)$_2$·2MeCN (appendix 2),[47] *i.e.* it contains two acetonitrile molecules per manganese instead of one. The effect of this is that for the preparation of the complexes not an exact ligand to metal ratio of 1:1 was used, but that a slight excess of the ligand was used. All complexes used in catalysis experiments were crystallized prior to use, which removed the ligand excess.

Complexes **4** and **5** both turned out to catalyze the epoxidation of different types of alkene substrates with H_2O_2. The highest activities were found in the epoxidation of cyclooctene and styrene type of substrates, while complex **5** turned out to be less effective with terminal linear alkene substrates. Reactions in acetone were higher yielding then reactions in acetonitrile. With acetone as solvent the epoxidation reaction pathway is likely to follow a metal-based pathway and much less so via a radical mechanism due to the radical scavenger properties of acetone. Another benefit of acetone is that it forms 2-hydroxy-2-hydroperoxypropane with H_2O_2. This compound gradually releases H_2O_2 as the reaction proceeds, maintaining a constant low oxidant concentration.[48]

For each of the complexes the presence of 4-methylimidazole or another imidazole additive is pivotal for achieving appreciable catalytic turnovers. The imidazole additive will probably function as axial ligand to manganese or might act as an acid-base catalyst to favor the heterolytic cleavage of the hydrogen peroxide. The influence of imidazoles has already been reported for porphyrin and salen complexes, to obtain efficient alkene epoxidation.[10,40-44] Beller and co-workers also reported on the beneficial use of 4-methylimidazole as additive in oxidation catalysis.[49] Why 4-methylimidazole provides the highest catalytic activities amongst the imidazole type additives remains unclear for now; sterics are likely to play a role. During the catalytic reactions 5 equivalents of 4-methylimidazole were used and not the 10 equivalents

used during the preliminary screenings, in order to prevent the formation of a manganese hexakis imidazole complex.[45] On the other hand, the catalytic activity of complex **5** with the 10 equivalents of imidazole turned out to be higher then when 5 equivalents were added; TON's were 115.7 and 94.0, respectively. Further studies are required to optimize and rationalize the ideal amount and the role of the 4-methylimidazole additive.

Overall, catalyst **5** gave the highest absolute TON value of 115.7 in these studies in the epoxidation of cyclooctene. The highest epoxide product formation percentage (55%, based on the amount of added substrate) was obtained with complex **5** in the epoxidation of styrene using substrate-limiting conditions (ratio 1:500:100). With cyclooctene as the substrate also the formation of small amounts of the *cis*-diol product was observed under high substrate loadings. The formation of a *cis*-diol product is likely to require the presence of two vacant *cis*-sites on the metal center.[30] This would mean that the **Py(ProMe)$_2$** ligand would need to rearrange during the catalytic cycle or that next to the labile triflate groups one or more donor atoms need to detach from the manganese center in order to accommodate two vacant *cis*-sites on the metal center. The dissociation of the ester carbonyl groups was reported earlier in iron oxidation catalysis.[30]

Both complexes turned out to induce enantioselectivity in the epoxidation of a pro-chiral olefin with hydrogen peroxide, as was demonstrated in the epoxidation of *trans*-beta-methylstyrene. Complex **4** gave the highest enantioselectivity of 35% using a ratio between catalyst, oxidant and substrate of 1:500:100. The higher enantioselectivity of complex **4** compared to complex **5** may be explained by the presence of the more bulky methyl ester groups instead of the hydroxyl groups in the corresponding ligands. The enantioselectivity is constant during the course of the reaction for both complexes, which indicates that a single oxidation mechanism is responsible for product formation.
Recently a related manganese(II) complex was reported that was used as efficient MRI contrast agent for vascular imaging. This application could possibly be of interest for our complexes reported here.[50]

2.5 Concluding remarks

We have reported on the synthesis and characterization of two manganese complexes based on a pyridine bis-proline framework. The catalytic conditions for these complexes were optimized, further more a screening for a suitable additive was done. Both complexes were tested as oxidation catalyst in the (enantioselective) epoxidation of olefins. The obtained ee (35%) is still moderate compared to the previous mentioned salen complexes reported by Pietikäinen[6-8] and needs to be further optimized for practical use of the complexes. Nowadays even aminopyridine

complexes are reported that obtain much higher ee's, over 90%. These complexes are reported by Sun,[20] Costas[22] and Bryliakov[51] The results obtained so far will used in ongoing research in our group to further optimize these kind of systems to obtain higher enantioselectivities with the use of hydrogen peroxide as oxidant.

2.6 Experimental section

General: Reactions with metal salts were carried out under an atmosphere of dry, oxygen-free N_2 using standard Schlenk techniques. Solvents were dried and freshly distilled prior to use. **Py(ProMe)$_2$ (1)**[26], **Py(ProOH)$_2$ (2)**[27] and Mn(OTf)$_2$.2MeCN[46] were prepared according to previously published procedures. Optical rotations ($[\alpha]_D^{21}$) were measured with a Perkin polarimeter 241. Elemental microanalyses were carried out by Mikroanalytisches Laboratorium Dornis and Kolbe, Mülheim a.d. Ruhr, Germany. Infrared spectra were recorded on a Perkin-Elmer Spectrum One FT-IR instrument. Solution IR spectra were recorded with a Mettler Toledo ReactIR^{TM} 1000 spectrometer with a SiComp^{TM} probe which was fitted in a reaction vessel under N_2 atmosphere. Solution magnetic moments were determined by Evans' NMR method in acetone-d_6/cyclohexane at 25 °C.[34,35] Gas chromatography analyses were performed on a Perkin-Elmer Autosystem XL GC (30 m, PE-17 capillary column), a Perkin-Elmer Autosystem XL GC (25 m*0.22 mm, Lipodex_E) and a Perkin-Elmer Clarus 500 GC (30 m, Econo-Cap EC-5) all with FID detector.

[Mn(OTf)$_2$(Py(ProMe)$_2$)] (4): A slightly yellow/beige solution of Mn(OTf)$_2$·2MeCN (0.75 mmol, 327 mg) in acetonitrile (15 mL) was added to a slightly yellow/beige solution of **1** (0.83 mmol, 300 mg) dissolved in acetonitrile (15 mL). After addition no color change was visible. The reaction mixture was stirred for 3 h at ambient temperature, followed by evaporation of the solvent *in vacuo*. The remaining white/beige solid was dissolved in a minimal amount of dry acetonitrile and precipitated by addition of dry diethyl ether affording a white solid in 74% yield (440 mg). Crystals suitable for X-ray crystal structure determination were obtained by slow vapor diffusion of diethyl ether into an acetonitrile solution of **4**. Anal. for $C_{21}H_{27}F_6Mn_1N_3O_{10}S_2$: calc. C 35.30, H 3.81, N 5.88; found C 35.19, H 3.72, N 5.81; $[\alpha]_D^{21}$ -29.0 deg cm^3 g^{-1} dm^{-1} (*c* 0.58, acetonitrile); IR (solid) ν (cm^{-1}): 2958.9, 1686.2, 1607.1, 1577.2, 1447.6, 1390.2, 1354.0, 1303.5, 1257.3, 1234.9, 1221.9, 1159.2, 1030.6, 944.4, 926.9, 894.7, 846.2, 795.7, 760.2. Solution magnetic moment (Evans' method): $\mu_{eff} = 5.55\ \mu_\beta$.

[Mn(OTf)$_2$(Py(ProOH)$_2$)] (5): A slightly yellow/beige solution of Mn(OTf)$_2$·2MeCN (0.59 mmol, 258 mg) in acetonitrile (10 mL) was added to a yellow solution of **2** (0.65 mmol, 200 mg) in acetonitrile (10 mL). After the addition the reaction mixture was yellow of color. The reaction mixture was stirred for 1.5 h at ambient temperature, followed by evaporation of the solvent *in vacuo*. The remaining yellow/brown

solid/foam was dissolved in a minimal amount of dry acetonitrile and precipitated by addition of dry diethyl ether affording a brownish solid in 72% yield (310 mg). Crystals suitable for X-ray crystal structure determination were obtained from an acetonitrile/diethyl ether solution of **5**. Anal. for $C_{19}H_{27}F_6Mn_1N_3O_8S_2$: calc. C 34.66, H 4.13, N 6.38; found C 34.78, H 4.20, N 6.46; $[\alpha]_D^{21}$ 23.7 deg cm^3 g^{-1} dm^{-1} (*c* 0.49, acetonitrile); IR (solid) ν (cm^{-1}): 3409.7, 2966.6, 1605.1, 1579.6, 1467.1, 1448.0, 1353.6, 1260.6, 1236.0, 1219.2, 1159.2, 1091.2, 1063.5, 1026.2, 958.9, 972.9, 902.6, 875.1, 832.8, 792.7, 761.2. Solution magnetic moment (Evans' method): μ_{eff} = 5.71 μ_β.

General oxidation procedure: To a solution of catalyst (3.5 μmol) in acetone (2 mL) was added alkene (1.4 mmol, 400 equiv.) and 4-methylimidazole (17.5 μmol, 5 equiv.) in acetone (0.8 mL) followed by slow drop wise addition of 0.5 mL of 3.5 M H_2O_2 solution in acetone (1.75 mmol, 500 equiv., diluted from 35% aqueous H_2O_2) over 30 min. The reaction mixture was stirred at ambient temperature and after 1 hour (from start of oxidant addition) internal standard (10 μL, cyclooctene: 1,2-dibromobenzene, all other substrates: bromobenzene) was added and the first sample was taken. After three hours a second sample was taken from the reaction mixture. To the aliquots of the reaction mixture was added Et_2O and these solutions were analyzed by GC. The products were identified and quantified by GC by comparison with authentic compounds. The reported values are the average of at least two independent runs.

X-ray crystal structure determinations: Reflections were measured on a Nonius KappaCCD diffractometer with rotating anode and graphite monochromator (λ = 0.71073 Å) up to a resolution of $(\sin\theta/\lambda)_{max}$ = 0.65 $Å^{-1}$ at a temperature of 150(2) K. Intensity data were integrated with the software Eval14[52] (compound **4**) or Eval15[53] (compound **5**). Absorption correction and scaling was performed based on multiple measured reflections with SADABS.[54] The starting coordinates of **4** were taken from the isostructural Fe compound, **5** was solved by automated Patterson methods.[55] Least-squares refinement was performed with SHELXL-97[56] against F^2 of all reflections. Non-hydrogen atoms were refined freely with anisotropic displacement parameters. Hydrogen atoms were introduced in calculated positions (**4**) or located in difference Fourier maps (**5**). C-H hydrogen atoms were refined with a riding model, O-H hydrogen atoms were refined freely with isotropic displacement parameters. Geometry calculations and checking for higher symmetry was performed with the PLATON program.[57]

CCDC 878083 (compound **4**) and 878084 (compound **5**) contain the supplementary crystallographic data for this paper. These data can be obtained free of charge from The Cambridge Crystallographic Data Centre via www.ccdc.cam.ac.uk/data_request/cif.

Compound 4: $C_{21}H_{27}F_6MnN_3O_{10}S_2$, Fw = 714,52, colorless needle, 0.48 x 0.18 x 0.15 mm^3, orthorhombic, $P2_12_12_1$ (no. 19), a = 9.00515(18), b = 13.2324(2), c = 24.3529(7) Å, V = 2901.89(11) Å^3, Z = 4, D_x = 1.635 g/cm^3, μ = 0.69 mm^{-1}. 72229 Reflections were measured, 6654 reflections were unique (R_{int} = 0.023), of which 6297 were observed [I>2σ(I)]. 390 Parameters were refined with no restraints. R1/wR2 [I > 2σ(I)]: 0.0247 / 0.0578. R1/wR2 [all refl.]: 0.0278 / 0.0596. S = 1.060. Flack parameter[58] x = -0.007(10). Residual electron density between -0.33 and 0.47 e/Å^3

Compound 5: $C_{19}H_{27}F_6MnN_3O_8S_2$, Fw = 658.50, colorless block, 0.42 x 0.27 x 0.18 mm^3, tetragonal, $P4_12_12$ (no. 92), a = b = 9.00716(7), c = 66.3715(3) Å, V = 5384.65(6) Å^3, Z = 8, D_x = 1.625 g/cm^3, μ = 0.74 mm^{-1}. 27288 Reflections were measured, 6185 reflections were unique (R_{int} = 0.018), of which 5972 were observed [I>2σ(I)]. 360 Parameters were refined with no restraints. R1/wR2 [I > 2σ(I)]: 0.0248 / 0.0602. R1/wR2 [all refl.]: 0.0264 / 0.0610. S = 1.093. Flack parameter[58] x = 0.014(11). Residual electron density between -0.26 and 0.37 e/Å^3.

References

1. Sheldon, R.A.; Kochi, J.K.; Metal-Catalyzed Oxidations of Organic Compounds (**1981**) Academic Press , New York.
2. Bäckvall, J-E. Modern Oxidations Methods (**2004**) Wiley-VCH, Weinheim.
3. Meunier, B. Biomimetic catalyzed by transition metal complexes (**1999**) Imperial College Press, London.
4. Costas, M.; Mehn, M.P.; Jensen, M.P.; Que, L. Jr. *Chem. Rev*. **2004**, *104*, 939-986.
5. Jacobson, E.N.; Zhang, W.; Muci, A.R.; Ecker, J.R.; Deng, L. *J. Am. Chem. Soc.* **1991**, *113*, 7063-7064.
6. Pietikäinen, P. *Tetrahedron Letters* **1994**, *35*, 941-944.
7. Pietikäinen, P. *Tetrahedron* **1998**, *54*, 4319-4326.
8. Haikarainen, A.; Sipilä, J.; Pietikäinen, P.; Pajunen, A.; Mutikainen, I. *Bioorg. Med. Chem.* **2001**, *9*, 1633-1638.
9. Irie, R.; Hosoyo, N.; Katsuki, T. *Synlett* **1994**, 255.
10. Schwenkreis, T.; Berkessel, A. *Tetrahedron Lett.* **1993**, *34*, 4785-4788.
11. Berkessel, A.; Frauenkron, M.; Schwenkreis, T.; Steinmetz, A.; Baum, G.; Fenske, D.; *J. Mol. Cat. A* **1996**, *113*, 321.
12. Berkessel, A.; Frauenkron, M.; Schwenkreis, T.; Steinmetz, A. *J. Mol. Cat. A* **1997**, *117*, 339-346.
13. Shitame, H.; Katsuki, T. *Tetrahedron Lett.* **2006**, *47*, 3203-3207.
14. Garcia-Bosch, I.; Ribas, A.; Costas, M. *Adv. Synth. Catal.* **2009**, *351*, 348-352.
15. Bolm, C.; Kadereit, D.; Valacchi, M. *Synlett* **1997**, 687.
16. Bolm, C.; Meyer, N.; Raabe, G.; Weyhermüller, T.; Bothe, E. *Chem. Commun.* **2000**, 2435.
17. Gómez, L.; Garcia-Bosch, I.; Company, A.; Sala, X.; Fontrodona, X.; Ribas, X.; Costas, M. *Dalton Trans.* **2007**, 5539-5545.
18. Wu, M.; Wang, B.; Wang, S.; Xia, C.; Sun, W. *Organic Letters* **2009**, *11*, 3622-3625.
19. Murphy, A.; Dubois, G.; Stack, T.D.P. *J. Am. Chem. Soc.* **2003**, *125*, 5250-5251.
20. Wang, B.; Miao, C.; Wang, S.; Xia, C.; Sun, W. *Chem. Eur. J.* **2012**, *18*, 6750-6753.
21. Ottenbacher, R.V.; Bryliakov, K.P.; Talsi, E.P. *Adv. Synth. Catal.* **2011**, *353*, 885-889.

22. Garcia-Bosch, I.; Gómez, L.; Polo, A.; Ribas, X.; Costas, M. *Adv. Synth. Catal.* **2012**, *354*, 65-70.
23. Lane, B.S.; Burgess, K. *Chem. Rev.* **2003**, *103*, 2457-2473.
24. de Faveri, G.; Ilyashenko, G.; Watkinson, M. *Chem. Soc. Rev.* **2011**, *40*, 1722-1760.
25. Talsi, E.P.; Bryliakov, K.P. *Coord. Chem. Rev.* **2012**, *256*, 1418-1434.
26. Gosiewska, S.; Cornelissen, J.L.M.; Lutz, M.; Spek, A.L.; van Koten, G.; Klein Gebbink, R.J.M. *Inorg. Chem.* **2006**, *45*, 4214-4227.
27. Gosiewska, S.; Lutz, M.; Spek, A.L.; Klein Gebbink, R.J.M. *Inorg. Chim. Acta* **2007**, *360*, 405-417.
28. Gosiewska, S.; Permentier, H.P.; Bruins, A.P.; van Koten, G.; Klein Gebbink, R.J.M. *Dalton Trans.* **2007**, 3365-3368.
29. Bruijnincx, P.C.A.; Lutz, M.; Spek, A.L.; Hagen, W.R.; Weckhuysen, B.M.; van Koten, G.; Klein Gebbink, R.J.M. *J. Am. Chem. Soc.* **2007**, *129*, 2275-2286.
30. Bruijnincx, P.C.A.; Buurmans, I.L.C.; Gosiewska, S.; Moelands, M.A.H.; Lutz, M.; Spek, A.L.; van Koten, G.; Klein Gebbink, R.J.M. *Chem. Eur. J.* **2008**, *14*, 1228-1237.
31. Pilati, T.; Forni. A. *J. Appl. Cryst.* **1998**, *31*, 503-504.
32 Bergström, P.Å.; French, R. *J. Phys. Chem.* **1995**, *99*, 12603-12611.
33. a) Aresta,M.; Quaranta, E.; Albinati, A. *Organometallics* **1993**, *12*, 2032. b) Aresta, M.; Dibenedetto, A.; Amodio, E.; Papai, I.; Schubert, G. *Inorg. Chem.* **2002**, *41*, 6550-6552.
34. Britovsek, G.J.P.; Gibson, V.C.; Spitzmesser, S.K.; Tellmann, K.P.; White, A.J.P.; Williams, D.J. *J. Chem. Soc., Dalton Trans.* **2002**, 1159-1171.
35. Evans, D.F.J *J. Chem. Soc.* **1959**, 2003-2005.
36. England, J.; Britovsek, G.J.P.; Rabadia, N.; White, A.J.P. *Inorg. Chem.* **2007**, *46*, 3752-3767.
37. Blakesley, D.W.; Payne, S.C.; Hagen, K.S. *Inorg. Chem.* **2000**, *39*, 1979-1989.
38. Börzel, H.; Comba, P.; Hagen, K.S.; Lampeke, Y.D.; Lienke, A.; Linti, G.; Merz, M.; Pritzkow, H.; Tsymbal, L.V.; *Inorg. Chim. Acta* **2002**, *337*, 407-419.
39. tBuOOH was also found to be inefficient as oxidant under these conditions.
40. Renaud, J.P.; Battioni, P.; Bartoli, J.F.; Mansuy, D. *J. Chem. Soc., Chem. Commun.* **1985**, 888-889.
41. Yuan, L.C.; Bruice, T.C. *J. Am. Chem. Soc.* **1986**, *108*, 1643-1650.
42. Balasubramanian, P.N.; Schmidt, E.S.; Bruice, T.C. *J. Am. Chem. Soc.* **1987**, *109*, 7865-7873.
43. Battioni, P.; Renoud, J.P.; Bartoli, J.F.; Reina-Artiles, M.; Fort, M.; Mansuy, D.; *J. Am. Chem. Soc.* **1988**, *110*, 8462-8470.
44. Haikarainen, A.; Sipilä, J.; Pietikäinen, P.; Pajunen, A.; Mutikainen, I. *Bioorganic & Medicinal Chemistry* **2001**, *9*, 1633-1638.
45. Moelands *et al.* manuscript in preparation (Chapter 3 of this thesis).
46. Bryan, P.S.; Dabrowiak, J.C. *Inorg. Chem.* **1975**, *14*, 296-299.
47. Lutz, M.; Schreurs, A.M.M.; Spek, A.L.; Moelands, M.A.H.; Klein Gebbink, R.J.M. *Acta. Cryst. C.* **2010**, *C66*, m9-m12.
48. Knops-Gerrits, P.-P.; de Vos, D.E.; Jacobs, P.A. *J. Mol. Catal. A.* **1997**, *117*, 57-70.
49. Bitterlich, B.; Anilkumar, G.; Gelalcha, F.G.; Spilker, B.; Grotevendt, A.; Jackstell, R.; Tse, M.K.; Beller, M. *Chem. Asian J.* **2007**, *2*, 521-529.
50. Su, H.; Wu, C.; Zhu, J.; Miao, T.; Wang, D.; Xia, C.; Zhao, X.; Gong, Q.; Song, B.; Ai, H. *Dalton Trans.* **2012**, *41*, 14480.
51. Lyakin, O.Y.; Ottenbacher, R.V.; Bryliakov, K.P.; Talsi, E.P. *ACS Catal.* **2012**, *2*, 1196-1202.
52. Duisenberg, A.J.M.; Kroon-Batenburg, L.M.J.; Schreurs, A.M.M. *J. Appl. Cryst.* **2003**, *36*, 220-229.
53. Schreurs, A.M.M.; Xian, X.; Kroon-Batenburg, L.M.J. *J. Appl. Cryst.* **2010**, *43*, 70-82.

54. Sheldrick, G.M. (**1999**). SADABS: Area-Detector Absorption Correction, v2.10, Universität Göttingen, Germany.
55. Beurskens, P.T.; Beurskens, G.; de Gelder, R.; Garcia-Granda, S.; Gould, R.O.; Smits, J.M.M. (**2008**). The DIRDIF2008 program system, Crystallography Laboratory, University of Nijmegen, The Netherlands.
56. Sheldrick, G.M. *Acta Cryst.* **2008**, *A64*, 112-122.
57. Spek, A.L. *Acta Cryst*. **2009**, *D65*, 148-155.
58. Flack, H.D. *Acta Cryst.* **1983**, *A39*, 876-881.

3

The effect of 4-methylimidazole on olefin epoxidations catalyzed by 2,6-pyridinylbisproline-based manganese complexes

In chapter 2 the catalytic potential of manganese complexes [Mn(**Py(ProMe)$_2$**)(OTf)$_2$] (**1**) and [Mn(**Py(ProOH)$_2$**)(OTf)$_2$] (**2**) for the epoxidation of alkenes was investigated. During this study it turned out that the addition of several equivalents of 4-methylimidazole had a positive effect on the catalytic potential of these complexes. Here, the investigations aimed at understanding the interaction of the 4-methylimidazole (4-MeIm) additive on these complexes, in particular with complex **1**, and with that on their reactivity in the epoxidation reaction of alkenes is reported. These investigations point at a relative weak interaction between 4-MeIm and **1**, leading to the formation of a catalytically active bis-imidazole adduct and ultimately to catalytically inert oligo-imidazole adducts such as a hexakis 4-MeIm Mn(II) complex. Binding of 2 equiv. of 4-MeIm to **1** was found to lead to a decrease in the intra-molecular coordination of the ester carbonyl groups and to their fluxional coordination behavior. It is proposed that non-coordinated carbonyl groups may aid the activation of H_2O_2 by means of hydrogen-bonding interactions.

3.1 Introduction

Manganese catalysts are widely explored for (enantioselective) oxidation and epoxidation reactions. Next to the proper design of the ligand around Mn, the addition of nitrogen or oxygen bases, such as imidazoles, pyridines and carboxylates, is studied in order to increase both the activity and selectivity of these catalysts. For instance the group of Costas has reported on the addition of acetic acid in catalytic olefin epoxidation by Mn^{Me,H}PyTACN complexes (^{Me,H}PyTACN = 1-(2′-pyridylmethyl)-4,7-dimethyl-1,4,7-triazacyclononane).[1] The addition of acetic acid prevents the use per acetic acid as the oxidant in this system and allows the reaction to be carried out with hydrogen peroxide. The group of Feringa reported on the addition of carboxylic acids in catalytic epoxidations by Mn(tmTACN) complexes (tmTACN = N,N',N"-trimethyl-1,4,7-triazacyclononane).[2] Other examples include the addition of imidazoles to manganese porphyrin[3-8] and salen[9,10] type complexes to result in an increased activity of the catalyst. The additives mostly act as additional ligands to the metal center. For instance, Renaud *et al.* have reported on the beneficial effect of imidazole in the epoxidation of styrene by [Mn(Cl)TPP] and [Mn(Cl)TMP] (TPP = tetraphenylporphyrin, TMP = tetramesitylporphyrin).[3] Meunier *et al.* reported on a ligand in which the imidazole group is covalently bound to the porphyrin framework and in this way functions as an additional fifth ligand.[7] Along a similar vein, Berkessel *et al.* reported on the preparation of Mn(III)salen ligands with an appended imidazole acting as a fifth axial donor ligand.[11,12] Pietikäinen has reported on the use of imidazole additives in the Mn(III)salen catalyzed asymmetric epoxidation of unfunctionalized alkenes.[9] In 2006 Katsuki *et al.* reported over the synthesis of pentacoordinated salen manganese complexes with an internal pyridine or *N*-methylimidazole ligand, which gave 97% ee in the epoxidation of chromene derivatives with hydrogen peroxide.[13] Next to increasing the catalytic activity, binding of additional ligands to manganese can favor heterolytic O–O bond cleavage of the initially formed metal-based intermediate upon reaction with e.g. H_2O_2, producing the reactive metal-oxo species. In this way the additives prevent the homolytic cleavage of the weak O-O bond, which would lead to the formation of O-centered radicals.[9] The base additives may furthermore function as an acid-base catalyst.[14]

In chapter 2 of this thesis two proline based manganese complexes, [Mn(**Py(ProMe)$_2$**)(OTf)$_2$] (**1**) and [Mn(**Py(ProOH)$_2$**)(OTf)$_2$] (**2**) were synthesized to function as catalyst in the epoxidation of alkenes (Figure 1).[15] During optimization studies the effect of different kinds of additives, especially imidazoles, on the catalytic activities of these complexes was investigated. From these studies it turned out that 4-methylimidazole (referred to as 4-MeIm) has a positive effect on the overall turnover number in the epoxidation reactions catalyzed by these complexes.

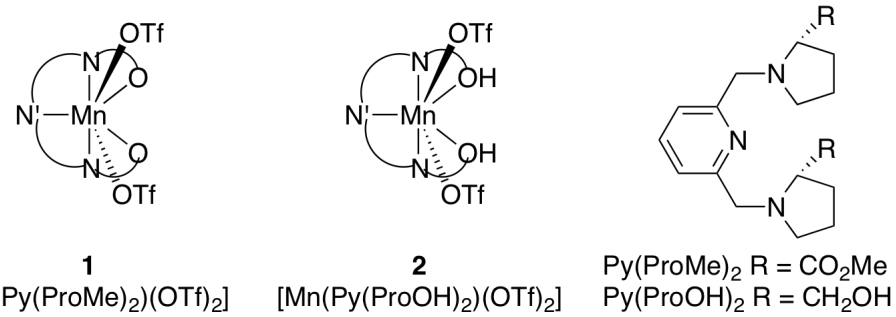

1 [Mn(Py(ProMe)$_2$)(OTf)$_2$] **2** [Mn(Py(ProOH)$_2$)(OTf)$_2$] Py(ProMe)$_2$ R = CO_2Me Py(ProOH)$_2$ R = CH_2OH

Figure 1. Representation of complexes **1** and **2**.

In this chapter we report on an investigation into the interaction of 4-MeIm with complexes **1** and **2** through a number of different spectroscopic techniques and into the influence of 4-MeIm on the reactivity of these complexes in epoxidation reactions. The outcome of this study can be used to further optimize catalytic oxidation reactions by these and related Mn-complexes.

3.2 Results

3.2.1 Binding of 4-MeIm to complexes 1 and 2

The investigations on the binding of 4-MeIm to the Mn-complexes was started by monitoring the replacement of the triflate ions by the imidazole using ^{19}F-NMR. ^{19}F NMR spectra of paramagnetic complexes can give a good indication whether the triflate anions function as bridging ligands (ca. +60 ppm), as terminal ligands (ca. –10 ppm) or as counter ions (ca. –80 ppm).[16,17] In earlier work on complexes **1** and **2**, no ^{19}F-NMR signal could be detected for complex **1** in both acetonitrile and acetone suggesting that the triflate ions are bound to Mn, while for **2** a broad fluorine peak at –70.8 ppm in acetonitrile was observed pointing at the exchange of triflate between bound en non-bound states.[15] Upon the addition of 4-MeIm (5 equiv.) a fluorine peak was observed for both complexes in each of these solvents (Table 1). In each case, a ^{19}F NMR signal was observed around –78.5 ppm, pointing at non-coordinated triflate anions.

Table 1. ^{19}F NMR data of complexes **1** and **2** in the absence and presence of 4-MeIm (5 equiv.).

Solvent	Complex **1** (ppm)	Complex **2** (ppm)
MeCN	-	–70.8
MeCN with 4-MeIm	–78.7	–79.1
Acetone	-	-
Acetone with 4-MeIm	–78.2	–78.2

For **2** a ^{19}F-NMR titration was carried out with 4-MeIm in acetone, i.e. the optimal solvent for catalytic epoxidations using **2** in conjunction with H_2O_2 (Figure 2). After the addition of 2 equivalents of 4-MeIm a signal started to appear that is caused by free triflate ions in solution. Upon increasing the amount of 4-MeIm, this signal increased in intensity and sharpened, indicating a further shifting of the coordination equilibrium away from the coordination of 4-MeIm to the manganese complex and towards the complete release of triflate ions.

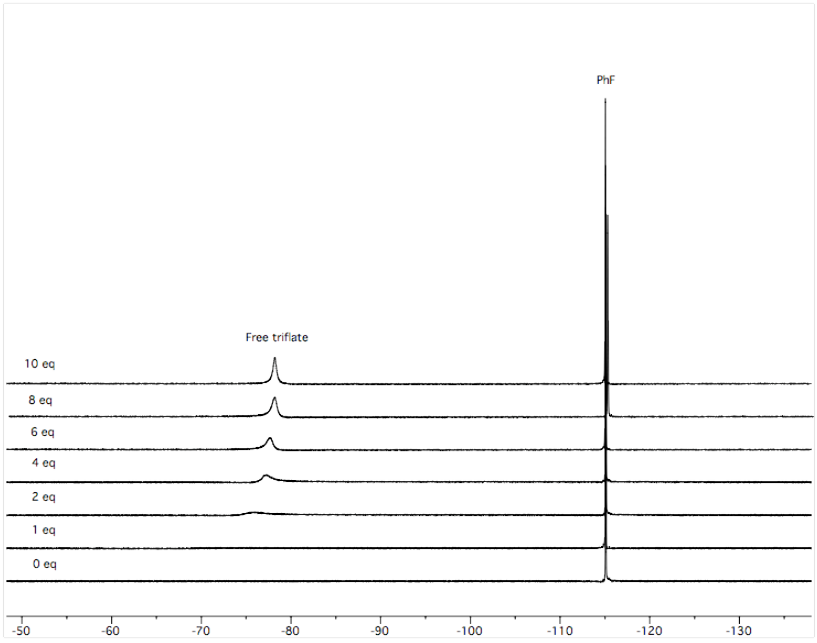

Figure 2. ^{19}F-NMR titration of complex **2** with different equivalents of 4-MeIm in acetone (PhF is used as reference).

Next, IR spectroscopy was used to monitor the binding of 4-MeIm to complex **1**, as the vibrational bands of the carbonyl groups of the proline moieties in the **Py(ProMe)$_2$** ligand are a good benchmark for metal ion coordination to these groups. The solution IR spectra in acetonitrile for the free ligand, complex **1**, and the complex after the addition of 4-MeIm (5 equiv.) are depicted in Figure 3. The ligand has a characteristic carbonyl vibration at 1745 cm^{-1}, which shifts to lower wavelength (1687 cm^{-1}) upon coordination of the carbonyl groups towards the manganese center. Upon addition of 4-MeIm (5 equiv.), two bands appear in the carbonyl vibration region at 1741 cm^{-1} and at 1691 cm^{-1}, respectively. The former of these peaks corresponds to a free carbonyl group, while the latter vibration can be attributed to a coordinated carbonyl group. This observation indicates that after the addition of 5 equiv. of 4-MeIm, the carbonyl groups in **1** are no longer fully coordinated to the manganese center and that coordinating 4-MeIm groups may partly replace these. Also in the triflate region between 1300 and 1050 cm^{-1} changes occur upon introduction of the imidazole additive. These changes correspond to a change in the binding of the triflate

groups. As already observed in earlier work,[15] in solution the coordinated triflate groups are replaced by acetonitrile solvent molecules. This effect is further enhanced by the addition of 4-MeIm, as only the signals of non-coordinated triflate anions are present in the region between 1270 and 1030 cm^{-1} (Figure 3, bottom).[18]

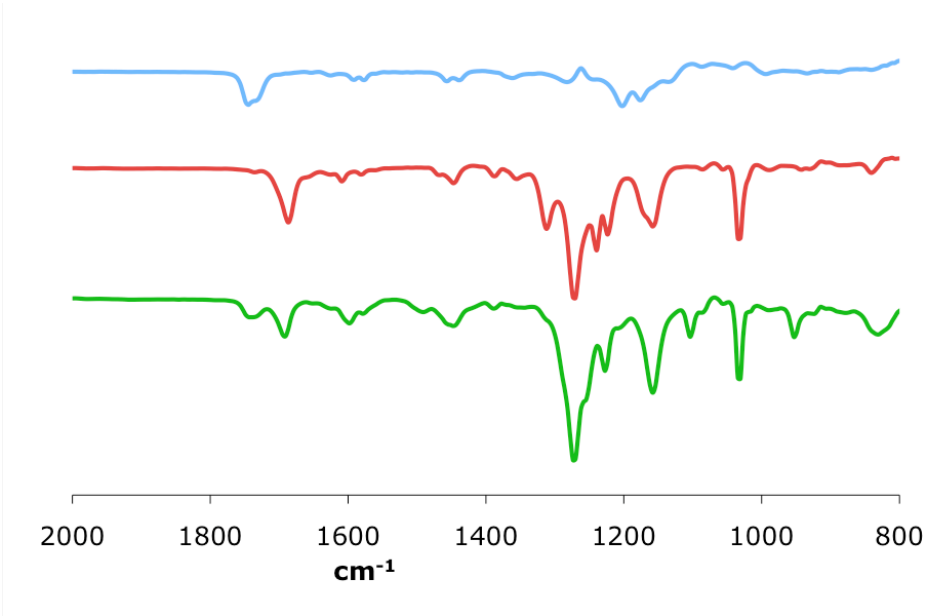

Figure 3. Solution IR spectra (acetonitrile) of ligand $Py(ProMe)_2$ (top) its corresponding $Mn(OTf)_2$ complex **1** (middle), and **1** with 4-MeIm (5 equiv.; bottom).

To study this effect in more detail a solution IR titration was carried out, by means of the addition of increasing amounts of 4-MeIm (0 – 10 equiv.) to a solution of complex **1** in acetonitrile (Figure 4). Upon the addition of 4-MeIm to **1**, the vibrational signals of non-coordinated carbonyl groups around 1740 cm^{-1} steadily increases in intensity, in particular after the addition of more than 3-4 equiv. of the imidazole. The signals around 1580 cm^{-1}, caused by the C=N bond from the pyridine moiety in the ligand and by the C=N bonds of 4-MeIm also increase in intensity, albeit in a more progressive manner. At the same time, the vibrational signal of the coordinated carbonyl group around 1680 cm^{-1} initially shifts to a slightly higher wavenumber and increases somewhat in intensity, before to decrease in intensity after the addition of 4 equivalents of 4-MeIm. This peak has almost disappeared after the addition of 10 equiv. of 4-MeIm. As was already mentioned above the coordination behavior of the triflate groups is at first influenced by the coordinating properties of the acetonitrile solvent. Next to that, added 4-MeIm also stimulates the decoordination of the triflate groups (Figure 3). Based on the titration shown in Figure 4, the addition of 4-MeIm causes the decoordination of the CO groups from the metal only after it has replaced the triflate anions. Carbonyl decoordination starts after the addition of 3-4 equiv. of 4-MeIm. The first equivalents are probably used to occupy the coordination sites of the

triflate groups. The more equivalents of 4-MeIm are added to **1**, the more the coordination equilibrium shifts towards non-coordinated carbonyl groups. The 4-MeIm groups then probably occupy these coordination sites (*vide infra*).

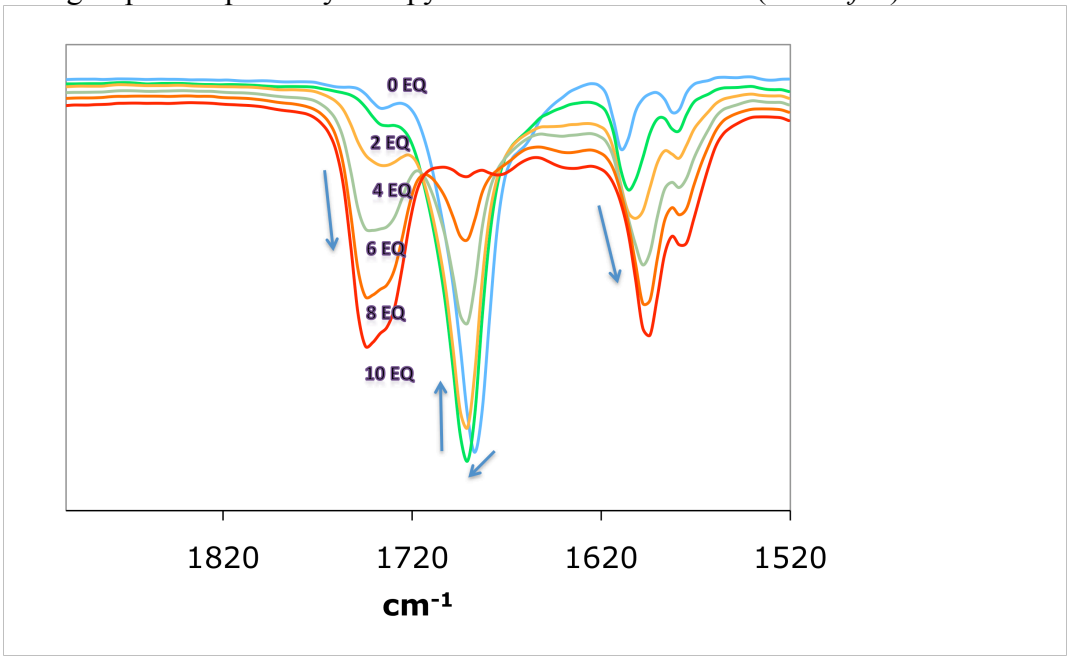

Figure 4. IR titration of **1** with 4-MeIm (0-10 equiv.) in acetonitrile.

The effect of adding 4-MeIm to **1** was also studied by recording EPR spectra of **1** in frozen acetonitrile solutions in the presence of increasing amounts of the additive (0-5 equiv.; Figure 5). The EPR spectrum of **1** shows a large and strongly isotropic signal around g = 3.46 and a less intense axial signal in the region between g = 2.07 and 1.81. Upon addition of 1 equiv. of 4-MeIm the spectrum changes to mainly a large axial signal with a high degree of anisotropy around g = 2.10. Upon the addition of the second equivalent of 4-MeIm, the spectrum simplifies considerably and only shows an axial six-line feature around g = 2 (exact g-values are: 2.06, 2.03, 1.98, 1.93, 1.88 and 1.80). This EPR pattern is characteristic for mononuclear Mn(II) complexes with a spin of $S = 5/2$ (number of lines = $2S + 1$).[19] There is some hyperfine coupling caused by the nitrogen donors present, but these are difficult to assign. No attempts were made to fully analyze or simulate this EPR feature. Further addition of 4-MeIm does not result in any further change in the overall spectrum, nor in the g-values. Given the low temperature at which these EPR spectra were recorded, these observations seem to indicate that binding of the first two equiv. of 4-MeIm (replacement of triflates) is facile, while the further binding of 4-MeIm and the simultaneous decoordination of carbonyl ligands is more difficult and requires more energy.

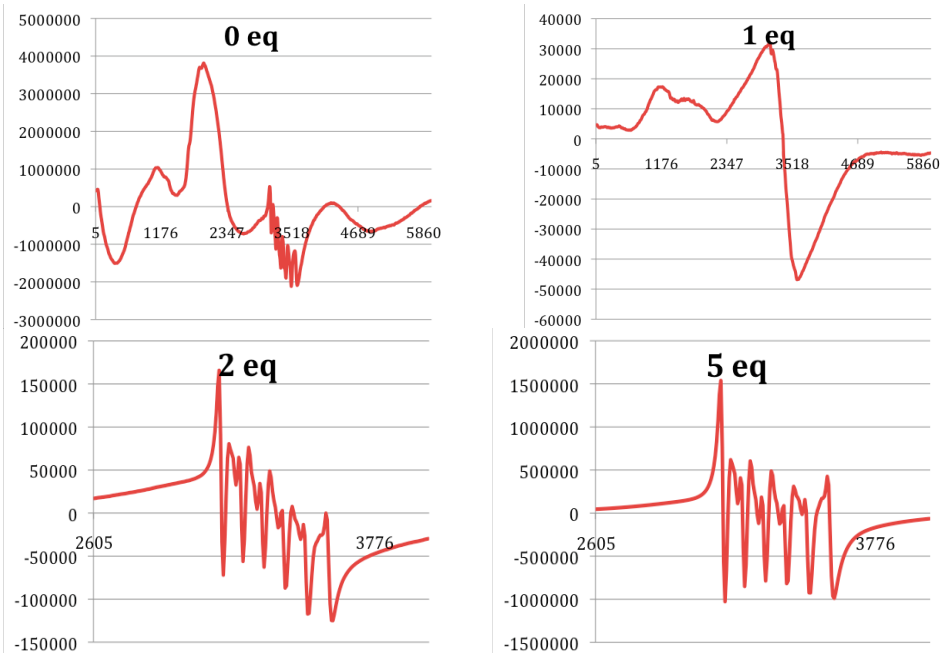

Figure 5. EPR titration of **1** with 4-MeIm (0-5 equiv.) in acetonitrile.

Finally, the binding of 4-MeIm to **1** was studied by means of ESI-MS. To this end ESI-MS measurements were carried out on acetone solutions of **1** in the presence of different amounts of 4-MeIm (0-10 equiv. and an excess). In the absence of 4-MeIm, the monocation $[Mn(\mathbf{Py(ProMe)_2})(OTf)_2]^+$ was clearly visible at m/z = 565.05, next to a less intense signal of the free ligand $(L+H)^+$ at m/z = 362.20. Upon addition of 4-MeIm in increasing amounts, the relative intensity of the $[Mn(\mathbf{Py(ProMe)_2})(OTf)_2]^+$ peak at m/z = 565 decreased. Furthermore, the peak of the free ligand at m/z = 362 increased in intensity. It was not possible to detect a complex ion that included both manganese and 4-MeIm along the series of additions of 4-MeIm. Finally, in the presence of a large excess of 4-MeIm, the $[Mn(\mathbf{Py(ProMe)_2})(OTf)_2]^+$ peak had completely disappeared.

3.2.2 Crystal structure of $[Mn(4\text{-MeIm})_6](OTf)_2$

During a crystallization experiment of complex $[Mn(\mathbf{Py(ProMe)_2})(OTf)_2]$ (**1**) in the presence of an excess of 4-MeIm in an attempt to obtain a crystal structure of a complex that included 4-MeIm coordinated to manganese, colorless crystals of a manganese hexakis 4-MeIm complex $[Mn(4\text{-MeIm})_6)](OTf)_2$ were obtained. The complex crystallizes in the trigonal space group R $\bar{3}$ (no. 148) with the Mn atom located on a site with $\bar{3}$ (C_{3i}) symmetry, the triflate anions have threefold rotation symmetry (C_3). $[Mn(4\text{-MeIm})_6)](OTf)_2$ is isostructural with the corresponding Ru complex.[20] For symmetry reasons, all Mn-N distances are equal (2.2565(10) Å), but the symmetry allows a deviation of the N-Mn-N angles from ideal (87.58(4) and 92.42(4) °). A molecular structure of (**1**) is depicted in Figure 6. The imidazole N-H

group acts as hydrogen bond donor with a triflate oxygen as acceptor. Overall this results in a hydrogen bonded 2D network parallel to the crystallographic *a,b*-plane.

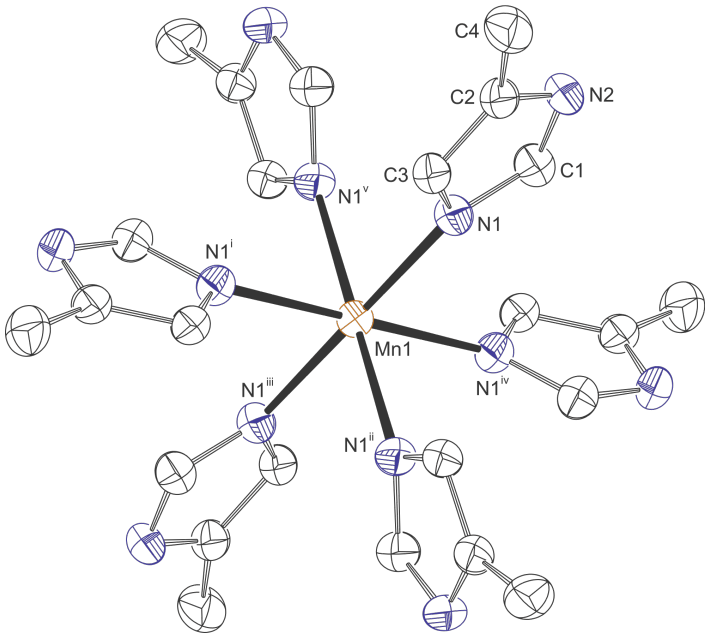

Figure 6. Molecular structure of the $[Mn(4\text{-MeIm})_6]^{2+}$ cation in the crystal. View along the *c*-axis. C-H hydrogen atoms and non-coordinating triflate groups have been omitted for clarity. Displacement ellipsoids are drawn at the 50% probability level. Symmetry operations *i*: -y, x-y, z; *ii*: y-x, -x, z; *iii*: -x, -y, -z;*iv*: y, y-x, -z; *v*: x-y, x, -z.

The crystals obtained after crystallization were used to test the catalytic potential of this hexakis(imidazole) complex in the oxidation of cyclooctene, in which the complex turned out to be completely inactive. This means that when certain amounts of the hexakis 4-MeIm complex are formed upon the addition of larger amounts of 4-MeIm in catalytic reactions with **1**, and mostly likely **2**, an overall lowered activity or to a complete cease in activity would be observed.

3.3 Catalysis

In the catalytic oxidation reactions using manganese complexes **1** and **2** reported in the previous chapter,[15] 4-MeIm was found to provide the highest reactivity and selectivity amongst a series of N-donor additives. To investigate the effect of the amount of 4-MeIm on the catalytic activity in more detail, the overall catalytic activity of **1** in the epoxidation of cyclooctene with H_2O_2 in acetone was monitored using increasing amounts of the additive (0-10 equiv., Figure 7). The results depicted here are the turnover numbers (TON) after 3 h using a catalyst:oxidant:substrate ratio of 1:500:400.

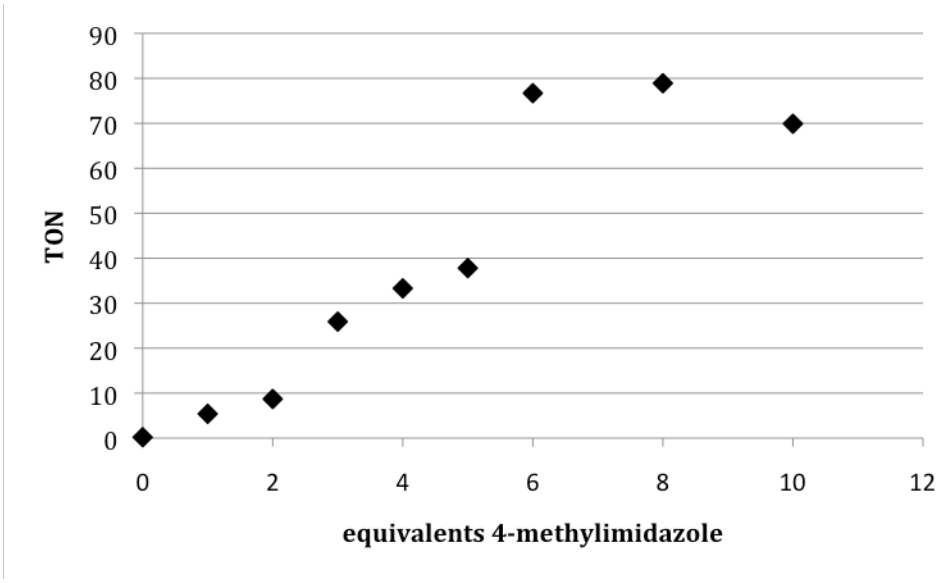

Figure 7. Effect of different amounts of 4-MeIm on the turnover number (TON) of **1** in the epoxidation of cyclooctene with H_2O_2 in acetone at RT.

With small amounts of 4-MeIm (0-2 equiv.) hardly any activity is observed. Increasing the amount of additive from 2-6 equiv. leads to a large increase in activity. Further addition of 4-MeIm (8 or 10 equiv.) does not significantly affect the reactivity, but ultimately leads to a small drop in activity. These different stages in activity can be explained by assuming that binding of 4-MeIm to **1** to form the catalytically active species is relatively weak and that the formation of this species shows saturation behavior. The S-shaped activity curve furthermore indicates that more than one equivalent of 4-MeIm binds to **1** and that either binding of the first equivalent of 4-MeIm is weaker than binding of a further equivalent or that the formation of the active catalyst species is presided by the formation of other, non-catalytically competent 4-MeIm adducts. The addition of more then 2 equiv. of 4-MeIm seems to lead to an overall shift of the binding equilibrium towards the formation of the catalytically active species, hence leading to an overall increase in activity. Upon the addition of more than 8 equiv. of 4-MeIm the hexakis(imidazole) complex starts to form, leading to a decreased catalytic activity. Based on the data presented in Figure 7 the optimal catalytic activity of **1** is obtained when using in between 5 to 8 equiv. of 4-MeIm.

To investigate the effect of varying amounts of 4-MeIm on the enantioselectivity of the epoxidations carried out by the Mn-complexes, the epoxidation of *trans*-beta-methylstyrene was monitored in the presence of different amounts of 4-MeIm (Table 3, Figure 8). For these catalytic reactions, complex [Mn(**Py(ProOH)$_2$**)(OTf)$_2$] (**2**) was used with a catalyst:oxidant:substrate ratio of 1:500:400. The TON and *ee* results depicted in Table 3 and Figure 8 are the catalytic results after 1 h.

Table 2. Effect of the amount of 4-MeIm on product enantioselectivity during the epoxidation of *trans*-beta-methylstyrene using complex **2**.[a]

Equiv. of 4-MeIm	TON[b]	ee (%)
0	2.1	8
1	5.6	14
2	8.8	15
3	13.2	16
4	16.9	22
5	24.6	25

[a] To a solution of catalyst (3.5 μmol) in acetone (2 mL) was added alkene (1.4 mmol, 400 equiv.) and 4-MeIm (17.5 μmol, 5 equiv.) in acetone (0.8 mL) followed by slow drop wise addition of 0.5 mL of 3.5 M H_2O_2 solution in acetone (1.75 mmol, 500 equiv., diluted from 35% aqueous H_2O_2) over 30 min, stirring was continued for another 30 min; [b] Yields expressed as turnover numbers (TON = mol product/mol catalyst.

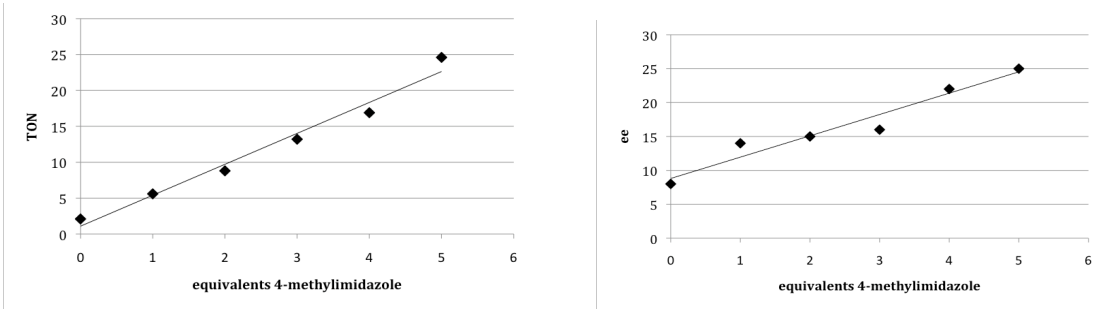

Figure 8. Graphical representation of the effect of 4-MeIm on the TON and product ee in the catalytic epoxidation of trans-beta-methylstyrene with **2**.

These experiments show, alongside a steady increase in TON, a significant increase of the enantioselectivity of the epoxide product upon increasing the amount of 4-MeIm. Going from 0 to 5 equiv. of 4-MeIm the enantioselectivity increases from 8% to 25%, while the TON increases from 2.1 to 24.6 per Mn.

In the above experiments, the activity of the complexes was monitored after 1 and 3 h, as well as after 1 night, which indicated that the TON further increased after the first hours of reaction. To determine the catalytic activity over time in a more detailed manner, the reaction of **1** with cyclooctene was monitored for a longer period of time using a catalyst:oxidant:substrate ratio of 1:500:400 and 5 equiv. of 4-MeIm. Figure 9 shows that the activity in the first 7 h steadily increases and results in over 60 turnovers after one night. The ultimate cease in activity may be explained by catalyst deactivation or by the complete consumption of hydrogen peroxide in either a productive or non-productive manner.

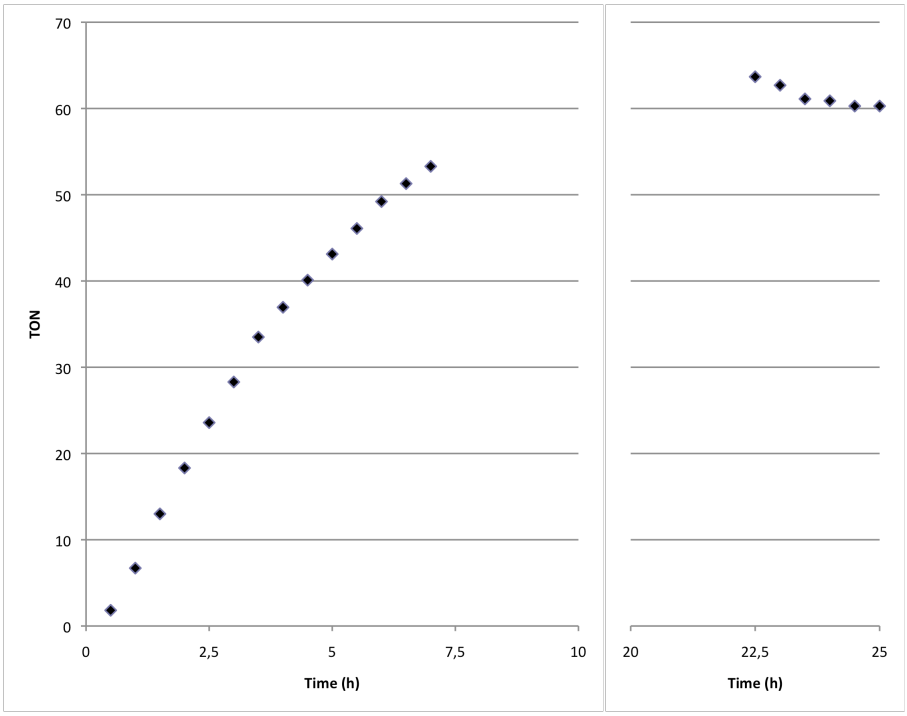

Figure 9. The epoxidation of cyclooctene with complex **1** followed in time using a ratio between catalyst:oxidant:substrate of 1:500:400.

3.4 Discussion

Our spectroscopic and catalytic investigations have provided us with a detailed picture of the equilibrium between the different species formed upon combining either complex **1** or **2** with a varying amount of 4-MeIm and allow us to correlate these to the observed catalytic activities (Figure 10). ^{19}F NMR showed that the addition of 4-MeIm in acetone releases the coordinating triflate groups from the complexes in an equilibrium process that requires several equivalents of 4-MeIm to fully release all triflates from Mn. In the previous chapter was already shown that the addition of a coordinating solvent like acetonitrile to the complexes also causes the full decoordination of the triflate groups.[15] Detailed IR investigations in acetonitrile showed minor changes in the carbonyl vibration upon the addition of the first equivalents of 4-MeIm. This may imply that 4-MeIm is able to replace acetonitrile molecules from the manganese coordination sphere. After the addition of 3 to 4 equivalents of 4-MeIm, the IR trace clearly shows the combined presence of coordinated and non-coordinated carbonyl groups. With the addition of more equivalents of the 4-MeIm this coordination equilibrium is pushed to the site in which the carbonyl groups no longer coordinate to the manganese center. At the amount of 5 equivalents, as used during the catalytic experiments, the triflate groups were released from the complex and the carbonyl groups are in an coordination equilibrium with the manganese center. A similar EPR titration at 77 K showed that the addition 2 equiv. of 4-MeIm led to a complete change of the EPR signal, while further addition of

4-MeIm did not lead to any further change in the signal. This observation implies that the binding of the first two equivalents of 4-MeIm, replacing either acetonitrile or triflate, is facile, while the decoordination of the carbonyl groups requires more energy and does take place at this temperature.

Figure 10 summarizes the combined spectroscopic observations and relates these to the catalytic properties of the various Mn-species involved. When the catalytic reactions are carried out without any 4-MeIm there is hardly any activity. The addition of 2 equivalents of 4-MeIm results in a small increase in catalytic activity due to a partial release of the triflate groups and partial coordination of 4-MeIm to the Mn-center. Upon increasing the amount of 4-MeIm to 5 equivalents, a considerable increase in catalytic activity is observed, which is related to a further shifting of the binding equilibrium towards the full release of the two triflate groups and coordination of two 4-MeIm moieties. The increased binding of 4-MeIm also leads to a flexible coordination behavior of the carbonyl groups, which partly release from the manganese center. With 5 equivalents of 4-MeIm, the highest catalytic activity (TON around 60-100) and product selectivity (ee values around 25-40%) are observed.[15] These data show that the species formed at this catalyst: 4-MeIm ratio is both the most kinetically competent as well as most enantio-discriminative.

Coordination of 4-MeIm to the Mn-center is likely to provide the proper steric and electronic environment for H_2O_2 activation and epoxidation. While the binding of 2 equiv. of 4-MeIm by the release of coordinating triflate ions would yield another 7-coordinated and saturated Mn-center, the coordinative flexibility of the relatively weak carbonyl donor groups allows for the formation of free coordination sites on the manganese center necessary for H_2O_2 binding. In a non-coordinated form, the carbonyl groups can participate in H_2O_2 activation by acting as a hydrogen bond acceptors. When the amount of 4-MeIm is further increased and an excess is added, the formation of an manganese hexakis 4-MeIm complex $[Mn(4\text{-MeIm})_6]^{2+}$ takes place. The formed 4-MeIm complex was found to be catalytically incompetent and during the reaction a brown solid (Mn_2O_3) was formed. Alkene epoxidation reactions using complexes **1** and **2** as the catalysts in combination with H_2O_2, therefore, require an optimized amount of 4-MeIm between 5-8 equiv. in order to obtain a decent activity as well selectivity. A number of different coordination equilibrium determines the optimal amount of 4-MeIm.

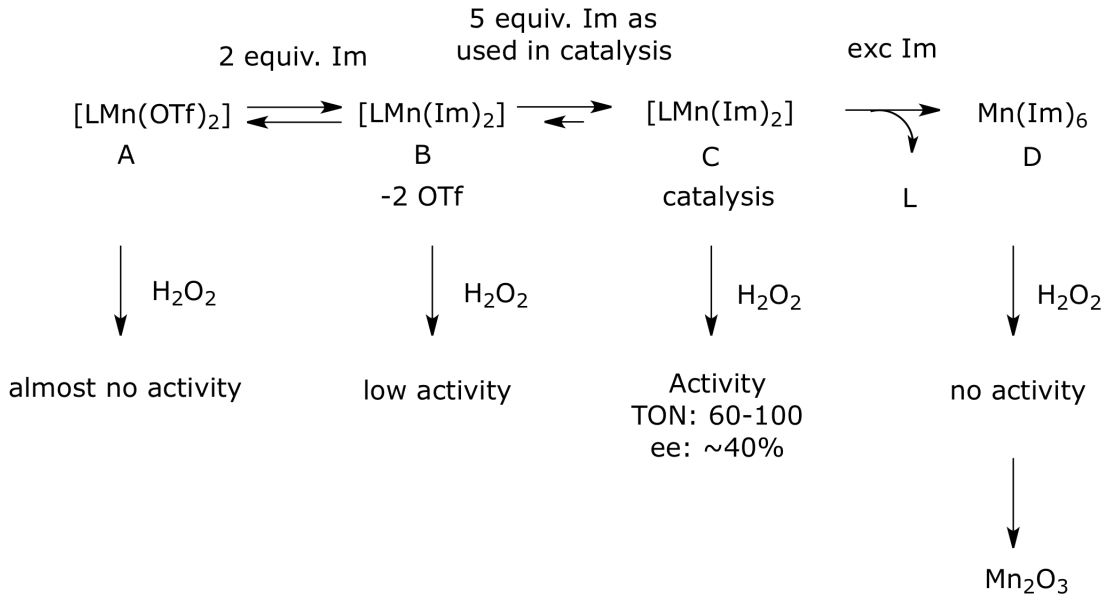

Figure 10. Effect of the 4-MeIm amount on the reactivity of complexes **1** and **2**.

3.5 Concluding remarks

In catalytic screenings, the design of the proper ligand is often of key importance. The use and the effect of possible additives may in some cases be of equal or even more importance on both the catalytic activity and scope of the overall catalytic system. The use of additives can give a true impulse to the catalytic performance of a catalyst, but the type and amount of additive should be carefully screened to obtain the maximum result and to understand the effect of the additive on catalysis.

These considerations have been illustrated during the catalytic screenings on the catalytic ability of two manganese complexes in combination with 4-MeIm as additive, as described in chapters 2 of this thesis. Based on all the combined spectroscopic and catalytic observations it can now be concluded that the number of equivalents of the additive 4-MeIm has a large influence on the overall catalytic performance of complexes **1** and **2** and goes through an optimum between 5-8 equivalents. This is the result of the intricate balance between a number of different coordination equilibrium that is at play in these mixed N,O-ligated manganese complexes in combination with a coordinating additive. It is believed that the observations described in these chapters are illustrative for catalysts derived from mixed donor ligands that include donor sites with distinctively different coordination properties.

3.6 Experimental section

General: The used solvents were dried and distilled before use. ^{19}F-spectra were recorded on a Varian 400 spectrometer at 400 MHz operating at 25 °C. Solution IR measurements were recorded with a Mettler Toledo ReactIR^{TM} 1000 spectrometer

with a SiComp^{TM} probe placed in a Schlenk under N_2 atmosphere. Experimental X-band EPR spectra were recorded on a Bruker EMX spectrometer equipped with a He temperature control cryostat system (Oxford Instruments). ESI-MS was measured on a Waters LCT Premier XE. GC analyses were performed on a Perkin-Elmer Clarus 500 GC (30 m, Econo-Cap EC-5) with FID detector. [Mn(Py(ProMe)$_2$)(OTf)$_2$] (**1**) and [Mn(Py(ProOH)$_2$)(OTf)$_2$] (**2**) were prepared according to published procedures.[15]

General oxidation procedure: To a solution of catalyst (3.5 μmol) in acetone (2 mL) was added alkene (1.4 mmol, 400 equiv.) and 4-MeIm (17.5 μmol, 5 equiv.) in acetone (0.8 mL) followed by slow drop wise addition of 0.5 mL of 3.5 M H_2O_2 solution in acetone (1.75 mmol, 500 equiv., diluted from 35% aqueous H_2O_2) over 30 min. The reaction mixture was stirred at ambient temperature and after 1 hour (from start of oxidant addition) internal standard (10 μL, cyclooctene: 1,2-dibromobenzene, all other substrates: bromobenzene) was added and the first sample was taken. After three hours a second sample was taken from the reaction mixture. To the aliquots of the reaction mixture was added Et_2O and these solutions were analyzed by GC. The products were identified and quantified by GC by comparison with authentic compounds. The reported values are the average of at least two independent runs.

X-ray crystal structure determination of [Mn(4-MeIm)$_6$](OTf)$_2$ (1): $[C_{24}H_{36}MnN_{12}](CF_3O_3S)_2$, Fw = 845.73, colorless block, 0.45 × 0.30 × 0.30 mm^3, trigonal, R $\overline{3}$ (no. 148), a = b = 12.8172(1), c = 20.5920(2) Å, V = 2929.65(4) Å^3, Z = 3, D_x = 1.438 g/cm^3, μ = 0.53 mm^{-1}. 23962 Reflections were measured on a Nonius KappaCCD diffractometer with rotating anode and graphite monochromator (λ = 0.71073 Å) at a temperature of 150(2) K up to a resolution of $(\sin\theta/\lambda)_{max}$ = 0.65 Å^{-1}. Intensity data were integrated with the HKL2000 software.[21] Absorption correction and scaling was performed with SADABS[22] (correction range 0.78-0.85). 1503 Reflections were unique (R_{int} = 0.034), of which 1368 were observed [I>2σ(I)]. Initial coordinates were taken from the isostructural Ru complex.[20] Least-squares refinement was performed with SHELXL-97[23] against F^2 of all reflections. Non-hydrogen atoms were refined freely with anisotropic displacement parameters. Hydrogen atoms were located in difference Fourier maps and refined freely with isotropic displacement parameters. 105 Parameters were refined with no restraints. R1/wR2 [I > 2σ(I)]: 0.0282 / 0.0719. R1/wR2 [all refl.]: 0.0316 / 0.0743. S = 1.054. Residual electron density between -0.36 and 0.19 e/Å^3. Geometry calculations and checking for higher symmetry was performed with the PLATON program.[24]

References

1. Garcia-Bosch, I.; Ribas, A.; Costas, M. *Adv. Synth. Catal.* **2009**, *351*, 348-352.
2. de Boer, J.W.; Brinksma, J.; Browne, W.R.; Meetsma, A.; Alsters, P.L.; Hage, R.; Feringa, B.L. *J. Am. Chem. Soc.* **2005**, *127*, 7990-7991.
3. Renaud, J.P.; Battioni, P.; Bartoli, J.F.; Mansuy, D. *J. Chem. Soc., Chem. Commun*. **1985**, 888-889.
4. Yuan, L.C.; Bruice, T.C. *J. Am. Chem. Soc.* **1986**, *108*, 1643-1650.
5. Balasubramanian, P.N.; Schmidt, E.S.; Bruice, T.C. *J. Am. Chem. Soc*. **1987**, *109*, 7865-7873.
6. Battioni, P.; Renoud, J.P.; Bartoli, J.F.; Reina-Artiles, M.; Fort, M.; Mansuy, D. *J. Am. Chem. Soc.* **1988**, *110*, 8462-8470.
7. Meunier, B.; de Carvalho, M.E.; Bortolini, O.; Momenteau, M. *Inorg. Chem.* **1988**, *27*, 161-164.
8. Takahashi, A.; Kurahashi, T.; Fujii, H. *Inorg. Chem.* **2009**, *48*, 2614-2625.
9. Pietikäinen, P. *Tetrahedron Lett.* **1994**, *35*, 941-944.
10. Haikarainen, A.; Sipilä, J.; Pietikäinen, P.; Pajunen, A.; Mutikainen, I. *Bioorg. Med. Chem.* **2001**, *9*, 1633-1638.
11. Schwenkreis, T.; Berkessel, A. *Tetrahedron Lett.* **1993**, *34*, 4785-4788.
12. Berkessel, A.; Frauenkron, M.; Schwenkreis, T.; Steinmetz, A. *J. Mol. Cat. A* **1997**, *117*, 339-346.
13. Shitame, H.; Katsuki, T. *Tetrahedron Lett.* **2006**, *47*, 3203-3207.
14. Meunier, B. *Chem. Rev.* **1992**, *92*, 1411-1456.
15. Moelands *et al.* manuscript in preparation (Chapter 2 of this thesis).
16. Blakesley, D.W.; Payne, S.C.; Hagen, K.S. *Inorg. Chem.* **2000**, *39*, 1979-1989.
17. Börzel, H.; Comba, P.; Hagen, K.S.; Lampeke, Y.D.; Lienke, A.; Linti, G.; Merz, M.; Pritzkow, H.; Tsymbal, L.V. *Inorg. Chim. Acta* **2002**, *337*, 407-419.
18. a) Aresta, M.; Quaranta, E.; Albinati, A. *Organometallics* **1993**, *12*, 2032-2043. b) Aresta, M.; Dibenedetto, A.; Amodio, E.; Papai, I.; Schubert, G. *Inorg. Chem.* **2002**, *41*, 6550-6552.
19. a) Warzeska, S.T.; Miccichè, F.; Mimmi, M.C.; Bouwman, E.; Kooijman, H.; Spek, A.L.; Reedijk, J. *J. Chem. Soc., Dalton Trans* **2001**, 3507-3512. b) Wu, J-Z.; Bouwman. E.; Mills, A.M.; Spek, A.L.; Reedijk, J. *Inorg. Chim. Acta* **2004**, *357*, 2694-2702.
20. Baird, I.R.; Rettig, S.J.; James, B.R.; Skov, K.A. *Can. J. Chem.* **1998**, *76*, 1379-1388.
21. Otwinowski, Z.; Minor, W.; *Methods in Enzymology, Volume 276* (C.W. Carter, Jr. & R.M. Sweet, Eds.) Academic Press (**1997**) 307-326.
22. Sheldrick, G. M. (**1999**). SADABS: Area-Detector Absorption Correction, Universität Göttingen, Germany.
23. Sheldrick, G.M. *Acta Cryst.* **2008**, *A64*, 112-122.
24. Spek, A.L. *J. Appl. Cryst.* **2003**, *36*, 7-13.

4

Manganese(II) complexes of azetidine and piperidine-based ligands derived from the Py(ProMe)$_2$ ligand framework

This work describes the synthesis and analysis of several chiral mixed N,O ligands and their corresponding manganese(II) complexes. The ligands were prepared by variation of the previously prepared **Py(ProMe)$_2$** ligand in the size of the ester tail and the substitution of the pyrrolidine ring by either a piperidine or an azetidine ring. Most of the ligands showed the same coordination behavior towards manganese as the parent ligand, i.e. the formation of pentagonal bipyramidal Mn-complexes with labile sites in axial positions. The azetidine-based ligand has a different coordination behavior. Although it does give a seven-coordinated Mn-center, its coordination geometry is highly distorted and the labile sites in this case are orientated in a *cis*-fashion. The investigation of the epoxidation properties of these complexes showed that it is the azetidine-derived ligand that provides the high activity to the corresponding manganese(II) triflate complexes.

4.1 Introduction

Nature functions as a continuous source of inspiration for the synthetic chemist. In the field of catalysis, one of the adopted strategies in catalyst development is the structural and functional mimicry of the active sites of metallo-enzymes that are able to carry out a particular type of reaction or that use a particular type of metal to bring about reactivity. This biomimetic approach in catalysis allows one to prepare synthetic analogues of these enzymes, which may serve to further understand their action, and at the same time allows for the development of bio-inspired catalysts that may be used in chemical synthesis. Once a certain mimic is found to posses the desired catalytic activity in the latter approach, its overall molecular design may be taken as a lead for further catalyst development and optimization, *e.g.* in terms of its reactivity toward a certain type of substrate or in terms of enantioselective transformations. Ligand variation is an important approach towards the development and optimization of these biomimetic catalysts.

In chapter 2 of this thesis,[1] biomimetic manganese complexes were developed for the catalytic oxidation of alkene substrates. These complexes are based on two biomimetic ligands (**Py(ProMe)$_2$** and **Py(ProOH)$_2$**), that were previously synthesized in our group by Gosiewska *et al.*[2,3] and that were used in combination with iron for the oxidation of alkene and alkane substrates. These manganese complexes are active in the epoxidation of various substrates. In the epoxidation of cyclooctene TON's up to 94 and substrate conversions up to 45% were obtained. Furthermore these manganese(II) complexes are a good extension of the limited number of manganese(II) complexes known in literature that are able to perform the enantioselective epoxidation of alkenes with hydrogen peroxide as the oxidant. With the pro-chiral substrate *trans*-beta-methylstyrene, ee's up to 35% were reached in the first screenings.

The crystal structure of the manganese complex [Mn(**Py(ProMe)$_2$**)(OTf)$_2$] reported earlier (chapter 2),[1] provides a good impression of the overall coordination geometry of the (**Py(ProMe)$_2$** and **Py(ProOH)$_2$**) ligands towards the manganese center in complexes of this type (Figure 1). The structure shows a cavity towards the manganese center in-between the two methyl-ester functionalities i.e. between oxygen O1 and O3. During the catalytic cycle a Mn-oxo species is presumably formed, which needs to be approached by the substrate. This means that the size of the cavity can influence the approach of the substrate towards the active intermediate responsible for oxygen transfer. Depending on the size of the cavity a substrate can bind towards the complex or cannot reach the activated manganese center for the reaction to occur. This will also have an effect on the enantioselectivity of the complex. The closer a substrate will fit into the cavity, the higher the enantioselectivity of the reaction is expected to be. This is comparable with the lock and key principle that is observed with enzymes.

The active intermediate in the epoxidation reactions is likely formed upon replacement of one of the triflate groups. For the subsequent oxygen transfer reaction to occur, the incoming substrate will therefore have to approach the active intermediate from the same side, which will be influenced by the size of the two nitrogen heterocycles attached to the central pyridine group. By changing these heterocycles, the cavity around the manganese center will be influenced; bigger heterocycles providing more steric hindrance, smaller heterocycles providing a larger cavity. Another point of consideration is the difference in donor strength of the nitrogen donor by changing the heterocycle ring sizes. Alternatively, the Mn-oxo is oriented within the equatorial N,N,N plane, i.e. by the decoordination of one of the ester groups as described in Chapter 3. In this case a variation of the substituent on the proline ring will lead to similar steric and electronic changes, e.g. by changing the size of the cavity around manganese and by changing the coordination behavior of the side chain toward the manganese center.

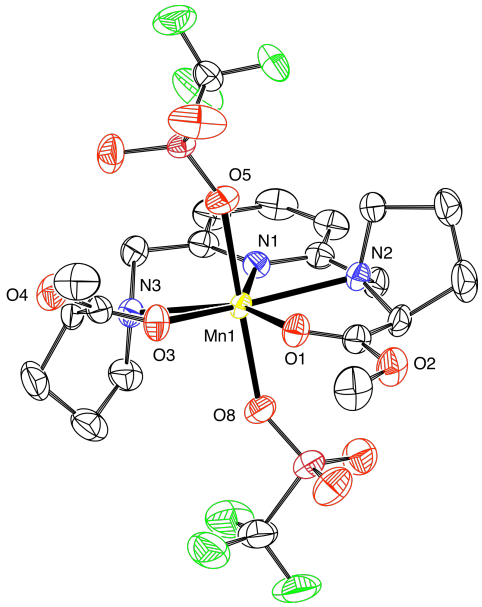

Figure 1. Crystal structure of [Mn(Py(ProMe)$_2$)(OTf)$_2$].[1]

Here, a variation study of the **Py(ProMe)$_2$** ligand manifold is reported. Structural variations in the ligand are carried out in the ester moiety, the substitution of the ester moiety by an alcohol moiety and in the ring containing the N-donor. In order to obtain a variation in the ring size, the 5-membered heterocyclic ring in the proline-based ligands is substituted by a four-membered azetidine ring (referred to as Aze) or a six-membered piperidine ring (referred to as Pip). An overview of the complete family of bis-prolinate ligands discussed in this chapter is depicted in Figure 2, together with their corresponding names. A full description is provided for the synthesis and characterization of this set of new mixed N,O ligands and their corresponding Mn(OTf)$_2$ complexes. The complexes have been tested in the catalytic oxidation of

alkenes using hydrogen peroxide as the oxidant. Finally, the catalytic performance of the complexes is correlated to the structure of the new set of biomimetic ligands.

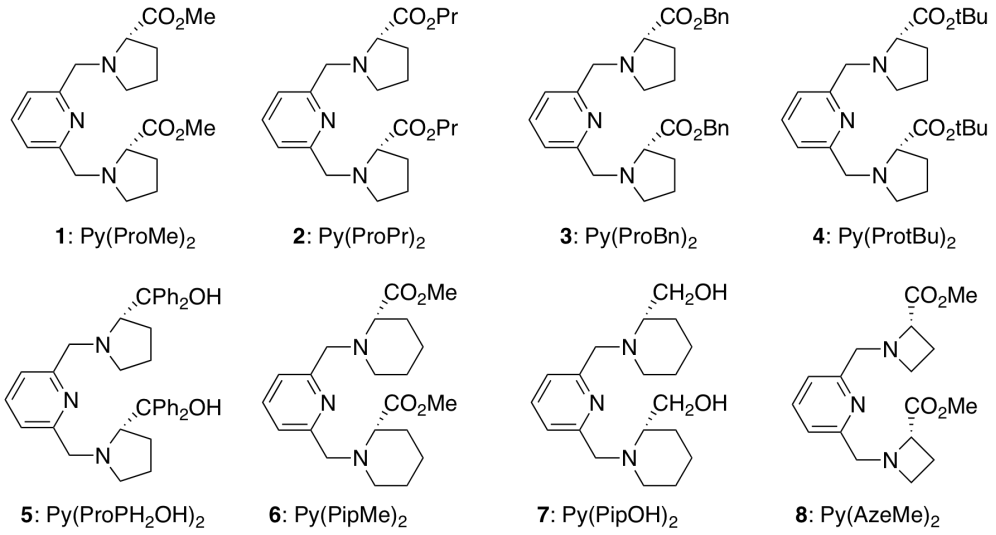

Figure 2. Overview of the ligands used in this study.

4.2 Results

4.2.1 Ligand synthesis

A small series of Py(ProR)$_2$ ligands in which R = propyl, benzyl and ^{t}Bu were synthesized according to a procedure reported by Chelucci *et al.*[4] (Scheme 1). To this end, the required proline ester was either prepared via an esterification reaction of proline with thionylchloride in propanol (**9**) or purchased from commercial sources (**10** and **11**). For the coupling of these esters to the central pyridine moiety, one equivalent of 2,6-bis(chloromethyl)pyridine was stirred overnight with 3 equivalents of the respective proline ester at 60 ºC in DMF with the addition of Na_2CO_3 and NaI. After purification by column chromatography, the ligands could be isolated as yellow oils in yields between 75 and 83%. The synthesis of ligand **5**, bearing bulky diphenyl carbinol moieties, was reported earlier.[3]

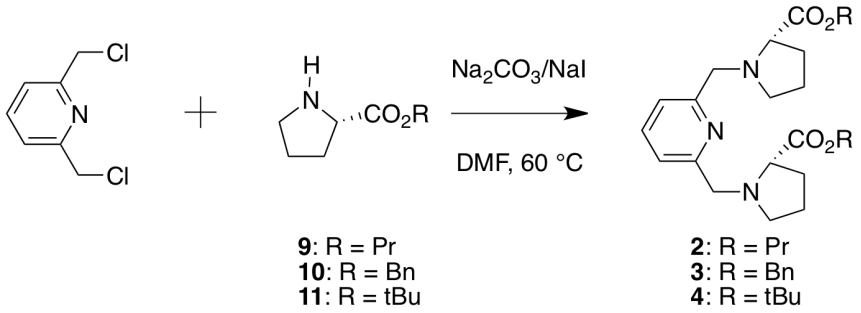

Scheme 1. Synthesis of the Py(ProR)$_2$ ligands with different ester groups.

The second ligand variation involves a change in the ring size of the amine heterocycle, *i.e.* changing the 5-membered pyrrolidine ring into a 6-membered piperidine (Pip) or 4-membered azetidine (Aze) ring. At the same time, the (L)-α-carboxy ester stereogenic center is maintained in the ligands. For the synthesis of the 6-membered piperidine ligands **6** and **7**, synthetic procedures reported by Gosiewska *et al.* for the corresponding 5-membered proline ligands were applied (Scheme 2).[2,3] For the synthesis of ligand **8** containing the 4-membered azetidine ring the procedure reported by Chelucci *et al.*[4] was used, applying a mixture of Na_2CO_3 and NaI in DMF. After purification via column chromatography the ligands **6**, **7**, and **8** were obtained as yellow/orange oils in 57, 36, and 94% yields, respectively.

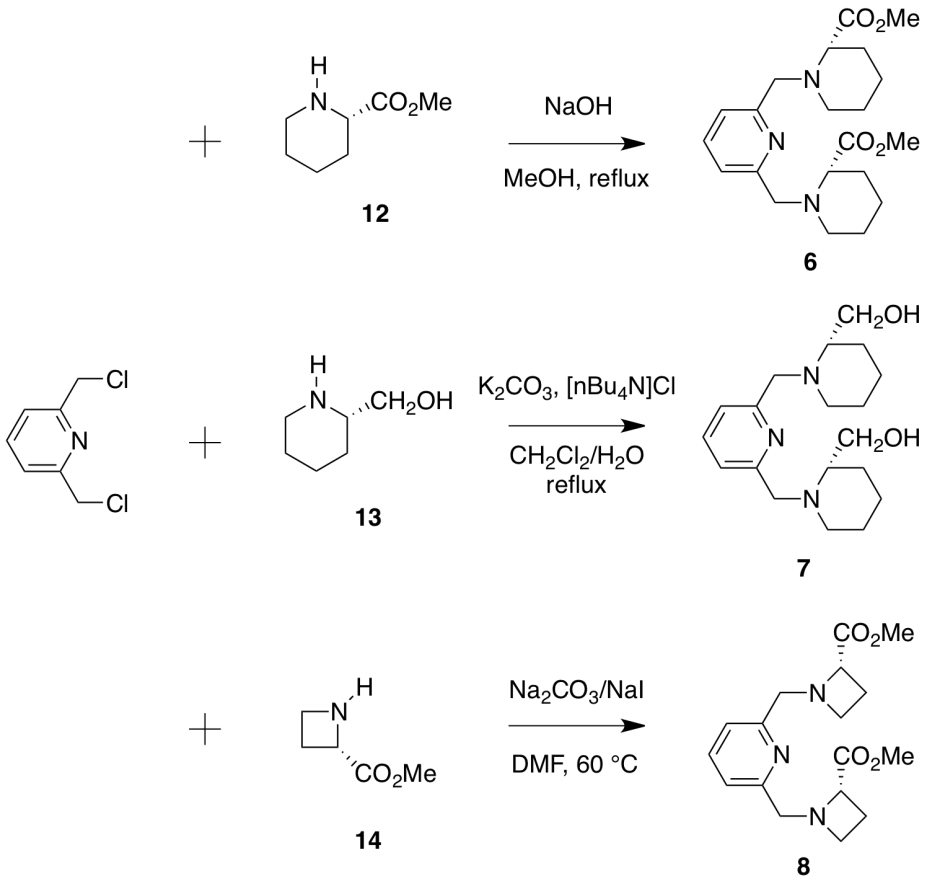

Scheme 2. Synthesis of the 4- and 6-membered ring analogues.

4.2.2 Preparation of metal complexes

For the series of mixed N,O-ligands, Mn-complexes were synthesized by reacting the ligand with an equimolar amount of $Mn(OTf)_2 \cdot MeCN$[5] in acetonitrile for 1-1.5 h under an inert N_2-atmosphere. The resulting complexes were isolated as solids via precipitation. All isolated complexes were stored under an inert nitrogen atmosphere. Table 1 provides an overview of the prepared complexes together with the isolated yield and the color of the isolated complexes.

Table 1. Overview of the prepared complexes.

Complex	Yield (%)	color	$[M\text{-}OTf]^+$, m/z
15: [Mn(**Py(ProPr)$_2$**)(OTf)$_2$]	68	white	621.153
16: [Mn(**Py(ProBn)$_2$**)(OTf)$_2$]	64	off-white	717.149
17: [Mn(**Py(ProtBu)$_2$**)(OTf)$_2$]	quant.	white	649.180
18: [Mn(**Py(ProPh$_2$OH)$_2$**)(OTf)$_2$]	97	green	813.232
19: [Mn(**Py(PipMe)$_2$**)(OTf)$_2$]	65	white	n.d.
20: [Mn(**Py(Pip)OH)$_2$**)(OTf)$_2$]	64	light brown	537.136
21: [Mn(**Py(AzeMe)$_2$**)(OTf)$_2$]	95	white	537.059

The isolated complexes were analyzed with ESI-MS and IR spectroscopy to get some initial information about their composition and structure. ESI-MS analysis showed a peak at an m/z value corresponding to the mono-cations $[M\text{-}OTf]^+$ for all complexes. When complex **15** was analyzed with ESI-MS after it was dissolved in MeOH, a peak of the free ligand was found together with two peaks of the ligand in which a methyl group replaced either one or two of the propyl groups. This observation indicates that in MeOH solution transesterification can take place towards the methyl ester ligand. The presence of the $[M\text{-}OTf]^+$ peak for each complex confirmed the expected structure of the complexes, a manganese center surrounded by one mixed N,O ligand and two triflate groups ([Mn(L)(OTf)$_2$]).

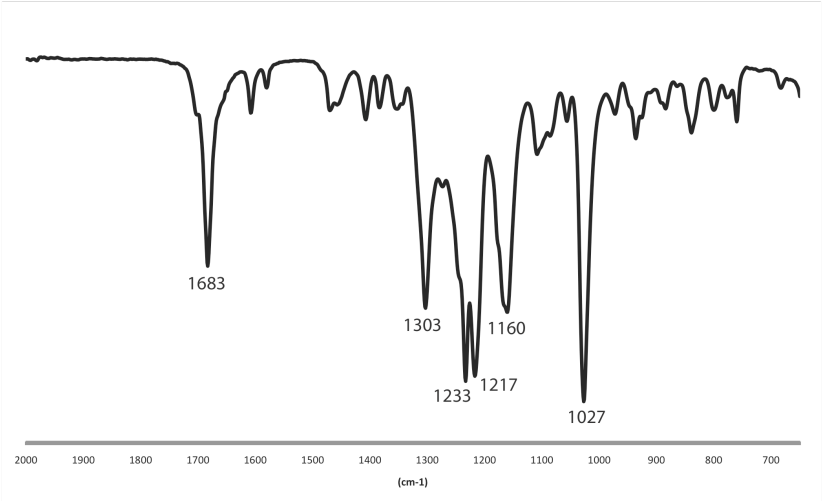

Figure 3. Solid-state IR spectrum of complex **15**.

IR analysis of the complexes was initially carried out in the solid state. Figure 3 shows the solid-state IR spectrum of complex **15** as an example, and depicts the informative vibrations pertaining to carbonyl and triflate fragments. The vibration of the carbonyl groups in **15** has shifted to lower wavelength compared to the vibration

of the free ligand (1728 cm^{-1}). This shift indicates the coordination of the carbonyl group towards the manganese center. For the triflate groups five vibrations are found at 1303 and 1233 (ν_{as} SO_3), 1217 (ν_s CF_3), 1160 (ν_{as} CF_3) and 1027 (ν_s SO_3) cm^{-1}. The double degenerate asymmetric SO_3 mode can be assigned to two components resulting from triflate anion coordination.[6] For the other complexes the same trend was seen in their solid state IR spectra: a shift in the carbonyl vibration due to the coordination to the manganese center and signals corresponding to coordinated triflate groups (see Table 2).

Table 2. Solid-state IR data of complexes **15-21**.

Complex	C=O vibration Free ligand (cm^{-1})	C=O vibration Complex (cm^{-1})	vibration triflate group (cm^{-1})
15: [Mn(**Py(ProPr)$_2$**)(OTf)$_2$]	1728	1683	1303, 1233, 1217, 1160, 1027
16: [Mn(**Py(ProBn)$_2$**)(OTf)$_2$]	1731	1683	1307, 1234, 1218, 1160, 1028
17: [Mn(**Py(ProtBu)$_2$**)(OTf)$_2$]	1724	1671	1308, 1235, 1217, 1153, 1028
18: [Mn(**Py(ProPh$_2$OH)$_2$**)(OTf)$_2$]			1281, 1235, 1222, 1161, 1026
19: [Mn(**Py(PipMe)$_2$**)(OTf)$_2$]	1733	1683	1310, 1236, 1213, 1158, 1021
20: [Mn(**Py(PipOH)$_2$**)(OTf)$_2$]			1307, 1235, 1219, 1158, 1028
21: [Mn(**Py(AzeMe)$_2$**)(OTf)$_2$]	1736	1689	1302, 1234, 1215, 1158, 1026

For complexes **15-17** IR spectra were additionally recorded in CH_2Cl_2 and MeCN solution. In both solvents it turned out that the carbonyl groups stay coordinated towards the manganese center: a single vibration is present at the same frequency as in the solid state. For the triflate groups a different effect is observed. In the non-coordinating solvent CH_2Cl_2 the same peaks were observed as in the solid state. However, in the coordinating solvent MeCN the doubly degenerate signal for the asymmetric SO_3 unit is replaced by an intensive signal around 1270 cm^{-1}. This change indicates the presence of non-coordinated triflate anions.[7] The triflate groups are therefore displaced by MeCN molecules in the Mn-coordination environment after dissolution of the complexes in acetonitrile. The solution IR data are compiled in

Table 3. Unfortunately no solution IR data could be obtained for the other complexes because these complexes were available in too small amounts.

Table 3. Solution IR data of complexes **15-17**.

Complex	Solvent	C=O vibration (cm^{-1})	triflate vibrations (cm^{-1})
15: [Mn(**Py(ProPr)$_2$**)(OTf)$_2$]	CH_2Cl_2	1683	1309, 1239, 1223, 1173, 1031
	MeCN	1679	1274, 1224, 1158, 1034
16: [Mn(**Py(ProBn)$_2$**)(OTf)$_2$]	CH_2Cl_2	1675	1309, 1239, 1223, 1162, 1034
	MeCN	1671	1270, 1224, 1158, 1034
17: [Mn(**Py(ProtBu)$_2$**)(OTf)$_2$]	CH_2Cl_2	1675	1309, 1239, 1223, 1173, 1034
	MeCN	1671	1270, 1224, 1158, 1034

4.2.3 Structural features of complexes in the solid state: X-ray crystal structures

For some of the prepared complexes it was possible to obtain crystals suitable for X-ray diffraction. Their structural features in the solid state are discussed below.

[Mn(**Py(ProPr)$_2$**)(OTf)$_2$] (**15**) Crystals suitable for X-ray diffraction were obtained via slow solvent evaporation of the solution that was removed after precipitation of the complex with CH_2Cl_2/Et_2O. The obtained structure is depicted in Figure 4.

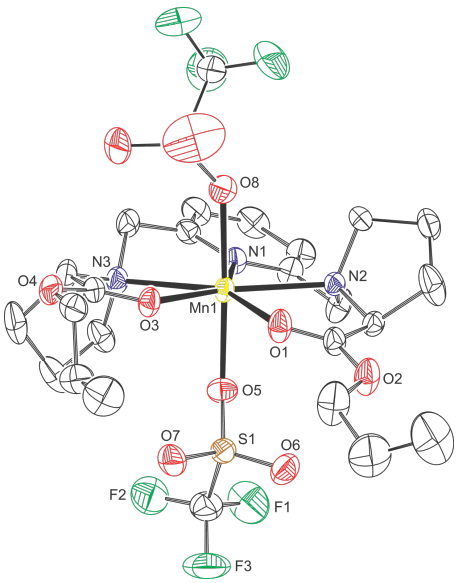

Figure 4. Molecular structure of complex **15** in the crystal. Displacement ellipsoid plot (50% probability). Only the major conformations of disordered proline rings, ester groups, and triflate ligands are shown. All hydrogen atoms and the partially occupied diethyl ether are omitted for clarity.

The manganese center in **15** is surrounded by a pentadentate ligand and two monodentate triflate groups, giving rise to a sevenfold-coordination geometry around the manganese(II) ion, which can be best described as distorted pentagonal bipyramidal (pbp, Figure 4). The manganese center resides in the equatorial plain and is surrounded by the three nitrogen atoms of the ligand as well as by the two oxygen atoms of the carbonyl groups from the ester moieties. The two κ^1-O bound triflate counter ions coordinate in the axial positions. The structure confirms the results obtained with the ESI-MS and IR measurements. Indeed, both the carbonyl and the triflate groups are found to coordinate to the manganese center. The propyl ester tails point away from the manganese center and in this way do not seem to increase the steric bulk around the metal.

The bond lengths and angles in **15** indicate a small distortion from a perfect pentagonal bipyramidal geometry (Table 4). The angles around manganese of the five equatorial donor atoms deviate slightly from the ideal value of 72°. Furthermore, the structure is not completely C_2-symmetric; *e.g.* the Mn-N3 bond length (2.567(2) Å) is significantly longer than the Mn-N2 bond length (2.395(2) Å). The *trans*-angle O(5)-Mn-O(8) of 176.93(8)° is very close to linear. The structure of **15** shows the same geometry as the complex [Mn(**Py(ProMe)$_2$**(OTf)$_2$] derived from the methyl ester ligand, reported earlier by us (chapter 2).[1] Furthermore, the bond lengths and angles in both complexes are very comparable to each other. For the other ester complexes **16** and **17** bearing a benzyl or *t*-butyl ester moiety, no X-ray quality crystals were obtained. Based on the combined IR data of these complexes, they are proposed to adopt a structure that is very similar to the structure of **15**.

Table 4. Selected bond lengths (Å) and angles (°) for **15**.

Bond length			Angle
Mn1-N1	2.220(2)	N1-Mn1-N2	71.89(8)
Mn1-N2	2.395(2)	N1-Mn1-N3	68.50(8)
Mn1-N3	2.567(2)	N2-Mn1-N3	140.23(7)
Mn1-O1	2.286(2)	N2-Mn1-O1	71.14(7)
Mn1-O3	2.1661(19)	N3-Mn1-O3	70.02(8)
Mn1-O5	2.211(2)	O1-Mn1-O3	79.31(7)
Mn1-O8	2.228(2)	O5-Mn1-O8	176.93(8)

Crystals of complexes [Mn(**Py(PipMe)$_2$**)(OTf)$_2$] (**19**) and [Mn(**Py(PipOH)$_2$**)(OTf)$_2$] (**20**) were obtained via solvent evaporation of the Et_2O/MeCN mixture that was left after the precipitation of the complex (Figure 5). In the asymmetric unit of the crystal structure of complex **20**, four independent molecules are present. Complex **19** adopts the typical sevenfold-coordination geometry (pbp) around the manganese(II) ion, also found for **15**. The ligand occupies the meridional plain and the two triflate groups are

bound in the axial positions giving rise to an approximately C_{2v} symmetric coordination polyhedron. Complex **20** also crystallizes in a distorted pentagonal bipyramidal (pbp) geometry, with a seven-coordinated manganese center. In this complex, the coordination occurs via the free electron pairs of the hydroxyl groups instead of carbonyl groups as in complex **19**. The coordinating triflate groups again occupy the axial positions.

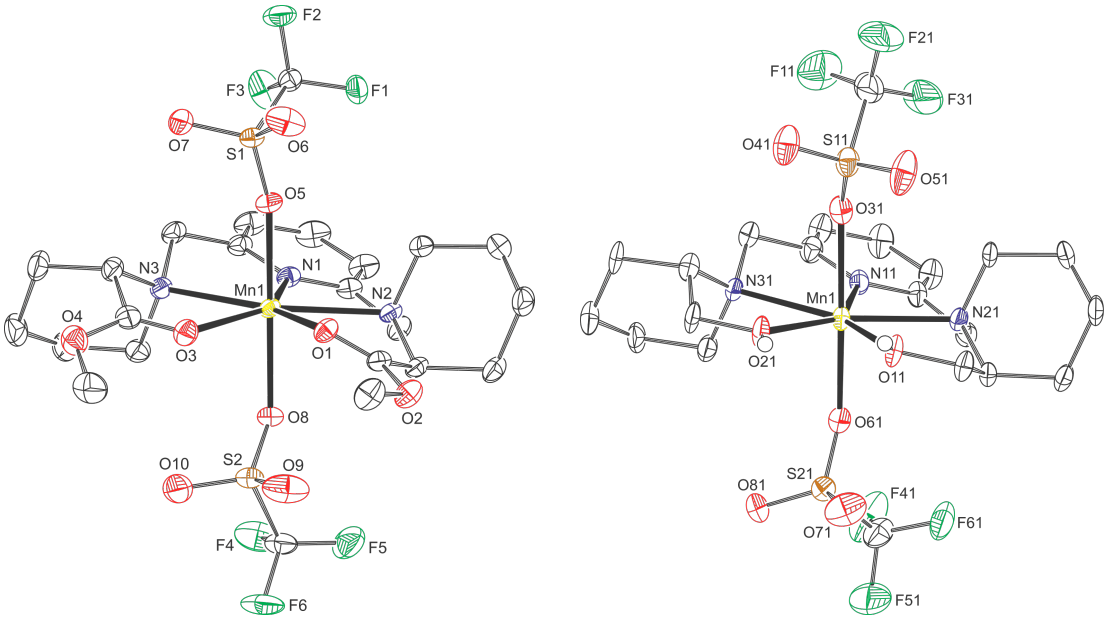

Figure 5. Molecular structures of complexes **19** and **20** in the crystal. Displacement ellipsoid plot (50% probability). For **20**, only one of four independent molecules is shown. C-H hydrogen atoms are omitted for clarity.

The selected bond lengths and angles for complex **19** and for all four residues of complex **20** are reported in Table 5. The values of complex **19** nicely reflect the almost perfect C_{2v} symmetry of the coordination environment; the bond lengths of Mn1-N2 and Mn1-N3 are almost equal, as are the bond lengths between Mn1-O5 and Mn1-O8. The sum of all *cis*-angles in the equatorial plane around the manganese center is 360.6(9)°, which indicates an essentially planar arrangement. The *trans*-angle O5-Mn1-O8 of 174.79(5)° between the coordinating oxygens of the triflate groups is nearly linear. For complex **20** the same trends in bond lengths and angles are observed as for complex **19**. The coordination polyhedra of the four independent molecules are almost C_2 symmetric. All piperidine rings of complexes **19** and **20** are best described as chair conformations.

Table 5. Selected bond lengths (Å) and angles (°) for **19** and **20**.

Complex **19**			Complex **20**			
Bond Length			Bond length			
			res x=1	res x=2	res x=3	res x=4
Mn1-N1	2.2312(11)	Mn1x-N1x	2.238(5)	2.232(5)	2.234(5)	2.226(5)
Mn1-N2	2.4166(11)	Mn1x-N2x	2.397(4)	2.421(4)	2.425(5)	2.401(5)
Mn1-N3	2.4453(11)	Mn1x-N3x	2.446(4)	2.431(4)	2.432(5)	2.443(5)
Mn1-O1	2.2547(9)	Mn1x-O1x	2.212(4)	2.216(4)	2.234(4)	2.219(4)
Mn1-O3	2.2283(11)	Mn1x-O2x	2.207(4)	2.217(4)	2.225(4)	2.224(4)
Mn1-O5	2.1693(10)	Mn1x-O3x	2.253(5)	2.206(4)	2.181(5)	2.266(4)
Mn1-O8	2.1894(10)	Mn1x-O6x	2.201(4)	2.271(4)	2.264(5)	2.198(4)
Angle			Angle			
			res x=1	res x=2	res x=3	res x=4
N1-Mn1-N2	71.80(4)	N1x-Mn1x-N2x	71.04(16)	71.07(17)	71.49(18)	71.49(17)
N1-Mn1-N3	70.68(4)	N1x-Mn1x-N3x	71.00(16)	71.01(17)	70.83(17)	70.76(17)
N2-Mn1-N3	142.34(4)	N2x-Mn1x-N3x	142.02(16)	141.99(17)	142.27(17)	142.24(16)
N2-Mn1-O1	69.64(4)	N2x-Mn1x-O1x	71.07(15)	70.99(15)	70.70(16)	70.74(16)
N3-Mn1-O3	70.93(4)	N3x-Mn1x-O2x	70.87(15)	71.04(16)	70.79(17)	70.84(16)
O1-Mn1-O3	77.55(4)	O1x-Mn1x-O2x	75.91(14)	75.83(15)	76.13(16)	76.05(16)
O5-Mn1-O8	174.97(5)	O3x-Mn1x-O6x	172.68(17)	171.73(16)	172.27(17)	173.01(16)

To investigate the effect of the substitution of the 5-membered pyrrolidine ring in the proline-based ligands by the six-membered piperidine ring on the steric surrounding around the manganese center, an overlay plot was prepared of the structure of piperidine complex **20** and the structure of the prolinol complex [Mn(**Py(ProOH)$_2$**)(OTf)$_2$], which was reported in chapter 2 (Figure 6).[1]

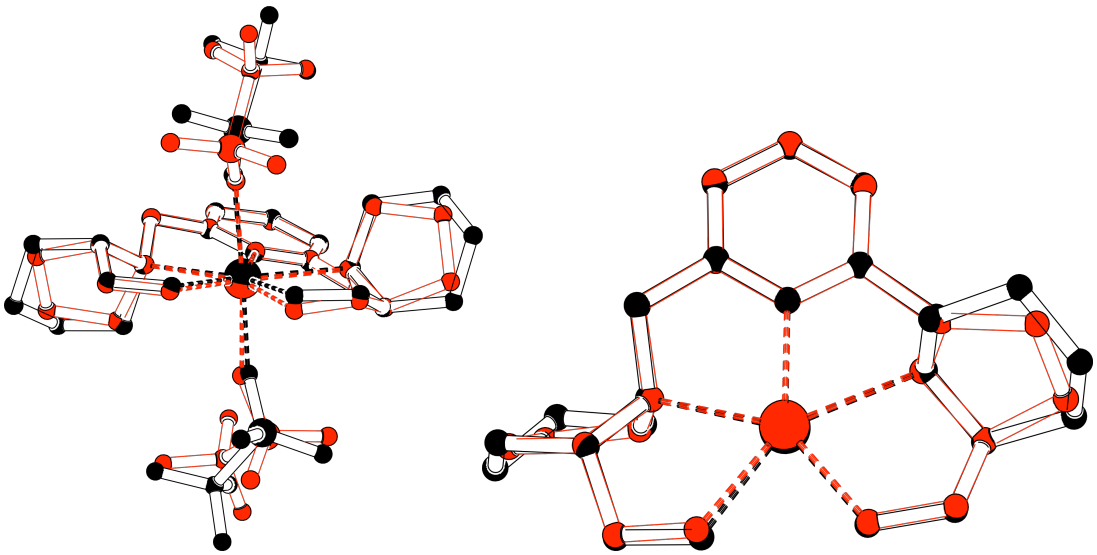

Figure 6. Crystal structure for complex **20** and [Mn(**Py(ProOH)$_2$**)(OTf)$_2$] placed on top of each other.

Figure 6 shows there is hardly any structural effect of the additional carbon atom in the piperidine rings on the surrounding of the manganese center. The size of the "active site" around manganese does not change significantly, and all the donor groups remain at almost the same position with respect to the manganese . The largest difference between the two structures is the folding of the ring of the nitrogen heterocycle. Based on this observation the substitution of the proline moiety by a substituted piperidine ring does not change the three-dimensional environment around the manganese center.

Vapor diffusion of Et_2O into a concentrated solution of complex [Mn(**Py(AzeMe)$_2$**(OTf)$_2$] (**21**) in MeCN lead to the formation of single crystals. The asymmetric unit of **21** contains the neutral complex **21-a**, the cationic compound **21-b**, and one non-coordinating triflate anion. The manganese complexes are shown in Figure 7. In both molecules the pyridine bis(azetidinate) ligand adopts a different structure than observed for any of the other **Py(ProR)$_2$** ligands.

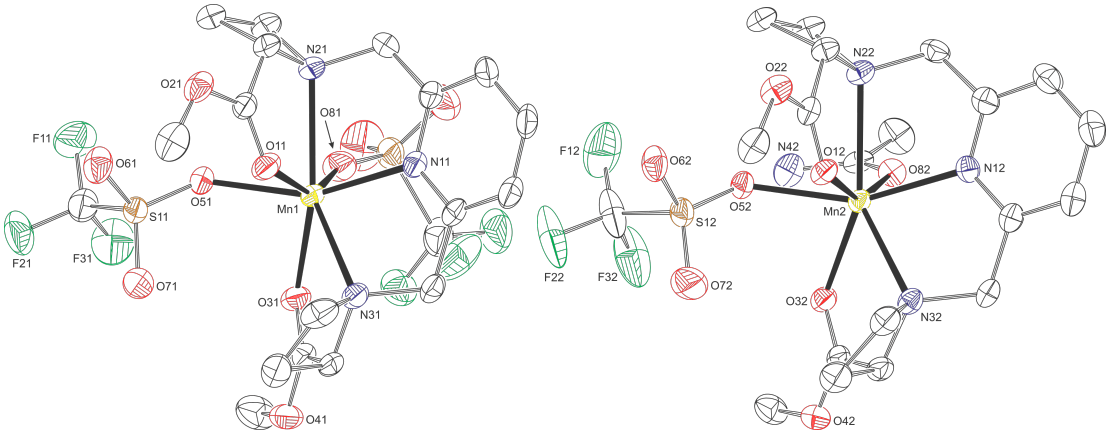

Figure 7. Displacement ellipsoid plot (50% probability) of the neutral molecule **21-a** (left) and the cationic **21-b** (right) in the asymmetric unit of crystal structure **21**. All hydrogen atoms are omitted for clarity.

Although both molecules are seven-coordinated manganese complexes, they do not adopt the pentagonal bipyramidal geometry as observed for the other seven-coordinated manganese complexes reported here. The neutral molecule **21-a** has a distorted geometry, which can be derived from a capped trigonal prism. The triangular faces are thereby O11-N11-N31 and O51-O81-O31, with atom N21 above one of the square faces. The two triangular planes are approximately parallel with an interplanar angle of 12.41(11)º. The cationic **21-b** shows a similar coordination geometry. Here, one triflate ligand is exchanged by an acetamide molecule. One triflate is now located in the crystal lattice and only connected by very weak C-H···O hydrogen bonds. In analogy to **21-a**, the trigonal prism in **21-b** is formed by the triangular faces O12-N12-N32 and O52-O82-O32. The interplanar angle between these faces is 5.71(10)º. The acetamide ligand is supposed to derive from the hydrolysis of acetonitrile solvent molecules, which may have been present as a contaminant in the solvent or may have formed under the influence of the Mn-complex. One N-H hydrogen atom of the acetamide moiety is involved in an intramolecular hydrogen bond to the coordinated triflate oxygen O52. The other N-H hydrogen atom forms an intermolecular hydrogen bond to triflate oxygen O91 of molecule **21-a**. In the IR spectrum of the complex after precipitation no free triflate group is visible. This would imply that the acetamide group is introduced during the crystallization.

The most apparent difference between these structures of **21** and the other seven-coordinated complexes described here is the position of the two labile, mono-dentate ligands in these structures. In **21** the mono-dentate ligands are found in a *cis*-position with respect to each other, while in all other complexes these are positioned in the axial (trans) positions of the overall pbp geometry. In relation to this geometrical change one of the ester groups in **21** occupies one of the axial position occupied by

one of the triflate groups in the other complexes. The other ester group is in-between axial and equatorial. As a result the C_2-like symmetry of the other complexes is not contained in **21**. Selected bond lengths and angles for the two molecules **21-a** and **21-b** are reported in Table 6.

Table 6. Selected bond lengths (Å) and angles (°) for both metal complexes in crystal structure **21**.

bis triflate complex (**21-a**)					
	Bond length		Angle		Angle
Mn1-N11	2.227(2)	N11-Mn1-N21	73.24(7)	N31-Mn1-O31	70.27(7)
Mn1-N21	2.409(2)	N11-Mn1-N31	72.19(7)	O11-Mn1-O31	127.10(7)
Mn1-N31	2.448(2)	N11-Mn1-O31	123.70(7)	O11-Mn1-O81	150.46(7)
Mn1-O11	2.3171(19)	N11-Mn1-O51	154.39(7)	O51-Mn1-O81	88.78(7)
Mn1-O31	2.2942(18)	N21-Mn1-N31	137.21(7)		
Mn1-O51	2.1771(18)	N21-Mn1-O11	72.18(7)		
Mn1-O81	2.1995(19)	N21-Mn1-O51	83.26(7)		
acetamide complex (**21-b**)					
	Bond length		Angle		Angle
Mn2-N12	2.224(2)	N12-Mn2-N22	72.45(7)	N32-Mn2-O32	72.22(7)
Mn2-N22	2.438(2)	N12-Mn2-N32	73.07(7)	O12-Mn2-O32	123.54(6)
Mn2-N32	2.420(2)	N12-Mn2-O32	129.68(7)	O12-Mn2-O82	151.89(6)
Mn2-O12	2.3090(17)	N12-Mn2-O52	154.33(7)	O52-Mn2-O82	97.21(6)
Mn2-O32	2.2543(17)	N22-Mn2-N32	137.71(7)		
Mn2-O52	2.2401(16)	N22-Mn2-O12	71.83(6)		
Mn2-O82	2.1617(17)	N22-Mn2-O52	83.35(6)		

The bond lengths and angles of the two structures do not show large differences. The largest difference is seen in the bond lengths between the coordinating triflates and acetamide groups. The Mn–O bond of the Mn-acetamide fragment (2.1617(17) Å) is significantly shorter than the other Mn–O bonds, while the Mn-O bond of the Mn-triflate fragment (2.2401(16) Å) in the acetamide structure is the shortest amongst these bonds. The O–Mn–O bond angles in the two structures are significantly different: in the acetamide structure this angle amounts to 97.21(6)°, while it is 88.78(7)° in the bis(triflate) structure. All other bond lengths and angles in the structures are very comparable. The azetidine rings in **21-a** and **21-b** are slightly bent with puckering amplitudes between 0.158(3) and 0.226(3) Å.

For manganese complex **18**, bearing bulky diphenylprolinol groups, no crystals suitable for structure determination could be obtained. On the other hand a crystal structure was obtained for the corresponding cobalt complex. This cobalt complex

[Co(**Py(ProPh$_2$OH)$_2$**)(CH$_3$CN)](OTf)$_2$ (**22**) was prepared via the reaction of one equivalent of ligand **PyProPh$_2$OH** (**5**) with cobalt triflate in a solvent mixture of acetonitrile and dichloromethane (1/1, v/v). Complex **22** was isolated as a gray/pink solid via precipitation with Et$_2$O. Crystals of this complex were obtained via vapor diffusion of Et$_2$O into a concentrated solution of the complex in MeCN.

The molecular structure of complex **22** represents a quite different geometry as the ones observed for the Mn complexes presented here (Figure 8). Instead of a seven-fold coordination number, the metal adopts a six-coordinated, distorted octahedral geometry. Although the **Py(ProPh$_2$OH)$_2$** ligand does act as a pentadentate ligand to cobalt in **22**, it shows a coordination mode that is different compared to the coordination of the other **Py(ProR)$_2$** ligands towards Mn reported here. While in the Mn-complexes the donor atoms arrange themselves within the equatorial coordination plane (with the exception of complexes **21-a** and **21-b**), the pentadentate ligand in **22** occupies 5 out of 6 positions in an octahedral complex, including the two formal axial positions. The presence of the bulky Ph$_2$OH groups seems to force the ligand to coordinate in this geometry. The remaining coordination position of the octahedral geometry is occupied by an acetonitrile solvent molecule, which coordinates in a position trans to the pyridine ring. The solid state IR spectrum of **22** taken before crystallization shows the presence of a coordinating triflate ion (1287 and 1235 (ν_{as} SO$_3$), 1222 (ν_s CF$_3$), 1161 (ν_{as} CF$_3$) and 1026 (ν_s SO$_3$) cm^{-1}). It is therefore likely that during crystallization from MeCN, a more strongly coordinating MeCN solvent molecule replaces the coordinating triflate.

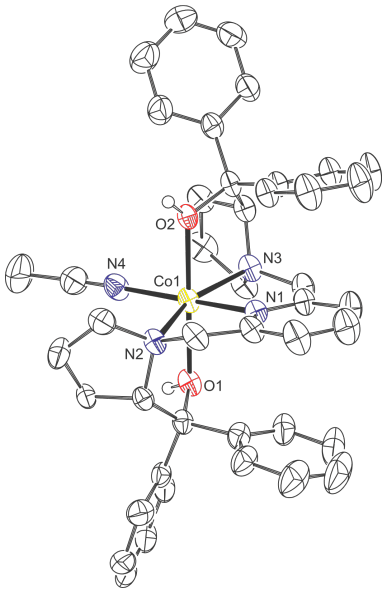

Figure 8. Molecular structure of complex **22** in the crystal. Displacement ellipsoid plot (50% probability). C-H hydrogen atoms, non-coordinated triflate anions, and non-coordinated acetonitrile are omitted for clarity.

The bond lengths and angles indicate that the coordination mode of the **Py(ProPh$_2$OH)$_2$** ligand around the cobalt center is almost symmetric (Table 7). The bond distances of Co1 to N2 and N3 are comparable and the same is true for the bond distances from Co1 to O1 and O2. The O1-Co1-O2 transoid angle of 174.37(8)° closely approaches the ideal value of 180°. The ideal angles for the octahedral geometry are not observed in **22** (e.g. N2–Co–N3 = 158.20(10)°) because of steric restriction of the ligand, which prevents its coordination in a perfect octahedral geometry. The same coordination behavior of the **Py(ProPh$_2$OH)$_2$** ligand was observed earlier for the corresponding iron complex.[3] Manganese complex **18** showed the same IR pattern as was observed for cobalt complex **22** (1281 and 1235 (ν_{as} SO_3), 1222 (ν_s CF_3), 1161 (ν_{as} CF_3) and 1026 (ν_s SO_3) cm^{-1}). Based on these data the coordination geometry of the corresponding manganese complex would be comparable.

Table 7. Selected bond lengths (Å) and angles (°) for **22**.

	Bond length		Angle		Angle
Co1-N1	2.029(3)	N1-Co1-N2	79.28(10)	N2-Co1-O2	106.07(9)
Co1-N2	2.213(3)	N1-Co1-N3	79.16(10)	N3-Co1-N4	104.67(11)
Co1-N3	2.204(2)	N1-Co1-N4	175.44(11)	N3-Co1-O1	98.16(9)
Co1-N4	2.071(3)	N1-Co1-O1	91.20(10)	N3-Co1-O2	77.90(9)
Co1-O1	2.178(2)	N1-Co1-O2	92.00(9)	N4-Co1-O1	90.69(11)
Co1-O2	2.148(2)	N2-Co1-N3	158.20(10)	N4-Co1-O2	86.47(10)
		N2-Co1-N4	97.01(11)	O1-Co1-O2	174.37(8)
		N2-Co1-O1	79.09(9)		

4.3 Oxidation catalysis

The catalytic properties of Mn-complexes **15**-**21** in oxidation reactions were tested in the epoxidation of olefins with the use of optimized reaction conditions from our previous studies, *i.e.* using H_2O_2 as the oxidant in acetone and with 5 equivalents of 4-methylimidazole as additive (Scheme 3). Catalytic runs were carried out at three different reagent ratios ranging from oxidant limiting conditions (Mn/oxidant/substrate, 1:500:1000) to substrate limiting conditions (1:500:100), and with cyclooctene and *trans*-beta-methylstyrene as benchmark substrates.

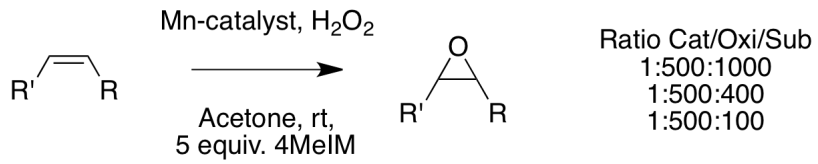

Scheme 3. General catalytic conditions.

A first activity screening was carried out with the proline-based complexes **15-18**, which differ in their ester side chains or the presence of bulky diphenylprolinol groups (Table 8).

Table 8. Catalytic epoxidations using complexes **15-18**.[a]

		TON[b]					
Complex		cyclooctene			*trans*-beta-methylstyrene (ee)		
	Conditions	1 hour	3 hour	1 night	1 hour	3 hour	1 night
15	1:500:1000	3.4	12.6	39.7	2.6 (5)	10.4 (15)	27.7 (14)
Py(ProPr)$_2$	1:500:400	3.0	11.1	42.7	1.7 (11)	9.2 (24)	27.3 (19)
	1:500:100	1.3	4.9	19.2	0.8 (20)	5.8 (27)	17.4 (33)
16	1:500:1000	13.8	46.2	73.3	18.9 (9)	32.6 (10)	25.7 (7)
Py(ProBn)$_2$	1:500:400	14.7	41.2	61.2	18.6 (26)	30.6 (19)	29.8 (17)
	1:500:100	6.5	20.4	27.1	14.3 (22)	21.0 (26)	ND (ND)
17	1:500:1000	0.9	0.8	1.4	0.0	1.1 (3)	0.5 (3)
Py(ProtBu)$_2$	1:500:400	0.4	0.4	1.0	0.0	0.2	0.7
	1:500:100	0.1	0.1	0.5	0.0	0.0	0.5
18	1:500:1000	1.3	1.4	1.3			
Py(ProPh$_2$OH)$_2$	1:500:400	0.3	0.6	0.6			
	1:500:100	0.1	0.2	0.4			

[a] Reaction conditions: see experimental section; [b] Activity depicted in turnover numbers: moles of product/moles of catalyst.

Among this set of complexes, complex **16** carrying benzyl ester moieties showed the best catalytic performance. In the best case, a TON of 73 was obtained for cyclooctene with the use of 1000 equivalents of substrate. Using 100 equivalents of substrate a TON of 27 was obtained, which corresponds to a conversion of 27%. The second best complex was complex **15** carrying propyl ester moieties. The two complexes with the bulky tBu ester and Ph_2OH side groups hardly gave any conversion towards the desired epoxide. At best 1.5 TON towards the epoxide using 1000 equivalents of cyclooctene was observed for both complexes.

The activity of the proline-derived complexes using oxidant limiting conditions (1:500:1000) and conditions (1:500:400) in which oxidant and substrate are present in

close to equal amounts are comparable. The same was also observed during the catalysis with the proline based [Mn(**Py(ProR)$_2$**)(OTf)$_2$] complex reported earlier by us (Chapter 2).[1] This means that the addition of more substrate has no real effect on the activity of the corresponding complexes.

The enantioselectivity in the epoxidation of *trans*-beta-methylstyrene is higher when a lower substrate loading was used. This same trend was also observed for the catalytic performance of the earlier reported complexes (Chapter 2).[1] With complex **15** an enantioselectivity of 33% was obtained at the lowest substrate loading (100 equiv.). This enantioselectivity is slightly lower than the enantioselectivity obtained with the Mn-complex derived from the corresponding methyl ester **Py(ProR)$_2$** ligand reported in Chapter 2. Enlarging the ester moieties to benzyl esters did not lead to a significant decrease in *ee*, however a further increase in size of the ester moieties turned out to be detrimental for catalytic activity and prevented a reliable *ee* analysis. During the catalytic reactions with *trans*-beta-methylstyrene also the formation of a small amount of benzaldehyde was detected. The amount of benzaldehyde varied between TON = 1 - 5 for the complexes **15** and **17**. For complex **16** a higher amount of benzaldehyde was formed. The amount seems to depend on the amount of substrate; the amount formed after 1 night going from the highest substrate loading to the lowest was 9.1, 5,3 and 4.0 respectively.

Next, the series of complexes **19-21** in which the ring size of the N-heterocyclic donor moieties is varied were tested in catalysis (Table 9). The piperidine-based complexes **19** and **20** hardly showed any activity in the epoxidation of both cyclooctene and *trans*-beta-methylstyrene. On the other hand the azetidine-based complex **21** turned out to be the most active complex in this study, in both the epoxidation of cyclooctene and *trans*-beta-methylstyrene. Next to the best activity, it also gave the highest enantioselectivity in the epoxidation of *trans*-beta-methylstyrene. In the reactions with cyclooctene as substrate, a conversion of 76% to the epoxide was obtained with **21** using 100 equiv. of substrate. Using *trans*-beta-methylstyrene as a substrate the best results were also obtained with the lowest substrate loading (100 equiv.). In the best case an *ee* of almost 40% was reached and a conversion to the epoxide of 75%. The observed ee was constant in time, which indicates that a single mechanism is operative for product formation. Also in this case some formation of benzaldehyde was observed. The amount formed after one night for complex **20** varied between TON = 0.5 - 5.1 at low or high substrate loadings, respectively, while for complex **21** after one night the amounts varied between TON = 1.8 - 2.9 respectively. These data show that **21** is a quite active and selective catalyst for the epoxidation of both aliphatic alkenes and styrenes.

Table 9. Catalytic epoxidations with complexes **19-21**.[a]

		TON[b]					
Complex		cyclooctene			*trans*-beta-methylstyrene (ee)		
	conditions	1 hour	3 hour	1 night	1 hour	3 hour	1 night
19	1:500:1000	1.2	1.0	1.0	0.0	0.0	0.0
$Py(PipMe)_2$	1:500:400	0.5	0.4	0.3	0.0	0.0	0.0
	1:500:100	0.2	0.1	0.1	0.0	0.0	0.0
20	1:500:1000	2.1	2.7	4.9	0.0	1.0	3.9(7)
$Py(PipOH)_2$	1:500:400	1.3	1.6	3.5	0.0	0.5	4.5(6)
	1:500:100	0.4	0.5	1.8	0.0	0.1	1.8(5)
21	1:500:1000	63.4	110.6	106.2	20.5(27)	48.6(29)	76.1(33)
$Py(AzeMe)_2$	1:500:400	54.4	120.6	119.7	25.8(34)	49.5(34)	94.8(36)
	1:500:100	33.8	66.0	75.7	15.6(39)	39.7(39)	74.2(39)

[a] For reaction conditions see experimental section; [b] Activity depicted in turnover numbers: moles of product/moles of catalyst.

4.4 Discussion

The series of Mn-complexes based on ligand variations around the parent **$Py(ProR)_2$** ligand design have shown some interesting relations between structure and activity in epoxidation reactions. The variation of the ester group in the parent **$Py(ProMe)_2$** ligand (from methyl to propyl, benzyl and tert-butyl) yielded highly similar seven-coordinated manganese complexes with a distorted pentagonal bipyramidal geometry around manganese, as judged by the structure of complex **15** derived from the propyl ester ligand. In the complexes, the ester tail of the proline moiety is pointing away from the manganese center and in that way is unlikely to influence the active site around manganese. The complexes derived from the $Py(ProPr)_2$ and **$Py(ProBn)_2$** ligands are active in epoxidation catalysis but are less active than the parent **$Py(ProMe)_2$** complex, while the **$Py(ProtBu)_2$** derived complex shows hardly any activity. In the latter case, steric hindrance could actually play a role, whereas in all these cases the low reactivity is possible due to the hydrolysis of the ester. The bulky diphenylprolinol complex **18** showed almost no catalytic activity. As shown by the structure of the corresponding octahedral cobalt complex, the structure of this complex is very different from the other complexes. Apparently, this coordination geometry does not provide access to active oxidation catalysts.

Changing the 5-membered heterocyclic ring in the proline-based ligands to either a piperidine or an azetidine ring leads to highly similar pentagonal bipyramidal structures in the former case, while in the latter case seven-coordinated manganese complexes are formed with a highly distorted geometry. Most strikingly, the structures derived from the **$Py(ProR)_2$** and **$Py(PipR)_2$** ligands bear labile sites in a

mutual *trans*-position, whereas in the structures derived from the **Py(AzeMe)$_2$** ligand these labile sites are *cis* with respect to each other. The smaller azetidine heterocycle in the **Py(AzeMe)$_2$** ligand is quite rigid with respect to its 5- and 6-membered congenders, which seems to prevent the meridional O,N,N,N,O coordination of the ligand due to ring strain. Due to this rigidity, the ligand cannot adopt the flattened structure to make it fit in the meridional plane and, consequently, the ester groups are forced to coordinate either in an axial or close to axial manner. In this way, the limited flexibility of the ligand overrules the electronic preference of the metal in determining the coordination geometry.

In fact, the number of documented coordination complexes that contain an azetidine donor ligand is limited (CSD search, 74 complexes). Amongst the chiral nitrogen heterocycles, azetidines seem to be the least well studied in coordination chemistry to date. In the examples that are reported the azetidines coordinate to palladium,[8-11] platinum,[8, 11,12] coper,[13-15] cobalt[16-18] or cadmium.[19] From these reports only a few report on catalytic studies done with these complexes, the resulting complexes are for instance used as chiral recognition reagent.[9] The catalytic reactions studied with these azetidine-based ligands include Suzuki-Miyaura cross-coupling,[10,20] Sonogashira cross-coupling,[21] and the addition of diethylzinc to aldehydes.[22] Furthermore, there are also some reports on complexes of azetidine carboxylic acids with cobalt, copper, zinc and nickel, in which the azetidines show the same coordination behavior (bidentate) as their proline analogues.[23,24]

The catalytic activity of the two piperidine complexes **19** and **20** is low and only a small amount of epoxide is formed. During the catalytic reactions with these complexes the formation of a brown solid was observed. This points to the formation of manganese oxide, which was not earlier observed with the other prepared complexes. Previously, we reported that manganese dioxide is not active in epoxidation catalysis.[26] While the decreased stability of these complexes under oxidizing conditions is not understood at this moment, the enlargement of the heterocyclic ring may affect the coordination strength of the N-donor. The importance of complex stability was further illustrated during a study on a series of related ligands (not shown). In these ligands either a phenyl ring or an ethyl bridge replaced the pyridine ring in the backbone of the **PyProMe** ligand. The Mn-complexes derived from these ligands are not active in the epoxidation of cyclooctene and *trans*-beta-methylstyrene, and release manganese oxide under epoxidation conditions. Apparently, the change in ligand backbone resulted in Mn-complexes with a lower kinetic stability upon treatment with H_2O_2. These observations indicate that in the absence of a sufficiently strongly chelating ligand, manganese ions will react with hydrogen peroxide to form manganese oxide, which is catalytically incompetent.

Azetidine-based complex **21** turned out as the most active epoxidation catalyst amongst the Mn-complexes tested in this study and outperforms the parent proline methyl ester complex.[1] In the best case with the lowest substrate loading (100 equiv.),

a conversion of 76% was reached for the epoxidation of cyclooctene and for *trans*-beta-methylstyrene a conversion of 75% was reached with an enantioselectivity of 40%. The difference in catalytic activity is likely related to the structure of this complex. As mentioned earlier in the structure of **21** two labile site are available in a *cis*-position, instead of a *trans*-position like in the other complexes. Another explanation for the higher activity may be found in the donor capacity of the N-heterocycle. However, it is difficult to characterize the donor strength of the heterocycles used through a single descriptor. Normally, when going to a smaller heterocycle by decreasing the number of methylene units in the ring a increase in nucleophilicity of the nitrogen atom is observed. This general rule counts for 'normal sized', i.e. five- and six-membered heterocycles, in the case of smaller heterocycles another factor comes into play. Due to ring strain in the smaller heterocycles, the nitrogen lone pair gets more s-character and with that its nucleophilic character decreases. Another way to differentiate the donor strength of the heterocycles used in this study is to consider the pK_a values of their conjugated acids; i.e. the more acidic the conjugated acid, the lower the donor strength of the heterocycle. The values for the heterocycles used in this study are; azetidine 11.29, pyrrolidine 11.31, and piperidine 11.22, they do not differ largely from each other. Based on these considerations, it could actually be the lower donor strength of the azetidine ring, as indicated by its lower nucleophilicity, which leads to the higher catalytic activity of azetidine complex **21**. Further investigations would be required to substantiate this explanation.

4.5 Concluding remarks

In search for chiral Mn-complexes derived from easily accessible chiral building blocks for the epoxidation of alkene substrates in total 7 different ligands derived on the benchmark ligand **Py(ProMe)$_2$** and their corresponding Mn-complexes have been examined. Most ligands show a highly similar coordination behavior towards manganese as was previously observed for the parent complex, a seven coordinated distorted pentagonal bipyramidal geometry comprising axial triflate ligands. The azetidine ligand **Py(AzeMe)$_2$**, however, provides a rather different and distorted 7-coordinated coordination geometry around manganese that creates two *cisoid* labile sites at the metal. The Mn-complex [Mn(OTf)$_2$(**Py(AzeMe)$_2$**)] turned out to be the most active catalysts amongst the complexes studied an outperforms the parent **Py(ProMe)$_2$** complex. Whereas this study has not provided access to a new class of highly enantioselective catalysts for the epoxidation of prochiral olefins, the catalytic properties of the azetidine-derived complex warrants further studies into the use of this largely non-explored heterocycle in coordination chemistry and homogeneous catalysis. Other applications of the complexes derived here may be in their use as MRI contrast agent for vascular imaging, as recently reported by the group of Ai for a

related manganese(II) complex based on a very similar mixed pyridine-piperidine ligand.[25]

4.6 Experimental section

General: Reactions with metal salts were carried out under an atmosphere of dry, oxygen-free N_2 using standard Schlenk techniques. Solvents were dried and freshly distilled prior to use. 2,6-bis(chloromethyl)pyridine,[27] $Mn(OTf)_2.2MeCN$,[5,28] and **Py(ProPh$_2$OH)$_2$ (5)**[3] were prepared according to previously published procedures. L-proline benzyl ester hydrochloride (**10**) and L-proline *tert* butyl ester hydrochloride (**11**) were bought commercially. Optical rotations ($[\alpha]_D^{21}$) were measured with a Perkin polarimeter 241. Elemental microanalyses were carried out by Mikroanalytisches Laboratorium Dornis and Kolbe, Mülheim a.d. Ruhr, Germany. Infrared spectra were recorded on a Perkin-Elmer Spectrum One FT-IR instrument. Solution IR spectra were recorded with a Mettler Toledo ReactIR^{TM} 1000 spectrometer with a SiComp^{TM} probe, which was fitted in a reaction vessel under N_2 atmosphere. ESI-MS was measured on a Waters LCT Premier XE. Solution magnetic moments were determined by Evans' NMR method in acetone-d_6/cyclohexane at 25 °C.[29,30] Gas chromatography analyses were performed on a Perkin-Elmer Autosystem XL GC (30m, PE-17 capillary column), a Perkin-Elmer Autosystem XL GC (25m*0.22mm, Lipodex_E) and a Perkin-Elmer Clarus 500 GC (30m, Econo-Cap EC-5) all with FID detector.

(S)-2-(^{n}Propoxycarbonyl)pyrrolidinium chloride (9): $SOCl_2$ (2.6 mL, 36 mmol) was added drop wise during 15 min to a solution of S-Proline (3.24 g, 28.1 mmol) in anhydrous nPrOH (20 mL) at 0 ºC. The white suspension was stirred and heated at 60 ºC overnight. The clear colorless solution was evaporated and dried in vacuo. The product was obtained as a slightly yellow oil a quantitative yield.
^{1}H NMR (400 MHz, $CDCl_3$, 25 °C): δ = 0.92 (t, 3H, $^3J_{HH}$ = 7.2 Hz, $CH_2CH_2CH_3$), 1.68 (sxt, 2H, $^3J_{HH}$ = 6.8 Hz, $CH_2CH_2CH_3$), 1.96-2.20 (m, 3H, CH_2 ring, γ and β to CO), 2.36-2.46 (m, 1H, CH_2 ring, β to CO), 3.42-3.62 (m, 2H, NCH_2 ring), 4.08-4.22 (m, 2H, $CH_2CH_2CH_3$), 4.40-4.50 (m, 1H, C*H* α to CO), 9.03 (s, b, 1H, N*H*H), 10.72 (s, b, 1H, NH*H*) ppm. ^{13}C {^{1}H} NMR (100 MHz, $CDCl_3$, 25 °C): δ = 10.4, 22.0, 23.8, 29.0, 46.1, 59.4, 68.6, 169.1 ppm. IR (solid) ν (cm^{-1}): 2965.4, 2879.0, 1690.4, 1739.8, 1560.4, 1458.4, 1396.4, 1354.3, 1222.8, 1092.6, 1057.4, 998.9, 968.5, 927.9, 903.7, 758.8, 676.1. $[\alpha]_D^{21}$ -43.3 deg cm^3 g^{-1} dm^{-1} (*c* 0.952, $CHCl_3$).

Py(ProPr)$_2$ (2): A white suspension of 2,6-bis(chloromethyl)pyridine (242 mg, 1.37 mmol), **9** (0.8 g, 4.13 mmol), NaI (83 mg, 0.55 mmol) and Na_2CO_3 (510.8 mg, 4.82 mmol) in anhydrous DMF (5 mL) was stirred at 60 ºC over night. The white suspension was taken up in H_2O and extracted with CH_2Cl_2. The organic phases were combined, washed with H_2O and a saturated solution of $NaHCO_3$ dried ($MgSO_4$),

filtered and evaporated. The product was purified by column chromatography (EtOAc/hexane 5/1). The product was obtained as yellow oil in 83% yield (0.48 g).
^{1}H NMR (400 MHz, $CDCl_3$, 25 °C): δ = 0.89 (t, 6H, $^{3}J_{HH}$ = 7.2 Hz, $CH_2CH_2CH_3$), 1.61 (q, 4H, $^{3}J_{HH}$ = 7.2 Hz, $CH_2CH_2CH_3$), 1.72-1.82 (m, 2H, CH_2 ring, γ to CO), 1.84-2.00 (m, 4H, CH_2 ring, β and γ to CO), 2.08-2.20 (m, 2H, CH_2 ring, β to CO), 2.46-2.54 (m, 2H, NC*H*H ring), 3.02-3.10 (m, 2H, NCH*H* ring), 3.36-3.42 (m, 2H, C*H* α to CO), 3.72 (d, 2H, $^{2}J_{HH}$ = 14.0 Hz, ArCH_2N), 3.96-4.05 (m, 4H, $CH_2CH_2CH_3$), 4.04 (d, 2H, $^{2}J_{HH}$ = 14 Hz, ArCH_2N), 7.32 (d, 2H, $^{3}J_{HH}$ = 7.6, Py*H*(3,5)), 7.58 (t, 1H, $^{3}J_{HH}$ = 7.6, Py*H*(4)) ppm. ^{13}C {^{1}H} NMR (100 MHz, $CDCl_3$, 25 °C): δ = 10.6, 22.2, 23.5, 29.5, 53.5, 60.3, 65.6, 66.3, 121.6, 137.0, 158.4, 174.7 ppm. IR (solid) ν (cm^{-1}): 2966.4, 2878.8, 2820.4, 1728.4, 1682.5, 1590.1, 1575.4, 1456.1, 1357.4, 1268.9, 1172.9, 1131.6, 1085.0, 1959.2, 992.2, 891.2, 793.5, 744.4. $[\alpha]_D^{21}$ -90.4 deg cm^3 g^{-1} dm^{-1} (*c* 0.784, $CHCl_3$). ESI-MS: m/z = 418.267 ($[M+H]^+$, calc. 418.271).

Py(ProBn)$_2$ (3): A white suspension of 2,6-bis(chloromethyl)pyridine (194 mg, 1.10 mmol), **10** (0.80 g, 3.31 mmol), NaI (66 mg, 0.46 mmol) and Na_2CO_3 (409 mg, 3.86 mmol) in anhydrous DMF (5 mL) was stirred at 60 ºC over night. The white suspension was taken up in H_2O and extracted with CH_2Cl_2. The organic phases were combined, washed with H_2O and a saturated solution of $NaHCO_3$ dried ($MgSO_4$), filtered and evaporated. The product was purified by column chromatography (EtOAc/hexane 5/1). The product was obtained as a slightly yellow oil in 75% yield (0.42 g).
^{1}H NMR (400 MHz, $CDCl_3$, 25 °C): δ = 1.72-1.82 (m, 2H, CH_2 ring, γ to CO), 1.84-2.02 (m, 4H, CH_2 ring, β and γ to CO), 2.08-2.20 (m, 2H, CH_2 ring, β to CO), 2.48-2-56 (m, 2H, NC*H*H ring), 3.02-3.10 (m, 2H, NCH*H* ring), 3.42-3.47 (m, 2H, C*H* α to CO), 3.74 (d, AB, 2H, $^{2}J_{HH}$ = 13.6 Hz, ArCH_2N), 4.03 (d, 2H, $^{2}J_{HH}$ = 13.6 Hz, ArCH_2N), 5.07 (d, 2H, $^{2}J_{HH}$ = 12.4 Hz, OCH_2Ph), 5.13 (d, AB, 2H, $^{2}J_{HH}$ = 12.4 Hz, OCH_2Ph), 7.26 (d, 2H, $^{3}J_{HH}$ = 7.6, Py*H*(3,5)), 7.28-7.34 (m, 10H, OCH$_2$*Ph*), 7.52 (t, 1H, $^{3}J_{HH}$ = 7.6, Py*H*(4)) ppm. ^{13}C {^{1}H} NMR (100 MHz, $CDCl_3$, 25 °C): δ = 23.6, 29.5, 53.6, 60.2, 65.4, 66.4, 121.7, 128.3, 128.4, 128.7, 136.2, 137.0, 158.2, 174.1 ppm. IR (solid) ν (cm^{-1}): 2959.8, 2877.6, 2817.9, 1730.8, 1589.9, 1575.3, 1498.0, 1455.7, 1356.6, 1263.4, 1211.0, 1162.6, 1129.0, 1082.8, 1029.3, 993.0, 906.6, 890.4, 803.8, 734.3, 696.1. $[\alpha]_D^{21}$ -74.9 deg cm^3 g^{-1} dm^{-1} (*c* 0.798, $CHCl_3$). ESI-MS: m/z = 514.263 ($[M+H]^+$, calc. 514.270).

Py(ProtBu)$_2$ (4): A white suspension of 2,6-bis(chloromethyl)pyridine (283 mg, 1.60 mmol), **11** (1.0 g, 4.81 mmol), NaI (96 mg, 0.64 mmol) and Na_2CO_3 (595 mg, 5.62 mmol) in anhydrous DMF (12 mL) was stirred at 60 ºC over night. The white suspension was taken up in H_2O and extracted with CH_2Cl_2. The organic phases were combined, washed with H_2O and a saturated solution of $NaHCO_3$ dried ($MgSO_4$),

filtered and evaporated. The product was purified by column chromatography (EtOAc/hexane 5/1). The product was obtained as yellow oil in 83% yield (0.59 g).
^{1}H NMR (400 MHz, $CDCl_3$, 25 °C): δ = 1.33 (s, 18H, C(C*H*)$_3$), 1.62-1.72 (m, 2H, CH_2 ring, γ to CO), 1.72-1.90 (m, 4H, CH_2 ring, β and γ to CO), 1.92-2.06 (m, 2H, CH_2 ring, β to CO), 2.34-2.44 (m, 2H, NC*H*H ring), 2.90-2.99 (m, 2H, NCH*H* ring), 3.14-3.22 (m, 2H, C*H* α to CO), 3.61 (d, 2H, $^2J_{HH}$ = 14.0 Hz, ArC*H*$_2$N), 3.99 (d, 2H, $^2J_{HH}$ = 14 Hz, ArC*H*$_2$N), 7.27 (d, 2H, $^3J_{HH}$ = 7.6, Py*H*(3,5)), 7.50 (t, 1H, $^3J_{HH}$ = 7.6, Py*H*(4)) ppm. ^{13}C {^{1}H} NMR (100 MHz, $CDCl_3$, 25 °C): δ = 23.4, 28.3, 29.4, 53.4, 60.3, 66.2, 80.7, 121.4, 137.0, 158.7, 173.6 ppm. IR (solid) ν (cm^{-1}): 2974.9, 2876.8, 2818.4, 1723.9, 1682.5, 1590.2, 1575.6, 1478.9, 1455.9, 1391.8, 1366.0, 1289.1, 1250.4, 1213.4, 1148.5, 1084.6, 1032.6, 991.8, 964.6, 845.0, 796.0, 766.5, 744.7. $[\alpha]_D^{21}$ 83.1 deg cm^3 g^{-1} dm^{-1} (*c* 0.744, $CHCl_3$). ESI-MS: m/z = 446.299 ([M+H]$^+$, calc. 446.302).

PipMe (12): $SOCl_2$ (0.51 mL, 6.97 mmol) was added drop wise during 15 min to a solution of L-Pipecolinic acid (0.75 g, 5.81 mmol) in anhydrous MeOH (15 mL) at 0 ºC. The white suspension was stirred and heated at 60 ºC for 1.5h. The solution was evaporated and the product was co-evaporated with toluene and dried in vacuo. The product was obtained as yellow/white solid in a quantitative yield.
^{1}H NMR (400 MHz, $CDCl_3$, 25 °C): δ = 1.52-1.64 (m, 1H, CH_2 ring, γ to CO), 1.78-1.92 (m, 2H, CH_2 ring, γ to CO and NCH$_2$C*H*H ring), 1.98-2.16 (m, 2H, CH_2 ring, β to CO and NCH$_2$CH*H* ring), 2.20-2.30 (m, 1H, CH_2 ring, β to CO), 3.04-3.18 (m, 1H, NC*H*H ring), 3.58-3.66 (m, 1H, NCH*H* ring), 3.82 (s, 3H, OCH_3), 3.90-3.98 (m, 1H, C*H* α to CO), 9.73 (s, b, 1H, N*H*H), 9.95 (s, b, 1H, NH*H*) ppm. ^{13}C {^{1}H} NMR (100 MHz, $CDCl_3$, 25 °C): δ = 21.7, 21.9, 25.8, 44.0, 53.4, 56.5, 168.9 ppm. IR (solid) ν (cm^{-1}): 2919.9, 2682.9, 2566.4, 2499.4, 2411.4, 1741.5, 1581.0, 1438.2, 1418.1, 1387.7, 1367.2, 1347.5, 1301.1, 1287.3, 1270.8, 1219.1, 1204.8, 1164.1, 1132.4, 1079.7, 1061.9, 1044.7, 1033.4, 988.0, 950.0, 920.4, 891.8, 846.4, 754.8, 688.9. $[\alpha]_D^{21}$ -4.5 deg cm^3 g^{-1} dm^{-1} (*c* 0.662, MeOH).

Py(PipMe)$_2$ (6): A solution of 2,6-bis(chloromethyl)pyridine (205 mg, 1.16 mmol) in MeOH (5 mL) was added to a solution of **12** (1,03 g, 5,76 mmol) in MeOH (5 mL). To this reaction mixture was added dropwise a solution of NaOH (279 mg, 6.97 mmol) in MeOH (5 mL) and the mixture was heated under reflux for 16h. After this the reaction mixture was evaporated. The product was dissolved in ether and washed with a saturated solution of $NaHCO_3$. The ether layers were collected, dried ($MgSO_4$), filtered and evaporated. The product was purified by column chromatography (EtOAc/MeOH 9/1). The product was obtained as yellow oil in 57% yield (0.26 g).
Anal. for $C_{21}H_{31}N_3O_4$: calc. C 64.76, H 8.02, N 10.79; found C 64.31, H 8.13, N 10.41. ^{1}H NMR (400 MHz, $CDCl_3$, 25 °C): δ = 1.32-1.42 (m, 2H, CH_2 ring, γ to CO), 1.50-1.64 (m, 6H, CH_2 ring, γ to CO and NCH$_2$C*H*$_2$ ring), 1.72-1.92 (m, 4H, CH_2 ring,

β to CO), 2.20-2.32 (m, 2H, NC*H*H ring), 2.92-3.03 (m, 2H, NCH*H* ring), 3.20-3.28 (m, 2H, C*H* α to CO), 3.60 (d, 2H, $^{2}J_{HH}$ = 14.8 Hz, ArCH_2N), 3.70 (s, 6H, OCH_3), 3.85 (d, 2H, $^{2}J_{HH}$ = 14.4 Hz, ArCH_2N), 7.36 (d, 2H, $^{3}J_{HH}$ = 7.6, Py*H*(3,5)), 7.60 (t, 1H, $^{3}J_{HH}$ = 7.6, Py*H*(4)) ppm. ^{13}C {^{1}H} NMR (100 MHz, $CDCl_3$, 25 °C): δ = 22.5, 25.5, 29.7, 50.7, 51.8, 62.3, 64.5, 121.4, 137.0, 158.3, 174.4 ppm. IR (solid) ν (cm^{-1}): 2936.1, 2855.8, 1733.0, 1590.8, 1575.3, 1455.5, 1436.4, 1367.2, 1278.7, 1260.9, 1190.6, 1162.8, 1128.1, 1061.1, 1011.1, 970.5, 784.2, 767.2. $[\alpha]_D^{21}$ -57.3 deg cm^3 g^{-1} dm^{-1} (*c* 0.545, MeCN). ESI-MS: m/z = 390.239 ($[M+H]^+$, calc. 390.239).

PipOH (13): L-Pipecolinic acid (0.75 g, 5.81 mmol) was added to a suspension of $LiAlH_4$ (330 mg, 8.71 mmol) in dry THF (10 mL) at ºC. The reaction mixture was refluxed for 2h, after which it was cooled to ambient temperature and quenched with 1.5 mL of a KOH solution (20%). The reaction mixture was filtered and the residue was refluxed again with new THF for 30 minutes. The hot mixture was filtered. The combined THF layers were dried ($MgSO_4$), filtrated and evaporated. Giving the product as slightly yellow oil in a quantitative yield.
^{1}H NMR (400 MHz, $CDCl_3$, 25 °C): δ = 1.02-1.14 (m, 1H, CH_2 ring, γ to CO), 1.22-1.42 (m, 2H, CH_2 ring, γ to CO and NCH_2CHH ring), 1.46-1.60 (m, 2H, CH_2 ring, β to CO and NCH_2CHH ring), 1.70-1.78 (m, 1H, CH_2 ring, β to CO), 2.52-2.62 (m, 2H, NCH_2 ring), 2.98-3.06 (m, 1H, C*H* α to CO), 3.32-3.36 (m, 1H, C*H*HOH), 3.46-3.52 (m, 1H, CH*H*OH) ppm. ^{13}C {^{1}H} NMR (100 MHz, $CDCl_3$, 25 °C): δ = 24.4, 26.3, 28.5, 46.5, 58.3, 66.3 ppm. IR (solid) ν (cm^{-1}): 3286.0, 2927.8, 2853.8, 1646.5, 1441.6, 1326.9, 1263.9, 1206.2, 1103.3, 1079.5, 1040.4, 993.0, 929.8, 844.1, 790.8. $[\alpha]_D^{21}$ +9.8 deg cm^3 g^{-1} dm^{-1} (*c* 0.72, $CHCl_3$).

Py(PipOH)$_2$ (7): 2,6-bis(chloromethyl)pyridine (76 mg, 0.43 mmol) and **13** (200 mg, 1.74 mmol) were dissolved in CH_2Cl_2. To this solution K_2CO_3 (360 mg. 2.6 mmol) in H_2O (3 mL) was added, followed by the addition of $[nBu_4N]Cl$ (12 mg, 0.043 mmol). The resulting mixture was vigorously stirred under reflux for 16h. The two layers were separated and the water layer was extracted with CH_2Cl_2 (2x). The combined organic layers were dried ($MgSO_4$), filtrated and evaporated. The product was purified by column chromatography (EtOAc/MeOH 1/1). The product could be isolated as orange oil in 36% yield (105 mg).
^{1}H NMR (400 MHz, $CDCl_3$, 25 °C): δ = 1.20-1.32 (m, 2H, CH_2 ring, γ to CO), 1.38-1.62 (m, 8H, CH_2 ring, β to CO and CH_2 ring, γ to CO and NCH_2CH_2 ring), 1.64-1.92 (m, 2H, CH_2 ring, β to CO), 2.14-2.22 (m, 2H, NC*H*H ring), 2.42-2.48 (m, 2H, C*H* α to CO), 2.76-2.84 (m, 2H, NCH*H* ring), 3.58-3.64 (m, 2H, CH_2OH), 3.71 (d, 2H, $^{2}J_{HH}$ = 14.8 Hz, ArCH_2N), 3.73-3.78 (m, 2H, CH_2OH), 4.00 (d, 2H, $^{2}J_{HH}$ = 14.4 Hz, ArCH_2N), 7.13 (d, 2H, $^{3}J_{HH}$ = 7.6, Py*H*(3,5)), 7.60 (t, 1H, $^{3}J_{HH}$ = 7.6, Py*H*(4)) ppm. ^{13}C {^{1}H} NMR (100 MHz, $CDCl_3$, 25 °C): δ = 24.1, 25.0, 28.6, 52.9, 58.9, 62.4, 64.2,

121.9, 137.5, 158.3 ppm. IR (solid) ν (cm^{-1}): 3265.6, 2928.8, 2855.1, 1735.9, 1592.3, 1575.5, 1454.6, 1441.6, 1371.9, 1337.1, 1291.4, 1265.3, 1153.4, 1059.6, 1037.5, 996.2, 927.8, 874.3, 769.4. $[\alpha]_D^{21}$ -70.3 deg cm^3 g^{-1} dm^{-1} (*c* 0.3, MeCN). ESI-MS: m/z = 334.247 ($[M+H]^+$, calc. 334.250).

AzeMe (14): $SOCl_2$ (0.22 mL, 2.97 mmol) was added drop wise during 15 min to a solution of L-azetidine-2-carboxylic acid (0.25 g, 2.47 mmol) in anhydrous MeOH (5 mL) at 0 ºC. The clear colorless solution was stirred and heated at 60 ºC for 1.5h. The solution was evaporated and the product was co-evaporated with toluene and dried in vacuo. The product was obtained as colorless oil in a quantitative yield.
^{1}H NMR (400 MHz, $CDCl_3$, 25 °C): δ = 2.66-2.88 (m, 2H, CH_2 ring, β to CO), 3.83 (s, 3H, OCH_3), 4.06-4.28 (m, 2H, NCH_2 ring), 5.14-5.26 (m, 1H, C*H* α to CO), 9.44 (s, b, 1H, N*H*H), 10.0 (s, b, 1H, NH*H*) ppm ^{13}C {^{1}H} NMR (100 MHz, $CDCl_3$, 25 °C): δ = 23.0, 44.0, 53.7, 57.5, 168.7 ppm. IR (solid) ν (cm^{-1}): 2852.7, 2604.4, 2417.9, 1740.9, 1563.2, 1439.1, 1381.4, 1251.3, 1224.5, 1052.8, 995.4, 972.0, 928.5, 856.9, 804.3, 757.7, 709.9. $[\alpha]_D^{21}$ -80.6 deg cm^3 g^{-1} dm^{-1} (*c* 0.45, MeCN).

Py(AzeMe)$_2$ (8): A white suspension of 2,6-bis(chloromethyl)pyridine (59 mg, 0.33 mmol), **14** (1.52 mg, 1.0 mmol), NaI (20 mg, 0.13 mmol) and Na_2CO_3 (124 mg, 1.17 mmol) in anhydrous DMF (6 mL) was stirred at 60 ºC over night. The white suspension was taken up in H_2O and extracted with CH_2Cl_2. The organic phases were combined, washed with H_2O and a saturated solution of $NaHCO_3$ dried ($MgSO_4$), filtered and evaporated. The product was obtained as yellow/orange oil in 94% yield (105 mg).
^{1}H NMR (400 MHz, $CDCl_3$, 25 °C): δ =2.17-2.26 (m, 2H, CH_2 ring, β to CO), 2.30-2.39 (m, 2H, CH_2 ring, β to CO), 2.97-3.06 (m, 2H, NCH_2 ring), 3.32-3.40 (m, 2H, NCH_2 ring), 3.58 (s, 6H, OCH_3), 3.68-3.71 (m, 2H, ArCH_2N), 3.84-3.90 (m, 3H, C*H* α to CO and ArCH_2N), 7.19 (d, 2H, $^3J_{HH}$ = 7.6, Py*H*(3,5)), 7.54 (t, 1H, $^3J_{HH}$ = 7.6, Py*H*(4)) ppm. ^{13}C {^{1}H} NMR (100 MHz, $CDCl_3$, 25 °C): δ = 22.1, 51.5, 51.9, 63.8, 64.9, 121.5, 137.1, 157.2, 173.2 ppm. IR (solid) ν (cm^{-1}): 3005.8, 2952.7, 2840.4, 1735.8, 1676.2, 1641.2, 1590.6, 1576.9, 1455.8, 1435.4, 1348.3, 1227.1, 1198.5, 1174.2, 1134.0, 1095.4, 1053.6, 1034.8, 993.0, 961.6, 915.8, 794.6, 766.3, 706.9. $[\alpha]_D^{21}$ -58.0 deg cm^3 g^{-1} dm^{-1} (*c* 0.52, MeCN) ESI-MS: m/z = 334.173 ($[M+H]^+$, calc. 334.177).

[Mn(Py(ProPr)$_2$(OTf)$_2$] (15): A slightly yellow/beige solution of Mn(OTf)$_2$.2MeCN (272 mg 0.63 mmol,) in acetonitrile (5 mL) was added to a yellow solution of Py(ProPr)$_2$ (**2**) (288.2 mg 0.69 mmol,) in acetonitrile (5 mL). After the addition the reaction mixture was yellow of color. The reaction mixture was stirred for 1h at ambient temperature, followed by evaporation of the solvent *in vacuo*. The remaining yellow/white solid/foam was dissolved in a minimal amount of dry dichloromethane

and precipitated by addition of dry diethyl ether affording an off white solid in 68% yield (327 mg). Crystals suitable for X-ray crystal structure determination were obtained by slow evaporation of the remaining dichloromethane diethyl ether solution. IR (solid) ν (cm^{-1}): 2974.0, 2883.0, 1683.0, 1607.6, 1580.3, 1469.8, 1407.3, 1383.4, 1352.4, 1303.2, 1233.1, 1216.8, 1160.4, 1026.8, 972.4, 939.2, 884.1, 839.1, 799.8, 760.0. $[\alpha]_D^{21}$ -39.1 deg cm^3 g^{-1} dm^{-1} (*c* 0.522, $CHCl_3$). ESI-MS: m/z = 621.153 ($[M\text{-}OTf]^+$, calc. 621.152).

[Mn(Py(ProBn)$_2$(OTf)$_2$] (16): A slightly yellow/beige solution of $Mn(OTf)_2$.2MeCN (134.3 mg 0.31 mmol,) in acetonitrile (5 mL) was added to a yellow solution of $Py(ProBn)_2$ (**3**) (175 mg 0.34 mmol,) in acetonitrile (5 mL). After the addition the reaction mixture was yellow of color. The reaction mixture was stirred for 1h at ambient temperature, followed by evaporation of the solvent *in vacuo*. The remaining white foam was dissolved in a minimal amount of dry dichloromethane and precipitated by addition of dry hexane and stored in the fridge for 48 hours, affording an off white solid in 64% yield (171 mg). IR (solid) ν (cm^{-1}): 2964.1, 1682.6, 1607.4, 1580.9, 1498.7, 1456.6, 1399.1, 1346.0, 1306.7, 1234.4, 1218.0, 1160.4, 1084.1, 1027.6, 954.2, 925.6, 835.8, 797.6, 755.2, 699.0. $[\alpha]_D^{21}$ -82.9 deg cm^3 g^{-1} dm^{-1} (*c* 0.284, $CHCl_3$). ESI-MS: m/z = 717.149 ($[M\text{-}OTf]^+$, calc. 717.153).

[Mn(Py(ProtBu)$_2$(OTf)$_2$] (17): A slightly yellow/beige solution of $Mn(OTf)_2$.2MeCN (175 mg 0.40 mmol,) in acetonitrile (5 mL) was added to a slightly yellow solution of $Py(ProtBu)_2$ (**4**) (198 mg 0.44 mmol,) in acetonitrile (5 mL). After the addition the reaction mixture was slightly yellow of color. The reaction mixture was stirred for 1h at ambient temperature, followed by evaporation of the solvent *in vacuo*. The remaining white oil/foam was dissolved in a minimal amount of dry acetonitrile and tried to precipitate by the addition of dry ether, no precipitate was formed. All the solvent was evaporated and the complex was isolated as a white solid in quantitative yield (334 mg).
IR (solid) ν (cm^{-1}): 3354.5, 2984.5, 1670.5, 1604.9, 1579.1, 1468.1, 1386.6, 1373.0, 1355.5, 1307.7, 1278.9, 1235.3, 1217.4, 1153.2, 1098.8, 1056.3, 1028.3, 927.4, 854.6, 827.8, 800.0, 782.1, 759.3, 737.2. $[\alpha]_D^{21}$ -42.8 deg cm^3 g^{-1} dm^{-1} (*c* 0.544, $CHCl_3$). ESI-MS: m/z = 649.180 ($[M\text{-}OTf]^+$, calc. 649.184).

[Mn(Py(ProPh$_2$OH)$_2$(OTf)]OTf (18): A slightly yellow/beige solution of $Mn(OTf)_2$.2MeCN (97 mg 0.22 mmol,) in acetonitrile (5 mL) was added to a white suspension of $Py(ProPh_2OH)_2$ (**5**) (150 mg 0.25 mmol,) in acetonitrile (5 mL). After the addition the reaction mixture was clear slightly green of color. The reaction mixture was stirred for 1.5 h at ambient temperature, followed by evaporation of the solvent *in vacuo*. The remaining green solid/foam was dissolved in a minimal amount

of dry acetonitrile and precipitated by addition of dry diethyl ether affording an green solid in 97% yield (209 mg). IR (solid) ν (cm^{-1}): 3342.9, 3063.1, 2975.7, 2891.8, 1662.1, 1608.0, 1585.4, 1495.0, 1469.9, 1450.0, 1431.7, 1280.9, 1234.5, 1222.0, 1161.4, 1060.6, 1025.8, 913.5, 886.0, 853.9, 778.1, 745.9, 705.8. $[\alpha]_D^{21}$ +0.3 deg cm^3 g^{-1} dm^{-1} (*c* 0.37, MeCN). ESI-MS: m/z = 813.232 ($[M\text{-}OTf]^+$, calc. 813.226).

[Mn(Py(PipMe)$_2$(OTf)$_2$] (19): A slightly yellow/beige solution of $Mn(OTf)_2.2MeCN$ (101 mg 0.23 mmol,) in acetonitrile (2.5 mL) was added to a slightly yellow solution of $Py(PipMe)_2$ (**6**) (100 mg 0.26 mmol,) in acetonitrile (2.5 mL). After the addition the reaction mixture was slightly yellow of color. The reaction mixture was stirred for 1h at ambient temperature, followed by evaporation of the solvent *in vacuo*. The remaining white solid was dissolved in a minimal amount of dry acetonitrile and precipitated by addition of dry ether, an white solid was isolated in 65% yield (112 mg). Crystals suitable for X-ray analysis were obtained via solvent diffusion of the Et_2O/MeCN mixture after precipitation.
Anal. for $C_{23}H_{31}F_6Mn_1N_3O_{10}S_2$: calc. C 37.20, H 4.21, N 5.66; found C 37.12, H 4.37, N 5.65. IR (solid) ν (cm^{-1}): 2950.6, 2868.9, 1771.9, 1682.6, 1605.6, 1576.6, 1453.7, 1386.6, 1362.5, 1310.4, 1235.6, 1212.8, 1158.3, 1131.4, 1116.1, 1095.2, 1066.9, 1021.3, 1010.5, 989.9, 955.1, 922.0, 904.4, 871.8, 852.9, 825.8, 810.2, 780.7, 761.3. $[\alpha]_D^{21}$ -43.3 deg cm^3 g^{-1} dm^{-1} (*c* 0.3, MeCN).

[Mn(Py(PipOH)$_2$(OTf)$_2$] (20): A slightly yellow/beige solution of $Mn(OTf)_2.2MeCN$ (89 mg 0.20 mmol,) in acetonitrile (5 mL) was added to a slightly orange solution of $Py(PipOH)_2$ (**7**) (105 mg 0.31 mmol,) in acetonitrile (5 mL). After the addition the reaction mixture was orange of color. The reaction mixture was stirred for 1.5h at ambient temperature, followed by evaporation of the solvent *in vacuo*. The remaining orange oil/solid was dissolved in a minimal amount of dry acetonitrile and precipitated by addition of dry ether, an light brown solid was isolated in 64% yield (90 mg). Crystals suitable for X-ray analysis were obtained via solvent diffusion of the Et_2O/MeCN mixture after precipitation.
IR (solid) ν (cm^{-1}): 3407.1, 2956.1, 1605.1, 1578.0, 1461.1, 1312.8, 1290.2, 1260.6, 1234.5, 1218.9, 1172.9, 1156.9, 1051.7, 1028.0, 994.8, 927.4, 892.5, 868.5, 849.4, 800.1, 773.5. $[\alpha]_D^{21}$ -39.3 deg cm^3 g^{-1} dm^{-1} (*c* 0.24, MeOH). ESI-MS: m/z = 537.136 ($[M\text{-}OTf]^+$, calc. 537.132).

[Mn(Py(AzeMe)$_2$(OTf)$_2$] (21): A slightly yellow/beige solution of $Mn(OTf)_2.2MeCN$ (108 mg 0.25 mmol,) in acetonitrile (3 mL) was added to a slightly yellow solution of $Py(AzeMe)_2$ (**8**) (92 mg 0.27 mmol,) in acetonitrile (7 mL). After the addition the reaction mixture was yellow of color. The reaction mixture was stirred for 1.5h at ambient temperature, followed by evaporation of the solvent *in vacuo*. The remaining orange/yellow oil/foam was dissolved in a minimal amount of dry acetonitrile and

precipitated by addition of dry ether, a white turbid solution was formed. The solvent was evaporated and the product was isolated as a white solid 95% yield (161 mg). Crystals suitable for X-ray analysis were obtained via vapor diffusion of Et_2O into a solution of complex 21 in MeCN.
IR (solid) ν (cm^{-1}): 3359.1, 2965.9, 1688.7, 1664.2, 1607.2, 1581.6, 1448.7, 1385.1, 1302.2, 1261.8, 1233.5, 1214.9, 1158.0, 1088.5, 1025.9, 974.5, 908.5, 797.5, 761.2, 726.4. $[\alpha]_D^{21}$ -2.25 deg cm^3 g^{-1} dm^{-1} (*c* 0.36, MeCN). ESI-MS: m/z = 537.059 ($[M-OTf]^+$, calc. 537.059).

[Co(Py(ProPh$_2$OH)$_2$)(OTf)]OTf (22): A clear pink solution of $Co(OTf)_2$ (88 mg 0.25 mmol,) in acetonitrile (10 mL) was added to a slightly yellow solution of Py(ProPh$_2$OH)$_2$ (**5**) (150 mg 0.25 mmol,) in dichloromethane (10 mL). After the addition the reaction mixture was clear purple of color. The reaction mixture was stirred for 1 h at ambient temperature, followed by evaporation of the solvent *in vacuo*. The remaining purple oil/solid was dissolved in a minimal amount of dry acetonitrile and precipitated by addition of dry diethyl ether affording a gray/pink solid in good yield. Crystals suitable for X-ray analysis were obtained via vapor diffusion of Et_2O into a solution of complex 22 in MeCN.
IR (solid) ν (cm^{-1}): 3268.7, 1587.7, 1495.0, 1474.0, 1450.2, 1432.6, 1286.8, 1235.2, 1222.6, 1160.9, 1057.9, 1026.3, 1001.0, 914.4, 884.6, 849.6, 782.2, 745.1, 706.7, 663.2. $[\alpha]_D^{21}$ +59.6 deg cm^3 g^{-1} dm^{-1} (*c* 0.314, MeCN). ESI-MS: m/z = 817.222 ($[M-OTf]^+$, calc. 817.221).

General oxidation procedure: To a solution of catalyst (3.5 μmol) in acetone (2 mL) was added alkene (1.4 mmol, 400 equiv.) and 4-methylimidazole (17.5 μmol, 5 equiv.) in acetone (0.8 mL) followed by slow drop wise addition of 0.5 mL of 3.5 M H_2O_2 solution in acetone (1.75 mmol, 500 equiv., diluted from 35% aqueous H_2O_2) over 30 min. The reaction mixture was stirred at ambient temperature and after 1 hour (from start of oxidant addition) internal standard (10 μL, cyclooctene: 1,2-dibromobenzene, all other substrates: bromobenzene) was added and the first sample was taken. After three hours a second sample was taken from the reaction mixture. To the aliquots of the reaction mixture was added Et_2O and these solutions were analyzed by GC. The products were identified and quantified by GC by comparison with authentic compounds. The reported values are the average of at least two independent runs.

X-ray crystal structure determinations: Reflections were measured on a Nonius KappaCCD diffractometer with rotating anode and graphite monochromator (λ = 0.71073 Å). Intensity data were integrated with Eval15[31] (compounds **15**, **19**, **20**), HKL2000[32] (compound 21) or Eval14[33] (compound 22). Absorption correction and

scaling was performed based on multiple measured reflections with SADABS.[34] The structures were solved by Direct Methods using the programs SHELXS-97[35] (**15**, **19**, **20**, **21**) or SIR-97[36] (**22**). Least-squares refinement was performed with SHELXL-97[35] against F^2 of all reflections. Non-hydrogen atoms were refined freely with anisotropic displacement parameters. Hydrogen atoms were introduced in calculated positions (**15**, **20**, **22**) or located in difference Fourier maps (**19**, **21**). C-H hydrogen atoms were refined with a riding model. The O-H hydrogen atoms in **20** were refined with a riding model, the N-H hydrogen atoms in **21** were refined freely with isotropic displacement parameters. The O-H hydrogen atoms of **22** were located in difference Fourier maps and kept fixed on their located position. Geometry calculations and checking for higher symmetry were performed with the PLATON program.[37] Further details of the crystal structure determinations are given in Table 10.

Compound 15: One proline ring, one triflate ligand and one ester moiety were refined with disorder models, respectively. The co-crystallized diethyl ether molecule was refined with a partial occupancy of 0.25. Restraints for distances, angles and displacement parameters were used for the disordered and partially occupied groups.

Compound 20: The crystal structure was refined as *pseudo*-orthorhombic twin with a twofold rotation about hkl=(001) as twin operation. The twin fraction refined to BASF = 0.3134(10). One of the triflate ligands was refined with a disorder model. Restraints for distances and angles were used in the disordered moiety.

Compound 22: One on the non-coordinated triflate anions was refined with a disorder model. Restraints for distances and angles were used in the disordered moiety. Restraints for displacement parameters were used for the disordered triflate and the non-coordinated acetonitrile.

Table 10. Details of the X-ray crystal structure determinations.

	15	**19**	**20**
formula	$C_{25}H_{35}F_6MnN_3O_{10}S_2 \cdot 0.25(C_4H_{10}O)$	$C_{23}H_{31}F_6MnN_3O_{10}S_2$	$C_{21}H_{31}F_6MnN_3O_8S_2$
Fw	789.15	742.57	686.55
crystal color	colorless	colorless	colorless
crystal size [mm^3]	0.60 × 0.51 × 0.36	0.30 × 0.25 × 0.21	0.54 × 0.43 × 0.12
T [K]	150(2)	150(2)	150(2)
crystal system	monoclinic	triclinic	monoclinic
space group	C2 (no. 5)	P1 (no. 1)	$P2_1$ (no. 4)
a [Å]	36.5534(14)	9.2988(4)	9.32357(7)
b [Å]	10.6920(3)	9.4491(3)	63.3559(8)
c [Å]	9.4292(2)	10.3882(4)	9.63623(11)
α [°]	-	81.988(2)	-
β [°]	96.304(1)	68.402(1)	90.022(1)
γ [°]	-	64.899(1)	-
V [$Å^3$]	3662.9(2)	768.38(5)	5692.15(11)
Z	4	1	8
D_{calc} [g/cm^3]	1.431	1.605	1.602
$(\sin\theta/\lambda)_{max}$ [$Å^{-1}$]	0.65	0.65	0.65
refl. measured/unique	39540 / 8420	21834 / 7053	60393 / 23997
parameters / restraints	522 / 303	410 / 3	1499 / 63
R1/wR2 [I>2σ(I)]	0.0392 / 0.1113	0.0191 / 0.0486	0.0554 / 0.1423
R1/wR2 [all refl.)]	0.0429 / 0.1148	0.0198 / 0.0490	0.0602 / 0.1472
Flack x[38]	-0.002(15)	0.002(6)	-0.001(14)
EXTI	-	0.0043(8)	-
S	1.072	1.039	1.072
ρ(min/max) [$eÅ^{-3}$]	-0.46 / 1.10	-0.22 / 0.28	-0.98 / 1.09

	21	**22**
formula	$[C_{20}H_{28}F_3MnN_4O_8S]$ $[C_{19}H_{23}F_6MnN_3O_{10}S_2]$ (CF_3O_3S)	$[C_{43}H_{46}CoN_4O_2]$ $(CF_3O_3S) \cdot C_2H_3N$
Fw	1432.00	1048.96
crystal color	colorless	purple
crystal size [mm^3]	0.30 × 0.27 × 0.09	0.45 × 0.18 × 0.18
T [K]	110(2)	150(2)
crystal system	monoclinic	orthorhombic
space group	$P2_1$ (no. 4)	$P2_12_12_1$ (no. 19)
a [Å]	9.1265(1)	14.2613(3)
b [Å]	16.7561(1)	15.6080(4)
c [Å]	19.2434(2)	21.4539(5)
β [°]	101.4999(3)	-
V [Å^3]	2882.71(5)	4775.4(2)
Z	2	4
D_{calc} [g/cm^3]	1.649	1.459
$(\sin\theta/\lambda)_{max}$ [Å^{-1}]	0.65	0.65
refl. measured/unique	77068 / 13255	71928 / 10621
parameters / restraints	788 / 1	696 / 333
R1/wR2 [I>2σ(I)]	0.0327 / 0.0753	0.0456 / 0.1019
R1/wR2 [all refl.)]	0.0416 / 0.0788	0.0664 / 0.1109
Flack x[38]	0.008(9)	0.005(13)
S	1.028	1.056
ρ(min/max) [eÅ^{-3}]	-0.39 / 0.60	-0.28 / 0.44

References

1. Moelands *et al.* manuscript in preparation (Chapter 2 of this thesis).
2. Gosiewska, S.; Cornelissen, J.J.L.M.; Lutz, A.L.; Spek, A.L.; van Koten, G.; Klein Gebbink, R.J.M. *Inorg. Chem.* **2006**, *45*, 4214-4227.
3. Gosiewska, S.; Lutz, M.; Spek, A.L.; Klein Gebbink, R.J.M. *Inorg. Chim. Acta* **2007**, *360*, 405-417.
4. Chelucci, G.; Falorni, M.; Giacomelli, G. *Tetrahedron-Asymmetr.* **1990**, *1*, 843.
5. Bryan, P.S.; Dabrowiak, J.C. *Inorg. Chem.* **1975**, *14*, 296-299
6. Bergström, P.Å.; French, R. *J. Phys. Chem.* **1995**, *99*, 12603-12611.
7. (a) Aresta, M.; Quaranta, E.; Albinati, A. *Organometallics* **1993**, *12*, 2032-2043. (b) Aresta, M.; Dibenedetto, A.; Amodio, E.; Papai, I.; Schubert, G. *Inorg. Chem.* **2002**, *41*, 6550-6552.
8. Voureka, E.; Tsangaris, J.M. *Transition Met. Chem.* **1996**, *21*, 244-249.
9. Marinetti, A.; Hubert, P.; Genêt, J.-P. *Eur. J. Org. Chem.* **2000**, 1815-1830.

10. Keller, L.; Sanchez, M.V.; Prim, D.; Couty, F.; Evano, G.; Marrot, J. *J. Organomet. Chem.* **2005**, *690*, 2306-2311.
11. Bertani, R.; Mozzon, M.; Benetollo, F.; Bombieri, G.; Michelin, R.A. *J. Chem. Soc., Dalton Trans.* **1990**, 1197.
12. Goto, M.; Tsutsui, H.; Matsuda, S.; Tanaka, Y.; Tsuruda, N.; Kurosaki, H. *Chem. Pharm. Bull.* **2004**, *52*, 47.
13. Nomoto, K.; Mino, Y.; Ishida, T.; Yoshioka, H.; Ota, N.; Inoue, M.; Takagi, S.; Takemoto, T. *Chem. Commun.* **1981**, 338
14. Mino, Y.; Ishida, T.; Ota, N.; Inoue, M.; Nomoto, K.; Yoshioka, H.; Takemoto, T.; Sugiura, Y.; Tanaka, H. *Inorg. Chem.* **1981**, 20, 3440.
15. Lee, Y.H.; Kim, H.Y.; Thuery, P.; Harrowfield, J.M.; Lim, W.T.; Kim, B.J.; Kim, Y. *J. Inclusion Phenom. Macrocyclic Chem.* **2009**, *65*, 65.
16. Geue, R.J.; McCarthy, M.G.; Sargeson, A.M.; Jorgensen, P.; Hazell, R.G.; Larsen, F.K. *Inorg. Chem.* **1985**, *24*, 2559.
17. Gahan, L.R.; Hambley, T.W. *Inorg. Chem.* **1987**, *26*, 2532.
18. Lee, Y.H.; Harrowfield, J.; Kim, Y.; Lim, W.T.; Park, Y.C.; Thuery, P. *Dalton Trans.* **2009**, 434.
19. Kobayashi, T.; Inomata, Y.; Takeuchi, T.; Howell, F.S. *Inorg. Chim. Acta*, **1997**, *258*, 109-112.
20. Lee, D.-H.; Lee, Y.H.; Kim, D.I.; Kim, Y.; Lim, W.T.; Harrowfield, J.M.; Thuéry, P.; Jin, M.-J.; Park, Y.C. Lee, I.-M. *Tetrahedron* **2008**, 64, 7178-7182.
21. Lee, D.-H.; Lee, Y.H.; Harrowfield, J.M.; Lee, I.-M.; Lee, H.I.; Lim, W.T.; Kim, Y.; Jin, M.-J. *Tetrahedron* **2009**, *65*, 1630.
22. Shi, M.; Jiang, J.-K. *Tetrahedron Asymmetry* **1999**, *10*, 1673-1679.
23. Lin, C.; Douglas, B.E. *J. Coord. Chem.* **1972**, *2*, 117-121.
24. White, C.R.; Joesten, M.D. *J. Coord. Chem.* **1976**, *6*, 53-57.
25. Su, H.; Wu, C.; Zhu, J.; Miao, T.; Wang, D.; Xia, C.; Zhao, X.; Gong, Q.; Song, B.; Ai, H. *Dalton Trans.* **2012**, *41*, 14480-14483.
26. Moelands *et al.* manuscript in preparation (Chapter 3 of this thesis).
27. Pauluccci, G.; Fischer, R.D.; Benetollo, F.; Sergagli, R.; Bombieri, G. *J. Organomet. Chem.* **1991**, *412*, 327-342.
28. Lutz, M.; Schreurs, A.M.M.; Spek, A.L.; Moelands, M.A.H.; Klein Gebbink, R.J.M. *Acta. Cryst. C.* (**2010**), C66, m9-m12.
29. Britovsek, G.J.P.; Gibson, V.C.; Spitzmesser, S.K.; Tellmann, K.P.; White, A.J.P.; Williams, D.J. *J. Chem. Soc., Dalton Trans.* **2002**, 1159-1171.
30. Evans, D.F. *J. Chem. Soc.* **1959**, 2003-2005.
31. Schreurs, A.A.M.; Xian, X.; Kroon-Batenburg, L.M.J. *J. Appl. Cryst.* **2010**, *43*, 70-82.
32. Otwinowski, Z.; Minor, W.; *Methods in Enzymology* Volume 276 (C.W. Carter, Jr. & R.M. Sweet, Eds.) Academic Press (**1997**) 307-326.
33. Duisenberg, A.J.M., Kroon-Batenburg, L.M.J., Schreurs, A.M.M. *J. Appl. Cryst.* **2003**, *36*, 2, 20-229.
34. Sheldrick, G. M. (**1999**). SADABS. Universität Göttingen, Germany.
35. Sheldrick, G.M. *Acta Cryst.* **2008**, *A64*, 112-122.
36. Altomare, A.; Burla, M.C.; Camalli, M.; Cascarano, G.L.; Giacovazzo, C.; Guagliardi, A.; Moliterni, A.G.G.; Polidori, G.; Spagna, R. *J. Appl. Cryst.* **1999**, *32*, 115-119.
37. Spek, A.L. *Acta Cryst.* **2009**, *D65*, 148-155
38. Flack, H.D. *Acta Cryst*. **1983**, *A39*, 876-881.

5

Facial triad modeling using ferrous pyridinyl prolinate complexes: synthesis and catalytic applications

A series of new chiral pyridinyl prolinate (**RPyProR**) ligands and their corresponding Fe(II) triflate and chloride complexes is reported. The ligands possess an NN'O coordination motive, as found in the active site of non-heme iron enzymes with the so-called 2-His-1-carboxylate facial triad. The coordination behavior of these ligands towards iron turned out to be dependent on the counter ion (chloride or triflate), the crystallization conditions (coordinating or non-coordinating solvents) and the presence of substituents on the ligand. In combination with $Fe(II)(OTf)_2$, coordinatively saturated complexes of the type $[Fe(L)_2](OTf)_2$ are formed, in which the ligands adopt a meridional coordination mode. The use of $FeCl_2$ in a non-coordinating solvent leads to 5-coordinated complexes $[Fe(L)(Cl)_2]$ with a meridional N,N',O ligand. Crystallization of these complexes from a coordinating solvent leads to 6-coordinated $[Fe(L)(solv)(Cl)_2]$ complexes (solv = methanol or acetonitrile), in which the N,N',O ligand is coordinated in a facial manner. For **RPyProR** ligands bearing a 6-Me substituent on the pyridine ring, solvent coordination and, accordingly, ligand rearrangement is prevented by steric constrains. The complexes were tested as oxidation catalysts in the epoxidation of alkene substrates in acetonitrile with hydrogen peroxide as the oxidant under oxidant limiting conditions. The complexes showed to be especially active in the epoxidation of styrene type of substrates (styrene and *trans*-beta-methylstyrene). In the best case, complex [Fe(**6-Me-PyProNH$_2$**)Cl_2] (**15**) allowed for 65% productive consumption of hydrogen peroxide toward epoxide and benzaldehyde products.

5.1 Introduction

Non-heme iron enzymes are involved in a large number of oxidative processes in biology and their modes of action constitute a source of inspiration for the design of synthetic oxidation catalysts.[1] In particular, the oxidation of non-activated C-H and C=C bonds using dioxygen as the formal oxidant are attractive to the synthetic chemist. Efforts towards modeling of the active sites of such enzymes have, therefore, not only focused on a further understanding of the enzyme activity and at reaching (electronic) structure activity relationships, but have also focused on the design of bio-inspired oxidation catalysts.[2]

Amongst these enzymes, the binuclear enzyme sMMO has attracted a lot of attention over the years because of its property to selectively oxidize methane to methanol.[3] More recently, a class of mono-nuclear non-heme iron enzymes that possess a so-called 2-His-1-carboxylate facial triad active site have found a widespread interest (Figure 1).[4,5] In the active site of these enzymes, the iron center is surrounded in a facial manner by two histidine ligands and one carboxylate ligand, from either glutamate or aspartate. Water molecules occupy the other three sites of the octahedron around iron in the resting state. These three 'vacant' sites are important for the overall reactivity of the enzymes, because they provide binding sites for substrate or co-factor molecules that are required for the oxidative transformations carried out by the enzymes.

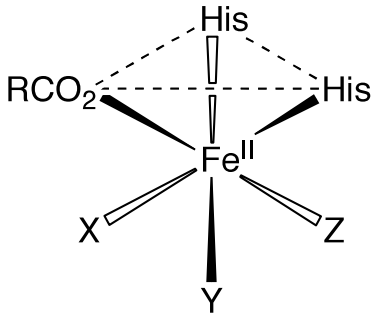

Figure 1. The 2-His-1-carboxylate facial triad.

Most striking besides the structural aspects of the active sites is the wide variety in the reaction patterns that are catalyzed by the members of the facial triad enzyme family. This reactivity includes, e.g., oxidative ring cleavage, *cis*-dihydroxylation, hydroxylation, desaturation, ring closure, and ring expansion. For a single structural entity this palette of reactivity is unprecedented in biology and rivals the reactivity diversity displayed by heme enzymes. Not surprisingly, the facial triad enjoys much interest in the bioinorganic field.

Different approaches have been followed to mimic the structural and reactivity features of the facial triad and to comprehend its overall reactivity. Que *et al.* reported on the preparation of a model of the α-ketoglutarate-dependent oxygenases, based on

the hydrotris(3,5-diphenylpyrazol-1-yl)borate(Tp^{Ph2}) ligand that coordinates to iron(II) in a facial manner via three nitrogen donor atoms.[6,7] Several other all-nitrogen ligands have been used as well to model the facial triad. Examples include tris(2-pyridylmethyl)amine (TPA),[8] N,N-bis-(2-pyridylmethyl)-N,N'-dimethyl-1,2-cyclohexanediamine (BPMCN)[9], and 1,4,7-triazacyclononane (TACN).[10] Attempts to mimic the structural features of the facial triad coordination environment in a more accurate manner, i.e. through the facial coordination of a combination of two nitrogen-based neutral donors and a mono- or bidentate carboxylate donor, were more recently described. Burzlaff and co-workers reported on the coordination chemistry of bispyrazolylacetate heteroscorpionate ligands towards iron.[11,12] Que and coworkers reported on the use of Ph-DPAH (di(2-pyridyl)methylbenzamide) which provides a neutral facial NNO coordination motif.[13] Interestingly, the complex $[Fe^{II}(Ph\text{-}DAPH)_2](OTf)_2$ is able to carry out the *cis*-dihydroxylation of alkenes using H_2O_2 as the oxidant and thereby mimics the reactivity of the Rieske dioxygenases. Furthermore, Que and Tolman have reported on an alternative strategy to prepare mononuclear iron(II) complexes with an NNO coordination mode, in which sterically encumbered carboxylato ligands in combination with bulky diamine ligands are used.[14]

Our interest in this field is the development of mixed N,O ligands and their use in catalytic oxidation chemistry. In an attempt to closely mimic the electronic properties next to the structural properties of the facial triad, we recently developed the bis(alkyl-imidazol-2-yl)propionate (BAIP) ligand family (Figure 2A). This ligand family combines a carboxylate donor moiety with two biologically relevant imidazole donor moieties in a predisposed facial manner and enables the synthesis of discrete $[M(BAIP)_2]$ and $[M(BAIP)(X)_2L]$ complexes, where M = Fe, Cu, Zn, $(X)_2$ are two anionic ligands or is a bidentate mono- or dianionic ligand, and L is a neutral donor ligand like H_2O or pyridine.[15] Substitution of the imidazole moieties in the BAIP-ligands allows for the variation of their steric and site isolating, as well as their solubility properties. Complexes of the type $[Fe(BAIP)(cat)(H_2O)]$, where (cat) is a mono-anionic bidentate (substituted) catechol ligand, were found to react with oxygen to accomplish cleavage of the catechol ring to afford extradiol cleavage products in excess to intradiol cleavage products (2:1 ratio, respectively) in 60% yield.[16] These complexes represent rather accurate structural and functional models for extra-diol cleaving dioxygenase enzymes. Upon substituting the carboxylate moiety in the BAIP ligands for a neutral carboxylic ester moiety (Figure 2B), the N,N,O facial capping propensity of the ligands is maintained and complexes of the type $[Fe(L)_2]^{2+}$ are obtained.[15c] Complexes of this type were found to be able to catalyze the combined *cis*-dihydroxylation and epoxidation of internal and external olefins. Burzlaff and co-workers have reported independently on the synthesis and metal coordination properties of members of the BAIP-ligand family,[17,18] while Holland *et al.* reported on the structure of $[Fe(BAIP)_2]$ complexes.[19]

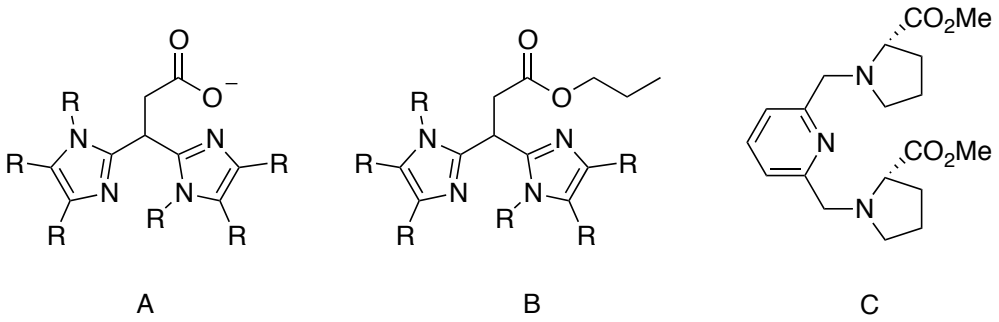

Figure 2. Mixed N,O ligands.

In an effort to extend the set of ligands that are able to coordinate to iron in a facial N,N,O manner, we have set out to investigate the coordination chemistry of a set of chiral ligands that would in principle allow for the development of enantioselective bio-inspired oxidation catalysts. The investigated set of ligands is composed of a (substituted) pyridine moiety connected to a (substituted) prolinate moiety (Figure 3). Ligands of this types were earlier reported by Chelucci and co-workers, and have recently been investigated by Paine *et al.* in combination with iron.[20] These pyridinyl prolinate ligands **RPyProR** are quite easily synthesized using proline and its derivatives as cheap chiral pool synthons. Earlier investigations by us have dealt with analogues of these ligands in which a central pyridine was combined with two proline-derived moieties (Figure 2C, $Py(ProMe)_2$). Those ligands behave as tridentate meridional or planar pentadentate NN'NOO ligands and render diastereopure seven-coordinated metal(II) complexes.[21]

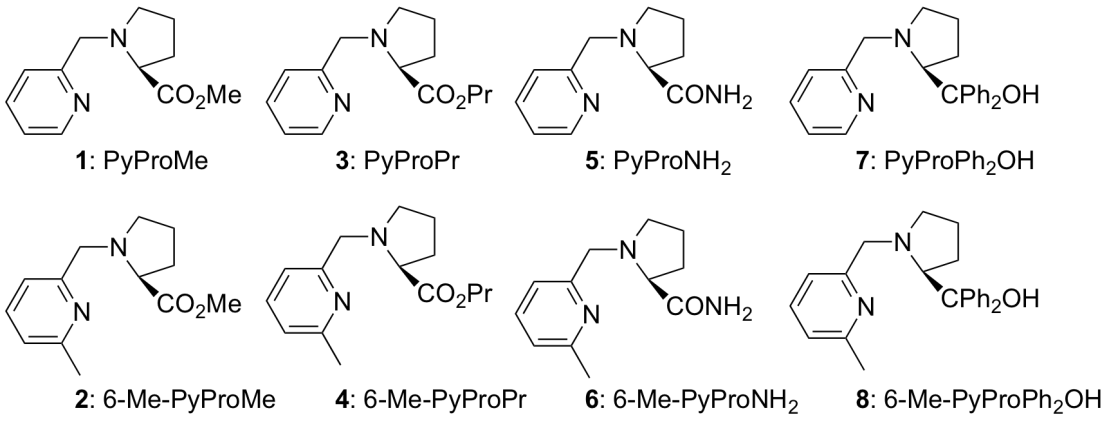

Figure 3. RPyProR ligands described in this study.

Here, we report on the synthesis and iron(II) coordination properties of ligands **1**-**8**, the structural analysis of the resulting complexes, and report on an initial evaluation of the ability of the resulting iron complexes to catalyze the epoxidation of a series of (pro-chiral) olefin substrates.

5.2 Results

5.2.1 Ligand synthesis

The synthesis of the parent ligand **PyProMe** (**1**) was earlier reported by Chelucci *et al.*[22] Following this synthesis route, ligands **6-Me-PyProMe** (**2**), **PyProPr** (**3**), and **6-Me-PyProPr** (**4**) were synthesized using the respective prolinate esters and (substituted) 2-chloromethylpyridine reagents (Scheme 1). Chelucci *et al.* also reported on the reaction of **1** with either NH_3 or PhMgBr to afford ligands **PyProNH$_2$** (**5**) and **PyProPh$_2$OH** (**7**), respectively. Amide ligand **6-Me-PyProNH$_2$** (**6**) and prolinol ligand **6-Me-PyProPh$_2$OH** (**8**) were synthesized in an analogues manner starting from the 2-methylpyridinyl ligand **6-Me-PyProMe** (**2**) (Scheme 1).

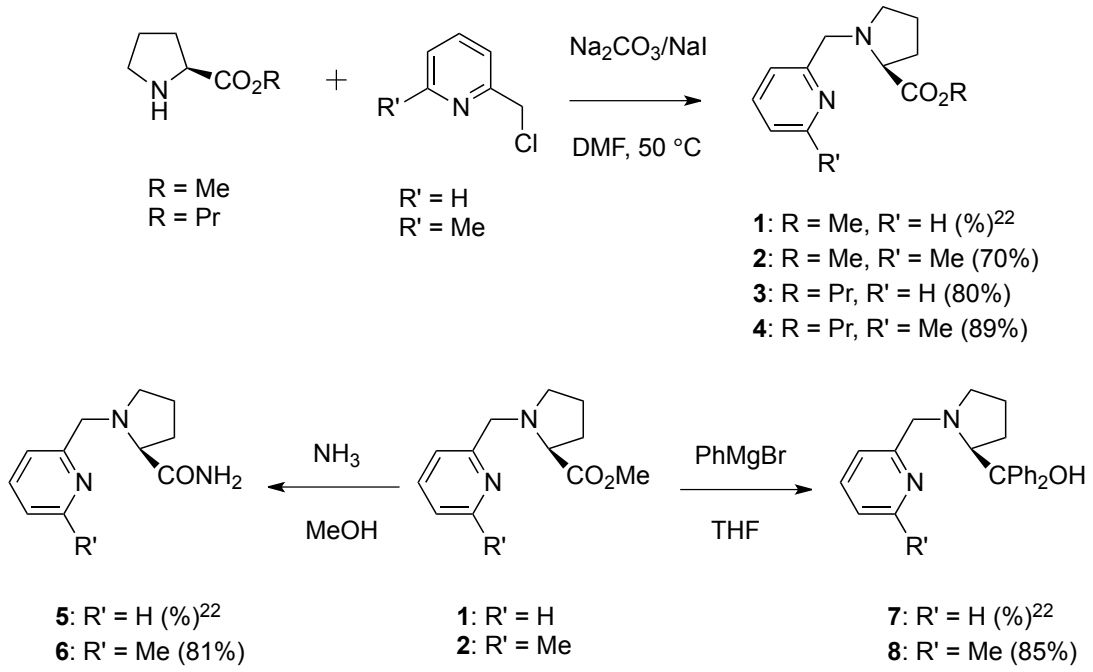

Scheme 1. Synthesis of ligands **1**-**8**.

5.2.2 Fe-triflate complexes

The complexation behavior of ligands **1-8** towards Fe(II) triflate was sturdied initially, thereby regarding the triflates as non-coordinating anions. A Job plot for ligand **1** and $Fe(OTf)_2{\cdot}2MeCN$ in acetonitrile shows the preferential formation of a 2:1 ligand:metal complex, suggesting that **1** acts either as a tridentate ligand to form a hexa-coordinated Fe-complex or as a bidentate ligand in combination with solvent or triflate coordination (Figure 4).

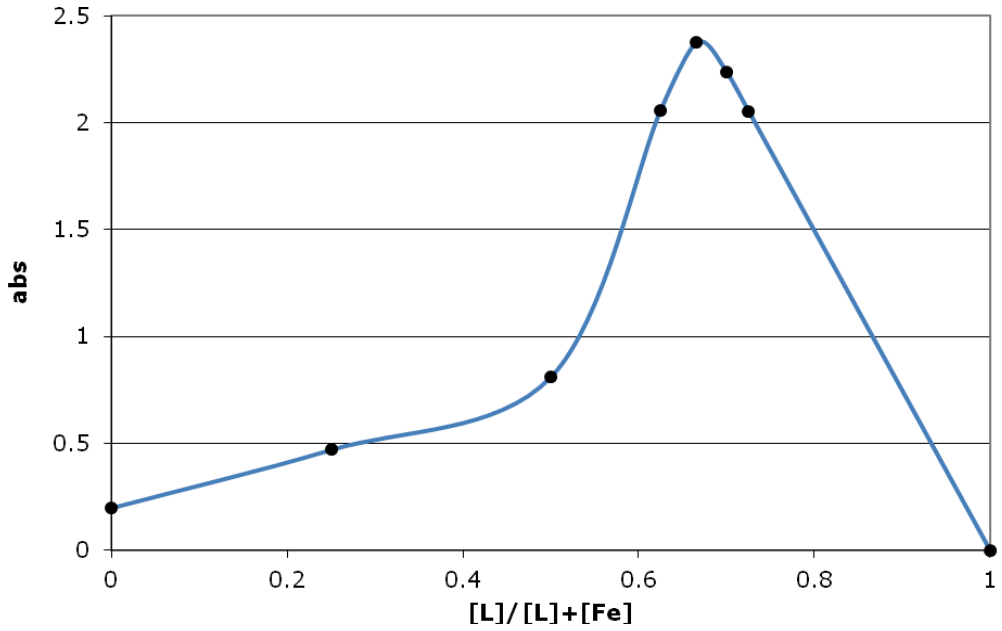

Figure 4. Job plot between $Fe(OTf)_2 \cdot 2MeCN$ and ligand **1**; the black dots represent the data points.

Accordingly, the 2:1 ligand:Fe complexes of ligands **3**, **5**, and **7** with $Fe(OTf)_2 \cdot 2MeCN$ were prepared on a preparative scale. To this end one equivalent of $Fe(OTf)_2 \cdot 2MeCN$ was reacted with two equivalents of the ligand in acetonitrile under an inert N_2-atmosphere for 1 h. Isolation via precipitation with Et_2O and recrystallization from $MeCN/Et_2O$ yielded complexes **9-11** as off-white (**9** and **11**) or yellow (**10**) powders in 60-90% yield (Scheme 2). These ferrous complexes are air sensitive and were stored in an inert atmosphere drybox.

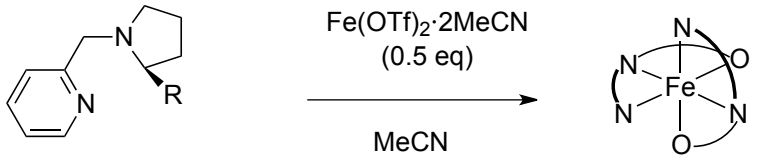

3: R = $CO_2{}^n$Pr
5: R = $CONH_2$
7: R = CPh_2OH

9: R = $CO_2{}^n$Pr; $[Fe^{II}(\mathbf{PyPro^nPr)_2}](OTf)_2$
10: R = $CONH_2$; $[Fe^{II}(\mathbf{PyProNH_2)_2}](OTf)_2$
11: R = CPh_2OH; $[Fe^{II}(\mathbf{PyProPh_2OH)_2}](OTf)_2$

Scheme 2. Synthesis of the triflate complexes **9-11**.

ESI-MS analysis of these isolated materials showed mono-cations of the composition $[Fe(L)_2(OTf)]^+$ as the parent peak. Elemental analysis corroborated the anticipated $Fe(L)_2(OTf)_2$ composition of the isolated materials. UV-Vis spectra recorded in MeCN showed typical ligand π-π^* and MLCT bands for octahedral Fe(II) complexes below 300 nm and in the 330-360 nm region, respectively. The solid state IR-

spectrum of complex **9** showed a distinctive vibration band at 1658 cm^{-1} (Figure 5), indicating that the carbonyl fragments in the complex are coordinated to the metal ion. For the free ligand (**3**), the carbonyl band is found at 1728 cm^{-1}. The symmetric and asymmetric vibrations of the CF_3 and SO_3 groups in **9** are found at 1255 (ν_{as} SO_3), 1223 (ν_s CF_3), 1148 (ν_{as} CF_3) and 1028 (ν_s SO_3) cm^{-1}, which points at the presence of non-coordinating triflate groups.[23]

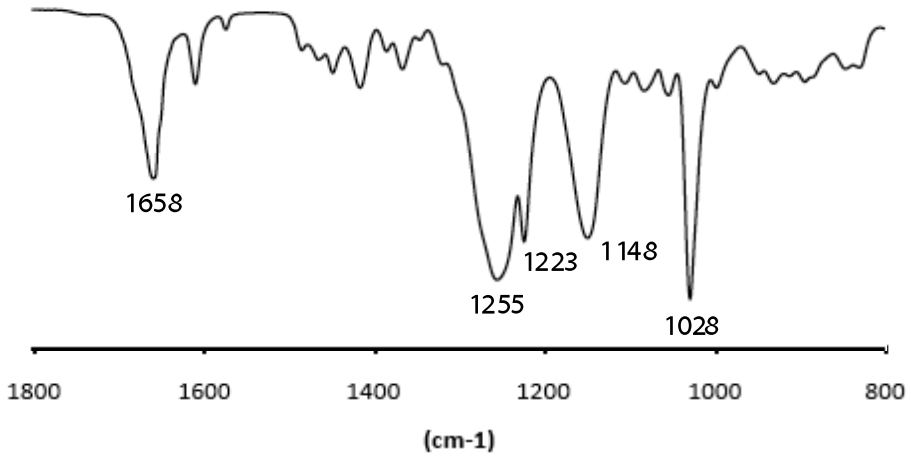

Figure 5. Solid-state IR spectrum of complex **9**.

Similar observations were made in the solution IR-spectrum (MeCN) of complex **9**. This indicates that no structural changes related to either carbonyl or triflate coordination take place and that the overall solid-state structure of **9** is maintained in solution. For solid complex **10**, the position of the carbonyl band at 1673 cm^{-1} also indicates coordination of this group to iron. In the free ligand (**5**), this band is also found at a relatively low energy (1669 cm^{-1}), which is most likely caused by intermolecular hydrogen bonding between carbonyl and amino groups. The position of the triflate bands also indicates that these ions are not coordinated to iron in complex **10**; vibration bands for the triflate groups are found at 1270 (ν_{as} SO_3), 1227 (ν_s CF_3), 1158 (ν_{as} CF_3) and 1031 (ν_s SO_3) cm^{-1}. For complex **11**, the situation is slightly different as the complex does not contain carbonyl groupings, but instead contains tertiary alcohol groupings. In the IR-spectra of complex **11** a broad peak is observed for the OH group around 3339 cm^{-1}. The peak of the OH group in the free ligand is found at a higher wavenumber (3395 cm^{-1}). The ROH groups in this complex most likely coordinate to iron, whereas they are not deprotonated according to the parent peak observed in ESI-MS ($[Fe(\mathbf{PyProPh_2OH})_2(OTf)]^+$, m/z = 893.269). The triflate groups in this complex are just as for complexes **9** and **10** not coordinated towards the iron center; triflate vibrations are found at 1277 (ν_{as} SO_3), 1223 (ν_s CF_3), 1157 (ν_{as} CF_3) and 1027 (ν_s SO_3) cm^{-1} for complex **11**.

Magnetic susceptibility measurements in solution using Evans' method[24,25] indicated μ_{eff} values of 4.86 (**9**, acetone), 4,46 (**10**, MeCN) and 4.58 (**11**, MeCN) μ_{β} for these complexes. While these values are somewhat below the theoretical value of 4.92 for an S = 2 system, these do indicate a high spin configuration for these iron(II) triflate complexes.

Twinned crystals suitable for X-ray diffraction were obtained for complex [Fe(**PyProNH$_2$**)$_2$](OTf)$_2$ **(10)** by slow vapor diffusion of diethyl ether into an acetonitrile solution of the complex. Crystal structure determination showed a very distorted octahedral geometry for the iron complex (Figure 6); selected bond lengths and angles are depicted in Table 1. Two **PyProNH$_2$** ligands coordinate in a meridional fashion around the iron center, corresponding to the ligand to metal ratio found in the Job plot (Figure 4). From each ligand, the nitrogen atoms of the pyridine and the proline ring coordinate to iron and the tridentate nature of the ligand is complemented by coordination of the carbonyl moiety. The triflate moieties are found as disordered, non-coordinating counter ions. The crystal structure showed furthermore that complex **10** is involved in a hydrogen-bonded one-dimensional chain.

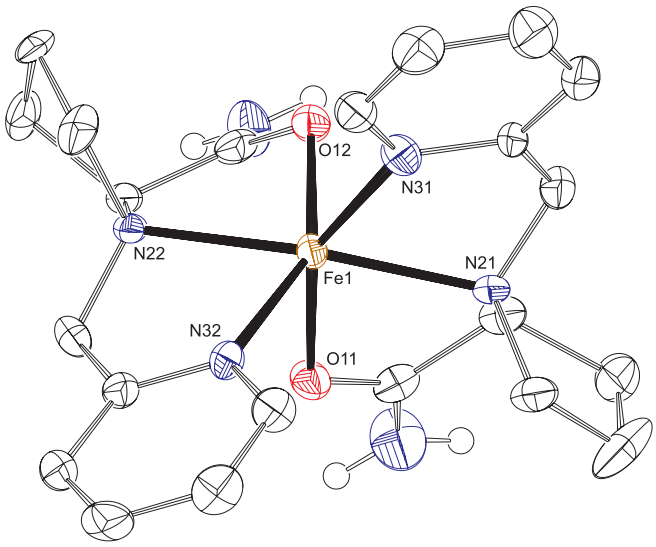

Figure 6. Displacement ellipsoid plot (50% probability) of **10**; C-H hydrogen atoms and non-coordinated triflate anions are omitted for clarity.

The meridional coordination mode of the tridentate ligands is most likely caused by steric reasons and gives rise to a trans orientation of the proline rings, the two Fe-O bonds are orientated *cis* to each other. The Fe-N distances vary between 2.132(5) and 2.197(5) Å, which are typical bond distances for high spin iron(II) complexes. The deviation from ideal octahedral geometry is reflected in the bond angles around iron (angular variance is 257.62 deg^2), which is caused by the geometrical restrictions of the ligands.

Table 1. Selected bond lengths (Å) and angles (°) for complex **10**.

Bond length			Angle
Fe1-N32	2.132(5)	N32-Fe1-N22	76.90(17)
Fe1-N22	2.197(5)	N32-Fe1-O12	151.82(18)
Fe1-O12	2.146(4)	N22-Fe1-O12	75.13(17)
Fe1-N31	2.148(5)	N31-Fe1-N21	77.26(18)
Fe1-N21	2.183(5)	N31-Fe1-O11	150.70(17)
Fe1-O11	2.164(4)	N21-Fe1-O11	74.09(17)
		N31-Fe1-N22	124.41(19)
		N22-Fe1-N21	154.94(16)

5.2.3 Fe-chloride complexes

The preparation of 1:1 iron to ligand complexes using the **PyProR** ligands **1-8** was envisioned through the use of an iron(II) source that contains coordinating counter ions. Indeed, complexes **12-15** were prepared via the reaction of one equivalent of the corresponding ligand with one equivalent of ferrous chloride in methanol under an inert N_2-atmosphere for 1 h. After precipitation with Et_2O, the complexes were isolated as yellow powders in 90-94% yield (Scheme 3). Complexes **12-15** were stored in an inert atmosphere drybox because of their air sensitivity.

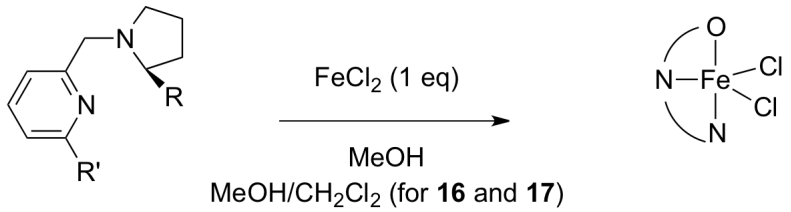

1: R = CO_2Me, R' = H
2: R = CO_2Me, R' = Me
5: R = $CONH_2$, R' = H
6: R = $CONH_2$, R' = Me
7: R = CPh_2OH, R' = H
8: R = CPh_2OH, R' = Me

12: R = CO_2Me, R' = H Fe^{II}(**PyProMe**)Cl_2
13: R = CO_2Me, R' = Me Fe^{II}(**MePyProMe**)Cl_2
14: R = $CONH_2$, R' = H Fe^{II}(**PyProNH$_2$**)Cl_2
15: R = $CONH_2$, R' = Me Fe^{II}(**MePyProNH$_2$**)Cl_2
16: R = CPh_2OH, R' = H Fe^{II}(**PyProPh$_2$OH**)Cl_2
17: R = CPh_2OH, R' = Me Fe^{II}(**MePyProPh$_2$OH**)Cl_2

Scheme 3. Synthesis of the chloride complexes **12-17**.

Ferrous chloride complexes **16** and **17** derived from the diphenylprolinol ligands **7** and **8** were prepared in a similar manner using a solvent mixture of methanol and dichloromethane (4:5, v/v) because of solubility reasons. Both complexes were isolated as yellow powders after precipitation in a yield of 90 and 85%, respectively (Scheme 3). Complexes **16** and **17** were also stored in an inert atmosphere drybox because of their air sensitivity.

ESI-MS analysis of the chloride complexes **12-17** showed a singly charged parent peak of composition $[Fe(L)(Cl)]^+$ in all cases and pointed at the formation of complexes with a metal to ligand ratio of 1:1. Elemental analysis corroborated the formation of complexes with an $[Fe(L)Cl_2]$ composition.

For these ferrous chloride complexes, IR spectroscopy is somewhat less informative than in the case of the ferrous triflate complexes due to the weak intensity of the Fe-Cl vibrational peaks. The solid-state IR spectrum of [Fe(**PyProMe**)Cl_2] (**12**) does show a clear vibration band of the carbonyl group at 1697 cm^{-1}. The corresponding vibration of the free ligand is found at 1732 cm^{-1}. This shift in energy clearly indicates the coordination of the carbonyl group to the iron center. The solution IR spectrum of [Fe(**PyProMe**)Cl_2] in MeCN shows the carbonyl vibration at 1702 cm^{-1}, which indicates that in solution the carbonyl group remains coordinated to iron.

For the 6-methylpyridine complex [Fe(**6-Me-PyProMe**)Cl_2] (**13**), the same trend in the vibration of the carbonyl group was observed for the free ligand, the prepared complex and the complex in solution (MeCN). Complexes [Fe(**PyProNH$_2$**)Cl_2] (**14**) and [Fe(**6-Me-PyProNH$_2$**)Cl_2] (**15**) showed a carbonyl vibration at respectively 1652 and 1656 cm^{-1} in their solid state IR spectra. In the free ligands, these bands are also found at a relatively low energy, which is again most likely caused by the intermolecular hydrogen bonding between the carbonyl and the amino groups. For the prolinol complexes [Fe(**PyProPh$_2$OH**)Cl_2] (**16**) and [Fe(**6-Me-PyProPh$_2$OH**)Cl_2] (**17**) a characteristic broad band around 3060 cm^{-1} for the ROH group was observed, which points to coordination of this moiety towards the metal center.

Magnetic susceptibility measurements in solution using Evans' method[24,25] showed the formation of high spin (S = 2) iron(II) chloride complexes. Detailed spectroscopic characteristics for complexes **12-17** are summarized in Table 2.

Table 2. Spectroscopic properties of complexes **12-17**.

Complex	C=O vibration free ligand (cm^{-1})	C=O vibration complex (cm^{-1})	UV-Vis[a] (nm)	ESI-MS (m/z) $[M-Cl]^+$	Evans μ_{eff} (μ_β)
12	1732	1697	291(866), 363 (501)	311.025	4.62
13	1732	1687	207(9910), 267(4282), 369(338)	325.041	5.07
14	1668	1652	385(469)	296.026	4.33
15	1625	1657	385(456)	310.040	5.10
16			255(7096), 292(5319)	425.091	4.88
17			205(21889), 261(7282), 316(4139)	449.106	5.23

[a] Extinction coefficients (M^{-1} cm^{-1}) are given in parentheses after each feature.

5.2.4 Structural features of the Fe chloride complexes in the solid state (X-ray crystal structures)

Fe(PyProMe)Cl_2 (12) Single crystals of **12** were obtained by either slow vapor diffusion of ether into a solution of **12** in dichloromethane, or by ether diffusion into a solution of **12** in methanol. These crystallization conditions lead to different crystal forms in which **12** adopts different coordination geometries (Figure 7).

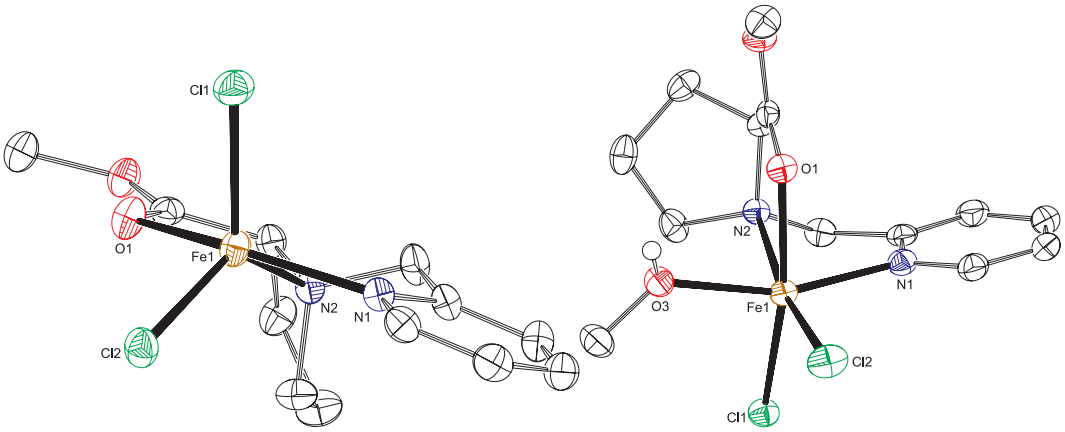

Figure 7. Molecular structures of complex **12** crystallized from a dichloromethane solution (**12a**, left) or a methanol solution (**12b**, right). Displacement ellipsoid plot (50% probability); C-H hydrogen atoms are omitted for clarity.

From a non-coordination solvent, complex **12a** crystallizes in a very distorted five-coordinated geometry, which cannot be described by a Berry pseudo-rotation pathway. The two largest angles at Fe1 are 149.78(6) (N1-Fe1-O1) and 126.96(5)º (Cl1-Fe1-Cl2), while one would expect 180º/120º for an ideal trigonal bipyramid and 150º/150º for a square pyramid. Using a coordinating solvent like methanol, the complex crystallizes in an octahedral geometry with a facial coordination mode of the **PyProMe** ligand. In the octahedral geometry a methanol solvent molecule is coordinated trans to the pyridine ring. Selected bond lengths and angles of **12a** and **12b** are depicted in Table 3.

Table 3. Selected bond lengths (Å) and angles (°) for **12b** (from MeOH) and **12a** (from CH_2Cl_2).

	Bond lengths			Angles	
	12b	**12a**		**12b**	**12a**
Fe1-N1	2.1856(14)	2.1749(18)	N1-Fe1-N2	74.86(5)	76.28(6)
Fe1-N2	2.2880(13)	2.1686(16)	N2-Fe1-O1	75.27(5)	73.55(6)
Fe1-O1	2.2210(12)	2.2830(15)	N1-Fe1-Cl1	94.71(4)	100.95(5)
Fe1-Cl1	2.4742(5)	2.3187(6)	N1-Fe1-Cl2	98.48(4)	99.25(5)
Fe1-Cl2	2.3303(5)	2.2810(6)	O1-Fe1-Cl1	163.93(3)	92.60(4)
Fe1-O3	2.1554(12)		O1-Fe1-Cl2	98.63(3)	100.05(4)
			N1-Fe1-O1	86.63(5)	149.78(6)
			Cl1-Fe1-Cl2	97.011(18)	113.01(2)
			N2-Fe1-Cl2	171.04(4)	126.96(5)

The observed Fe-N bond lengths are all in agreement with high spin (S = 2) iron(II) complexes. The bond length towards Cl1 in **12b** is much longer compared to the other Fe-Cl bond lengths. Cl1 is the acceptor of an intermolecular hydrogen bond with the hydroxyl atom of the coordinated methanol of a neighboring complex as hydrogen bond donor.

Fe(6-Me-PyProMe)Cl_2 (13) Crystals of **13** suitable for X-ray diffraction were obtained by slow vapor diffusion of ether into a solution of **13** in methanol. Despite the presence of the coordinating solvent methanol, the crystal structure of **13** shows a five-coordinated iron center (Figure 8) and is therefore similar to **12a** (from CH_2Cl_2) and not to **12b** (from MeOH). Again, the coordination polyhedron of **13** is very distorted and does not follow a Berry pseudorotation pathway. The largest angles at Fe1 are 153.71(6) (N1-Fe1-O1) and 127.01(2)º (Cl1-Fe1-Cl2).

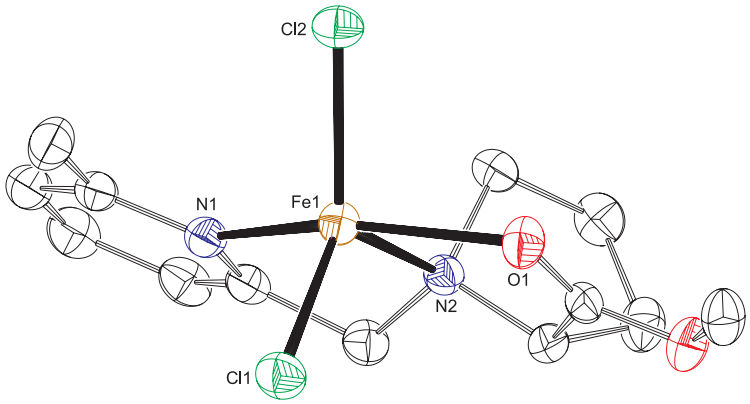

Figure 8. Molecular structure of complex **13** crystallized from a methanol solution. Displacement ellipsoid plot (50% probability); all hydrogen atoms are omitted for clarity.

The observation that complex **13** does not pick up a methanol molecule in its coordination sphere upon crystallization from methanol, most likely arises from the presence of the methyl group at the 6-position of the pyridine ring in **6-Me-PyProMe**. This methyl group provides some steric bulk and seems to prevent the rearrangement of the **6-Me-PyProMe** ligand from a *mer* to a *fac* coordination mode by blocking the concomitant rearrangement of the two chloride ligands. The methyl group is probably also the reason for the larger Cl-Fe-Cl angle in **13** (127.01(2)º) compared to **12a** (113.01(2)º). Selected bond lengths and angles for **13** are shown in Table 4.

Table 4. Selected bond lengths (Å) and angles (°) for complex **13**.

Bond length		Angle	
Fe1-N1	2.1866(17)	N1-Fe1-N2	78.53(6)
Fe1-N2	2.1512(17)	N2-Fe1-O1	75.33(6)
Fe1-O1	2.2610(15)	N1-Fe1-Cl1	99.88(5)
Fe1-Cl1	2.3011(6)	N1-Fe1-Cl2	102.73(5)
Fe1-Cl2	2.2804(6)	O1-Fe1-Cl1	88.83(4)
		O1-Fe1-Cl2	91.23(4)
		N1-Fe1-O1	153.71(6)
		Cl1-Fe1-Cl2	127.01(2)

Fe(PyProNH$_2$)Cl$_2$ (14) and Fe(6-Me-PyProNH$_2$)Cl$_2$ (15) Crystals suitable for X-ray analysis were obtained by slow vapor diffusion of ether into a acetonitrile solution of **14** and a methanol solution of complex **15**. Compound **14** crystallizes in an octahedral geometry with a facial coordination of the **PyProNH$_2$** ligand and with the additional coordination of an acetonitrile molecule (Figure 9). The acetonitrile ligand is coordinated trans to the proline nitrogen, while in complex **12b** the methanol ligand is coordinated trans to the pyridine nitrogen. The crystal structure also showed that complex **14** is able to form a hydrogen-bonded two-dimensional network in the crystallographic *a,b*-plane. On the other hand compound **15** was obtained as a five-coordinated iron complex with a square-pyramidal geometry ($\tau = 0.28$)[26] (Figure 9). The basal plane is formed by the tridentate ligand and the chlorine atom Cl2. The iron center Fe1 is 0.73 Å above this plane. The largest angles at Fe1 are 147.29(3) and 130.66(4)º. The amide group of complex **15** is involved in a one-dimensional hydrogen-bonding network towards the chloride atoms of neighboring complexes. Probably also in this case, just like for complex **13**, the presence of the methyl group on the pyridine ring prevents the coordination of a solvent molecule, giving rise to a five coordinated iron center.

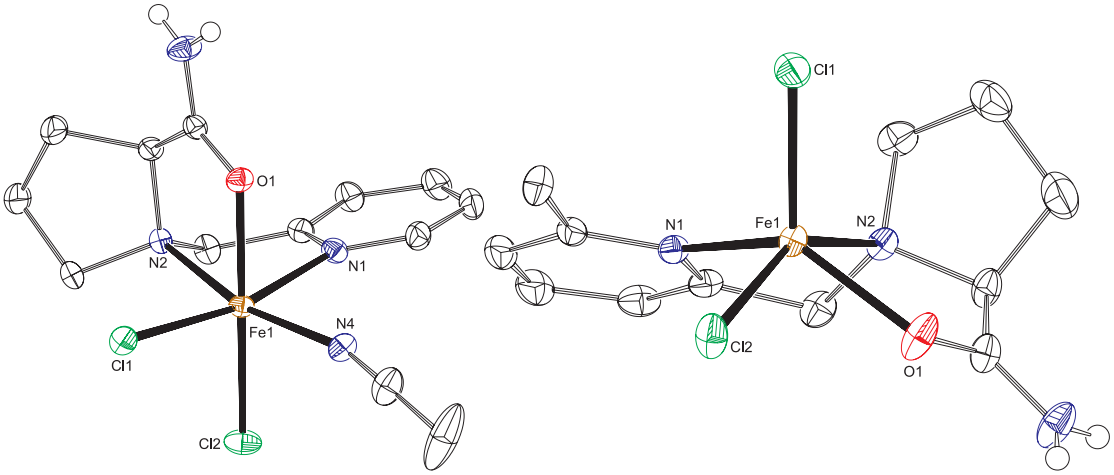

Figure 9. Molecular structures of complex **14** crystallized from an acetonitrile solution (left) and complex **15** crystallized from a methanol solution (right). Displacement ellipsoid plot (50% probability); C-H hydrogen atoms are omitted for clarity.

The proline ring in both structures has the envelope conformation, for complex **14** (cosform 0.966, sinform 0.034)[27] and for complex **15** (cosform 0.804, sinform 0.196).[27] Selected bond lengths and angles of complexes **14** and **15** are depicted in Table 5.

Table 5. Selected bond lengths (Å) and angles (°) for complex **14** and **15**.

	Complex **14**	Complex **15**		Complex **14**	Complex **15**
	Bond Lengths			Angles	
Fe1-N1	2.2264(15)	2.1598(11)	N1-Fe1-N2	75.37(5)	76.51(4)
Fe1-N2	2.2319(14)	2.2767(11)	N2-Fe1-O1	79.18(5)	74.81(4)
Fe1-O1	2.1176(13)	2.0941(11)	N1-Fe1-Cl1	168.72(4)	104.37(3)
Fe1-Cl1	2.4809(5)	2.3147(4)	N1-Fe1-Cl2	92.76(4)	98.98(3)
Fe1-Cl2	2.3873(5)	2.3660(4)	O1-Fe1-Cl1	87.97(4)	121.53(4)
Fe1-N4	2.1900(16)		O1-Fe1-Cl2	174.14(4)	84.99(3)
			N1-Fe1-O1	83.01(5)	130.66(4)
			Cl1-Fe1-Cl2	95.723(17)	106.956(15)
			N2-Fe1-Cl2	95.86(4)	147.29(3)

The Fe-O bond lengths of these two complexes are significantly shorter then the other reported Fe-O bond lengths. This difference can be explained by the presence of the amide group. The carbonyl group in an amide bond has a higher partial negative charge compared to the carbonyl group in an ester bond due to the lower

electronegativity of nitrogen compared to oxygen. This difference causes that the amide carbonyl group binds stronger to the iron center.

Fe(PyProPh$_2$OH)Cl$_2$ (16) and Fe(6-Me-PyProPh$_2$OH)Cl$_2$ (17) For the last two complexes crystals suitable for X-ray analyses were obtained by diffusion of ether into a dichloromethane solution of the corresponding complex. Figure 10 shows the two molecular structures. For both complexes **16** and **17,** two independent residues (Res 1 and Res 2) are present in the asymmetric unit. Both complexes also turned out to form hydrogen-bonded dimers between the two independent molecules.

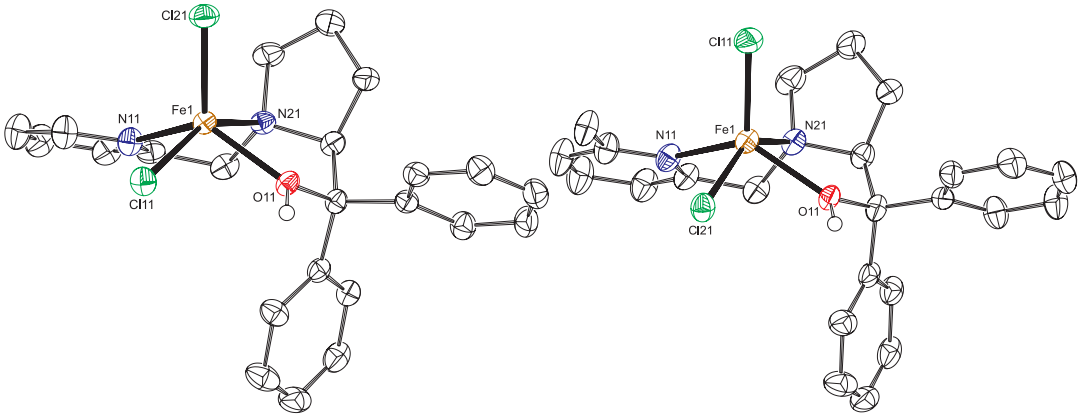

Figure 10. Molecular structures of complexes **16** and **17**. Displacement ellipsoid plot (50% probability); C-H hydrogen atoms and the co-crystallized CH_2Cl_2 solvent molecule in **16** are omitted for clarity. For both structures, only one of two independent residues is shown.

In **16**, both independent molecules have a five-coordinated iron center with a geometry between square pyramidal and trigonal bipyramidal (τ = 0.43/0.37)[26]. The two independent molecules in **17** have a square pyramidal geometry (τ = 0.28/0.24)[26] with the basal plane formed by the tridentate ligand and one chlorine. The iron center is 0.82/0.81 Å above this plane. Selected bond lengths and angles for both residues of complexes **16** and **17** are depicted in Table 6.

Table 6. Selected bond lengths (Å) and angles (°) for complex **16** and **17**.[a]

	Complex **16**		Complex **17**	
	Res 1	Res 2	Res 1	Res 2
	Bond lengths			
Fex-N1x	2.1227(18)	2.1354(18)	2.160(2)	2.153(3)
Fex-N2x	2.2800(18)	2.2125(17)	2.240(3)	2.193(3)
Fex-O1x	2.0858(15)	2.1347(14)	2.123(2)	2.1431(19)
Fex-Cl1x	2.3890(6)	2.3666(6)	2.2565(9)	2.2580(9)
Fex-Cl2x	2.2542(6)	2.2604(6)	2.3825(9)	2.3663(9)
	Angles			
N1x-Fex-N2x	76.41(7)	74.96(7)	77.51(10)	75.63(10)
N2x-Fex-O1x	74.73(6)	73.38(6)	73.40(9)	73.47(8)
N1x-Fex-Cl1x	92.30(6)	90.88(5)	111.38(8)	113.58(7)
N1x-Fex-Cl2x	112.82(6)	113.09(6)	92.17(8)	90.34(7)
O1x-Fex-Cl1x	90.17(4)	91.84(4)	119.52(6)	115.03(6)
O1x-Fex-Cl2x	120.13(5)	119.68(5)	85.67(6)	89.86(6)
N1x-Fex-O1x	124.63(7)	124.56(7)	126.54(9)	128.07(9)
Cl1x-Fex-Cl2x	103.77(2)	104.17(2)	109.76(4)	109.71(3)

[a] x = residue 1 or 2.

The bond lengths differ slightly between the two complexes. The bond length Fex - N1x is slightly longer for complex **17**, which also in this case may be due the presence of the methyl group in the six position on the pyridine ring. Furthermore, the angle between the two chloride atoms is larger for the complex with the methyl group at the six position of the pyridine ring. For comparison, a quaternion plot of the different residues in crystals of **16** and **17** is presented in Figure 11, which clearly shows the similarity of the four structures. The most apparent differences are the orientation of the two phenyl rings of the diphenylprolinol moiety and the Cl-Fe-Cl angle. Overall the pyridine methyl group has no large structural influence in this case.

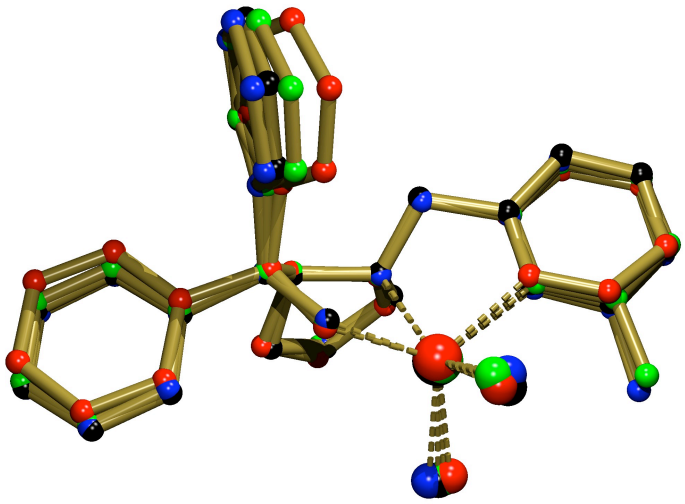

Figure 11. Quaternion fit of all residues in the crystals of **16** and **17** (**16**: Red (res1) and black (res2); **17**: green (res1) and blue (res2)).

5.3 Oxidation catalysis

Iron(II) complexes **9-17** were tested as catalysts for the epoxidation of alkene substrates. For the catalytic screening acetonitrile was chosen as solvent and hydrogen peroxide was used as sacrificial oxidant. A ratio between catalyst, oxidant and substrate of 1:100:500 (oxidant limiting conditions) was used during these screenings (Scheme 4).

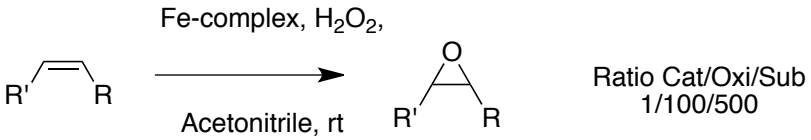

Scheme 4. General representation of catalytic conditions.

In total four different benchmark substrates were used, cyclooctene, 1-octene, styrene and *trans*-beta-methylstyrene. *Trans*-beta-methylstyrene was used to examine the enantio-inducing ability of the chiral iron(II) complexes. Product formation was monitored by GC after 1 and 3 h, and after 1 night.

Table 7 shows the conversion data (TON in epoxide/benzaldehyde) in the reactions with the triflate complexes **9–11** derived from **PyProMe**, **PyProNH$_2$** and **PyProPh$_2$OH**. Among these complexes, **10** showed the highest activity towards all four substrates, while complex **9** and in particular the more bulky complex **11** showed poor activities. As it turned out, 1-octene is not a suitable substrate for these complex systems, as there is hardly any conversion to the epoxide product. In the best case, for complex **10,** a conversion towards the epoxide of 3.3% is obtained based on the amount of added hydrogen peroxide. The highest conversion to epoxide products was

observed with *trans*-beta-methylstyrene, although no appreciable enantioselectivity was found. In the best case a conversion towards the epoxide of 35% is reached based on the amount of oxidant used, with the total productive consumption of hydrogen peroxide of 51% (formation of epoxide and benzaldehyde). Benzaldehyde formation was observed both in the reactions with styrene and *trans*-beta-methylstyrene. In fact, in the case of **9** and **11** more benzaldehyde then epoxide is formed out of styrene after 1 night (9 equiv. for **9** and 4.5 equiv. for **11**). Complex **10** produces an equal amount of epoxide and benzaldehyde after 1 night. In the reactions with *trans*-beta-methylstyrene the epoxide is the predominant product after 1 night. Overall, the activity of these triflate complexes is rather poor, except perhaps for complex **10** in combination with styrenes. The low activity of the complexes is likely caused by the fact that these complexes are coordinatively saturated; it seems that at least one dative bond needs to be broken before the complexes can interact with either the substrate or the oxidant.

Table 7. Oxidation of alkenes catalyzed by complexes **9-11**.[a]

	TON[b]											
Complex	cyclooctene			1-octene			Styrene (benzaldehyde)			*trans*-beta-methylstyrene (benzaldehyde)		
	1 h	3 h	1 night	1 h	3 h	1 night	1 h	3 h	1 night	1 h	3 h	1 night
9 $CO_2{}^nPr$	1.1	2.3	4.8	0.4	0.6	0.7	1.3 (4.8)	2.4 (7.0)	2.7 (9.0)	5.7 (8.4)	10.0 (9.8)	22.9 (13.9)
10 $CONH_2$	4.9	7.9	14.5	1.8	2.5	3.3	6.6 (9.8)	7.9 (11.4)	14.1 (14.4)	20.6 (13.6)	24.4 (14.0)	35.0 (15.9)
11 CPh_2OH	0.6	1.1	1.3	0.1	0.2	0.3	0.9 (2.8)	0.9 (3.7)	1.0 (4.5)	3.5 (5.0)	6.7 (7.0)	8.7 (7.0)

[a] Reaction conditions: 0.5 mL of 700 mM H_2O_2 solution in acetonitrile (0.35 mmol, 100 equiv., diluted from 35% aqueous H_2O_2) was slowly added over 30 min to a stirred solution of 3 mL acetonitrile containing catalyst (3.5 μmol) and substrate (1.75 mmol) at ambient temperature, stirring was continued for another 30 min. After 1 hour from the start internal standard was added (10 μL, cyclooctene: 1,2-dibromobenzene, all other substrates: bromobenzene) and the first samples were taken and analyzed by GC; [b] Moles of product/moles of catalyst.

The chloride complexes **12**–**17** showed an overall higher reactivity profile compared to the triflate complexes **9**–**11** in the oxidation reactions (Table 8). At the same time, several trends are rather similar amongst the two series of complexes. In all cases, aliphatic olefins and in particular external olefins (1-octene) are converted in only a

small number of turnovers, while styrenes give higher and in some cases good turnover numbers. In addition, the amide-appended complexes **10** and **15** give the highest activities in these series, while the most bulky complexes **11**, **16**, and **17** give the lowest activities. For *trans*-beta-methylstyrene, amide complex **15**, [Fe(**6-Me-PyProNH$_2$**)Cl$_2$], gives 50 turnovers in epoxide formation, which corresponds to 50% productive H_2O_2 consumption. Significant benzaldehyde formation was also observed with styrene substrates in the case of complexes **12** – **17** (Table 8).

Table 8. Oxidation of alkenes catalyzed by complexes **12**-**17**.[a]

	TON[b]											
Complex	cyclooctene			1-octene			Styrene (benzaldehyde)			*trans*-beta-methylstyrene (benzaldehyde)		
	1 h	3 h	1 night	1 h	3 h	1 night	1 h	3 h	1 night	1 h	3 h	1 night
12 CO_2Me	5.6	8.6	12.1	1.2	1.9	3.5	8.5 (7.0)	13.1 (10.9)	15.1 (11.8)	20.8 (9.6)	29.4 (12.8)	29.1 (10.6)
13 $MeCO_2Me$	1.2	3.5	9.9	0.3	0.5	2.9	1.4 (5.9)	2.3 (8.5)	13.6 (9.6)	3.8 (10.2)	7.0 (13.7)	30.5 (11.6)
14 $CONH_2$	4.3	5.4	7.7	0.9	1.3	2.7	6.1 (2.6)	8.6 (4.0)	9.1 (13.7)	18.2 (4.0)	25.9 (5.9)	24.7 (13.3)
15 $MeCONH_2$	5.8	13.2	17.5	1.1	3.2	7.0	6.0 (3.6)	13.1 (7.8)	28.2 (13.6)	10.7 (5.5)	27.3 (11.5)	49.2 (15.0)
16 CPh_2OH	2.3	3.8	7.3	0.6	0.9	1.7	3.9 (2.9)	6.0 (5.5)	10.0 (10.7)	10.4 (6.0)	17.0 (8.7)	24.9 (11.1)
17 $MeCPh_2OH$	2.0	2.7	6.4	0.4	0.6	1.9	2.2 (2.3)	2.9 (3.6)	5.7 (9.3)	6.5 (4.5)	9.8 (6.1)	12.5 (7.8)

[a] For reaction conditions see Table 7; [b] Moles of product/moles of catalyst.

In order to provide an overview of the overall activity of the chloride complexes, the cumulative formation of epoxides and aldehydes as a measure for productive H_2O_2 consumption is shown in Figure 12. The graph clearly shows the overall effect of the 6-Me-pyridine substituent on the catalytic activity. For **12** and **13** only minor changes are observed, whereas for **16** and **17** reactivity clearly goes down. In contrast, for amide complexes **14** and **15** inclusion of a methyl-substituent leads to a substantial increase in reactivity. Clearly, the highest activity is obtained for complex **15**, with a maximum of 65% productive H_2O_2 conversion with *trans*-beta-methylstyrene. Also for this series of catalysts, a mediocre enantioselectivity was found in the epoxide formation out of styrenes. No attempts were made to further optimize these ee values.

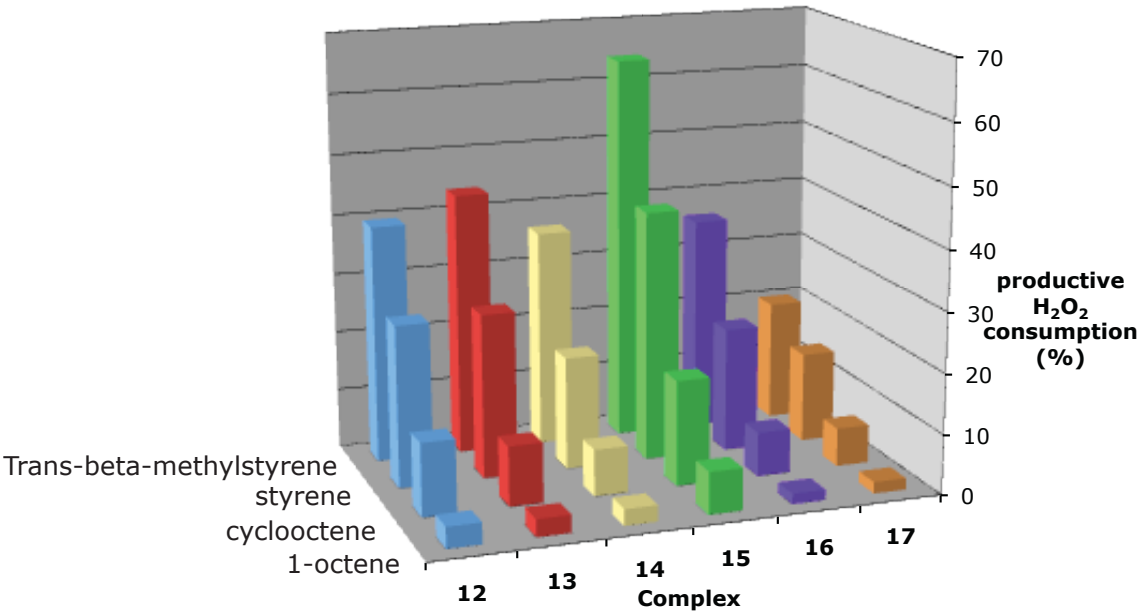

Figure 12. Productive consumption of oxidant after 1 night for complexes **12-17**.

5.4 Discussion

In the present investigations we have explored the coordination chemistry of a series of simple pyridinyl prolinate and pyridinyl diphenylproline ligands with respects to Fe(II). Whereas the parent ligand of the series reported here (*S*)-methyl-1-(pyridin-2-ylmethyl)pyrrolidine-2-carboxylate **(PyProMe)** has been studied by Paine *et al.* in relation with iron-mediated catechol oxidation,[20] the current extended series of pyridinyl proline ligands (**RPyProR**) allows for a more general description of the coordination properties of this ligand family. The specific interest in these ligands combines the ease of synthesis of these chiral ligands and their anticipated mimicry of the 2-His-1-carboxylate facial triad coordination mode as found in certain mononuclear non-heme iron enzymes. Our synthetic efforts have resulted in a full structural characterization of most of the reported Fe(II) complexes and show the coordinative flexibility of the N,N,O pyridinyl proline fragment acting either as a meridional or as a facial ligand.

Closed-shell, octahedral structures of the type $[Fe(L)_2]^{2+}$ were formed when iron triflate was used as the iron source. This is a rather common observation for tridentate ligands and has also been observed for related tridentate ligands of the N,N,O type. In our earlier studies on BAIP and $BAIP^R$ type ligands, the formation of similar octahedral closed-shell structures were observed in cases where non-coordinating counter ions were used, albeit that in these cases the ligands coordinate in a facial rather than in the meridional manner to iron like observed for complex **10**.[15c,28]

In particular when anionic N,N,O ligands are used, the formation of octahedral bis-ligand complexes is difficult to avoid. Attempts to form discrete [Fe(II)(L)X] or

[Fe(III)(L)X_2] complexes derived from the family of BAIP-ligands have proven difficult so far. In most reported cases did the thermodynamic $[Fe(L)_2]^{0/1+}$ complexes form. Burzlaff and co-workers also reported on their difficulties in synthesizing mono-ligand complexes derived from the bis(pyrazolyl)proprionate ligand family. Ultimately, they succeeded in synthesizing $[Fe(L)Cl_3]^-$ in which iron is in the oxidation state 3+.[12] The major differences between the **RPyProR** ligands and the BAIP as well as the bis(pyrazolyl)proprionate ligand families are the predisposed facial coordination modes of the latter ligands and their anionic nature in comparison to the neutral **PyPro** ligands.

Using $FeCl_2$ as the source of iron does in combination with a **PyPro** ligand lead to the formation of discrete $[Fe(L)Cl_2]$ complexes that have a penta-coordinated iron center, which would at best be described as square pyramidal (τ values vary from 0.24 to 0.45). Following the square pyramidal description the **PyPro** ligands coordinate to iron as a N,N,O meridional ligand in these cases, positioning the two chloride ligands in 'equatorial' positions. Examples of discrete square pyramidal structures in non-heme iron chemistry include complexes derived from pyridine(bis-imine) ligands.[29,30] Other examples of meridionally coordinated N,N,O ligands are reported with cobalt, zinc and copper.[31-33]

Detailed analysis of the 5-coordinated structures reported here (7 in total) shows that none of these structures are found on a Berry pseudo-rotation trajectory (Table 9).

Table 9. Berry pseudo-rotation of the reported complexes.

	δ_{24}[a]	θ_{24}[a]	θ_{15}[a]
12a	39.11	126.96(5)	149.78(6)
13	44.02	115.14(5)	153.71(6)
15	14.49	130.66(4)	147.29(3)
16_mol1	22.24	124.63(7)	150.14(5)
16_mol2	18.82	124.56(7)	147.02(5)
17_mol1	14.83	126.54(9)	143.20(8)
17_mol2	11.69	128.07(9)	142.72(7)

[a] for a definition of δ_{24}, θ_{24}, and θ_{15}[34]

This again shows that the coordination geometry of these complexes is ill-defined and can, accordingly, actually not be labeled as square pyramidal. An analysis of the CSD-database[35] revealed 14 other 5-coordinated $FeCl_2$ complexes bearing an N,N,O ligand.[36] Of these complexes, also none obeys the Berry trajectory. A graphical representation of the 14 structures found in the CSD-database and our 7 structures reported here is depicted in the Graph 1.

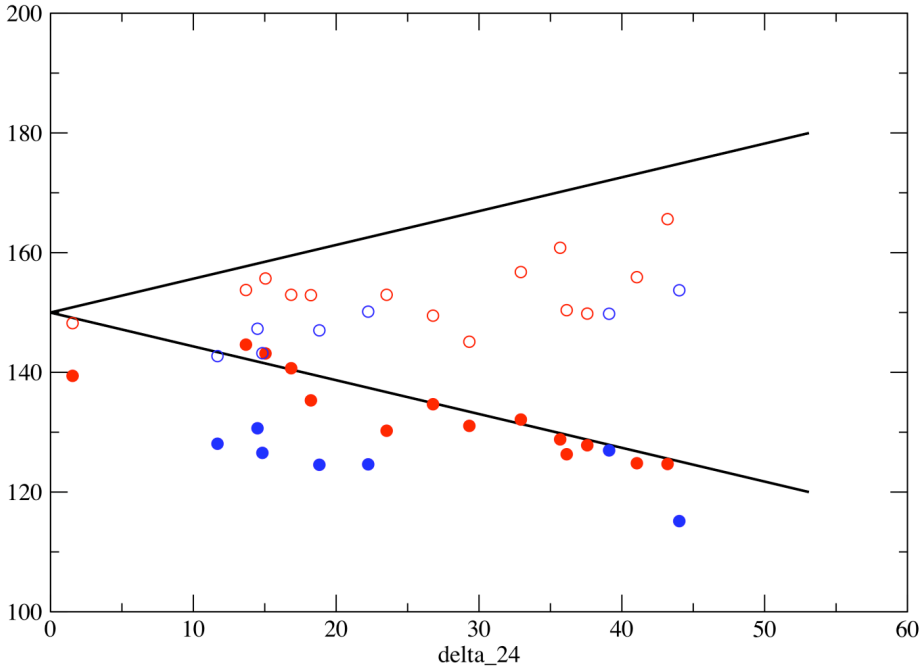

Graph 1. Graphical representation of the Berry pseudo-rotation pathway screening. The seven structures reported here are represented as the blue dots. The 14 structures extracted from the CSD-database are represented as the red dots.[33] The open circles correspond to the 1,5-angle and the filled circles to the 2,4-angle. Furthermore the theoretical Berry pathway is draw as the black lines.

Vahrenkamp and co-workers have earlier noticed this feature in 5-coordinated Zn(II) complexes and have proposed an adapted description of the Berry trajectory in these systems.[37] The current set of Fe(II) complexes is limited in number and does not allow for a similar analysis at this stage. Current efforts in our lab involve the expansion of the set of 5-coordinated $FeCl_2$ complexes in order to arrive at a more detailed structural description of such complexes.

The coordination flexibility of the **PyPro** ligands is shown by the complexes that form when their trigonal bipyramidal complexes are crystallized from coordinating solvents like methanol or acetonitrile. In such solvents, these complexes accommodate one solvent molecule in the coordination sphere of iron and, accordingly, form octahedral complexes of the type $[Fe(L)(solv)Cl_2]$. In these cases the coordination geometry of the **RPyProR** ligand becomes facial. The coordination of solvent molecules is only observed in complexes that contain a **PyPro** ligand with an unsubstituted pyridine moiety. Introduction of a methyl group at the 6-position of this moiety prevents the coordination of solvent molecules at the *cis*-position with respect to the pyridine N-

donor, most likely due to steric constrains. Solvent coordination at the *trans*-position is also prevented because the size of the methyl substituent prevents the reorientation of the chloride ligands, i.e. positioning of the Fe-Cl vector within the plane defined by the pyridine ring is not possible. Where the pyridine 6-position in nitrogen ligands is often used to steer substrate approach to the metal center[38] and the electronics at the metal (spin state),[8b] inclusion of a substituent at this position in the **RPyProR** ligand framework prevents a meridional to facial ligand coordination change and locks the **RPyProR** framework in a meridional conformation.

All prepared complexes **9-17** were tested in the catalytic oxidation of different alkenes using hydrogen peroxide as the oxidant. During the catalytic reactions oxidant limiting conditions were used to allow putative short-live oxygenated metal species to be trapped rapidly by the excess of substrate. It turned out that the triflate complexes perform far less compared to the chloride-based complexes. This can be explained by the fact that the triflate complexes are close-shell complexes with a fully occupied octahedral coordination sphere around iron. These complexes can, therefore, only react via inner-sphere pathways with external reagents such as alkene substrates or oxidants after one or more existing coordination bonds are broken. The chloride complexes turned out to be much more reactive. Several of the crystal structures of these complexes nicely show how solvent molecules can be accommodated in their coordination sphere to obtain six-coordinate complexes. The formation of oxygenated complexes of the type $[Fe(L)(Cl)_2(ox)]$ is therefore not restricted due to the lack of coordination sites.

The observation of the lower activity of the triflate complexes is also somewhat surprising. We have earlier reported that related coordinatively saturated $[Fe(\mathbf{BAIP})_2]^{2+}$ complexes are active as epoxidation/dihydroxylation catalysts and have postulated that open coordination sites in these systems may form by means of ester moiety dissociation.[15c] In addition, the $[Fe(Ph\text{-}DPAH)_2]^{2+}$ system that was studied was Que *et al.* has similar coordination features and at the same time is very active in the dihydroxylation of olefins (TON's of 8 are obtained, ratio catalyst:oxidant:substrate 1:10:1000).[13] In this case the authors have assumed that full dissociation of one of the facial N,N,O ligands takes place prior to any catalytic turn-over. Given the lower turn-over numbers of the **PyPro**-derived iron triflate complexes ligand dissociation does not seem to take place for these complexes and accordingly TON's are lower.

The overall structure of the **RPyProR** ligands has a distinct effect on the catalytic activity of their complexes. Complexes derived form bulky diphenylprolinol ligands gave the lowest activities, both in case of the triflate as well as the chloride complexes and for all substrates. A combination of alcohol instead of ester or amide coordination and enhanced steric bulk could lead to a less electron-rich metal center (electronic effect) and a less favorable olefin substrate attack on the oxygenated active species

(steric effect). In all cases, complexes derived from amide-appended **RPyProR** ligands gave the better catalysts, i.e. higher productive consumption of H_2O_2 was found. The higher activity of these complexes may be explained by the stronger Fe-O bonds that are formed by the amide ligands, which could lead to enhanced catalyst life-times. On the other hand, the short Fe-O bond lengths to the amide moieties indicate an enhanced electron donation, which will lead to more electron-rich Fe-centers and, in turn, to lower oxidation potentials. Finally, the amino groups of the primary amide may have a stabilizing role on putative high-valent iron-oxygen intermediates by means of acting as a hydrogen bond donor. Similar effects were recently found for amide $BAIP^R$ Fe(II) complexes.[28]

Concerning the reactivity of the **RPyProR** systems towards different olefin substrates, it is clear that these show a higher reactivity towards the more electron-deficient styrenes than to the more electron-rich aliphatic olefins. This observation seems to point to a nucleophilic nature of the active species in the oxidations. This seems to make sense given the neutral nature of the more reactive $Fe(II)Cl_2$ complexes and of their putative high-valent intermediates, in particular in the presence of coordinating chlorides. In the oxidation experiments with the pro-chiral *trans*-beta-methylstyrene substrate no appreciable enantioselectivity was observed. This can probably be rationalized by the involvement of a radical-based reaction pathway, which tends to result in racemic product distributions. This assumption is corroborated by the large extent of benzaldehyde formation in the oxidation of styrenes by the **PyPro** systems. On the other hand, the use of *trans*-beta-methylstyrene as the substrate did result in the highest TON's for these systems. With amide complex **15**, a useful conversion of the oxidant towards the epoxide of almost 50% was reached, and an overall productive conversion of the oxidant of almost 65% was found.

Finally, the role of the substitution of the pyridine moiety in the PyPro ligands on their reactivity may be pointed out. In the case of the chloride complexes **12**-**17**, the reactivity remains about equal between **12** and **13**, it increases considerably between **14** and **15**, but decreases between **16** and **17**. Although there is no clear trend, it seems that complexes without the 6-methyl substituent on pyridine have a higher initial activity compared to the complexes with the methyl group (Table 8). On the other hand, complexes bearing the 6-methyl group do stay active over the whole course of the reaction. This reactivity difference can be explained by assuming a longer life time of species involved in the catalytic cycle for the complexes with the methyl group due to steric congestion. The fact that complexes derived from the methyl-substituted ligands do not accommodate a solvent molecule as the sixth ligand, could also implicate a higher barrier for the formation of six-coordinate oxygenated intermediates for these complexes. This would either suggest that these systems operate via a different pathway or that different kinetics are at play within a similar pathway.

Few other Fe-based catalyst based on a mixed N,N,O ligand manifold, in particular ones based on proline, are known to perform the epoxidation of alkenes using H_2O_2. Examples include the BAIP and Ph-DAPH systems (*vide supra*). Paine *et al.* reported on a study using the parent ligand (**PyProMe**) in relation with iron-catalyzed catechol oxidation instead of the epoxidation of alkenes.[20] Beller and co-workers reported in 2007 on the use of ligands derived from the L-proline backbone.[39] These ligands were used in the epoxidation of aromatic alkenes (*trans*-stilbene) and gave for the first time ee's above 20%. Unfortunately no reactions were done on non-aromatic alkenes. We have previously reported on the use of iron complexes derived from bis-proline substituted pyridine ligands for the oxidation of alkenes with hydrogen peroxide as oxidant.[21] These complexes showed a low activity towards the epoxidation of various alkenes.

5.5 Concluding remarks

In conclusion, a series of readily available chiral tripodal N,N,O ligands derived from proline were developed. The structural characterization of several Fe(II) complexes has show that these ligands can adopt a meridional or a facial coordination mode in 6-coordinated complexes. On the other hand, the 5-ccordinated complexes show ill-defined geometries that do not obey a Berry-type description. Depending on the size and nature of the substituents at both the proline and at the pyridine ring, the coordination mode of these ligands may change upon binding of a solvent molecule. This allows for the formation of complexes of the type $[Fe(L)(solv)Cl_2]$, where L is a facial and neutral N,N,O ligand. The further development of such complexes is of interest in modeling the features of the 2-His-1-carboxylate facial triad found in mono-nuclear non-heme iron enzymes.

The use of iron complexes derived from the **PyPro** ligands results in reasonable turnover numbers for both epoxide and benzaldehyde products, albeit that no substantial enantioselectivity has been observes thus far. These results may be used as guidelines in the further development of bio-inspired non-heme iron oxidation catalyst based on cheap chiral building blocks.

5.6 Experimental section

General: Air-sensitive organic reactions and reactions with metal salts were carried out under an inert, N_2 atmosphere using standard Schlenk techniques. Solvents were dried and distilled before use. Chemicals were either commercially obtained and used as received or reproduced from literature. ^1H and ^{13}C NMR spectra were recorded on a Varian 400 spectrometer at 400 MHz and 100 MHz, respectively, operating at 25 °C. Infrared spectra were recorded with a Perkin-Elmer Spectrum One FT-IR instrument. Solution IR measurements were recorded with a Mettler Toledo ReactIR™ 1000 spectrometer with a SiComp™ probe under N_2 atmosphere. ESI-MS was measured on a Waters LCT Premier XE. UV-Vis spectra were recorded on a

Varian Cary 50. Solution magnetic moments were determined by the Evans' NMR method in acetone-d_6/cyclohexane (95/5 *v*/*v*) or in acetonitrile-d_3/cyclohexane (95/5 *v*/*v*) at 25 °C.[24,25] GC analyses were performed on a Perkin-Elmer Clarus 500 GC (30 m, Econo-Cap EC-5) with FID detector. Elemental microanalyses were carried out by the Mikroanalytisches Laboratorium KOLBE, Mülheim an der Ruhr, Germany. $Fe(OTf)_2 \cdot 2MeCN$,[40] (*S*)-2-(methoxycarbonyl)pyrrolidinium chloride,[41] (*S*)-methyl-1-(pyridin-2-ylmethyl)pyrrolidine-2-carboxylate **(PyProMe) (1)**,[22] 1-(pyridin-2-ylmethyl)pyrrolidine-2-carboxamide **($PyProNH_2$) (5)**,[22] diphenyl(1-(pyridin-2-ylmethyl)pyrrolidin-2-yl)methanol **($PyProPh_2OH$) (7)**,[22] were prepared according to published procedures.

(*S*)-2-(*n*-Propoxycarbonyl)pyrrolidinium chloride: $SOCl_2$ (2.6 mL, 36 mmol) was added dropwise during 15 min with stirring to anhydrous *n*-propanol (12 mL) at 0 ºC. *S*-proline (3.24 g, 28.1 mmol) was added to this solution at 0 ºC. The white suspension was stirred and heated to 60 ºC. After 24 h the light brown solution was evaporated and dried in vacuo (<0.1 mbar) with stirring at 75 ºC for 4 h to leave a light brown, viscous oil, which was used in the subsequent reaction without further purification (5.32 g, 98%).
^{1}H NMR (300 MHz, DMSO-d_6, 25 ºC): δ = 0.90 (t, 3H, $^3J_{HH}$ = 7.2 Hz, CH_3), 1.64 (sxt, 2H, $^3J_{HH}$ = 7.2 Hz, $CH_2CH_2CH_3$), 1.83-2.03 (m, 3H, CH_2 ring, γ and β to CO), 2.19-2.33 (m, 1H, CH_2 ring, β to CO), 3.13-3.28 (m, 2H, NCH_2 ring), 4.06-4.19 (m, 2H, $CH_2CH_2CH_3$), 4.33-4.38 (m, 1H, C*H* α to CO), 9.15 (s, b, 1H, NHH), 10.33 (s, b, 1H, NHH) ppm. ^{13}C {1H} NMR (100 MHz, CDCl3, 25 °C): δ = 10.4, 22.0, 23.8, 29.0, 46.1, 59.4, 68.6, 169.1 ppm. IR (film): ν = 2965.4, 2879.0, 1690.4, 1739.8, 1560.4, 1458.4, 1396.4, 1354.3, 1222.8, 1092.6, 1057.4, 998.9, 968.5, 927.9, 903.7, 758.8, 676.1 cm^{-1}. [α]D^{21} -43.3 deg cm^3 g^{-1} dm^{-1} (c 0.952, $CHCl_3$).

2-(Chloromethyl)pyridinium chloride: A cooled solution of $SOCl_2$ (2.1 mL, 29 mmol) in anhydrous CH_2Cl_2 (50 mL) was added dropwise during 30 min with stirring to a colorless solution of pyridin-2-ylmethanol (2.20 g, 20.2 mmol) in anhydrous CH_2Cl_2 (50 mL) at 0 ºC. After 60 min stirring at 0 ºC, the white turbid solution was allowed to reach ambient temperature. After 60 min, the solution was quenched with *n*-propanol (3.5 mL), stirred for 15 min, evaporated, and dried *in vacuo* to leave a white powder, which was used in the subsequent reaction without further purification (3.31 g, quant.).
^{1}H NMR (400 MHz, DMSO-d_6, 25 ºC): δ = 4.98 (s, 2H, ArCH_2), 7.75 (dd, 1H, $^3J_{HH}$ = 7.6 Hz, $^3J_{HH}$ = 5.6 Hz, Py*H*(5)), 7.92 (d, 1H, $^3J_{HH}$ = 8.0 Hz, Py*H*(3)), 8.29 (t, 1H, $^3J_{HH}$ = 7.8 Hz, Py*H*(4)), 8.76 (d, 1H, $^3J_{HH}$ = 5.4 Hz, Py*H*(6)) ppm. ^{13}C{^{1}H} NMR (100 MHz, DMSO-d_6, 25 ºC): δ = 42.9, 125.5, 125.8, 143.2, 145.2, 153.1 ppm.

2-(Chloromethyl)-6-methylpyridinium chloride: $SOCl_2$ (1.2 mL, 17 mmol) in anhydrous CH_2Cl_2 (28 mL) was reacted with (6-methylpyridin-2-yl)methanol (1.41 g, 11.4 mmol) in anhydrous CH_2Cl_2 (28 mL) in the same manner as described for 2-(chloromethyl)pyridinium chloride. After the solution reached ambient temperature the solution was stirred for an additional 60 min at 60 ºC after which the reaction was quenched with ^{n}PrOH (2.0 mL), stirred for 15 min, evaporated, and dried *in vacuo* to leave a white powder, which was used in the subsequent reaction without further purification (2.04 g, quant.).
^{1}H NMR (400 MHz, DMSO-d_6, 25 ºC): δ = 2.69 (s, 3H, ArC*H*$_3$), 5.01 (s, 2H, ArC*H*$_2$), 7.69 (d, 1H, $^3J_{HH}$ = 7.6 Hz, Py*H*(5)), 7.78 (d, 1H, $^3J_{HH}$ = 8.0 Hz, Py*H*(3)), 8.26 (t, 1H, $^3J_{HH}$ = 8.0 Hz, Py*H*(4)) ppm. ^{13}C{^{1}H} NMR (100 MHz, DMSO-d_6, 25 ºC): δ = 41.9, 62.5, 123.5, 126.2, 143.9, 151.8, 155.5 ppm.

(*S*)-Methyl-1-((6-methylpyridin-2-yl)methyl)pyrrolidine-2-carboxylate (6-Me-PyProMe) (2): A yellow suspension of 2-(chloromethyl)-6-methylpyridinium chloride (9.62 g, 54.0 mmol), (*S*)-2-(methoxycarbonyl)pyrrolidinium chloride (12.2 g, 73.5 mmol), NaI (3.08 g, 20.5 mmol) and Na_2CO_3 (19.0 g, 179 mmol) in anhydrous DMF (140 mL) was stirred at 50 ºC. After 16 h the reaction was taken up in H_2O (280 mL) and extracted with CH_2Cl_2 (5 x 100 mL). The organic phases were combined, washed with H_2O (120 mL), dried (Na_2SO_4), filtered and evaporated. The remaining orange oil was subjected to column chromatography (SiO_2 (900 mL), Et_2O/Et_3N 100:1 → 100:2 (*v*/*v*), R_f = 0.3-0.4). A remaining impurity (^{1}H NMR ($CDCl_3$): 6.82-6.88 (m) and 7.17-7.21 (m)) was removed by heating the oil *in vacuo* (<0.5 mbar) at 90 ºC for 2 h to leave a yellow oil (8.57 g, 70%).
^{1}H NMR (400 MHz, $CDCl_3$, 25 ºC): δ = 1.77-2.01 (m, 3H, CH_2 ring, γ and β to CO), 2.10-2.21 (m, 1H, CH_2 ring, β to CO), 2.53 (s, 3H, ArC*H*$_3$), 2.53-2.59 (m, 1H, NC*H*H ring), 3.09-3.14 (m, 1H, NCH*H* ring), 3.42-3.46 (m, 1H, C*H* α to CO), 3.65 (s, 3H, C*H*$_3$), 3.80 (d, 1H, $^2J_{HH}$ = 13.6 Hz, ArC*H*HN), 4.01 (d, 1H, $^2J_{HH}$ = 13.6 Hz, ArCH*H*N), 7.01 (d, 1H, $^3J_{HH}$ = 7.6 Hz, Py*H*(5)), 7.28 (d, 1H, $^3J_{HH}$ = 7.6 Hz, Py*H*(3)), 7.54 (t, 1H, $^3J_{HH}$ = 7.6 Hz, Py*H*(4)) ppm. ^{13}C{^{1}H} NMR (100 MHz, $CDCl_3$, 25 ºC): δ = 23.4, 24.5, 29.5, 51.9, 53.7, 60.3, 65.5, 120.5, 121.8, 137.0, 157.6, 158.0, 174.5 ppm. IR (film): ν = 2951.6, 1732.2, 1591.4, 1577.9, 1455.8, 1435.4, 1358.2, 1275.0, 1196.0, 1169.4, 1087.1, 1038.4, 995.4, 933.2, 890.9, 783.4, 758.1 cm^{-1}. UV-Vis (MeCN) [λ_{max}, nm (ε, M^{-1} cm^{-1})]: 207 (7587), 265 (4096). $[\alpha]_D^{21}$ –72.1 deg cm^3 g^{-1} dm^{-1} (c 1.1, $CHCl_3$). Anal. for $C_{13}H_{18}N_2O_2$ (234.29): calc. C 66.64, H 7.74, N 11.96; found C 66.54, H 7.83, N 11.90.

***n*-Propyl-1-(pyridin-2-ylmethyl)pyrrolidine-2-carboxylate (PyProPr) (3):** An orange suspension of 2-(chloromethyl)pyridinium chloride (3.30 g, 20.1 mmol), (*S*)-2-(*n*-propoxycarbonyl)pyrrolidinium chloride (5.32 g, 26.8 mmol), NaI (1.19 g, 7.94 mmol) and Na_2CO_3 (7.29 g, 68.8 mmol) in anhydrous DMF (54 mL) was stirred at 50

ºC. After 25 h the resulting pink suspension was taken up in H_2O (110 mL) and extracted with CH_2Cl_2 (5 x 30 mL). The organic phases were combined, washed with H_2O (50 mL), dried (Na_2SO_4), filtered and evaporated. The remaining red oil was subjected to column chromatography (SiO_2 (250 mL), Et_2O/hexanes/Et_3N 75:25:2 (*v*/*v*), R_f = 0.3). A remaining impurity (^{1}H NMR ($CDCl_3$): 6.83-6.87 (m) and 7.18-7.22 (m)) was removed by heating the oil *in vacuo* (<0.1 mbar) at 110 ºC for 1 h to leave a dark yellow oil (3.99 g, 80%).

^{1}H NMR (400 MHz, $CDCl_3$, 25 ºC): δ = 0.91 (t, 3H, $^3J_{HH}$ = 7.2 Hz, C*H*$_3$), 1.63 (sxt, 2H, $^3J_{HH}$ = 7.2 Hz, CH$_2$C*H*$_2$CH$_3$), 1.78-2.03 (m, 3H, CH$_2$ ring, γ and β to CO), 2.12-2.23 (m, 1H, CH$_2$ ring, β to CO), 2.53-2.60 (m, 1H, NC*H*H ring), 3.08-3.13 (m, 1H, NCH*H* ring), 3.43-3.46 (m, 1H, C*H* α to CO), 3.80 (d, 1H, $^2J_{HH}$ = 13.6 Hz, ArC*H*HN), 3.99-4.08 (m, 2H, C*H*$_2$CH$_2$CH$_3$), 4.10 (d, 1H, $^2J_{HH}$ = 13.6 Hz, ArCH*H*N), 7.13 (dd, 1H, $^3J_{HH}$ = 7.6 Hz, $^3J_{HH}$ = 4.8 Hz, Py*H*(5)), 7.46 (d, 1H, $^3J_{HH}$ = 7.6 Hz, Py*H*(3)), 7.64 (t, 1H, $^3J_{HH}$ = 7.6 Hz, Py*H*(4)), 8.50 (d, 1H, $^3J_{HH}$ = 4.8 Hz, Py*H*(6)) ppm. ^{13}C{^{1}H} NMR (100 MHz, $CDCl_3$, 25 ºC): δ = 10.5, 22.1, 23.3, 29.4, 53.5, 60.2, 65.5, 66.3,122.2, 123.5, 136.6, 149.0, 158.9, 174.1 ppm. IR (film): ν = 2967.0, 1728.2, 1588.8, 1569.9, 1473.9, 1433.3, 1360.5, 1269.9, 1174.1, 1086.8, 1059.3, 1046.3, 993.5, 934.6, 897.1, 757.7 cm^{-1}. UV-Vis (MeCN) [λ_{max}, nm (ε, M^{-1} cm^{-1})]: 202 (7617), 261 (3024). $[\alpha]_D^{21}$ –65.4 deg cm^3 g^{-1} dm^{-1} (c 0.8, $CHCl_3$). Anal. for $C_{14}H_{20}N_2O_2$ (248.32): calc. C 67.71, H 8.12, N 11.28; found C 67.64, H 8.17, N 11.25.

***n*-Propyl-1-((6-methylpyridin-2-yl)methyl)pyrrolidine-2-carboxylate (6-Me-PyProPr) (4):** A yellow suspension of 2-(chloromethyl)-6-methylpyridinium chloride (2.02 g, 11.3 mmol), (*S*)-2-(*n*-propoxycarbonyl)pyrrolidinium chloride (2.99 g, 15.4 mmol), NaI (0.68 g, 4.5 mmol) and Na_2CO_3 (4.13 g, 39.0 mmol) in anhydrous DMF (31 mL) was stirred at 50 ºC. After 25 h the faintly yellow suspension was taken up in H_2O (60 mL) and extracted with CH_2Cl_2 (5 x 25 mL). The organic phases were combined, washed with H_2O (20 mL), dried (Na_2SO_4), filtered and evaporated. The remaining orange oil was subjected to column chromatography (SiO_2 (200 mL), Et_2O/hexanes/Et_3N 75:25:2 (*v*/*v*), R_f = 0.4). A remaining impurity was removed by heating the oil *in vacuo* (<0.1 mbar) at 110 ºC for 60 min to leave a yellow oil (2.65 g, 89%).

^{1}H NMR (400 MHz, $CDCl_3$, 25 ºC): δ = 0.91 (t, 3H, $^3J_{HH}$ = 7.2 Hz, CH$_2$CH$_2$C*H*$_3$), 1.62 (sxt, 2H, $^3J_{HH}$ = 7.2 Hz, CH$_2$C*H*$_2$CH$_3$), 1.75-2.01 (m, 3H, CH$_2$ ring, γ and β to CO), 2.10-2.20 (m, 1H, CH$_2$ ring, β to CO), 2.51-2.57 (m, 1H, NC*H*H ring), 2.52 (s, 3H, ArC*H*$_3$), 3.07-3.12 (m, 1H, NCH*H* ring), 3.39-3.43 (m, 1H, C*H* α to CO), 3.76 (d, 1H, $^2J_{HH}$ = 14.0 Hz, ArC*H*HN), 3.97-4.07 (m, 2H, C*H*$_2$CH$_2$CH$_3$), 4.04 (d, 1H, $^2J_{HH}$ = 14.0 Hz, ArCH*H*N), 7.00 (d, 1H, $^3J_{HH}$ = 7.6 Hz, Py*H*(5)), 7.29 (d, 1H, $^3J_{HH}$ = 7.6 Hz, Py*H*(3)), 7.52 (t, 1H, $^3J_{HH}$ = 7.6 Hz, Py*H*(4)) ppm. ^{13}C{^{1}H} NMR (100 MHz, $CDCl_3$, 25 ºC): δ = 10.5, 22.1, 23.4, 24.5, 29.5, 53.6, 60.3, 65.5, 66.2, 120.3, 121.7, 136.9,

157.5, 158.3, 174.2 ppm. IR (film): ν = 2967.7, 1728.6, 1591.5, 1578.1, 1456.4, 1357.7, 1267.0, 1173.4, 1086.8, 1059.2, 1040.2, 991.7, 935.4, 900.8, 782.9, 757.5 cm^{-1}. UV-Vis (MeCN) [λ_{max}, nm (ε, M^{-1} cm^{-1})]: 207 (8018), 265 (4347). $[\alpha]_D^{21}$ –65.8 deg cm^3 g^{-1} dm^{-1} (c 0.7, $CHCl_3$). Anal. for $C_{15}H_{22}N_2O_2$ (262.35): calc. C 68.67, H 8.45, N 10.68; found C 68.57, H 8.65, N 10.63.

1-((6-Methylpyridin-2-yl)methyl)pyrrolidine-2-carboxamide (6-Me-PyProNH$_2$) (6): A colorless solution of **2** (3.48 g, 14.9 mmol) in anhydrous MeOH (60 mL) was saturated with NH_3 at 0 ºC for 30 min. The solution was allowed to reach ambient temperature and after 6 days was evaporated to dryness. The remaining yellow oil was dissolved in a small amount of eluent and subjected to column chromatography (SiO_2 (400 mL), Et_2O/MeOH/Et_3N 30:1:1 → 30:3:1 (*v*/*v*), R_f = 0.3-0.4). A remaining impurity (^{1}H NMR ($CDCl_3$): 6.83-6.86 (m) and 7.17-7.21 (m)) was removed by heating *in vacuo* (<0.5 mbar) at 100 ºC for 2 h to leave a yellow, highly viscous oil, which solidified upon standing for several weeks (2.65 g, 81%).
^{1}H NMR (400 MHz, $CDCl_3$, 25 ºC): δ = 1.72-1.85 (m, 2H, CH_2 ring, γ to CO), 1.94-2.02 (m, 1H, CH_2 ring, β to CO), 2.21-2.31 (m, 1H, CH_2 ring, β to CO), 2.48-2.55 (m, 1H, NC*H*H ring), 2.53 (s, 3H, ArC*H*$_3$), 3.07-3.12 (m, 1H, NCH*H* ring), 3.37 (s (br), 1H, C*H* α to CO), 3.72 (d, 1H, $^2J_{HH}$ = 13.6 Hz, ArC*H*HN), 3.99 (d, 1H, $^2J_{HH}$ = 13.6 Hz, ArCH*H*N), 5.58 (s (br), 1H, N*H*H), 7.03 (d, 1H, $^3J_{HH}$ = 7.6 Hz, Py*H*(5)), 7.06 (d, 1H, $^3J_{HH}$ = 7.6 Hz Py*H*(3)), 7.53 (t, 1H, $^3J_{HH}$ = 7.6 Hz, Py*H*(4)), 8.01 (s (br), 1H, NH*H*) ppm. ^{13}C{^{1}H} NMR (100 MHz, $CDCl_3$, 25 ºC): δ = 24.4, 24.6, 30.7, 54.3, 61.1, 67.4, 119.8, 122.1, 137.1, 157.7, 158.4, 177.9 ppm. IR (solid): ν = 3388.2, 3191.1, 2972.0, 2920.6, 2872.6, 2825.5, 1624.5, 1594.4, 1576.8, 1460.0, 1402.2, 1374.8, 1331.9, 1310.0, 1275.1, 1235.0, 1196.8, 1156.3, 1111.2, 983.3, 899.8, 785.6 cm^{-1}. UV-Vis (MeCN) [λ_{max}, nm (ε, M^{-1} cm^{-1})]: 199 (8820), 265 (4012). $[\alpha]_D^{21}$ –42.3 deg cm^3 g^{-1} dm^{-1} (c 0.6, $CHCl_3$). Anal. for $C_{12}H_{17}N_3O$ (219.28): calc. C 65.73, H 7.81, N 19.16; found C 65.64, H 7.76, N 19.05.

(1-((6-Methylpyridin-2-yl)methyl)pyrrolidin-2-yl)diphenylmethanol (6-Me-PyProPh$_2$OH) (8): Cut and oven-dried Mg turnings were stirred and heated under N_2. After 30 min they were wetted with anhydrous THF and treated with 8 drops of 1,2-dibromoethane. The mixture was heated for 5 min, stirred for 30 min, diluted with THF (15 mL), and subsequently treated dropwise during 40 min with a solution of anhydrous bromobenzene in THF (30 mL) with stirring. After stirring for 20 h the mixture was concentrated *in vacuo* (to 24 mL). The grey suspension was cooled to 0 ºC and subsequently treated dropwise during 60 s *via cannula* with a solution of **2** (2.14 g, 9.14 mmol) in THF (10 mL) with vigorous stirring. The green solution was allowed to reach ambient temperature. After 60 min of stirring the solution was acidified with 2 M HCl (40 mL), and after 30 min the aqueous phase was basified to pH 8 with 2 M NaOH. After separation of the organic phase, the aqueous phase was

extracted with CH_2Cl_2 (2 x 80 mL, 1 x 40 mL). The combined organic phases were washed with H_2O (60 mL), dried (Na_2SO_4), filtered, and evaporated. The remaining yellow solid was dissolved in CH_2Cl_2 (10 mL), purified by column chromatography (SiO_2 (250 mL), hexanes/EtOAc 4:1 → 0:1 (*v*/*v*), R_f (hexanes/EtOAc 2:1) = 0.4), and dried *in vacuo* to leave a white powder (2.80 g, 85%).
^{1}H NMR (400 MHz, $CDCl_3$, 25 ºC): δ = 1.66 (s (br), 2H, CH_2 ring, γ to CO), 1.79 (s (br), 1H, CH_2 ring, β to CO), 1.92-2.02 (m, 1H, CH_2 ring, β to CO *H*), 2.44-2.65 (m, 1H, NC*H*H ring), 2.49 (s, 3H, ArCH_3), 3.03 (s (br), 1H, NCH*H* ring), 3.40 (s (br), 2H, C*H* α to CO and ArC*H*HN), 4.12 (s (br), 1H, ArCH*H*N), 5.16 (s (br), 1H, O*H*), 6.93 (d, 1H, $^3J_{HH}$ = 7.6 Hz Py*H*(5)), 6.97 (d, 1H, $^3J_{HH}$ = 7.6 Hz, Py*H*(3)), 7.08 (t, 1H, $^3J_{HH}$ = 7.2 Hz, *p*-Ph*H*), 7.16 (t, 1H, $^3J_{HH}$ = 7.6 Hz, *p*-Ph*H*), 7.22 (t, 2H, $^3J_{HH}$ = 7.6 Hz, *m*-Ph*H*), 7.29 (t, 2H, $^3J_{HH}$ = 7.6 Hz, *m*-Ph*H*), 7.48 (t, 1H, $^3J_{HH}$ = 7.6 Hz, Py*H*(4)), 7.58 (d, 2H, $^3J_{HH}$ = 7.6 Hz, *o*-Ph*H*), 7.68 (d, 2H, $^3J_{HH}$ = 7.6 Hz, *o*-Ph*H*) ppm. $^{13}C\{^1H\}$ NMR (100 MHz, $CDCl_3$, 25 ºC): δ = 24.5, 29.8, 55.9, 62.3, 71.3, 78.2, 119.5, 121.5, 125.9, 126.4, 126.6, 128.2, 128.3, 136.8, 146.5, 157.4 ppm. IR (solid): ν = 3267.6, 2966.6, 2947.0, 2821.8, 1592.1, 1577.5, 1487.2, 1449.1, 1393.0, 1300.0, 1250.0, 1206.3, 1155.8, 1135.0, 1106.4, 1083.3, 1062.1, 1032.5, 962.3, 944.3, 924.9, 895.6, 870.1, 832.1, 795.0, 767.4, 753.3, 711.1, 703.3, 658.7 cm^{-1}. UV-Vis (MeCN) [λ_{max}, nm (ε, M^{-1} cm^{-1})]: 203 (55625), 265 (7885). $[\alpha]_D^{21}$ +54.3 deg cm^3 g^{-1} dm^{-1} (c 0.6, $CHCl_3$). Anal. for $C_{24}H_{26}N_2O$ (358.48): calc. C 80.41, H 7.31, N 7.81; found C 80.46, H 7.37, N 7.78.

[Fe(PyProPr)$_2$](OTf)$_2$ (9): A solution of Fe(OTf)$_2$·2MeCN (725 mg, 1.66 mmol) in anhydrous, degassed MeCN (23 mL) was added *via cannula* with stirring to a solution of **3** (0.83 g, 3.3 mmol) in MeCN (23 mL). Immediately upon addition a color change to yellow was observed. After 60 min stirring at RT the solvent was evaporated *in vacuo* to leave an orange foam. The product was purified twice by the addition of Et_2O (2x 30 mL) to a solution of the product in MeCN (2 x 7 mL) with stirring (for 16 h, for 1 h). The colorless supernatants were removed *via cannula*. The remaining red-brown oil was dried *in vacuo* to leave an orange foam. Stirring *in vacuo* resulted in a white powder with an orange-pink hue (1.11 g, 78%).
IR (solid): ν = 2973.1, 1658.7, 1608.8, 1447.4, 1415.6, 1365.6, 1254.8, 1222.9, 1148.4, 1104.7, 1081.9, 1052.9, 1028.0, 930.0, 845.9, 767.9 cm^{-1}. IR (MeCN): ν = 2250 (νCN), 1664 (νCO), 1274 ($\nu_{as}SO_3$), 1224 (ν_sCF_3), 1158 ($\nu_{as}CF_3$), 1034 (ν_sSO_3) cm^{-1}. UV-Vis (MeCN) [λ_{max}, nm (ε, M^{-1} cm^{-1})]: 205 (13387), 260 (6357), 354 (593). $[\alpha]_D^{21}$ 0 deg cm^3 g^{-1} dm^{-1} (c 0.6, MeCN). Anal. for $C_{30}H_{40}F_6FeN_4O_{10}S_2$ (850.62): calc. C 42.36, H 4.74, N 6.59; found C 42.18, H 4.75, N 6.62. ESI-MS: m/z = 701.191 ([M-OTf]$^+$, calc. 701.192). Solution magnetic moment (Evans' method): μ_{eff} = 4.86 μ_B.

[Fe(PyProNH$_2$)$_2$](OTf)$_2$ (10): A solution of Fe(OTf)$_2$·2MeCN (476 mg, 1.09 mmol) in anhydrous, degassed MeCN (15 mL) was added *via cannula* with stirring to a

solution of **5** (0.46 g, 2.2 mmol) in MeCN (15 mL). Immediately upon addition a color change to yellow was observed. After 60 min stirring at RT the solvent was evaporated *in vacuo* to leave a bright yellow foam. The product was precipitated by the addition of Et_2O (40 mL) to a solution of the product in MeCN (5 mL) with stirring for 60 min. The colorless supernatant was removed *via cannula*. The remaining yellow powder was recrystallized from MeCN (5 mL) by the addition of Et_2O (25 mL) and dried *in vacuo* (752 mg, 90%). Slow vapor diffusion of Et_2O into a concentrated solution of **10** in MeCN yielded yellow, needle-shaped crystals suitable for X-ray diffraction.
IR (solid): ν = 3353.1, 1673.6, 1592.4, 1481.8, 1439.7, 1249.9, 1224.5, 1149.2, 1106.5, 1055.0, 1026.8, 991.7, 926.6, 843.5, 781.6, 757.2 cm^{-1}. IR (MeCN): ν = 2250 (νCN), 1668 (νCO), 1270 ($\nu_{as}SO_3$), 1227 (ν_sCF_3), 1158 ($\nu_{as}CF_3$), 1031 (ν_sSO_3) cm^{-1}. UV-Vis (MeCN) [λ_{max}, nm (ε, M^{-1} cm^{-1})]: 365 (785). $[\alpha]_D^{21}$ +208 deg cm^3 g^{-1} dm^{-1} (c 0.3, MeCN). Anal. for $C_{24}H_{30}F_6FeN_6O_8S_2$ (764.50): calc. C 37.71, H 3.96, N 10.99; found C 37.85, H 4.06, N 11.05. ESI-MS: m/z = 615.125 ($[M\text{-}OTf]^+$, calc. 615.130). Solution magnetic moment (Evans' method): μ_{eff} = 4.46 μ_B.

$[Fe(PyProPh_2OH)_2](OTf)_2$ (11): A solution of $Fe(OTf)_2 \cdot 2MeCN$ (636 mg, 1.46 mmol) in anhydrous, degassed MeCN (20 mL) was added *via cannula* with stirring to a solution of **7** (1.01 g, 2.93 mmol) in CH_2Cl_2 (22 mL). Immediately upon addition a color change to bright yellow was observed. After 60 min stirring at RT the solvent was evaporated *in vacuo* to leave a yellow solid. The product was recrystallized twice by the addition of Et_2O (50 mL, 65 mL) to a solution of the product in MeCN (10 mL, 12 mL). The yellow supernatants were removed *via cannula*. The remaining off-white powder was dried *in vacuo* (939 mg, 62%). IR (solid): ν = 3338.5 (b), 2972.4, 1610.1, 1574.4, 1491.5, 1449.3, 1430.2, 1277.0, 1243.6, 1222.6, 1156.8, 1110.6, 1074.9, 1055.2, 1027.0, 936.1, 889.4, 844.3, 768.9, 747.8, 707.3, 696.3, 663.9 cm^{-1}. UV-Vis (MeCN) [λ_{max}, nm (ε, M^{-1} cm^{-1})]: 204 (65048), 259 (12570), 331 (3900). $[\alpha]_D^{21}$ -21 deg cm^3 g^{-1} dm^{-1} (c 0.5, MeCN). Anal. for $C_{48}H_{48}F_6FeN_4O_8S_2$ (1042.88): calc. C 55.28, H 4.64, N 5.37; found C 55.20, H 4.99, N 5.46. ESI-MS: m/z = 893.269 ($[M\text{-}OTf]^+$, calc. 893.265). Solution magnetic moment (Evans' method): μ_{eff} = 4.58 μ_B.

$[Fe(PyProMe)Cl_2]$ (12): A solution of $FeCl_2$ (81 mg, 0.64 mmol) in anhydrous, degassed MeOH (4 mL) was added *via cannula* with stirring to a solution of **1** (140 mg , 0.64 mmol) in MeOH (4 mL). Immediately upon addition a color change to yellow was observed. After 60 min stirring at RT the solvent was evaporated *in vacuo* to leave a yellow solid/oil. The product was precipitated by the addition of Et_2O to a solution of the product in MeOH. The colorless supernatant was removed *via cannula*. The remaining yellow powder was dried in a stream of N_2 and subsequently *in vacuo* (206 mg, 93%). Slow vapor diffusion of Et_2O into a concentrated solution of **12** in MeOH yielded yellow crystalline needles suitable for X-ray diffraction. Slow solvent

diffusion of Et_2O into a concentrated solution of **12** in CH_2Cl_2 at RT yielded yellow, blocky crystals suitable for X-ray diffraction.
IR (solid): ν = 3285.4 (b), 2966.7, 2907.4, 1696.6, 1602.3, 1568.7, 1476.8, 1442.0, 1388.4, 1366.0, 1346.2, 1296.9, 1271.8, 1254.5, 1171.2, 1099.4, 1077.4, 1050.4, 1025.8, 996.4, 958.6, 931.9, 912.1, 872.8, 859.0, 825.6, 783.1, 771.3, 665.2 cm^{-1}. IR (MeCN): ν = 2247 (νCN), 1668 (νCO) cm^{-1}. UV-Vis (MeCN) [λ_{max}, nm (ε, M^{-1} cm^{-1})]: 291 (866), 363 (501). $[\alpha]_D^{21}$ +24.9 deg cm^3 g^{-1} dm^{-1} (c 0.42, MeCN). Anal. for $C_{13}H_{20}Cl_2FeN_2O_3$ (379.06): calc. C 41.19, H 5.32, N 7.39; found C 41.11, H 5.71, N 7.26. ESI-MS: m/z = 311.025 ($[M-Cl]^+$, calc. 311.025). Solution magnetic moment (Evans' method): μ_{eff} = 4.62 μ_B.

[Fe(6-Me-PyProMe)Cl_2] (13): Reacting $FeCl_2$ (100 mg, 0.79 mmol) with **2** (185 mg, 0.79 mmol) in the manner described for **12** yielded **13** as a yellow powder (258 mg, 90%). Slow vapor diffusion of Et_2O into a concentrated solution of **13** in MeOH yielded yellow, blocky crystals suitable for X-ray diffraction.
IR (solid): ν = 2982.4, 2925.3, 1687.4, 1604.5, 1571.2, 1442.6, 1391.1, 1313.1, 1266.0, 1223.0, 1182.3, 1162.0, 1082.4, 1049.8, 1033.1, 1012.0, 984.0, 941.0, 921.5, 872.8, 839.9, 818.2, 786.5, 733.3 cm^{-1}. IR (MeCN): ν = 2250 (νCN), 1702 (νCO) cm^{-1}. UV-Vis (MeCN) [λ_{max}, nm (ε, M^{-1} cm^{-1})]: 207 (9910), 267 (4282), 369 (338). $[\alpha]_D^{21}$ +29.6 deg cm^3 g^{-1} dm^{-1} (c 0.448, MeCN). Anal. for $C_{13}H_{18}Cl_2FeN_2O_2$ (361.05): calc. C 43.25, H 5.03, N 7.76; found C 43.18, H 5.14, N 7.83. ESI-MS: m/z = 325.041 ($[M-Cl]^+$, calc. 325.041). Solution magnetic moment (Evans' method): μ_{eff} = 5.07 μ_B.

[Fe(PyProNH_2)Cl_2] (14): Reacting $FeCl_2$ (104 mg, 0.82 mmol) with **5** (168 mg, 0.82 mmol) in the manner described for **12** yielded **14** as a yellow powder (245 mg, 90%). Slow vapor diffusion of Et_2O into a concentrated solution of **14** in MeCN yielded yellow, blocky crystals suitable for X-ray diffraction.
IR (solid): ν = 3315.1, 3162.0, 2972.0, 1652.3, 1602.1, 1476.1, 1444.5, 1383.9, 1299.6, 1155.1, 1102.8, 1052.1, 1019.1, 963.2, 927.8, 766.5 cm^{-1}. IR (MeCN): ν = 2247 (νCN), 1668 (νCO) cm^{-1}. UV-Vis (MeCN) [λ_{max}, nm (ε, M^{-1} cm^{-1})]: 385 (469). $[\alpha]_D^{21}$ +60 deg cm^3 g^{-1} dm^{-1} (c 0.3, MeOH). ESI-MS: m/z = 296.026 ($[M-Cl]^+$, calc. 296.025). Solution magnetic moment (Evans' method): μ_{eff} = 4.33 μ_B.

[Fe(6-Me-PyProNH_2)Cl_2] (15): Reacting $FeCl_2$ (102 mg, 0.80 mmol) with **6** (176 mg, 0.80 mmol) in the manner described for **12** yielded **15** as a yellow powder (260 mg, 94%). Slow vapor diffusion of Et_2O into a concentrated solution of **15** in MeOH yielded yellow, needle-shaped crystals suitable for X-ray diffraction.
IR (solid): ν = 3322.0, 3250.9, 3170.8, 2964.0, 2900.9, 1656.9, 1604.7, 1591.4, 1467.2, 1455.7, 1384.6, 1357.3, 1304.8, 1218.3, 1168.5, 1123.8, 1101.0, 1015.0, 895.1, 797.6, 781.8 cm^{-1}. UV-Vis (MeCN) [λ_{max}, nm (ε, M^{-1} cm^{-1})]: 385 (456). $[\alpha]_D^{21}$ +71 deg cm^3 g^{-1} dm^{-1} (c 0.4, MeOH). Anal. for $C_{12}H_{17}Cl_2FeN_3O$ (346.03): calc. C

41.65, H 4.95, N 12.14; found C 41.48, H 4.91, N 11.96. ESI-MS: m/z = 310.040 ($[M-Cl]^+$, calc. 310.041). Solution magnetic moment (Evans' method): μ_{eff} = 5.10 μ_B.

[Fe(PyProPh$_2$OH)Cl$_2$] (16): Reacting $FeCl_2$ (72 mg, 0.57 mmol) with **7** (197 mg, 0.57 mmol) in CH_2Cl_2 (5 mL) in the manner described for **12** yielded **16** as a yellow powder (242 mg, 90%). Slow solvent diffusion of Et_2O into a concentrated solution of **16** in CH_2Cl_2 yielded yellow, blocky crystals suitable for X-ray diffraction.
IR (solid): ν = 3060.0, 2988.8 1605.0, 1483.4, 1444.4, 1369.4, 1343.9, 1325.3, 1275.4, 1176.8, 1152.4, 1066.2, 1049.7, 1011.8, 960.8, 940.3, 905.4, 855.7, 778.4, 752.1, 696.5, 665.0 cm^{-1}. UV-Vis (MeCN) [λ_{max}, nm (ε, M^{-1} cm^{-1})]: 255 (7096), 292 (5319). $[\alpha]_D^{21}$ -32 deg cm^3 g^{-1} dm^{-1} (c 0.1, MeCN). Anal. for $C_{23}H_{24}Cl_2FeN_2O$ (471.20): calc. C 58.63, H 5.13, N 5.95; found C 58.58, H 5.20, N 5.86. ESI-MS: m/z = 435.091 ($[M-Cl]^+$, calc. 435.093). Solution magnetic moment (Evans' method): μ_{eff} = 5.44 μ_B.

[Fe(6-Me-PyProPh$_2$OH)Cl$_2$] (17): Reacting $FeCl_2$ (75 mg, 0.59 mmol) with **8** (212 mg, 0.59 mmol) in CH_2Cl_2 (5 mL) in the manner described for **12** yielded **17** as a yellow powder (245 mg, 85%). Slow solvent diffusion of Et_2O into a concentrated solution of **17** in CH_2Cl_2 yielded yellow, blocky crystals suitable for X-ray diffraction.
IR (solid): ν = 3059.0, 2974.3, 1606.2, 1574.6, 1491.4, 1463.1, 1446.7, 1382.0, 1345.3, 1321.9, 1274.4, 1160.9, 1084.7, 1067.3, 1037.2, 1005.9, 907.7, 853.9, 782.9, 747.4, 705.5, 695.0, 657.4 cm^{-1}. UV-Vis (MeCN) [λ_{max}, nm (ε, M^{-1} cm^{-1})]: 205 (21889), 261 (7282), 316 (4139). $[\alpha]_D^{21}$ +19 deg cm^3 g^{-1} dm^{-1} (c 0.1, MeCN). Anal. for $C_{24}H_{26}Cl_2FeN_2O$ (485.23): calc. C 59.41, H 5.40, N 5.77; found C 59.33, H 5.36, N 5.66. ESI-MS: m/z = 449.106 ($[M-Cl]^+$, calc. 449.108). Solution magnetic moment (Evans' method): μ_{eff} = 5.23 μ_B.

Protocol for catalytic olefin oxidation: To a solution of Fe-complex (3.5 μmol) in anhydrous, degassed acetonitrile was added substrate (1.75 mmol) to obtain a total volume of 3.0 mL. Subsequently, 0.5 mL of oxidant solution (700 mM solution in acetonitrile diluted from 35% aqueous H_2O_2) was added portion wise in 30 min. The reaction mixture was stirred at room temperature and after 1 h (from start of oxidant addition) internal standard (10 μL, cyclooctene: 1,2-dibromobenzene, all other substrates: bromobenzene) was added and the first sample was taken. To an aliquot of the reaction mixture was added diethyl ether. The sample was analyzed by GC. The products were identified and quantified by comparison with authentic compounds.

X-ray crystal structure determinations: Reflections were measured on a Nonius KappaCCD diffractometer with rotating anode and graphite monochromator (λ = 0.71073 Å). Intensity data were integrated with the software Eval14 [42] (compound **10**), Eval15[43] (compound **15**) or HKL2000[44] (compounds **12a, 12b, 13, 14, 16, 17**).

Absorption correction and scaling was performed based on multiple measured reflections with SADABS[45] (**10**-**15**) or SORTAV[46] (**16**, **17**). The structures were solved by Direct Methods using the programs SHELXS-97[47] (**10**, **12b**, **13**-**17**) or SIR-97[48] (**12a**). Least-squares refinement was performed with SHELXL-97[47] against F^2 of all reflections. Non-hydrogen atoms were refined freely with anisotropic displacement parameters. Hydrogen atoms were introduced in calculated positions (**10, 12a, 13**) or located in difference Fourier maps (**12b, 14-17**). Hydrogen atoms were refined with a riding model, the N-H or O-H hydrogen atoms of **12b, 14,** and **15** were refined freely with isotropic displacement parameters. The crystal structure of **10** was refined as a twin with (-1,0,0 / 0,-1,0 / 1,0,1) as twin matrix (pseudo-orthorhombic C-centered lattice). The twin fraction refined to 0.4877(13). The triflate anions in **10** were refined with disorder models using restraints for distances and angles and for the approximation of isotropic behavior. Geometry calculations and checking for higher symmetry was performed with the PLATON program[49].Further details of the crystal structure determinations are given in the Tables 10-14.

Table 10. Experimental details of crystal structure **10**.

	10
formula	$[C_{22}H_{30}FeN_6O_2](CF_3O_3S)_2$
Fw	764.51
crystal color	yellow
crystal size [mm^3]	0.54x0.08x0.06
T [K]	150(2)
crystal system	monoclinic
space group	$P2_1$ (No. 4)
a [Å]	7.0198(6)
b [Å]	18.956(2)
c [Å]	11.9392(7)
β [º]	107.114(3)
V [$Å^3$]	1518.4(2)
Z	2
D_{calc} [g/cm^3]	1.672
$(\sin \theta/\lambda)_{max}$ [$Å^{-1}$]	0.61
refl. measured/unique	20320 / 5667
parameters / restraints	517 / 454
R1/wR2 [I>2σ(I)]	0.0317 / 0.0568
R1/wR2 [all refl.)]	0.0394 / 0.0595
Flack x[50]	0.00(2)
S	1.068
ρ(min/max) [$eÅ^{-3}$]	-0.26 / 0.27

Table 11. Experimental details of crystal structures **12a** and **12b**.

	12a	**12b**
formula	$C_{12}H_{16}Cl_2FeN_2O_2$	$C_{13}H_{20}Cl_2FeN_2O_3$
Fw	347.02	379.06
crystal color	yellow	yellow
crystal size [mm^3]	0.36x0.18x0.09	0.42x0.18x0.12
T [K]	150(2)	150(2)
crystal system	hexagonal	orthorhombic
space group	$P6_5$ (No. 170)	$P2_12_12_1$ (No. 19)
a [Å]	8.3897(1)	11.5923(1)
b [Å]	-	11.6358(1)
c [Å]	35.4893(5)	12.1043(2)
V [$Å^3$]	2163.32(5)	1632.70(3)
Z	6	4
D_{calc} [g/cm^3]	1.598	1.542
$(\sin\theta/\lambda)_{max}$ [$Å^{-1}$]	0.65	0.65
refl. measured/unique	11159 / 3256	28909 / 3728
parameters / restraints	173 / 1	196 / 0
R1/wR2 [$I>2\sigma(I)$]	0.0252 / 0.0507	0.0223 / 0.0491
R1/wR2 [all refl.)]	0.0300 / 0.0528	0.0251 / 0.0503
Flack x[50]	-0.015(11)	0.000(10)
S	1.072	1.071
ρ(min/max) [$eÅ^{-3}$]	-0.21 / 0.21	-0.22 / 0.21

Table 12. Experimental details of crystal structure **13**.

	13
formula	$C_{13}H_{18}Cl_2FeN_2O_2$
Fw	361.04
crystal color	yellow
crystal size [mm^3]	0.36x0.09x0.09
T [K]	150(2)
crystal system	orthorhombic
space group	$P2_12_12_1$ (No. 19)
a [Å]	8.0901(1)
b [Å]	12.9326(2)
c [Å]	14.6255(2)
V [$Å^3$]	1530.21(4)
Z	4
D_{calc} [g/cm^3]	1.567
$(\sin \theta/\lambda)_{max}$ [$Å^{-1}$]	0.65
refl. measured/unique	27410 / 3509
parameters / restraints	183 / 0
R1/wR2 [$I>2\sigma(I)$]	0.0271 / 0.0615
R1/wR2 [all refl.)]	0.0337 / 0.0647
Flack x^{50}	-0.012(13)
S	1.075
ρ(min/max) [$eÅ^{-3}$]	-0.29 / 0.29

Table 13. Experimental details of crystal structures **14** and **15**.

	14	**15**
formula	$C_{13}H_{18}Cl_2FeN_4O$	$C_{12}H_{17}Cl_2FeN_3O$
Fw	373.06	346.04
crystal color	yellow	yellow
crystal size [mm^3]	0.42x0.18x0.06	0.60x0.27x0.18
T [K]	110(2)	150(2)
crystal system	triclinic	monoclinic
space group	P1 (No. 1)	$P2_1$ (No. 4)
a [Å]	6.8899(1)	8.89008(11)
b [Å]	7.4891(1)	8.19097(10)
c [Å]	9.0561(1)	10.05615(16)
α [º]	113.7230(8)	-
β [º]	92.0237(7)	90.575(1)
γ [º]	107.1842(6)	-
V [$Å^3$]	402.305(9)	732.236(17)
Z	1	2
D_{calc} [g/cm^3]	1.540	1.569
$(\sin\theta/\lambda)_{max}$ [$Å^{-1}$]	0.65	0.65
refl. measured/unique	9765 / 3636	26417 / 3374
parameters / restraints	199 / 3	181 / 1
R1/wR2 [$I>2\sigma(I)$]	0.0215 / 0.0488	0.0154 / 0.0401
R1/wR2 [all refl.)]	0.0229 / 0.0496	0.0157 / 0.0404
Flack x^{50}	0.000(9)	-0.008(8)
S	1.084	1.069
ρ(min/max) [$eÅ^{-3}$]	-0.21 / 0.25	-0.27 / 0.26

Table 14. Experimental details of crystal structures **16** and **17**.

	16	**17**
formula	$C_{23}H_{24}Cl_2FeN_2O \cdot 0.5CH_2Cl_2$	$C_{24}H_{26}Cl_2FeN_2O$
Fw	513.66	485.22
crystal color	yellow	yellow
crystal size [mm^3]	0.48x0.27x0.24	0.36x0.18x0.15
T [K]	150(2)	150(2)
crystal system	monoclinic	monoclinic
space group	$P2_1$ (No. 4)	$P2_1$ (No. 4)
a [Å]	11.2439(1)	11.1681(2)
b [Å]	12.5035(1)	12.3970(2)
c [Å]	16.7671(2)	16.8766(3)
β [º]	101.8532(4)	103.6971(8)
V [$Å^3$]	2306.99(4)	2270.13(7)
Z	4	4
D_{calc} [g/cm^3]	1.479	1.420
$(\sin \theta/\lambda)_{max}$ [$Å^{-1}$]	0.65	0.65
refl. measured/unique	38678 / 10555	34625 / 10331
parameters / restraints	550 / 1	543 / 1
R1/wR2 [I>2σ(I)]	0.0286 / 0.0712	0.0409 / 0.0846
R1/wR2 [all refl.)]	0.0308 / 0.0728	0.0546 / 0.0914
Flack x[50]	-0.012(8)	-0.005(11)
S	1.030	1.051
ρ(min/max) [$eÅ^{-3}$]	-0.61 / 0.44	-0.33 / 0.54

References

1. Meunier, B. *Biomimetic Oxidations Catalyzed by Transition Metal Complexes*, Imperial College Press, London, **1999**.
2. Costas, M.; Mehn, M.P.; Jensen, M.P.; Que, L. Jr. *Chem. Rev.,* **2004**, *104*, 939-986.
3. (a) Rosenzweig, A.C.; Frederick, C.A.; Lippard, S.J.; Nordlund, P. *Nature,* **1993**, *366*, 537-543. (b) Rosenzwieg, A.C.; Nordlund, P.; Takahara, P.M.; Frederick, C.A.; Lippard, S.J. *Chem. Biol.,* **1995**, *2*, 409-418. (c) Elango, N.; Radhakrishnam, R.; Froland, W.A.; Waller, B.J.; Earhart, C.A.; Lipscomb, J.D.; Ohlendorf, D.H. *Prot. Sci*., **1997**, *6*, 556-568.
4. Bruijnincx, P.C.A.; van Koten, G.; Klein Gebbink, R.J.M. *Chem. Soc. Rev*., **2008**, *37*, 2716-2744.
5. (a) Kovaleva, E.G.; Lipscomb, J.D. *Nature Chem. Biol*., **2008**, *4*, 186-193. (b) Koehntop, K.D.; Emerson, J.P.; Que, L. Jr. *J. Biol. Inorg. Chem*., **2005**, *10*, 87-93.
6. Hegg, E.L.; Ho, R.Y.K.; Que, L. Jr. *J. Am. Chem. Soc.,* **1999**, *121*, 1972-1973.
7. Mehn, M.P.; Fujisawa, K.; Hegg, E.L.; Que, L. Jr. *J. Am. Chem. Soc.,* **2003**, *125*, 7828-7842.

8. (a) Dong, Y.; Fujii, H.; Hendrich, M.P.; Leising, R.A.; Pan, G.; Randall, C.R.; Wilkinson, E.C.; Zang, Y.; Que, L. Jr.; Fox, B.G.; Kauffmann, K.; Münck, E. *J. Am. Chem. Soc*., **1995**, *117*, 2778-2792. (b) Zang, Y.; Kim, J.; Dong, Y.; Wilkinson, E.C.; Appelman, E.H.; Que, L. Jr. *J. Am. Chem. Soc*., **1997**, *119*, 4197-4205. (c) Kim, C.; Chen, K.; Kim, J.; Que, L. Jr. *J. Am. Chem. Soc*., **1997**, *119*, 5964-5965. (d) Chen, K.; Que, L. Jr. *J. Am. Chem. Soc*., **2001**, *123*, 6327-6337. (e) Chen, K.; Costas, M.; Kim, J.; Tipton, A.; Que, L. Jr. *J. Am. Chem. Soc*., **2002**, *124*, 3026-3235. (f) Ryu, J.Y.; Kim, J.; Costas, M.; Chen, K.; Nam, W.; Que, L. Jr. *Chem. Commun.,* **2003**, 1288-1289.
9. Costas, M.; Tipon, A.K.; Chen, K.; Jo, D.-W.; Que, L. Jr. *J. Am. Chem. Soc*., **2001**, *123*, 6722-6723.
10. (a) Wieghardt, K.; Pohl, K.; Gebert, W. *Angew. Chem., Int. Ed. Engl.,* **1983**, *22*, 727. (b) Shul'pin, B.B.; Nizova, G.V.; Kozlov, Y.N.; Gonzales Cuervo, L.; Süss-Fink, G. *Adv. Synth. Catal*., **2004**, *346*, 317-332.
11. Beck, A.; Weibert, B.; Burzlaff, N. *Eur. J. Inorg. Chem.,* **2001**, 521-527.
12. Beck, A.; Barth, A.; Hübner, E.; Burzlaff, N. *Inorg. Chem.,* **2003**, *42*, 7182-7188.
13. Oldenburg, P.D.; Shteinman, A.A.; Que, L. Jr. *J. Am. Chem. Soc.,* **2005**, *127*, 15672-15673.
14. Friesse, S.J.; Kucera, B.E.; Que, L. Jr.; Tolman, W.B. *Inorg. Chem.,* **2006**, *45*, 8003-8005.
15. (a) Bruijnincx, P.C.A.; Lutz, M.; Spek, A.L.; van Faassen, E.E.; Weckhuysen, B.M.; van Koten, G.; Klein Gebbink, R.J.M. *Eur. J. Inorg. Chem*., **2005**, 779-787. (b) Bruijnincx, P.C.A.; Lutz, M.; den Breejen, J.P.; Spek, A.L.; van Koten, G.; Klein Gebbink, R.J.M. *J. Biol. Inorg. Chem.,* **2007**, *12*, 1181-1196. (c) Bruijnincx, P.C.A.; Buurmans, I.L.C.; Gosiewska, S.; Moelands, M.A.H.; Lutz, M.; Spek, A.L.; van Koten, G.; Klein Gebbink, R.J.M. *Chem. Eur. J*., **2008**, *14*, 1228-1237.
16. Bruijnincx, P.C.A.; Lutz, M.; Spek, A.L.; Hagen, W.R.; Weckhuysen, B.M.; van Koten, G.; Klein Gebbink, R.J.M. *J. Am. Chem. Soc*., **2007**, *129*, 2275-2286.
17. Peters, L.; Hübner, E.; Burzlaff, N. *J. Organomet. Chem.,* **2005**, *690*, 2009-2016.
18. Burzlaff, N. *Angew. Chem. Int. Ed.,* **2009**, *48*, 5580-5582.
19. Rocks, S.S.; Brennessel, W.W.; Machonkin, T.E.; Holland, P.L. *Inorg. Chim. Acta*., **2009**, *362*, 1387-1390.
20. Paria, S.; Halder, P.; Paine, T.K. *Inorg. Chem.,* **2010**, *49*, 4518-4523.
21. (a) Gosiewska, S.; Cornelissen, J.L.M.; Lutz, M.; Spek, A.L.; van Koten, G.; Klein Gebbink, R.J.M. *Inorg. Chem.,* **2006**, *45*, 4214-4227. (b) Gosiewska, S.; Lutz, M.; Spek, A.L.; Klein Gebbink, R.J.M. *Inorg. Chim. Acta,* **2007**, *360*, 405-417.
22. Chelucci, G.; Falorni, M.; Giacomelli, G. *Tetrahedron-Asymmetr.,* **1990**, *1*, 843.
23. Bergström, P.Å.; French, R. *J. Phys. Chem.,* **1995**, *99*, 12603-12611.
24. Britovsek, G.J.P.; Gibson, V.C.; Spitzmesser, S.K.; Tellmann, K.P.; White, A.J.P.; Williams, D.J. *J. Chem. Soc., Dalton Trans.,* **2002**, 1159-1171.
25. Evans, D.F. *J. Chem. Soc.,* **1959**, 2003-2005.
26. Addison, A.W.; Rao, T.N.; Reedijk, J.; van Rijn, J.; Verschoor, G.C. *J. Chem. Soc Dalton Trans.,* **1984**, 1349-1356.
27. Evans, G.G.; Boeyens, J.A. *Acta Cryst*., **1989**, *B45*, 581-590.
28. Moelands, M.A.H.; Nijsse, S.; Folkertsma, E.; de Bruin, B.; Lutz, M.; Spek, A.L.; Klein Gebbink, R.J.M. *Inorg. Chem.* **2013**, *52*, 7394.
29. Small, B.L.; Brookhart, M. *Marcomolecules,* **1999**, *32*, 2120-2130.
30. Pelascini, F.; Wesolek, M.; Peruch, F.; Lutz, P.J. *Eur. J. Inorg. Chem.,* **2006**, *21*, 4309-4316.
31. Dowling, C.; Murphy, V.J.; Parkin, G. *Inorg. Chem.,* **1996**, *35*, 2415-2420.
32. Biswas, M.; Pilet, G.; El Fallah, M.S.; Ribas, J.; Mitra, S. *Inorg. Chim. Acta,* **2008**, *361*, 387-392.
33. Amoroso, A.J.; Burrows, M.W.; Coles, S.J.; Haigh, R.; Farley, R.D.; Hursthouse, M.B.; Jones, M.; Malik, K.M.A.; Murphy, D.M. *Dalton Trans.,* **2008**, 506-513.
34. Holmes,; R.R. *Progress in Inorganic Chemistry* **1984**, *32*, 119-235.

35. Allen, F.H. *Acta Cryst*. **2002**, *B58*, 380-388.
36. (a) Argay, G.; Kalman, A.; Leovac, V.M. *Acta Crystallogr., Sect. C: Cryst. Struct. Commun.,* **1999***, 55*, 1440. (b) Yampol'skaya, M.A.; Shova, S.G.; Simonov, Y.A.; Gerbeleu, N.V.; Turte, K.I.; Zavodnik, V.E. *Russ. J. Inorg. Chem.,* **1985***, 30*, 1221. (c) Bernhardt, P.V.; Chin, P.; Sharpe, P.C.; Wang, J.-Y. C.; Richardson, D.R.; *J. Biol. Inorg. Chem.*, **2005***, 10*, 761. (d) Urakami, D.; Inoue, K.; Hayami, S. *Acta Crystallogr., Sect. E: Struct. Rep. Online,* **2009***, 65*, m800. (e) Liu, H.; Kou, Y.-Y.; Feng, L.; Li, D.-D.; Gao, C.-Y.; Tian, J.-L.; Zhang, J.-Y.; Yan, S.-P. *Appl. Organomet. Chem.,* **2010***, 24*, 636. (f) Tomic, Z.D.; Leovac, V.M.; Jacimovic, Z.K.; Giester, G.; Zaric, S.D. *Inorg. Chem. Commun.,* **2006***, 9*, 833. (g) Kleigrewe, N.; Steffen, W.; Blomker, T.; Kehr, G.; Frohlich, R.; Wibbeling, B.; Erker, G.; Wasilke, J.-C.; Wu, G.; Bazan, G.C. *J. Am. Chem. Soc.*, **2005**, *127*, 13955. (h) Gibson, V.C.; Redshaw, C.; Solan, G.A.; White, A.J.P.; Williams, D.J. *Organometallics,* **2007***, 26*, 5119. (i) O'Reilly, R.K.; Gibson, V.C.; White, A.J.P.; Williams, D.J. *J. Am. Chem. Soc.*, **2003***, 125*, 8450. (j) Kaul, F.A.R.; Puchta, G.T.; Frey, G.D.; Herdtweck, E.; Herrmann, W.A. *Organometallics*, **2007**, *26*, 988. (k) Hardman, N.J.; Fang, X.; Scott, B.L.; Wright, R.J.; Martin, R.L.; Kubas, G.J. *Inorg. Chem.*, **2005**, *44*, 8306. (l) Wu, W.-S.; Liu, S.-X. *Chem. J. Chin. Univ. (Chinese Edition)* **2003***, 24*, 2137. (m) Yamaguchi, Y.; Ando, H.; Nagaya, M.; Hinago, H.; Ito, T.; Asami, M.; *Chem. Lett.*, **2011**, *40*, 983.
37. Vahrenkamp, H. *Acc. Chem. Res.* **1999**, *32*, 589.
38. Company, A.; Gómez, L.; Fontrodona, X.; Ribas, X.; Costas, M. *Chem. Eur. J.,* **2008**, *14*, 5727-5731.
39. Gelalcha, F.G.; Bitterlich, B.; Anilkumar, G.; Tse, M.K.; Beller, M. *Angew. Chem. Int. Ed.,* **2007**, *46*, 7293-7296.
40. Hagen, K.S. *Inorg. Chem.,* **2000**, *39*, 5867-5869.
41. Suster, G.; Stoykova, S.A.; Linden, A.; Heimgartner, H. *Helv. Chim. Acta,* **2000**, *83*, 2961-2974.
42. Duisenberg, A.J.M.; Kroon-Batenburg, L.M.J.; Schreurs, A.M.M. *J. Appl. Cryst., **2003***, *36*, 220-229.
43. Schreurs, A.M.M.; Xian, X.; Kroon-Batenburg, L.M.J. *J. Appl. Cryst.,* **2010**, *43*, 70-82.
44. Otwinowski, Z.; Minor, W. *Methods in Enzymology, Volume 276* (C.W. Carter, Jr. & R.M. Sweet, Eds.) Academic Press (**1997**) 307-326.
45. Sheldrick, G.M. **1999**, SADABS: Area-Detector Absorption Correction, v2.10, Universität Göttingen, Germany.
46. Blessing, R.H. *Acta Cryst.,* **1995**, *A51*, 33-38.
47. Sheldrick, G.M. *Acta Cryst.,* **2008**, *A64*, 112-122.
48. Altomare, A.; Burla, M.C.; Camalli, M.; Cascarano, G.L.; Giacovazzo, C.; Guagliardi, A.; Moliterni, A.G.G.; Polidori, G.; Spagna, R. *J. Appl. Cryst.,* **1999**, *32*, 115-119.
49. Spek*,* A.L. *Acta Cryst.,* **2009**, *D65*, 148-155.
50. Flack, H.D. *Acta Cryst.,* **1983**, *A39*, 876-881.

6

Bio-inspired non-heme iron complexes derived from an extended series of N,N,O-ligated BAIP ligands

A series of mononuclear Fe(II) triflate complexes based on the 3,3-bis(1-alkylimidazole-2-yl)propionate ester (**BAIP**) ligand scaffold are reported. In these complexes the tripodal N,N,O **BAIP** ester ligand is varied by *i)* changing the ester moiety (*n*-Pr, *tert*-Bu esters, *n*-Pr amide), *ii)* changing the methylimidazole moieties into methylbenzimidazole moieties, and *iii)* changing the methylimidazole moieties into 1-ethyl-4-isopropylimidazole moieties. The general structure of the resulting complexes comprises two facially capping **BAIP** ligands around a coordinatively saturated octahedral Fe(II) center, with either a *transoid* or *cisoid* orientation of the N,N,O donor manifold depending on the combined steric and electronic demand of the ligands. In case of the sterically most encumbered ligand, a 4-coordinated all N-coordinated complex is formed as well, which co-crystallizes with the 6-coordinated complex. In combination with the catalytic properties of the new complexes in the epoxidation/*cis*-dihydroxylation of cyclooctene with H_2O_2, in terms of turn-over number and *cis*-diol formation, these studies provide a number of insights for further ligand design and catalyst development aimed at Fe-mediated *cis*-dihydroxylation.

Based on: Moelands, M.A.H.; Nijsse, S.; Folkertsma, E.; de Bruin, B.; Lutz, M.; Spek, A.L.; Klein Gebbink. R.J.M. *Inorg. Chem.* **2013**, *52*, 7394-7410.

6.1 Introduction

Oxidation reactions are important in the production of bulk and fine chemicals. More than 20% of all organic products made in the chemical industry are obtained via catalytic oxidation reactions.[1] The catalysts used in these reactions have an additional role when the stereochemistry of the oxidation product is of interest, for instance in the production of building blocks for the pharmaceutical industry. Of particular interest in this respect are catalysts that are able to bring about the stereo-selective *cis*-dihydroxylation of alkenes to the corresponding vicinal diols.

Several procedures are known to selectively oxidize alkene substrates to the corresponding *cis*-diols, but in most cases these reactions are associated with several unwanted drawbacks or problems.[2] For example, osmium tetroxide can be used catalytically in the presence of a secondary oxidant (e.g. hydrogen peroxide) to facilitate alkene *cis*-dihydroxylation.[3] The Sharpless AD mix α and β are commercially available osmium-based reagent mixtures for the asymmetric dihydroxylation of alkenes.[4] Although these systems are very reliable, the obvious disadvantages of the use of osmium are its price and toxicity. Several examples of alkene *cis*-dihydroxylation using ruthenium as an alternative to osmium have been reported.[5-7] Unfortunately, these ruthenium systems are not as selective as the osmium ones and, in addition, ruthenium may still be considered as an expensive metal. Alternatively, $KMnO_4$ may be used for alkene *cis*-dihydroxylation, albeit that stoichiometric amounts of this oxidant have to be used.[8,9] Catalytic systems based on manganese have been reported by Feringa[10] and Che.[11]

The answer to a good alternative for osmium in *cis*-dihydroxylation reactions might be found in nature, where several classes of metallo-enzymes catalyze a wide variety of oxidation reactions. One important class of enzymes in the perspective of *cis*-dihydroxylations are the Rieske oxygenases.[12] These dioxygenases are found in soil bacteria and catalyze the first step in the biodegradation of aromatic compounds by performing a *cis*-dihydroxylation on the arene substrate.[13] Because this reaction is regio- and stereospecific it was investigated extensively over the past two decades resulting in a range of crystallographic and mechanistic studies. The enzyme that is most studied is naphthalene dioxygenase (NDO), which catalyzes the *cis*-dihydroxylation of naphthalene to *cis*-(1R,2S)-1,2-dihydronaphtalene-1,2-diol. The combined crystallographic data on Rieske dioxygenases show that the catalytic sites of these dioxygenases are very similar. They all consist of a mononuclear iron center anchored to the enzyme by two histidine residues and a mono- or bidentate carboxylate ligand from either an aspartate or a glutamate residue (Figure 1). Depending on the coordination mode of the carboxylate, this active site architecture is referred to as either the 2-His-1-carboxylate facial triad (monodentate carboxylate)[14] or as the 2-His-1-carboxylate structural motif (bidentate carboxylate binding).[12] Because iron adopts an octahedral geometry in these enzymes, there are respectively three or two vacant sites left to bind substrate, dioxygen and/or cofactor ligands. If

none of these are bound, the sites are either occupied by weakly bounded solvent molecules or are vacant.

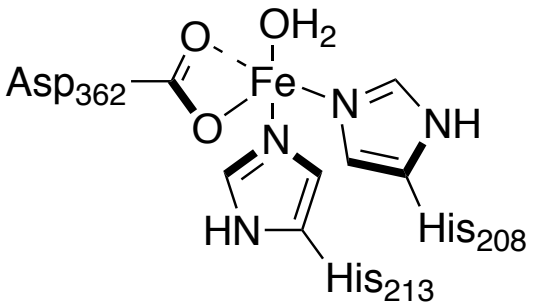

Figure 1. Structure of the mono-iron(II) active site in naphthalene 1,2-dioxygenase.

The interest in the catalytic properties of the Rieske dioxygenase have led to several endeavors trying to grasp its structure and reactivity in synthetic model systems. The structure of the 2-His-1-carboxylate facial triad structural motif has, in addition, become a designer platform for the development of synthetic Fe-based dihydroxylation catalysts. The group of Que was the first to synthesize a successful catalyst based on the active site of NDO.[15] The compound [Fe(II)(6-Me_3-TPA)(CH_3CN)$_2$](ClO_4)$_2$ (6-Me_3-TPA = tris[(6-methylpyridin-2-yl)methyl]amine) is able to convert a number of aliphatic alkenes to the corresponding *cis*-diol products (in combination with some epoxide by-products) with the use of hydrogen peroxide as oxidant. As a critical structural feature the Fe(6-Me_3-TPA) complex contains two labile *cis*-coordination sites that are occupied by CH_3CN molecules. Que and coworkers later reported on the synthesis of the chiral Fe(II) complex [Fe(6-Me-BPBP)(OTf)$_2$] (BPBP = Bis(pyridinylmethyl)bipyrrolidine) that is able to form *cis*-diols out of olefins in up to 97% ee.[17] These systems are currently the most selective iron-based catalysts for the dihydroxylation of olefins. Other Fe-based systems able to carry out *cis*-dihydroxylations include systems based on bispidine and on (bi)cyclic tetraaza ligands.[18]

A typical feature of the above systems is that these all contain an all-nitrogen ligand donor set, instead of the mixed N,O donor set found in the Rieske dioxygenases. In addition, these systems do not follow the facially capping tridentate designer mold laid down by the 2-His-1-carboxylate facial triad. In 2005, Que and coworkers reported on the Ph-DPAH ligand (DPAH = di(2-pyridyl)methylbenzamide) which has an N,N,O donor set.[16] The corresponding iron complex [Fe(II)(Ph-DPAH)$_2$](OTf)$_2$ has an octahedral geometry in which the two carbonyl oxygen donors are *trans* to each other. Although this iron complex is coordinatively saturated it does catalyze the oxidation of olefins. During these reactions one ligand most likely dissociates from the iron center to make three sites available for substrate and hydrogen peroxide binding. The complex forms the *cis*-diol as the major product for a range of olefins

with conversions of 50-80% based on the amount of hydrogen peroxide added and does so with retention of the olefin configuration.

Along a similar vein, other N,N,O ligands are currently explored in order to mimic the structural aspects of the 2-His-1-carboxylate facial triad more accurately. Examples of ligands that are used in these studies in combination with iron include the scorpionate-type bis(pyrazol-1-yl) acetates,[19] and mixed proline-pyridine ligands.[20] Iron complexes of bispyrazolyl acetate ligands have been quite extensively by Burzlaff and co-workers,[19c] while more recently Jones *et al.* have developed some sterically encumbered versions of these ligands.[21]

In recent papers, we have reported on the syntheses of iron(II) complexes derived from a new class of facial N,N,O ligands.[22-24] The tripodal 3,3-bis(1-alkylimidazole-2-yl)propionate (**BAIP**) ligands contain two imidazole groups and a carboxylate moiety to mimic the histidine and the aspartate residues in the active site of NDO (Figure 2). These anionic N,N,O ligands form mononuclear iron complexes in the presence of an additional anionic ligand, for instance catecholate. In the absence of such additional ligands, coordinatively saturated [Fe(**BAIP**)$_2$] complexes are formed, which were found inactive as oxidation catalysts.[23] Changing the carboxylate into a carboxylate ester changes the coordination properties of these ligands. Depending on the counter ion and the solvent that is used, either a *trans* bis-ligand complex or bis-solvent bis-ligand adduct is formed (Figure 2). In the latter adduct, the **BMIP^{nPr}** ligands (**BMIP^{nPr}** = propyl 3,3-bis(1-methylimidazole-2-yl)propionate) act as N,N donors and two MeOH molecules coordinate to iron in a *cis* fashion. When the *trans* bis-ligand complex [Fe(**BMIP^{nPr}**)$_2$](OTf)$_2$ is used in the oxidation of alkenes with H_2O_2, next to the formation of the epoxide product also the formation of the *cis*-diol product is observed.[23] The observation of the *cis*-diol products indicates the flexibility of the ligand system, because for the *cis*-diol product to be formed, two labile *cis* sites are deemed necessary on the metal center. The [Fe(**BMIP^{nPr}**)$_2$](OTf)$_2$ complex most likely rearranges in solution to a structure that is similar as observed for the MeOH adduct.

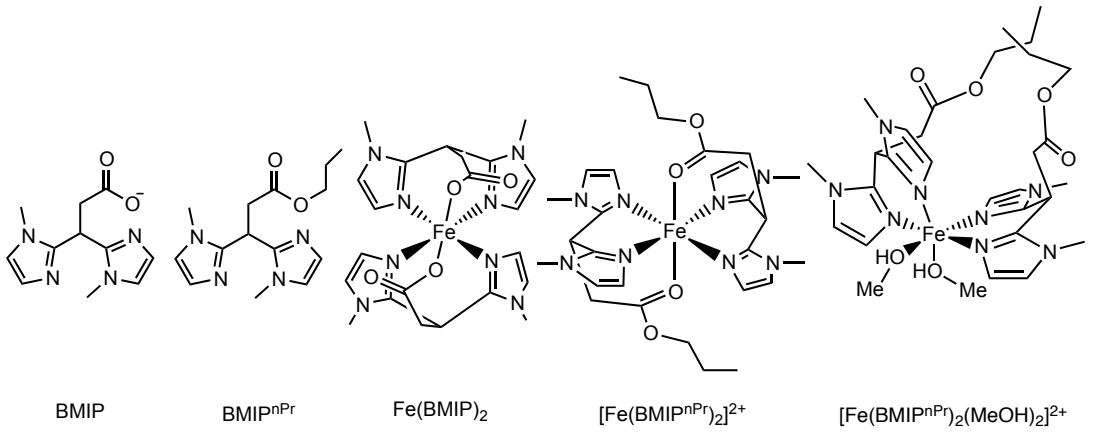

Figure 2. The ligands 3,3-bis(1-methylimidazole-2-yl)propionate (**BMIP**) and propyl 3,3-bis(1-methylimidazole-2-yl)propionate (**BMIP^{nPr}**) and some of their iron(II) complexes.

Here, we report on an extension of this work by the synthesis of several analogues of the **BMIP^{nPr}** ligand in the search for more selective *cis*-dihydroxylation catalysts based on iron. A number of seven different ligands have been investigated, which can be divided into three different groups (Figure 3). In the first group the two 1-methylimidazole donors of the **BMIP** structure are combined with different ester or amide donors. In the second group the 1-methylimidazole donors are substituted for 1-methylbenzimidazole donors to induce more steric bulk around the nitrogen donors and to make the ligand more soluble in apolar solvents. The third ligand group is comprised of the ligand in which the 1-methylimidazole donors have been replaced by 1-ethyl-4-isopropylimidazole donors. The coordination behavior of these *N,N,O* ligands towards iron and the catalytic behavior of the resulting complexes in the oxidation of cyclooctene are investigated.

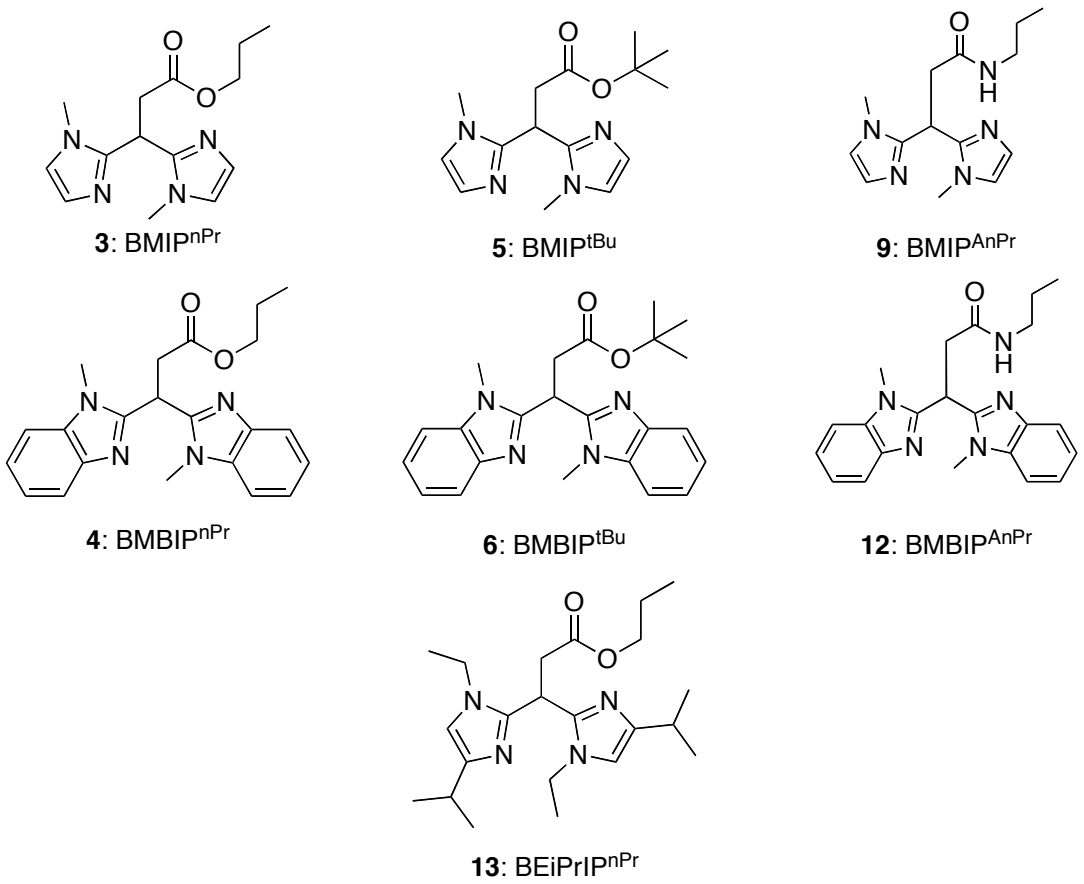

Figure 3. Overview of BAIP-type ligands.

6.2 Results and discussion

6.2.1 Ligand synthesis

Ligands **BMIP^{nPr}** (**3**) and **BMBIP^{nPr}** (**4**) have been synthesized according to a synthetic route previously reported by our group,[25] that was also employed for the synthesis of ligands **BMIP^{tBu}** (**5**) and **BMBIP^{tBu}** (**6**) (Scheme 1). The starting bis(1-methylimidazole-2-yl)methane (**1**)[26,27] and bis(1-methylbenzimidazole-2-yl)methane (**2**)[28] compounds can easily be synthesized on a multigram scale. Lithiation of these bis(imidazole)methane's at the methylene position using *n*-BuLi at –78 °C, followed by the addition of either *n*-propylbromoacetate or tert-butylbromoacetate yielded propyl 3,3-bis(1-methylimidazole-2-yl)propionate, **BMIP^{nPr}** (**3**), propyl 3,3-bis(1-methylbenzimidazole-2-yl)propionate, **BMBIP^{nPr}** (**4**), *tert*-butyl 3,3-bis(1-methylimidazole-2-yl)propionate, **BMIP^{tBu}** (**5**) and *tert*-butyl 3,3-bis(1-methylbenzimidazole-2-yl)propionate, **BMBIP^{tBu}** (**6**), respectively, in good yields (83-94%).

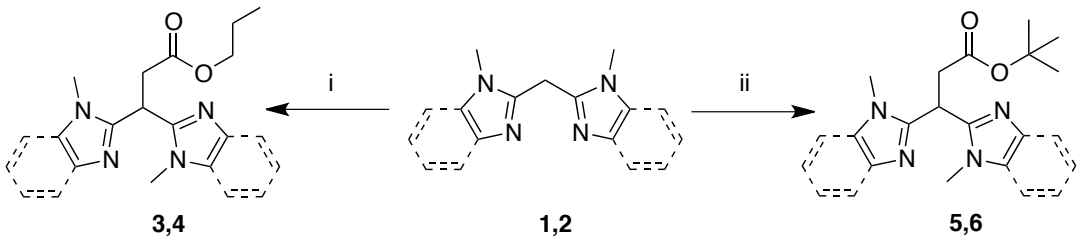

Scheme 1. Synthesis of the ligands 3-6. *i*) a. *n*-BuLi, THF, –78 °C, 1 h; b. propyl bromoacetate, –78 °C to rt, overnight; *ii*) a. *n*-BuLi, THF, –78 °C, 1h; b. *tert*-butyl bromoacetate, –78 °C to rt, overnight.

The preparation of the amide-appended ligands 3,3-bis(1-methylimidazol-2-yl)-*N*-propylpropanamide, **BMIP^{AnPr}** (**9**) and 3,3-bis(1-methylbenzimidazol-2-yl)-*N*-propylpropanamide, **BMBIP^{AnPr}** (**12**) proceeded via the preparation of an active ester intermediate (Scheme 2). First the propyl ester ligands **3** and **4** were hydrolyzed using 1 equivalent of KOH.[25] The resulting carboxylic acids were turned into an active ester by a DCC coupling according to a modified procedure by Suijkerbuijk *et al.*[29] The yield of **8** (43%) was much lower compared to the yield of **11** (85%), which was caused by the low solubility of acid **7** in THF. In the last step the active esters were reacted with propylamine to yield the desired amide ligands **9** and **12** in 25% and 90% isolated yield after recrystallization. Preparation of the **BEiPrIP^{nPr}** ligand (**13**) with two 1-ethyl-4-isopropylimidazole donors was previously reported by us.[30]

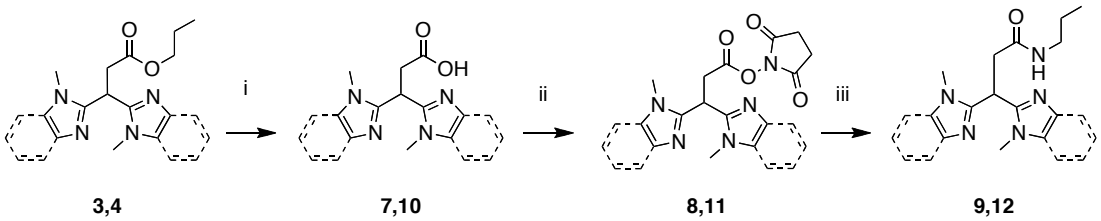

Scheme 2. Synthesis of the amide ligands **9** and **12**. *i*) a. 1 equiv. KOH, THF, rt; b. 1 equiv. HCl; *ii*) NHS, DCC, pyridine, THF, 35-40 °C; *iii*) propylamine, CH_2Cl_2, rt.

6.2.2 Fe triflate complexes

For the set of seven ligands, the corresponding iron bis-ligand complexes were synthesized in the same way as reported for the **BMIP^{nPr}** complex (Scheme 3).[23] For the preparation of the complexes, the appropriate ligand was mixed in a 2:1 ratio with $Fe(OTf)_2 \cdot 2MeCN$[31] in methanol for 1 h. After removal of the solvent, recrystallization of the resulting brown or (off) white powders from an acetonitrile/diethyl ether mixture yielded the iron complexes [Fe(**BMIP^{nPr}**)$_2$](OTf)$_2$ (**14**),[23] [Fe(**BMIP^{tBu}**)$_2$](OTf)$_2$ (**15**), [Fe(**BMBIP^{nPr}**)$_2$](OTf)$_2$ (**17**), [Fe(**BMBIP^{tBu}**)$_2$](OTf)$_2$ (**18**), [Fe(**BMBIP^{AnPr}**)$_2$](OTf)$_2$ (**19**) and [Fe(**BEiPrIP^{nPr}**)$_2$](OTf)$_2$ (**20**) as crystalline solids in high yields (79 to 95%); the yield of **20** was much lower (34%) as the result

of two consecutive crystallization steps in its purification. The corresponding iron bis-ligand complex **16** derived from ligand **BMIP^{AnPr}** was not synthesized as isolated material, but was instead prepared *in situ* for catalytic testing.

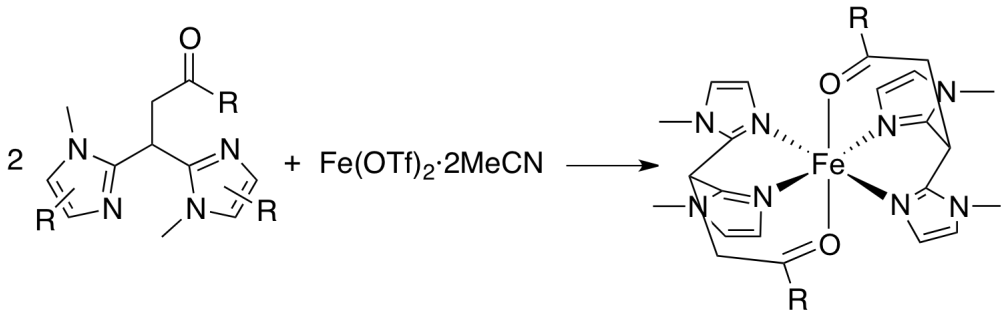

14: [Fe(**BMIP^{nPr}**)$_2$](OTf)$_2$
15: [Fe(**BMIP^{tBu}**)$_2$](OTf)$_2$
16: [Fe(**BMIP^{AnPr}**)$_2$](OTf)$_2$
17: [Fe(**BMBIP^{nPr}**)$_2$](OTf)$_2$
18: [Fe(**BMBIP^{tBu}**)$_2$](OTf)$_2$
19: [Fe(**BMBIP^{AnPr}**)$_2$](OTf)$_2$
20: [Fe(**BEiPrIP^{nPr}**)$_2$](OTf)$_2$

Scheme 3. Synthesis of iron triflate complexes **14-20** (a generalized structure is shown).

These paramagnetic complexes were characterized by different techniques including single crystal X-ray structure determination, IR spectroscopy, and ESI-MS analysis. All prepared complexes were stored as dry powders under a nitrogen atmosphere. Benzimidazole amide complex **19** proved quite sensitive towards oxidation even under these storage conditions. The color of a dry powder of **19** turned red overnight, which indicates the oxidation of Fe(II) to Fe(III) in this complex.

High resolution mass spectroscopic analysis (ESI-MS) proved very conclusive on the composition of the isolated materials. In all cases mono-cations of the composition $[Fe(L_2)(OTf)]^+$ were recorded as the parent peak. This composition is in agreement with the anticipated composition of the complexes as $[Fe(L_2)](OTf)_2$, as based on the first generation complex [Fe(**BMIP^{nPr}**)$_2$](OTf)$_2$.[23]

IR spectra were recorded for the different complexes, both in the solid state and in solution. The IR spectrum of [Fe(**BMIP^{nPr}**)$_2$](OTf)$_2$ (**14**) in the solid state showed a clear vibration band of the carbonyl group at 1691 cm^{-1}, whereas the frequency of the carbonyl vibration in the free ligand was found at 1727 cm^{-1}. This frequency shift indicates coordination of the carbonyl group to the iron center. The symmetric and asymmetric vibrations of the CF_3 and SO_3 groups of the triflate anions in [Fe(**BMIP^{nPr}**)$_2$](OTf)$_2$ were found at 1259 (ν_{as} SO_3), 1216 (ν_s CF_3), 1152 (ν_{as} CF_3), 1030 (ν_s SO_3) cm^{-1}, which indicates that these are non-coordinating ions.[32] Similar observations were made in the solid state for complexes **15**, **18**, and **19**, pointing to similar solid state structures as imposed for **14** (Table 1).

Table 1. Solid state IR vibrations of complexes **14**, **15**, **18** and **19**.

Complex	Ligand ν(C=O)(cm^{-1})	complex ν(C=O)(cm^{-1})	triflate vibrations ν(cm^{-1})
[Fe(**BMIP^{nPr}**)$_2$](OTf)$_2$ **14**	1727	1691	1259, 1216, 1152, 1030
[Fe(**BMIP^{tBu}**)$_2$](OTf)$_2$ **15**	1726	1692	1258, 1224, 1144, 1029
[Fe(**BMBIP^{tBu}**)$_2$](OTf)$_2$ **18**	1720	1665	1260, 1226, 1150, 1030
[Fe(**BMBIP^{AnPr}**)$_2$](OTf)$_2$ **19**	1656	1628	1244, 1223, 1151, 1028

In the case of benzimidazole complex [Fe(**BMBIP^{nPr}**)$_2$](OTf)$_2$ (**17**), two carbonyl stretching vibrations were found, a strong vibration at 1694 cm^{-1} and a shoulder at 1709 cm^{-1}, which both point at coordinating carbonyl groups (free ligand at 1734 cm^{-1}). Probably both the *cis*- and *trans*-isomer of the complex are present in the solid state. For [Fe(**BEiPrIP^{nPr}**)$_2$](OTf)$_2$ (**20)** several carbonyl-stretching vibrations were observed. Just like in **17**, two bands that correspond to coordinating carbonyl groups were found (1705, 1691 cm^{-1}), again implying the presence of both *cis*- and *trans*-isomers. In addition a strong vibration was found for a non-coordinating carbonyl moiety at 1736 cm^{-1} (free ligand 1734 cm^{-1}). This indicates that at least three different forms of the complex are present in the solid state. Based on these IR data, the triflate groups do not coordinate to iron in the solid state in complexes **17** and **20**.

For several of the complexes solution IR spectra were recorded in acetonitrile. In previous work on complex **14** it was found that in solution some of the carbonyl oxygens detach from the iron center to create a vacant site,[23] to which either a triflate ion or a solvent molecule could coordinate. For [Fe(**BMIP^{nPr}**)$_2$](OTf)$_2$ (**14**) two distinct C=O stretching vibrations were observed, one at 1737 cm^{-1} (non-coordinated) and one at 1702 cm^{-1} (coordinated; Figure 4). When the imidazole donors are substituted for benzimidazole donors as in [Fe(**BMBIP^{nPr}**)$_2$](OTf)$_2$ (**17**), only one C=O vibration corresponding to a coordinated carbonyl group was present at 1691 cm^{-1}. However, this intense peak has small shoulders indicating the possible presence of other species in solution.

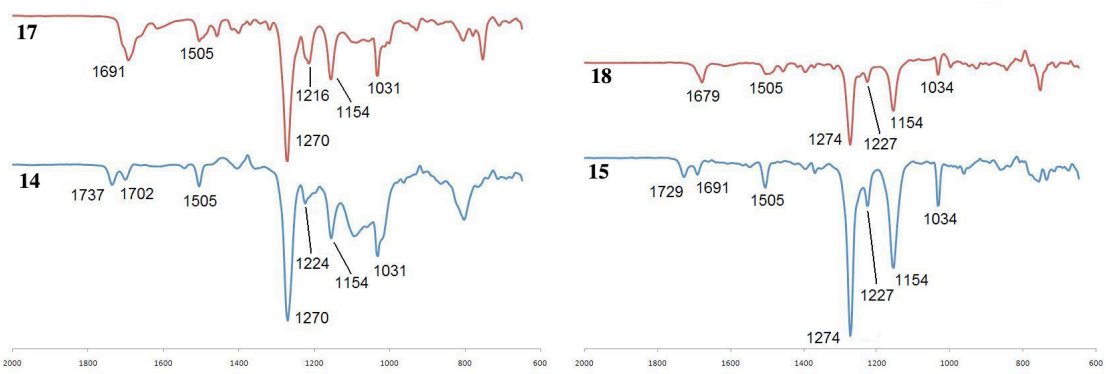

Figure 4. Solution IR spectra of complexes **14**, **17** (left) and **15**, **18** (right) in acetonitrile. Vibrational energies are given in wavenumbers (cm^{-1}).

For [Fe(**BMIP^{tBu}**)$_2$](OTf)$_2$ (**15**) and for the corresponding benzimidazole compound [Fe(**BMBIP^{tBu}**)$_2$](OTf)$_2$ (**18**) similar IR features were observed in acetonitrile (Figure 4, right). Compound **15** again showed two distinct carbonyl peaks and compound **18** showed one sharp carbonyl peak. These observations indicate that the presence of the benzimidazole group hinders/prevents the decoordination of the carbonyl groups in solution. Figure 4 also shows the triflate vibrations for the four complexes in the 1000 – 1300 cm^{-1} region. These vibrations are characteristic of non-coordinated triflates.[32] Due to the low yielding synthesis of the amide ligands no solution IR spectrum could be obtained for the corresponding Fe-compounds.

6.2.3 Structural features of the iron triflate complexes in the solid state (X-ray crystal structures)

Crystals of complexes **14-20** suitable for X-ray analysis were obtained by slow vapor diffusion of diethyl ether into a solution of the corresponding complex in acetonitrile. The crystal structures for the first group of complexes with the imidazole backbone, [Fe(**BMIP^{nPr}**)$_2$](OTf)$_2$ (**14**), [Fe(**BMIP^{tBu}**)$_2$](OTf)$_2$ (**15**), and [Fe(**BMIP^{AnPr}**)$_2$](OTf)$_2$ (**16**) are depicted in Figure 5.

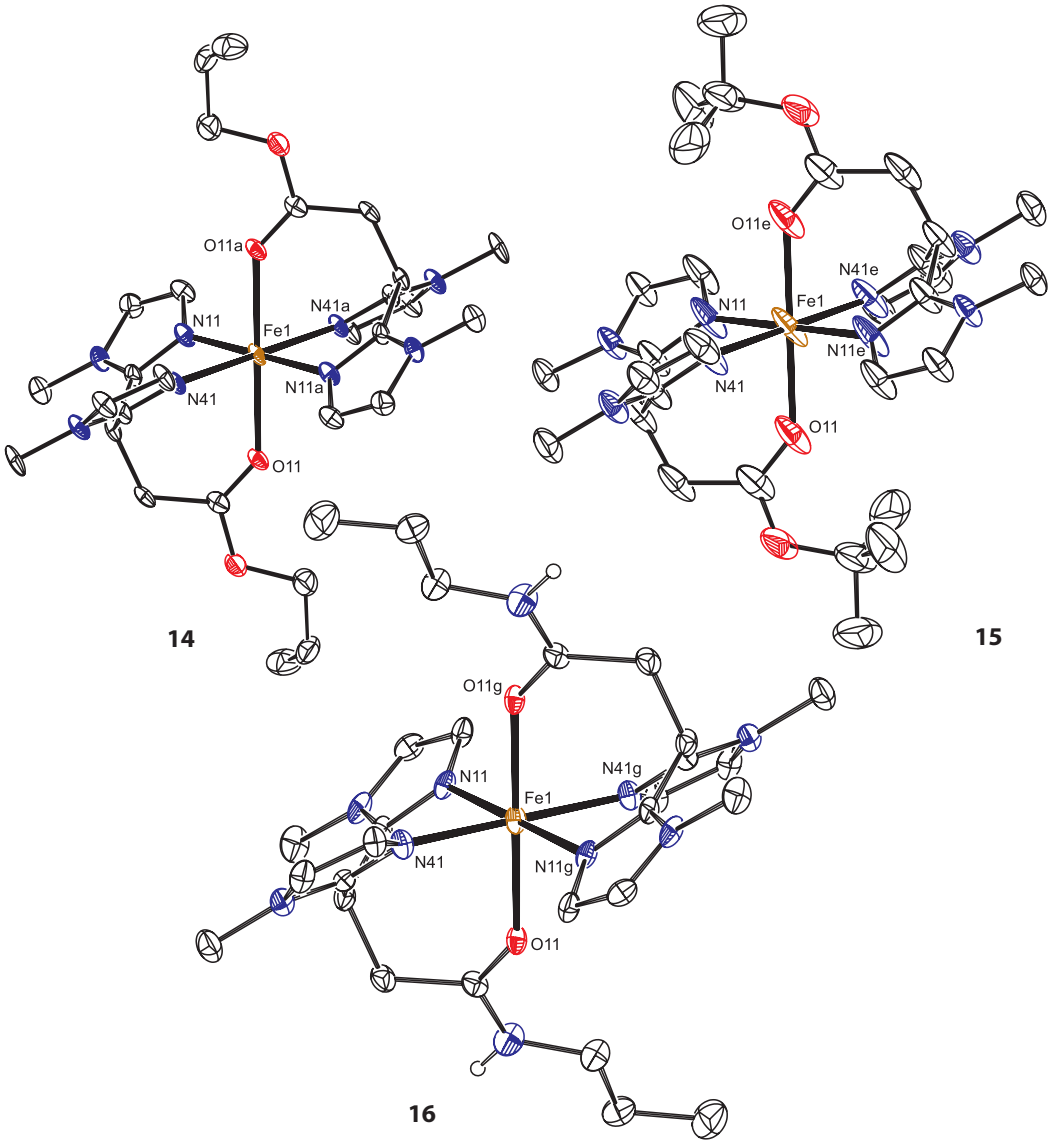

Figure 5. Molecular structures of the cationic complexes **14-16** in the crystal. Displacement ellipsoid plots (30% probability); all C-H hydrogen atoms, non-coordinated triflate anions, and non-coordinated acetonitrile molecules are omitted for clarity. In **14**, only one of four independent molecules is shown and only the major conformation of the disordered *n*-propyl moiety is displayed. In **15**, only one of two independent molecules is depicted. Symmetry operations: a) –x, –y, –z; e) 1–x, –y, 1–z; g) 1–x, 1–y, 1–z.

In the crystal structures of complexes **14-16** the Fe atoms of all molecules are located on inversion centers. The complexes have a nearly ideal octahedral geometry. Both ligands in these complexes are coordinated in a facial manner around the iron center with the two coordinating carbonyl groups in *trans* position with respect to each other. The two ester complexes **14** and **15** are very much alike. Their ester moieties point away from the iron center and do not exert a noticeable effect on the coordination geometry around iron. Amide ligand **BMIP^{AnPr}** coordinates in the same way to iron as

the **BMIP^{nPr}** ligand, *i.e.* the amide moiety coordinates to iron via its carbonyl grouping and the propyl amide tails point away from iron. Bruijnincx *et al.* earlier reported on a structure of complex **14**.[23] In that case the crystals were obtained from a MeOH/Et_2O mixture and a different structure was obtained, [Fe(**BMIP^{nPr}**)$_2$(MeOH)$_2$](OTf)$_2$, in which the two ligands coordinate to iron via the nitrogen donor atoms only and two molecules of MeOH are coordinated in a *cis* fashion to the iron center (see Figure 2). A structure of the corresponding tetraphenylborate complex [Fe(**BMIMP^{nPr}**)$_2$](BPh$_4$)$_2$ was also reported.[23] In this case the structure matches the structure of **14** reported here.

Table 2 shows selected bond lengths and angles for complexes **14-16**, for each complex the data for all independent residues in the asymmetric unit are shown. The observed Fe-N bond lengths vary between 2.105(3) Å and 2.147(6) Å and are characteristic of iron(II) high-spin complexes with imidazole-like ligands.[33,34] Overall, the variation of bond lengths in the individual complexes is very small, as can be seen in the quadratic elongation $\langle\lambda_{oct}\rangle$.[35] The intra-ligand N-Fe-N angles are all smaller than 90°, reflecting the small 'bite-angle' of the bis-imidazole methane moiety, while all inter-ligand N-Fe-N angles are larger than 90°. All complexes have a significant angular variance σ_{oct}^2.[35] Comparison of all independent molecules in the crystal structures of **14-16** shows only minor differences in the bond lengths and angles. The variation in the ester moiety in the first group of **BMIP** ligands, therefore, does not have a large effect on the overall structure of the corresponding [Fe(**BAIP**)$_2$](OTf)$_2$ complexes.

Table 2. Selected bond lengths (Å) and angles (°) for complexes **14-16**.[a]

	14				**15**		**16**
	Bond lengths						
	Res 1 (x=1, y=a)	Res 2 (x=2, y=b)	Res 3 (x=3, y=c)	Res 4 (x=4, y=d)	Res 1 (x=1, y=e)	Res 2 (x=2, y=f)	Res 1 (x=1, y=g)
Fex-N1x	2.123 (5)	2.144 (5)	2.126 (5)	2.130 (5)	2.115 (4)	2.140 (3)	2.147 (6)
Fex-N4x	2.124 (4)	2.124 (5)	2.136 (5)	2.127 (5)	2.137 (4)	2.105 (3)	2.107 (7)
Fex-O1x	2.249 (4)	2.174 (4)	2.186 (4)	2.229 (4)	2.145 (4)	2.167 (3)	2.157 (5)
$<\lambda_{oct}>$[b]	1.006	1.004	1.004	1.005	1.005	1.006	1.005
	Angles						
N1x-Fex-N4x	85.35 (18)	85.78 (19)	85.31 (19)	85.21 (18)	85.14 (14)	84.66 (10)	83.9(2)
N1x-Fex-O1x	87.26 (17)	85.88 (17)	88.82 (17)	86.37 (16)	86.85 (14)	85.12 (10)	86.6(2)
N1x-Fex-N4xy	94.63 (18)	94.22 (19)	94.69 (19)	94.79 (18)	94.86 (14)	95.34 (10)	96.1(2)
N1x-Fex-O1xy	92.74 (17)	94.12 (17)	91.18 (17)	93.63 (16)	93.15 (14)	94.88 (10)	93.4(2)
N4x-Fex-O1x	86.33 (16)	89.43 (17)	85.89 (17)	87.49 (17)	85.46 (16)	86.99 (10)	89.5(2)
N4x-Fex-O1xy	93.67 (16)	90.56 (17)	94.11 (17)	92.51 (17)	94.54 (16)	93.01 (10)	90.5(2)
σ_{oct}^2 (deg^2)[c]	15.43	12.59	14.68	15.57	19.80	22.43	17.76

[a] Symmetry operations: a) –x, –y, –z; b) –x, 1–y, –z; c) 1–x, –y, 1–z; d) 1–x, 1–y, –z; e) 1–x, –y, 1–z; f) –x, –y, 1–z; g) 1–x, 1–y, 1–z.

[b] $\langle\lambda_{oct}\rangle = \sum_{i=1}^{6}(l_i/l_o)^2/6$

[c] $\sigma_{oct}^2 = \sum_{i=1}^{12}(\theta_i - 90°)^2/11$

The structures of the three complexes of the benzimidazole group, [Fe(**BMBIP^{nPr}**)$_2$](OTf)$_2$ (**17**), [Fe(**BMBIP^{tBu}**)$_2$](OTf)$_2$ (**18**), and [Fe(**BMBIP^{AnPr}**)$_2$](OTf)$_2$ (**19**) are shown in Figure 6. In contrast to the centrosymmetric complexes **14-16**, complex **17** is located on a twofold rotation axis with a *cisoid* coordination of the ligands. The basal plane of **17** is formed by the symmetry related nitrogen atoms N31 and N31a and oxygen atoms O21 and O21a (a=

x, 0.5-y, 0.5-z). The symmetry related nitrogen atoms N11 and N11a are above and below this plane. Both solid state and solution IR spectra of complex **17** indicate the presence of more than one species, which does not rule out the presence of an isomer of **17** in which the oxygen donors are in *trans* position. Most likely, the *cis* isomer crystallizes preferentially. This different coordination behavior of benzimidazole complex **17** compared to its imidazole derivative **14** might be caused by the presence of the more bulky benzimidazole groups which precludes the formation of a single thermodynamic conformer. On the other hand, the structure of [Cu(**BMBIP**)$_2$] comprising the analogues anionic benzimidazole propionate ligand was earlier found to crystallize in a *transoid* manner,[25] which could indicate an additional role for the ester moiety in determining the overall structure.

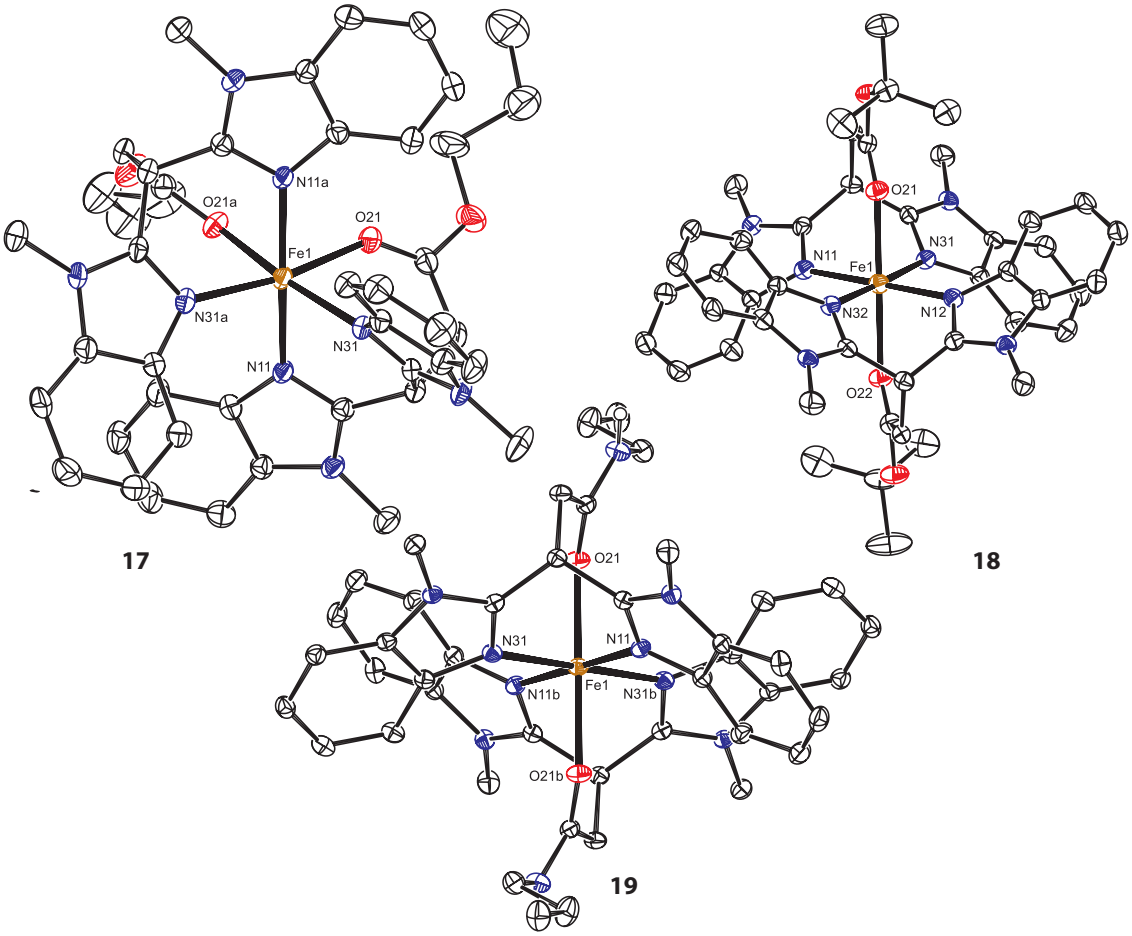

Figure 6. Molecular structures of the cations of complexes **17-19** in the crystal. Displacement ellipsoid plots (30% probability); all C-H hydrogen atoms, non-coordinated triflate anions, and non-coordinated acetonitrile molecules are omitted for clarity. Symmetry operations: a) x, 0.5-y, 0.5-z; b) 1–x, 1–y, 1–z.

Complex **18** and **19** show the same coordination geometry as complexes **14-16**, a distorted octahedral coordination with the carbonyl oxygens in *trans* positions. While complex **19** is again centrosymmetric, complex **18** is located on a general position and has no molecular symmetry. Nevertheless, the distortion of the octahedral geometry in **18** is only slightly larger than in the other complexes. The N,N,O ligands in **18** are different from those in **17** in the sense that the n-propylester moieties in **17** are exchanged for *tert*-butyl ester moieties in **18**. In this case, the steric bulk of these *tert*-butyl groups seem to 'suppress' or 'overrule' the steric effect of the benzimidazole groups. A *cis*-orientation of the *tert*-butyl ester groups most likely is unfavorable due to steric congestion of these groups in this orientation. Introduction of an n-propyl amide group in **BMBIP^{AnPr}** also results in a *trans* octahedral complex (**19**). In this case, steric reasons are less likely to be at play, as the n-propyl ester moiety in **BMBIP^{nPr}** allowed the formation of *cis* complexes. It therefore seems more reasonable that electronic effects result in the *trans* disposition of the amide oxygen donors. The amides are stronger donors than the esters and seem to overrule steric arguments (*vide infra)*. Selected bond lengths and angles for complexes **17-19** are shown in Table 3.

Very similar trends in bond lengths and angles are found for **17-19** as compared to those of the first group of complexes **14-16**. All bond lengths are in agreement with high spin (S = 2) iron(II) complexes. As found for complexes **14-16**, the intra-ligand N-Fe-N angles in **17-19** are smaller than 90°, reflecting the small 'bite-angle' of the bis-benzimidazole methane moiety. In complex **19**, the Fe-O bond length is considerable shorter than in **17** and **18**, which indeed suggests that the carbonyl oxygen atoms in this complex are more tightly bound to the iron center. This effect is reflected amongst the series of complexes reported here by overall shorter Fe-O bond lengths for the amide complexes (2.0886(13) and 2.157(5) Å) compared to the ester complexes (2.145(4) till 2.249(4) Å).

Table 3. Selected bond lengths (Å) and angles (°) for complexes **17**-**19**.[a]

	complex **17** (y=a)	complex **19** (y=b)		complex **18**
	Bond lengths			Bond lengths
Fe1-N11	2.115(3)	2.1426(15)	Fe1-N11	2.140(4)
Fe1-N31	2.115(3)	2.1584(15)	Fe1-N31	2.128(4)
Fe1-O21	2.180(3)	2.0886(13)	Fe1-O21	2.195(3)
			Fe1-N12	2.132(4)
			Fe1-N32	2.122(4)
			Fe1-O22	2.203(3)
$<\lambda_{oct}>$	1.010	1.004		1.005
	Angle			Angle
N11-Fe1-N31	87.31(13)	83.99(6)	N11-Fe1-N31	83.54(15)
N11-Fe1-O21	86.22(12)	89.57(6)	N11-Fe1-O21	88.65(14)
N11-Fe1-N11y	173.91(19)	180	N11-Fe1-N32	95.51(15)
N11-Fe1-N31y	96.48(13)	96.01(6)	N12-Fe1-N31	96.49(15)
N11-Fe1-O21y	89.23(12)	90.43(6)	N12-Fe1-N32	84.47(15)
N31-Fe1-N31y	103.4(2)	180	N12-Fe1-O22	87.74(14)
N31-Fe1-O21	86.81(13)	89.54(6)	N31-Fe1-O21	87.24(14)
N31-Fe1-O21y	169.54(13)	90.46(6)	N32-Fe1-O22	87.58(14)
O21-Fe1-O21y	83.12(17)	180	O21-Fe1-O22	178.91(13)
			N11-Fe1-N12	179.68(17)
			N31-Fe1-N32	178.40(16)
σ_{oct}^2 (deg^2)	34.12	13.25		17.08

[a] Symmetry operations: a) x, 0.5-y, 0.5-z; b) 1–x, 1–y, 1–z.

[Fe(**BEiPrIP^{nPr}**)$_2$](OTf)$_2$ (**20**) crystallizes in the non-centrosymmetric space group *P*1 with three independent metal complexes in the unit cell, of which two have a tetrahedral coordination geometry and one has an octahedral geometry. Figure 7 shows both the structure of the octahedral residue and the structure of one of the tetrahedral residues. The structure of the octahedral residue is reminiscent of the structure of complex **17**, *i.e.* an overall octahedral coordination geometry in which the oxygen donor atoms are found in *cisoid* positions. The combined bond lengths and angles again show a deviation from the ideal octahedral geometry, mostly caused by the tripodal structure of the ligand (Table 4). The bond lengths are in agreement with a high spin (S = 2) iron(II) complex. In this residue, all bond lengths around Fe are larger than in **17**. In particular the Fe-O bond lengths are remarkable longer than in **17** (2.252(3)/2.303(3) *vs* 2.180(3) Å, resp.). These elongated bonds most likely reflect the overall steric demand of the **BEIPrIP^{nPr}** ligand as compared to the parent **BMIP^{nPr}** and **BMBIP^{nPr}** ligands.

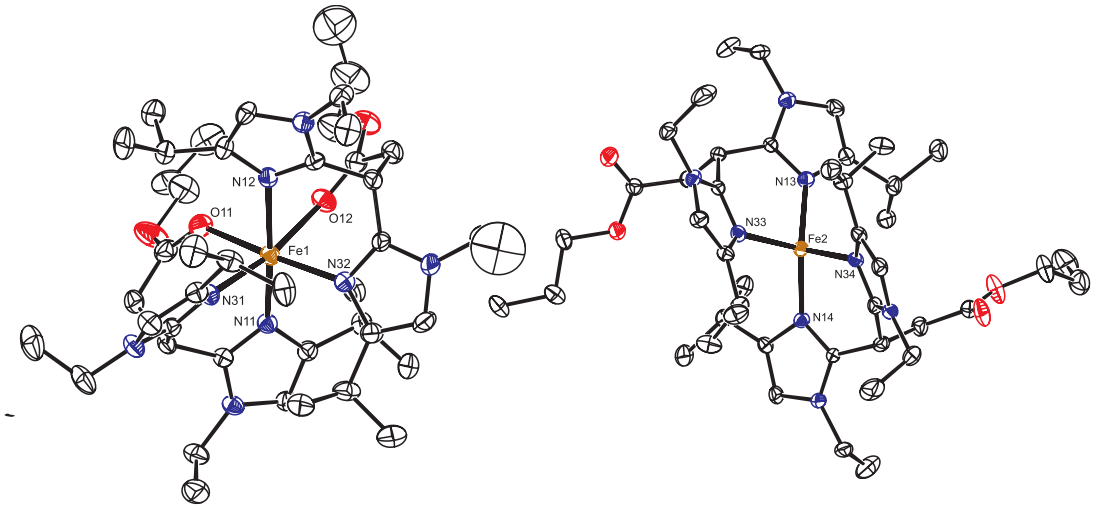

Figure 7. Molecular structures of the octahedral and the tetrahedral forms of the $[Fe(\mathbf{BEiPrIP^{nPr}})_2]^{2+}$ cation in the crystal structure of **20**. Displacement ellipsoid plots (30% probability); all hydrogen atoms, non-coordinated triflate anions, and non-coordinated solvent molecules are omitted for clarity. Only the major disorder components of the n-propyl groups are shown.

Table 4. Selected bond lengths (Å) and angles (°) for the octahedral geometry of **20**.

Bond length		Angle		Angle	
Fe1-N11	2.136(3)	N11-Fe1-N12	168.80(13)	N12-Fe1-O12	79.57(11)
Fe1-N12	2.133(3)	N11-Fe1-N31	92.31(13)	N31-Fe1-N32	98.45(13)
Fe1-N31	2.154(3)	N11-Fe1-N32	95.69(12)	N31-Fe1-O11	90.65(12)
Fe1-N32	2.137(3)	N11-Fe1-O11	79.98(12)	N31-Fe1-O12	170.40(12)
Fe1-O11	2.252(3)	N11-Fe1-O12	93.17(11)	N32-Fe1-O11	170.10(12)
Fe1-O12	2.303(3)	N12-Fe1-N31	93.78(13)	N32-Fe1-O12	88.84(12)
		N12-Fe1-N32	92.70(13)	O11-Fe1-O12	82.56(11)
		N12-Fe1-O11	90.55(12)		
$<\lambda_{oct}>$	1.012	σ_{oct}^2 (deg^2)	37.09		

In the tetrahedral residues of **20**, the **BEIPrIP^{nPr}** ligands act as bidentate nitrogen ligands, while the propyl ester moieties do not coordinate to iron and rather point away from the metal center. Selected bond length and angles for the two tetrahedral residues are shown in Table 5. Steric bulk caused by the ethyl and isopropyl groups makes that the ester groups do not coordinate to the metal center in the tetrahedral complex. In the octahedral coordination mode, this bulk results in elongated Fe-O bonds. The tetrahedral N-Fe-N angles vary between 95.4 and 135.3°, and are far from the ideal geometry of 109°. The bond lengths in the tetrahedral residues are the shortest among all structures presented in this study. Steric factors seem to play a decisive role in this. Because the enhanced overall steric bulk of the **BEIPrIP^{nPr}**

ligand prevents the coordination of the oxygen donors, the nitrogen donor moieties can approach the iron(II) ion more closely. The remarkable presence of two different coordination geometries or **20** in the solid state explains the presence of three carbonyl peaks in its IR spectrum (*vide infra*).

Table 5. Selected bond lengths (Å) and angles (°) for the two tetrahedral residues in **20**.

Bond length		Angle		Angle	
Residue 1					
Fe2-N13	2.022(3)	N13-Fe2-N14	134.35(14)	N14-Fe2-N33	111.27(13)
Fe2-N14	2.025(3)	N13-Fe2-N33	95.59(13)	N14-Fe2-N34	95.89(13)
Fe2-N33	2.048(3)	N13-Fe2-N34	112.84(13)	N33-Fe2-N34	104.38(13)
Fe2-N34	2.057(3)				
$<\lambda_{tet}>^{[a]}$	1.049	σ_{tet}^2 (deg^2)	207.57		
Residue 2					
Fe3-N15	2.041(3)	N15-Fe3-N16	104.34(13)	N16-Fe3-N35	110.98(13)
Fe3-N16	2.045(3)	N15-Fe3-N35	95.42(13)	N16-Fe3-N36	95.54(12)
Fe3-N35	2.027(3)	N15-Fe3-N36	112.51(13)	N35-Fe3-N36	135.33(13)
Fe3-N36	2.026(3)				
$<\lambda_{tet}>^{[b]}$	1.052	σ_{tet}^2 (deg^2)	219.60		

[a] $\langle \lambda_{tet} \rangle = \sum_{i=1}^{4} (l_i / l_o)^2 / 4$

[b] $\sigma_{tet}^2 = \sum_{i=1}^{6} (\theta_i - 109.47°)^2 / 5$

We are not aware of many examples in the literature in which two different coordination geometries of the same molecular metal complex are present within one crystal.[36] Because both geometries of **20** are present in the same unit cell, this should indicate that their energies are almost equal and that the transition energy between the two geometries is low. To provide more insight in the ground state energy difference between both geometries, DFT geometry optimizations were performed at the bp86, SV(P) level. Improved energies were obtained with single point SCF energy calculations at the b3-lyp TZVP level. In these calculations simplified versions of the ligands were used, in which all alkyl tails were substituted for methyl groups in order to limit computing time. The resulting calculated structures are in agreement with the octahedral and tetrahedral geometries in the crystal of **20** (Figure 8, Table 6). Comparison of the calculated structures with the experimental crystal structures shows that the geometry around the iron center is the same and that no clear differences in the overall structures are present. The calculated bond lengths and angles are comparable with the data obtained from the crystal structures of the two different geometries (Table 4 and 5). The substitution of all alkyls for methyl groups

could cause minor differences between the geometry of the crystal structure and the calculated structures, but as all alkyl tails are found on the outside of the overall structures and all of them point away from the metal center, only a small deviation is to be expected between the energy value of the structure with alkyl chains compared to the calculated structure with methyl groups. The difference in energy between the two geometries was computed to be 5.6 kcal/mol in favor of the octahedral geometry. This small energy difference points out that the octahedral and tetrahedral structures may well coexist in solution and in the solid state.

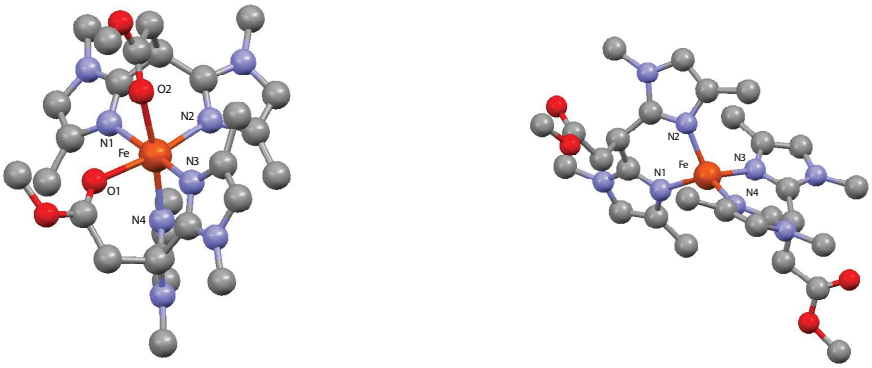

Figure 8. Calculated structures (DFT) of the two geometries of complex **20**.

Table 6. Bond length (Å) and angles (°) of the calculated DFT structures of complex **20**.

Octahedral				Tetrahedral			
Bond Length			Angle	Bond length			Angle
Fe-N1	2.186	O1-Fe-N1	88.0	Fe-N1	2.050	N1-Fe-N2	94.9
Fe-N2	2.155	N1-Fe-N2	87.5	Fe-N2	2.051	N2-Fe-N3	111.6
Fe-N3	2.187	N2-Fe-N3	100.4	Fe-N3	2.048	N3-Fe-N4	94.8
Fe-N4	2.154	N3-Fe-O1	83.0	Fe-N4	2.047	N1-Fe-N4	130.4
Fe-O1	2.191	O1-Fe-O2	85.6				
Fe-O2	2.192	O1-Fe-N2	171.8				
		O2-Fe-N4	171.9				

The different coordination modes of **BAIP**-type ligands around iron point out that the coordination geometry of this ligand system is quite amendable and sensitive to changes in the overall ligand structure. This could also mean that it may be difficult to point out what the real structure of an active species is during catalysis. It could be possible that multiply species are present in solution and that some of these are kinetically more competent than others. Earlier studies did demonstrate the coordination flexibility of **BAIP** ligands.[23] A good example of the coordination

flexibility of these ligands is the characterization of [Fe(**BMIP^{nPr}**)$_2$(MeOH)$_2$](OTf)$_2$ in which two MeOH molecules have replaced the ester donors and further rearranged the ligands in order to coordinate in a mutual *cis* position. The current study shows that IR-spectroscopy provides an insightful view on the coordination mode of the **BAIP** ligands. A combination of solid state and solution IR spectra did indicate the presence of different coordination conformers for complexes **17** and **20**, based on the coordinating/non-coordinating nature of the carbonyl moieties. Furthermore, the IR studies indicated that complexes with an imidazole backbone are more prone to rearrangement in solution, involving both dissociation of ester donor moieties and coordination of solvent molecules. The difference in coordination flexibility between the imidazole and benzimidazole ligands can be explained by the more electron-deficient nature of the benzimidazole donor compared to the imidazole donor and accordingly, a stronger interaction between the metal and the ester moieties in the benzimidazole complexes.

6.2.4 Magnetic susceptibility measurements

The magnetic moments of all reported iron(II) complexes were determined in acetonitrile at 298 K using Evans' NMR method.[37,38] All complexes showed magnetic moments consistent with high spin (S = 2) iron(II) centers. For complexes **16** and **19** no magnetic moments were determined, but according to the bond lengths in the crystal structures of **16** and **19**, a high spin configuration was also assigned to these complexes. An overview of the spectroscopic properties of all the complexes **14-20** is summarized in Table 7.

Table 7. Properties of the synthesized complexes.

Complex	C=O-position	ν(C=O)(cm^{-1})	Δν(C=O)(cm^{-1})[a]	μ_{EFF} (μ_B)
[Fe(**BMIP^{nPr}**)$_2$](OTf)$_2$ **14**	*trans*	1691	36	5.1
[Fe(**BMIP^{tBu}**)$_2$](OTf)$_2$ **15**	*trans*	1692	33	5.1
[Fe(**BMIP^{AnPr}**)$_2$](OTF)$_2$ **16**	*trans*	n.a.	n.a.	n.a. (HS)[b]
[Fe(**BMBIP^{nPr}**)$_2$](OTf)$_2$ **17**	*cis, (trans)*	1709, 1694	25, 40	5.1
[Fe(**BMBIP^{tBu}**)$_2$](OTf)$_2$ **18**	*trans*	1665	55	5.3
[Fe(**BMBIP^{AnPr}**)$_2$](OTf)$_2$ **19**	*trans*	1628	28	n.a. (HS)[b]
[Fe(**BEiPrIP^{nPr}**)$_2$](OTf)$_2$ **20**	*cis,*[c] (trans)	1736[d],1705[c], 1691[c]	2, 29, 43	5.1

[a] Compared to the free ligand; [b] Indicated by Fe-N bond lengths; [c] Octahedral; [d] Tetrahedral.

6.2.5 CV measurements

The oxidation potentials of Fe(II) complexes **14**, **18** and **19** were investigated by means of cyclic voltammetry. These complexes showed (quasi)reversible, single wave features that indicate clean 1-electron Fe(II)/Fe(III) oxidation-reduction processes (Table 8, Figure 9).

Table 8. Summarized cyclic voltammetry data for complexes **14**, **18** and **19**.

Complex	E 1/2 (V)	ΔE_p (mV)
[Fe(**BMIP^{nPr}**)$_2$](OTf)$_2$ **14**	0.735	175
[Fe(**BMBIP^{tBu}**)$_2$](OTf)$_2$ **18**	0.910	80
[Fe(**BMBIP^{AnPr}**)$_2$](OTf)$_2$ **19**	0.595	60

The cyclic voltammetry measurements showed that amide complex **19** is oxidized at a much lower potential ($E_{p,a}$ = 0.63 V) in comparison to that of the ester complexes **14** and **18** ($E_{p,a}$ = 0.82 and 0.95 V), making complex **19** more sensitive towards oxidation. Complex **19** was at first isolated as an off-white crystalline solid just like the other complexes, but the color of the isolated complex turned red after one day upon storage. This change in color points to the oxidation of the Fe(II) complex to an Fe(III) complex. The same observation was also made during catalysis in which the reaction mixture turned red when **19** was used as the catalyst. The lower oxidation potential of **19** likely results from a combination of (more) electron-deficient benzimidazole donors and strong amide donors (as shown by the short Fe-O distance in the crystal). This combination is also expected to lead to a complex with a diminished coordination flexibility and high conformational integrity. The latter aspect may be reflected in the close to Nernstian ΔE_p in CV for the redox change between Fe(II) and Fe(III) in **19**. The observation that complex **14** is oxidized at a lower potential than complex **18** seems to reflect the relative electron-donating abilities of the imidazole donor with respect to the benzimidazole donor groupings.

In Figure 9 the cyclic voltammogram of the benzimidazole amide complex **19** is combined with the voltammogram of the benzimidazole ester complex **18**. Unfortunately no CV measurements could be carried out on amide complex **16**, due to the low yield of the complex.

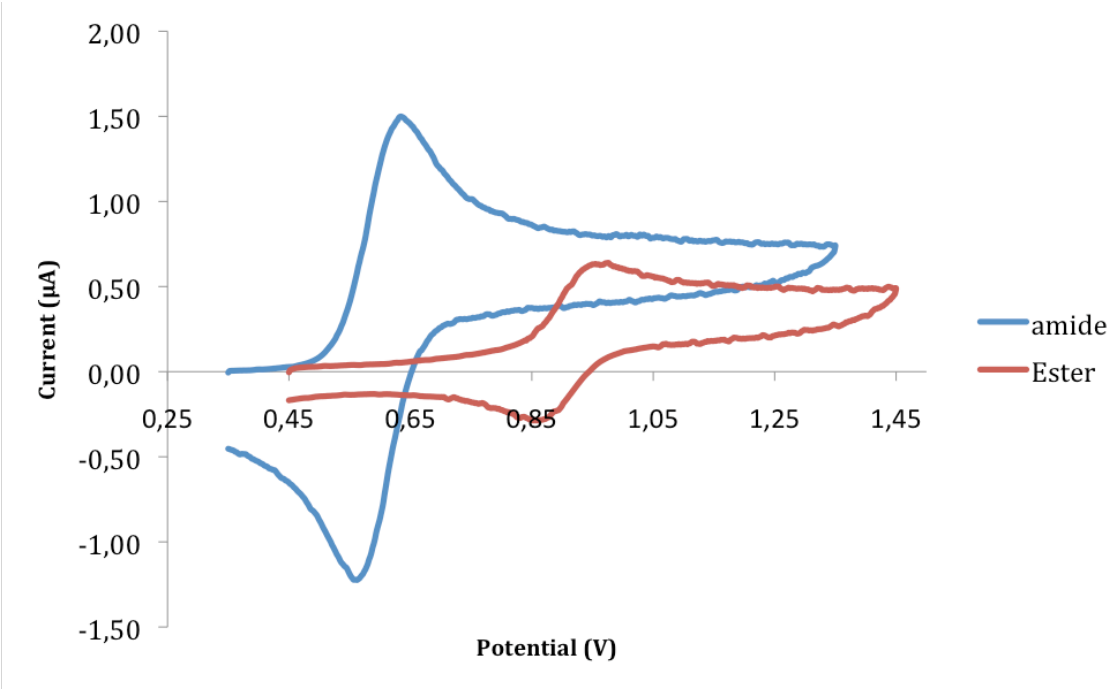

Figure 9. Cyclic voltammograms of complexes **18** and **19**.

6.3 Oxidation catalysis

The ability of complexes **14**-**20** to catalyze the oxidation of olefins was investigated by using cyclooctene as a benchmark substrate (Scheme 4). The oxidations were carried out in acetonitrile at ambient temperature and under a nitrogen atmosphere, using H_2O_2 as the sacrificial oxidant. The oxidant was added drop wise over a period of 20 minutes, to minimize the chance for peroxide disproportionation. The reactions were carried out with different ratios between catalyst, oxidant, and substrate. In all cases, the substrate was present in a large excess (oxidant limiting conditions). The reactions were monitored by GC, samples were taken 1 h and 3 h after the first drop of oxidant was added to the reaction mixture, as well as after running the reaction for one night (Table 9).

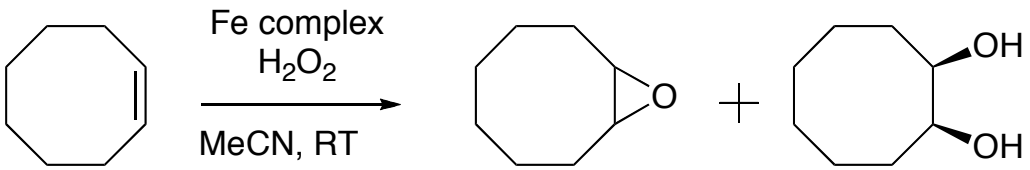

Scheme 4. General representation of the oxidation of cyclooctene.

Table 9. Overview catalytic results.

complex	equiv. H_2O_2	equiv. substrate	epoxide[a]			*cis*-diol[a]			conversion	epoxide:diol
			1h	3h	1night	1h	3h	1night	%[b]	ratio[c]
14	20	500	3.3	3.0	2.7	1.4	1.2	1.8	23	1.5 : 1
	20	1000	3.7	3.1	3.1	1.5	1.3	1.9	25	1.6 : 1
	100	1000	7.1	6.6	8.2	1.0	1.0	1.5	10	5.5 : 1
15	20	500	2.8	2.7	2.4	-	-	-	12	> 100 : 1
	20	1000	3.4	3.1	2.4	-	-	-	12	> 100 : 1
	100	1000	5.1	5.3	5.7	-	-	-	6	> 100 : 1
16	20	500	1.0	1.1	0.9	-	-	-	5	> 100 : 1
	20	1000	1.3	1.5	1.0	0.1	0.1	0.1	5	10 : 1
	100	1000	2.5	3.4	4.8	-	-	0.1	5	48 : 1
17	20	500	1.6	1.8	1.7	0.1	0.2	0.4	11	4.3 : 1
	20	1000	1.7	1.6	1.5	0.3	0.3	0.5	10	3 : 1
	100	1000	3.4	4.0	6.0	0.1	0.1	0.1	6	60 : 1
18	20	500	1.1	1.0	0.8	-	-	-	4	> 100 : 1
	20	1000	1.4	1.1	0.9	-	0.1	-	5	> 100 : 1
	100	1000	2.3	2.8	3.3	-	-	-	3	> 100 : 1
19	20	500	1.0	1.1	0.7	0.8	0.7	0.5	6	1.4 : 1
	20	1000	1.2	1.3	0.8	1.4	1.3	0.8	8	1 : 1
	100	1000	2.9	3.3	4.3	0.4	0.6	0.1	4	43 : 1
20	20	500	1.0	1.0	1.2	0.1	0.1	0.1	7	12 : 1
	20	1000	1.3	1.3	1.6	0.1	0.1	0.1	9	16 : 1
	100	1000	2.0	2.3	2.9	-	-	0.1	3	29 : 1

[a] Yields expressed as turnover numbers (TON = mol product/mol catalyst); [b] Conversion of H_2O_2 into epoxide and cis-diol after 1 night; [c] After 1 night.

Overall, all tested complexes are able to oxidize cyclooctene albeit with rather low TON's and low productive H_2O_2 consumption. This observation is in line with earlier studies on the oxidation of cyclooctene with [Fe(**BMIP^{nPr}**)$_2$](OTf)$_2$ and [Fe(**BMIP^{nPr}**)$_2$](BPh$_4$)$_2$.[23] In the present case, productive H_2O_2 conversion varies between 5-25% after one night of reaction time, which corresponds to a range of 0-10 turn-overs per iron. For the first group of complexes (**14**-**16**), complex **14** was most active. The use of 20 equiv. H_2O_2 per iron resulted in a productive conversion of H_2O_2 from 23% and 25% after one night with different amounts of substrate (500 and 1000 equiv., resp.) These conditions resulted in an epoxide to diol ratio of 1.5:1 and 1.6:1. An increase of the oxidant loading to 100 equiv. resulted in an increase in turn-over number to 10 (10% productive H_2O_2 consumption) and a change in epoxide/cis-diol ratio to 5.5:1. For complexes **15** and **16** the overall catalytic characteristics are lower,

and only minor traces of diol are formed. The overall catalytic activity of **14** is the highest amongst the complexes tested here.

The reactivity of the group of benzimidazole complexes (**17**-**19**) is comparable to the activity of complex **16**. The most interesting results in this group of complexes were obtained with amide complex **19**. In this case, an equal amount of epoxide and *cis*-diol was formed at a catalyst:oxidant:substrate ratio of 1:20:1000. Although the amount of *cis*-diol product is lower than the amount produced by complex **14**, in the latter case larger amounts of epoxides were formed. During the catalytic reactions with complex **19**, a change in color from off-white to red was observed upon addition of the oxidant (*vide supra*). For all the other complexes the color of the solution changed to dark yellow/orange after the addition of hydrogen peroxide. Based on its crystal structure, complex **17** [Fe(**BMBIP^{nPr}**)$_2$](OTf)$_2$ might have been expected to be a good candidate as a *cis*-dihydroxylation catalyst because of the *cis*-coordination of the two carbonyl groups. However, **17** gave a 3:1 ratio of epoxide and cis-diol product at best. This observation adds to the notion that the *cisoid* structure as observed by X-Ray crystallography is one of several conformers of **17** and apparently does not stand out in kinetic competence during catalysis. Complex **20** was amongst the least active complexes in this study. A small amount of epoxide was formed and in some cases a small trace of diol was observed at a H_2O_2 conversion between 3 and 7%.

Few other Fe-based catalyst, in particular ones based on a mixes N,N,O ligand manifold, are known to perform *cis*-dihydroxylations of alkenes using H_2O_2 and cyclooctene is not always included as a substrate in these studies. The Ph-DPAH based system reported by Que *et al.* shows a selectivity towards the diol in the oxidation of cyclooctene of 14:1 with a TON value of 7.0 towards the diol product.[16] Later, this system was optimized through ligand derivatization to exclusively yield the diol product in styrene oxidation (TON = 9.4) and 1-octene oxidation (TON = 7.7).[39] Cyclooctene was not included as a substrate in this study. The same group also reported on a polydentate mixed N,O ligand derived from Kemp's acid of which the corresponding Fe(II) complex is able to oxidize 1-octene to the epoxide and diol in a 1:6 ratio albeit with a TON value lower than 1 per iron.[40] These data show that turnover values in *cis*-dihydroxylation reactions using mixed N,O ligands in combination with iron are, in general, low. The *cis*-dihydroxylation activity of non-heme iron complexes derived from all nitrogen-ligands has been described somewhat more extensively (*vide supra*). The most active systems reported so far are derived from the PyTACN ligand system reported by the group of Costas. These systems show TON values for diols up to 140 and a diol/epoxide ratio up to 4.9 in the oxidation of cyclooctene (300 equiv. H_2O_2 was used). All of these studies used large excesses (~1000 equiv.) of alkene substrate per iron.[41]

The overall low activity of the complexes presented here pose a challenge for further improvement or even practical use. Issues that could be at play here, next to metal release from the ligand manifold, are structural integrity of the complexes and diol

product inhibition. Our investigation on the structure of iron complexes based on the **BAIP** ligand family have shown the coordination flexibility of these ligands in solution as well as in the solid state. Accordingly, this may lead to multiple species under catalytic conditions, with a variation in activity and specificity. For the **BAIP** ligands our investigations show that a change from imidazole to benzimidazole donors prevents ester dissociation from the metal. On the one hand this reduces the number of solution species, while on the other hand the creation of vacant sites on the metal is hampered. In effect this has led to a lower activity for the benzimidazole complexes. Another factor that influences product formation and turnover, and which is less discussed, is the possibility of product inhibition. Although reaction mixtures involving H_2O_2 tend to be acidic, the formation of stable iron-diolate complexes cannot be excluded. Such complexes seem to lack sufficient open coordination sites to accommodate a *cis*-dihydroxylation pathway and are proposed to be inactive. We have previously reported on Fe-catecholate complexes derived from BAIP ligands and found that these are rather stable or show catechol-based chemistry.[22] Release of diols from Fe-diolate complexes leading to increased TONs may be accomplished by the use of a proper reaction medium. This matter is currently investigated in our labs.

6.4 Concluding remarks

In summary, we have presented an extension of the **BAIP** ester ligand family and have studied the coordination chemistry of the new ligands towards $Fe(OTf)_2$. These studies have shown the intrinsic property of these ligands to bind to iron in a facial N,N,O manner, thereby mimicking the 2-His-1-carboxylate facial triad found in mononuclear non-heme iron enzymes. The coordination flexibility of the ligands also manifested itself in these studies, where next to *trans* bis-ligand arrangements also *cis* arrangements are possible and where tetrahedral, all nitrogen coordination can be enforced by steric bulk. Although these studies have so far not led to the development of improved olefin *cis*-dihydroxylation catalyst, they do provide designer tools for the further development of bio-mimetic mono-nuclear non-heme iron complexes and for steering the reactivity of such complexes in catalysis. In particular the role of benzimidazole donors in providing a well-defined tripodal coordination mode of the ligands in solution, the electron-rich nature of amide donors which may help to stabilize higher oxidation states of the metal, and the subtle role of steric factors in the balance between site-isolation and coordination mode integrity are of interest. These considerations are currently included in the design of new ligands and their corresponding non-heme iron complexes, with the aim to arrive at site-isolated mono-nuclear complexes 'capped' by a single N,N,O ligand that feature enhanced activities in the catalytic *cis*-dihydroxylation of olefins.

6.5 Experimental section

General: Air-sensitive reactions were carried out under an inert, N_2 atmosphere using standard Schlenk techniques. The used solvents were dried and distilled before use. The chemicals were commercially obtained and used as received or were reproduced from literature. ^{1}H and ^{13}C NMR spectra were recorded on a Varian 400 spectrometer at 400 MHz and 100 MHz respectively operating at 25 °C. Infrared spectra were recorded with a Perkin-Elmer Spectrum One FT-IR instrument. Solution IR measurements were recorded with a Mettler Toledo ReactIR^{TM} 1000 spectrometer with a SiComp^{TM} probe placed in a Schlenk under a N_2 atmosphere. GC-MS measurements were measured on a Perkin-Elmer Autosystem XL gas chromatograph with an attached Perkin-Elmer Turbomass Upgrade mass spectrometer. High-resolution ESI-MS data were acquired on a Waters LCT Premier XE machine. Solution magnetic moments were determined by the Evans' NMR method in acetone-d_6/cyclohexane (95/5 *v*/*v*) or in acetonitrile-d_3/cyclohexane (95/5 *v*/*v*) at 25 °C.[37,38] GC analyses were performed on a Perkin-Elmer Clarus 500 GC (30 m, Econo-Cap EC-5) with FID detector. Elemental microanalyses were carried out by the Mikroanalytisches Laboratorium KOLBE, Mülheim an der Ruhr, Germany. Cyclic voltammograms were recorded in a single compartment cell under a dry nitrogen atmosphere. The cell was equipped with a Pt working electrode, a Pt wire counter electrode and a Ag/AgCl reference electrode. The potential control was achieved with a PAR Model 263A potentiostat. Bis(1-methylimidazol-2-yl)methane (**1**),[26,27] bis(1-methylbenzimidazol-2-yl)methane (**2**),[28] propyl 3,3-bis(1-methyl(benz)imidazol-2-yl)propionate (**BMIP^{nPr}** (**3**), **BMBIP^{nPr}** (**4**)),[25] 3,3-bis(1-methyl(benz)imidazol-2-yl)propionic acid (**7**,**10**),[25] propyl 3,3-bis(1-ethyl-4-isopropylimidazol-2-yl)propionate (**BEiPrIP^{nPr}**, (**13**)),[30] Fe(OTf)$_2$·2MeCN[31] and [Fe(**BMIP^{nPr}**)$_2$](OTf)$_2$ (**14**),[23] were prepared according to published procedures.

***tert*-Butyl 3,3-bis(1-methylimidazol-2-yl)propionate, BMIP^{tBu} (5):** A solution of *n*-butyllithium (0.48 mL, 0.77 mmol, 1.6 M in hexanes) was added drop wise to a stirring solution of bis(1-methylimidazol-2-yl)methane (**1**) (134 mg, 761 µmol) in THF (4 mL) at -78°C. The greenish solution was stirred for 1 hour at -78 °C, followed by the drop wise addition of *t*-butyl bromoacetate (115 µL, 779 µmol). The mixture was allowed to rise to room temperature and was quenched with H_2O (10 mL). All volatiles were evaporated *in vacuo* and the water layer was extracted with ethyl acetate (4 x 10 mL) and the combined organic layers were dried over magnesium sulfate, filtered and concentrated *in vacuo*. The product was obtained as a clear yellow oil (216 mg, 90%).

^{1}H NMR (400 MHz, $CDCl_3$, 25 °C): δ = 1.16 (s, 9H, OC(C*H*$_3$)$_3$), 3.03 (d, 2H, $^3J_{HH}$ = 7.6 Hz, CHC*H*$_2$), 3.32 (s, 6H, NC*H*$_3$), 4.74(t, 1H, $^3J_{HH}$ = 8.0 Hz, C*H*CH$_2$), 6.58 (d, 2H, $^3J_{HH}$ = 0.8 Hz, H$_{imid}$), 6.71 (d, 2H, $^3J_{HH}$ = 0.8 Hz, H$_{imid}$) ppm. ^{13}C {1H} NMR (100 MHz, $CDCl_3$, 25 °C): δ = 28.0, 32.9, 34.7, 37.6, 80.9, 122.1, 127.0, 145.4, 170.3 ppm.

IR (solid): ν (cm^{-1}): 3107.0, 2977.4, 2932.3, 1725.5 1520.5, 1491.0, 1455.9, 1411.4, 1392.9, 1366.0, 1310.9, 1280.4, 1249.7, 1151.1, 1133.7, 857.6, 763.7, 738.3. ESI-MS: m/z = 291.182 ($[M+H]^+$, calc. 291.182).

***tert*-Butyl 3,3-bis(1-methylbenzimidazol-2-yl)propionate, $BMBIP^{tBu}$ (6):** A solution of *n*-butyllithium (0.75 mL, 1.2 mmol, 1.6 M in hexanes) was added drop wise to a stirring solution of **2** (308 mg, 1.11 mmol) in THF (20 mL) at -78°C. The greenish solution was stirred for 1 hour at -78 °C, followed by the drop wise addition of *t*-butyl bromoacetate (165 µL, 1.11 mmol). The mixture was allowed to rise to room temperature and was quenched with H_2O (15 mL). All volatiles were evaporated *in vacuo* and the water layer was extracted with ethyl acetate (2 x 25 mL) and the combined organic layers were dried over magnesium sulfate, filtered and concentrated *in vacuo*. The product was obtained as an off-white solid (407 mg, 94%).
^{1}H NMR (400 MHz, $CDCl_3$, 25 °C): δ = 1.33 (s, 9H, OC(CH_3)$_3$), 3.50 (d, 2H, $^3J_{HH}$ = 7.6 Hz, CHCH_2), 3.81 (s, 6H, NCH_3), 5.48 (m, 1H, CHCH$_2$), 7.27 (m, 6H, $H_{benzimid}$), 7.76 (m, 2H, $H_{benzimid}$) ppm. ^{13}C {1H} NMR (100 MHz, $CDCl_3$, 25 °C): δ = 28.2, 30.7, 36.1, 37.4, 81.7, 109.6, 119.7, 122.7, 123.3, 136.5, 151.2, 169.8 ppm. IR (solid) ν (cm^{-1}): 3046.3, 2934.1, 2871.2, 1719.6, 1614.6, 1467.3, 1438.8, 1359.7, 1331.5, 1145.2, 981.2, 741.9. ESI-MS: m/z = 391.215 ($[M+H]^+$, calc. 391.213).

NHS 3,3-bis(1-methylimidazol-2-yl)propionate (8): N-hydroxysuccinimide (373 mg, 3.25 mmol) and N,N'-dicyclohexylcarbodiimide (670 mg, 3.25 mmol) were added to a stirring suspension of **7** (759 mg, 3.24mmol) in dry THF (250 mL), followed by the addition of pyridine (1.5 mL, 18.5 mmol). A reflux condenser was put on top of the flask and the reaction mixture was stirred on an oil bath at 40 °C overnight after which the reaction mixture was still a white suspension. After stirring at 45 °C for an additional 3 hours the white solid particles were filtered off, followed by the evaporation of the solvent *in vacuo* yielding a yellow/white solid which was dissolved in dichloromethane. The precipitated urea was filtered off and the dichloromethane was evaporated *in vacuo*. The remaining solid was dissolved again in dichloromethane and the precipitate was filtered off again. This cycle was repeated until no more precipitate was formed (3 cycles). The yellowish solid was recrystallized from a dichloromethane/diethyl ether mixture at -30 °C overnight yielding an off-white solid (450 mg, 43%). Not entirely pure, some dicyclohexylurea was present according to NMR.
^{1}H NMR (400 MHz, $CDCl_3$, 25 °C): δ = 2.63 (s, 4H, C(O)CH_2), 3.25 (d, 2H, $^3J_{HH}$ = 6.4 Hz, CHCH_2), 3.48 (s, 6H, NCH_3), 4.98 (t, 1H, $^3J_{HH}$ = 8.0 Hz, CHCH$_2$), 6.72 (s, 2H, H_{im}), 6.87 (s, 2H, H_{im}) ppm. ^{13}C {1H} NMR (100 MHz, dmso-d6, 25 °C): δ = 25.7, 32.3, 33.1, 38.8, 123.1, 125.9, 145.8, 173.2, 174.1 ppm. ESI-MS: m/z = 332.135 ($[M+H]^+$, calc. 332.136).

3,3-bis(1-methylimidazol-2-yl)-*N*-propylpropanamide, BMIP^{AnPr} (9) : Propylamine (112 µL, 1.38 mmol) was added to a solution of **8** (450 mg, 1.36 mmol) in dichloromethane (20 mL). The colorless solution was stirred for 48 hours at room temperature. The reaction mixture was washed with a saturated $NaHCO_3$ solution (2 x 15 mL) and H_2O (2 x 15 mL). The combined aqueous layers were extracted with dichloromethane (1 x 15 mL) and the combined organic layers were dried over magnesium sulfate, filtrated and evaporated *in vacuo* yielding a white solid which was recrystallized from a dichloromethane/diethyl ether mixture (95 mg, 25%).
^{1}H NMR (400 MHz, $CDCl_3$, 25 °C): δ = 0.81 (t, 3H, $^3J_{HH}$ = 7.4 Hz, $NHCH_2CH_2CH_3$), 1.40 (sextet, 2H, $^3J_{HH}$ = 7.2 Hz, $NHCH_2CH_2CH_3$), 3.11 (m, 2H, $NHCH_2CH_2CH_3$), 3.14 (d, 2H, $^3J_{HH}$ = 7.6 Hz, $CHCH_2$), 3.50, (s, 6H, NCH_3), 4.83 (t, 1H, $^3J_{HH}$ = 7.2 Hz, $CHCH_2$), 6.53 (m, 1H, $NHCH_2CH_2CH_3$), 6.77 (s, 2H, H_{im}), 6.93 (s, 2H, H_{im}) ppm. ^{13}C {1H} NMR (100 MHz, $CDCl_3$, 25 °C): δ = 11.5, 22.8, 33.3, 33.8, 39.1, 41.5, 122.1, 126.8, 145.8, 170.4 ppm. IR (solid) ν (cm^{-1}): 3231.9, 3050.7, 2970.1, 2937.1, 2875.7, 1650.6, 1562.8, 1489.0, 1473.9, 1278.7, 1237.9, 1133.3, 1084.1, 971.1, 924.7, 843.0, 761.0, 738.2, 694.3. ESI-MS: m/z = 276.187 ($[M+H]^+$, calc. 276.182).

NHS 3,3-bis(1-methylbenzimidazol-2-yl)propionate (11): N-hydroxysuccinimide (166 mg, 1.44 mmol) and N,N'-dicyclohexylcarbodiimide (303 mg, 1.47 mmol) were added to a stirring suspension of **10** (480 mg, 1.44 mmol) in dry THF (200 mL), followed by the addition of pyridine (1.5 mL, 18.5 mmol). A reflux condenser was put on top of the flask and the reaction mixture was stirred on an oil bath at 35 °C for 3 h and at room temperature overnight. The reaction mixture became a clear yellow solution upon heating to 35 °C again and stirring at 35 °C was continued for another 8 hours, followed by stirring at room temperature for 3 days. Some white precipitate (N,N'-dicyclohexylurea) was present which was filtered off, followed by the evaporation of the solvent *in vacuo* yielding a yellow/white solid, which was dissolved in dichloromethane. The precipitated urea was filtered off and the dichloromethane was evaporated *in vacuo*. The remaining solid was dissolved again in dichloromethane and the precipitate was filtered off again. This cycle was repeated until no more precipitate was formed (4 cycles). The yellowish solid was recrystallized from a dichloromethane/diethyl ether mixture at -30 °C overnight yielding a slightly yellow solid (529 mg, 85%).
^{1}H NMR (400 MHz, $CDCl_3$, 25 °C): δ = 2.76 (s, 4H, $C(O)CH_2$), 3.73 (s, 6H, NCH_3), 3.94 (d, 2H, $^3J_{HH}$ = 7.6 Hz, $CHCH_2$), 5.50 (t, 1H, $^3J_{HH}$ = 7.6 Hz, $CHCH_2$), 7.27 (m, 6H, $H_{benzimid}$), 7.79 (m, 2H, $H_{benzimid}$) ppm. ^{13}C {1H} NMR (100 MHz, $CDCl_3$, 25 °C): δ = 25.7, 30.5, 33.5, 35.8, 109.6, 120.2, 122.7, 123.4, 136.6, 142.0, 150.1, 166.8, 168.8 ppm. IR (solid) ν (cm^{-1}): 2936.7, 1813.9, 1782.0, 1728.3, 1502.5, 1469.4, 1438.2, 1363.4, 1287.3, 1197.2, 1156.2, 1094.8, 1062.6, 980.3 869.0, 809.2, 743.4. ESI-MS: m/z = 432.163 ($[M+H]^+$, calc. 432.167).

3,3-bis(1-methylbenzimidazol-2-yl)-*N*-propylpropanamide, BMBIP^{AnPr} (12): Propylamine (48 µL, 580 µmol) was added to a solution of **11** (250 mg, 579 µmol) in dichloromethane (10 mL). The colorless solution was stirred overnight at room temperature. The reaction mixture was washed with a saturated $NaHCO_3$ solution (2 x 5 mL) and H_2O (1 x 5 mL). The combined aqueous layers were extracted with dichloromethane (1 x 5 mL) and the combined organic layers were dried over magnesium sulfate, filtrated and evaporated *in vacuo* yielding a white solid (195 mg, 90%).
^{1}H NMR (400 MHz, $CDCl_3$, 25 °C): δ = 0.77 (t, 3H, $^3J_{HH}$ = 7.4 Hz, $NHCH_2CH_2CH_3$), 1.37 (sextet, 2H, $^3J_{HH}$ = 7.2 Hz, $NHCH_2CH_2CH_3$), 3.12 (q, 2H, $^3J_{HH}$ = 6.7 Hz, $NHCH_2CH_2CH_3$), 3.40 (d, 2H, $^3J_{HH}$ = 6.8 Hz, $CHCH_2$), 3.73 (s, 6H, NCH_3), 5.32 (t, 1H, $^3J_{HH}$ = 7.2 Hz, $CHCH_2$), 6.38 (m, 1H, $NHCH_2CH_2CH_3$), 7.29 (m, 6H, $H_{benzimid}$), 7.73 (m, 2H, $H_{benzimid}$) ppm. ^{13}C {1H} NMR (100 MHz, $CDCl_3$, 25 °C): δ = 11.4, 22.8, 30.3, 31.1, 35.4, 39.3, 41.6, 109.5, 120.0, 122.4, 123.0, 136.4, 142.3, 152.1, 170.3 ppm. IR (solid) ν (cm^{-1}): 3235.1, 3057.2, 2930.0, 1656.2, 1555.9, 1507.8, 1464.0, 1439.9, 1395.5, 1281.9, 1262.4, 1240.0, 1092.7, 773.6, 740.3. Anal. for $C_{22}H_{25}N_5O$ (375.47): calc. C 70.38, H 6.71, N 18.65; found C 70.59, H 7.05, N 18.43.

[Fe(BMIP^{tBu})$_2$](OTf)$_2$ (15): To a solution of **BMIP^{tBu} (5)** (216 mg, 744 µmol) in acetonitrile (2 mL) was added a solution of $Fe(OTf)_2$·2MeCN (171 mg, 370 µmol) in acetonitrile (2 mL) and the yellowish reaction mixture was stirred for 1 hour at RT. The solvent was evaporated *in vacuo* and the remaining brown solid was recrystallized from an acetonitrile/diethyl ether mixture at -30 °C overnight to optimize the yield. The product was obtained as a brown crystalline solid (270 mg, 95%). Single crystals suitable for X-ray diffraction were obtained by slow vapor-diffusion of diethyl ether into a solution of **15** in acetonitrile.
IR (solid) ν (cm^{-1}): 2983.2, 1692.2, 1506.7, 1396.5, 1370.3, 1258.1, 1223.5, 1144.1, 1029.4, 988.7, 962.1, 948.2, 852.7, 831.8, 754.3, 734.4. Solution magnetic moment (Evans' method): μ_{eff} = 5.1 μ_B. ESI-MS: m/z = 785.235 ($[M\text{-}OTf]^+$, calc. 785.236).

[Fe(BMIP^{AnPr})$_2$](OTf)$_2$ (16): Compound **9** (13 mg, 48 µmol) was mixed with $Fe(OTf)_2$·2MeCN (11 mg, 24 µmol) in acetonitrile (16 mL) prior to use it in catalysis. From the remaining solution single crystals were grown by slow vapor-diffusion of diethyl ether into it for X-ray analysis and no further analysis was performed on the crystals.

[Fe(BMBIP^{nPr})$_2$](OTf)$_2$ (17): To a solution of **BMBIP^{nPr} (4)** (195 mg, 518 µmol) in methanol (5 mL) was added a solution of $Fe(OTf)_2$·2MeCN (114 mg, 259 µmol) in methanol (4 mL) and the reaction mixture was stirred for 40 min at RT. The solvent was evaporated *in vacuo* and the remaining white solid was recrystallized from an

acetonitrile/diethyl ether mixture at -30 °C overnight to optimize the yield. The solvent, which had a deep red color, was removed with a cannula and the remaining crystalline solid was washed with diethyl ether and dried *in vacuo*. The product was obtained as an off-white crystalline solid (254 mg, 89%). Single crystals suitable for X-ray diffraction were obtained by slow vapor-diffusion of diethyl ether into a solution of **17** in acetonitrile.
IR (solid) ν (cm^{-1}): 3510.2, 3058.2, 2967.6, 1708.8, 1693.7, 1618.4, 1493.7, 1455.6, 1401.0, 1258.5, 1208.1, 1160.5, 1030.6, 927.1, 739.1. Solution magnetic moment (Evans' method): μ_{eff} = 5.1 μ_B. Anal. for $C_{46}H_{48}F_6FeN_8O_{10}S_2$ (1106.89): calc. C 49.91, H 4.37, N 10.12; found C 49.39, H 4.53, 10.03.

[Fe(BMBIP^{tBu})$_2$](OTf)$_2$ (18): To a solution of **BMBIP^{tBu} (6)** (158 mg, 405 μmol) in methanol (5 mL) was added a solution of Fe(OTf)$_2$·2MeCN (89 mg, 203 μmol) in methanol (5 mL) and the yellowish reaction mixture was stirred for 45 min at RT. The solvent was evaporated *in vacuo* and the remaining off- white solid was recrystallized from an acetonitrile/diethyl ether mixture at -30 °C overnight to optimize the yield. The solvent, which had a brownish color, was removed with a cannula leaving the white crystalline solid (198 mg, 86%). Single crystals suitable for X-ray diffraction were obtained by slow vapor-diffusion of diethyl ether into a solution of **18** in acetonitrile.
IR (solid) ν (cm^{-1}): 2981.9, 1665.1, 1490.5, 1454.0, 1418.2, 1398.0, 1373.2, 1260.1 1226.1, 1149.8, 1029.5, 1010.5, 995.1, 844.5, 745.9. Solution magnetic moment (Evans' method): μ_{eff} = 5.3 μ_B. ESI-MS: m/z = 985.294 ([M-OTf]$^+$, calc. 985.298).

[Fe(BMBIP^{AnPr})$_2$](OTf)$_2$ (19): To a solution of **BMBIP^{AnPr} (12)** (154 mg, 410 μmol) in methanol (7 mL) was added a solution of Fe(OTf)$_2$·2MeCN (90mg, 205 μmol) in methanol (4 mL) and the reaction mixture was stirred for 30 min at RT. The solvent was evaporated *in vacuo* and the remaining off- white solid was recrystallized from an acetonitrile/diethyl ether mixture at -30 °C overnight to optimize the yield. The solvent was removed with a cannula leaving the off-white crystalline solid (178 mg, 79%). Single crystals suitable for X-ray diffraction were obtained by slow vapor-diffusion of diethyl ether into a solution of **19** in acetonitrile. The off-white crystalline solid turned red after 1 day (in a Schlenk under N_2 atmosphere).
IR (solid) ν (cm^{-1}): 3297.7, 3104.9, 2965.1, 1628.3, 1565.0, 1504.9, 1481.0, 1454.8, 1277.0, 1244.4, 1223.3, 1151.7, 1028.1, 741.0. ESI-MS: m/z = 955.292 ([M-OTf]$^+$, calc. 955.299).

[Fe(BEiPrIP^{nPr})$_2$](OTf)$_2$ (20): Fe(OTf)$_2$.2MeCN (86 mg, 197 μmol) was added to a stirring solution of **BEiPrIP^{nPr} (13)** (153 mg, 394 μmol) in methanol (4 mL) and the dark brown solution stirred for 30 min at RT. The solvent was evaporated *in vacuo* and the remaining dark oil was recrystallized twice from an acetonitrile/diethyl ether

mixture at -30 °C leaving a yellow crystalline solid which was washed with diethyl ether (50 mg, 34%). Crystals suitable for X-ray diffraction were obtained by slow vapor-diffusion of diethyl ether into a solution of **20** in acetonitrile.
IR (solid) ν (cm^{-1}): 3109.1, 2968.3, 2879.0, 1736.0, 1704.8, 1691.5, 1583.1, 1497.1, 1495.2, 1388.1, 1365.3, 1258.6, 1223.6, 1147.5, 1087.4, 1030.6, 975.4, 803.0. Solution magnetic moment (Evans' method): μ_{eff} = 5.1 μ_B. ESI-MS: m/z = 981.455 ($[M\text{-}OTf]^+$, calc. 981.454).

Catalysis protocol: To a solution of catalyst (3 μmol) in acetonitrile (2 mL) was added *cis*-cyclooctene (500 or 1000 equiv.) and acetonitrile (to bring the total volume to 2.5 mL). 1,2-dibromobenzene (10 μL) was added as internal standard and subsequently, 0.5 mL of oxidant solution (20 or 100 equiv., diluted from 35% aqueous H_2O_2 with acetonitrile) was added drop wise over 20 min. The reaction mixture was stirred at room temperature and after 1h the first sample was taken. Diethyl ether was added to the sample to precipitate the iron complex after which it was analyzed by GC.

X-ray crystal structure determinations: Reflections were measured on a Nonius KappaCCD diffractometer with rotating anode and graphite monochromator (λ = 0.71073 Å) at a temperature of 150(2) K. Intensity data were integrated with the software Eval14[42] (compound **14** and **16**), Eval15[43] (compound **15**) or HKL2000[44] (compounds **17**-**20**). Absorption correction and scaling was performed based on multiple measured reflections with SADABS[45] (**14**-**16**) or SORTAV[46] (**18**-**20**). In compound **17**, no absorption correction was considered necessary. The structures were solved by Direct Methods using the programs SHELXS-97[47] (**14**-**17**, **19**-**20**) or SIR-97[48] (**18**). Least-squares refinement was performed with SHELXL-97[47] against F^2 of all reflections. Non-hydrogen atoms were refined freely with anisotropic displacement parameters. Hydrogen atoms were introduced in calculated positions (**14-18, 20**) or located in difference Fourier maps (**19**). Hydrogen atoms were refined with a riding model, the N-H hydrogen atom of **19** was refined freely with isotropic displacement parameters. Restraints for distances and angles and for the approximation of isotropic behavior were used for triflate and acetonitrile. In **14**, **16**, **17**, **18**, and **20**, triflate anions were refined with disorder models, respectively. In **14** the acetonitrile was refined with partial occupancy and a propyl ester moiety with a disorder model. The crystal structures of **15** and **20** contain voids [594 (compound **15**) and 282 $Å^3$ / unit cell (compound **20**)] filled with disordered acetonitrile solvent molecules. Their contribution to the structure factors was secured by back-Fourier transformation with the SQUEEZE routine of PLATON,[49] resulting in 112 (compound **15**) and 70 electrons / unit cell (compound **20**). Geometry calculations and checking for higher symmetry was performed with the PLATON program.[49]

Further details of the crystal structure determinations are given in Tables 10-12.

Table 10. Experimental details of crystal structures **14**-**16**.

	14	**15**	**16**
formula	$[C_{28}H_{40}FeN_8O_4](CF_3O_3S)_2 \cdot 1.95(CH_3CN)$	$[C_{30}H_{44}FeN_8O_4](CF_3O_3S)_2$ + disordered acetonitrile	$[C_{28}H_{42}FeN_{10}O_2](CF_3O_3S)_2$
Fw	986.73	934.72[*]	904.71
crystal color	colorless	colorless	colorless
crystal size [mm^3]	0.63x0.42x0.04	0.18x0.16x0.12	0.90x0.21x0.03
crystal system	triclinic	monoclinic	triclinic
space group	$P\bar{1}$ (no. 2)	$P2_1/n$ (no. 14)	$P\bar{1}$ (no. 2)
a [Å]	14.3823(2)	17.2165(5)	8.6294(5)
b [Å]	14.6648(4)	13.1126(4)	10.7097(8)
c [Å]	22.2031(7)	20.2556(13)	11.4184(6)
α [°]	87.999(1)	90	65.829(4)
β [°]	88.800(1)	91.338(2)	88.557(3)
γ [°]	89.251(1)	90	81.683(2)
V [$Å^3$]	4678.7(2)	4571.4(4)	951.95(10)
Z	4	4	1
D_{calc} [g/cm^3]	1.401	1.358[*]	1.578
$(\sin\theta/\lambda)_{max}$ [$Å^{-1}$]	0.55	0.53	0.48
refl. measured/ unique	47185 / 12969	46455 / 5600	6170 / 1681
parameters / restraints	1227 / 469	545 / 195	334 / 187
R1/wR2 [I>2σ(I)]	0.0680 / 0.1657	0.0488 / 0.1275	0.0665 / 0.1626
R1/wR2 [all refl.)]	0.1102 / 0.1909	0.0628 / 0.1355	0.0827 / 0.1741
S	1.078	1.148	1.106
ρ(min/max) [$eÅ^{-3}$]	-0.61 / 1.37	-0.85 / 0.68	-0.50 / 0.70

[*] Derived values do not contain the contribution of the disordered solvent.

Table 11. Experimental details of crystal structures **17-19**.

	17	**18**	**19**
formula	$[C_{44}H_{48}FeN_8O_4]$ $(CF_3O_3S)_2$ $\cdot 2(CH_3CN)$	$[C_{46}H_{52}FeN_8O_4]$ $(CF_3O_3S)_2$ $\cdot 5(CH_3CN)$	$[C_{44}H_{50}FeN_{10}O_2]$ $(CF_3O_3S)_2$ $\cdot 2(CH_3CN)$
Fw	1189.00	1340.22	1187.04
crystal color	colorless	colorless	yellow
crystal size [mm^3]	0.36x0.09x0.09	0.42x0.10x0.08	0.57x0.30x0.12
crystal system	orthorhombic	monoclinic	monoclinic
space group	Pnna (no. 52)	$P2_{1/}c$ (no. 14)	$P2_{1/}c$ (no. 14)
a [Å]	16.6451(2)	11.7689(2)	14.9769(1)
b [Å]	18.8376(3)	26.0832(6)	11.8607(1)
c [Å]	17.5683(3)	22.7901(6)	17.6525(2)
α [°]	90	90	90
β [°]	90	112.8675(8)	122.6929(5)
γ [°]	90	90	90
V [$Å^3$]	5508.61(14)	6446.1(3)	2638.96(4)
Z	4	4	2
D_{calc} [g/cm^3]	1.434	1.381	1.494
$(\sin\theta/\lambda)_{max}$ [$Å^{-1}$]	0.55	0.56	0.65
refl. measured/unique	44453 / 3850	52160 / 9198	45526 / 6063
parameters / restraints	388 / 81	858 / 267	366 / 0
R1/wR2 [$I>2\sigma(I)$]	0.0597 / 0.1721	0.0632 / 0.1562	0.0418 / 0.1173
R1/wR2 [all refl.)]	0.0833 / 0.1897	0.1127 / 0.1851	0.0552 / 0.1275
S	1.057	1.077	1.093
ρ(min/max) [$eÅ^{-3}$]	-0.34 / 1.30	-0.38 / 0.53	-0.60 / 0.64

Table 12. Experimental details of crystal structure **20**.

	20
formula	$[C_{44}H_{72}FeN_8O_4](CF_3O_3S)_2$ + disordered acetonitrile
Fw	1131.09[*]
crystal color	yellow
crystal size [mm^3]	0.26x0.24x0.06
crystal system	triclinic
space group	*P*1 (no. 1)
a [Å]	12.7766(1)
b [Å]	13.9229(1)
c [Å]	27.2566(4)
α [°]	80.8220(3)
β [°]	84.8511(4)
γ [°]	67.7105(7)
V [$Å^3$]	4426.61(8)
Z	3
D_{calc} [g/cm^3]	1.273[*]
(sin θ/λ_{max} [$Å^{-1}$]	0.65
refl. measured/unique	88288 / 39932
parameters / restraints	2142 / 2229
R1/wR2 [I>2σ(I)]	0.0496 / 0.1116
R1/wR2 [all refl.)]	0.0786 / 0.1264
S	0.999
Flack x[50]	0.537(9)
ρ(min/max) [$eÅ^{-3}$]	-0.32 / 0.57

[*] Derived values do not contain the contribution of the disordered solvent.

DFT geometry optimizations. The geometry optimizations were carried out with the Turbomole program[51a,b] coupled to the PQS Baker optimizer.[52] Geometries were fully optimized as minima at the ri-DFT BP86[53] level using the Turbomole SV(P) basis set[51c,d] on all atoms. Improved energies were obtained with single point energy calculations at the DFT b3-lyp,[54] def-TZVP[51c-f] level of theory.

References

1. Tanase, S.; Bouwman, E. *Adv. Inorg. Chem*. **2006**, *58*, 29-75.
2. Bataille, C.J.R.; Donohoe, T.J. *Chem. Soc. Rev*. **2011**, *40*, 114-128.
3. Schroeder, M. *Chem. Rev.* **1980**, *80*, 187-213.
4. Sharpless, K.B.; Amberg, W.; Bennani, Y.L. Crispino, G.A.; Hartung, J.; Jeong, K.-S.; Kwong, H.-L. Morikawa, K.; Wang, Z.-M.; Xu, D.; Zhang, X.-L. *J. Org. Chem.* **1992**, *57*, 2768-2771.
5. Yip, W.-P.; Ho, C.-M.; Zhu, N.; Lau, T.-C.; Che, C.-M. *Chem. Asian. J*. **2008**, *3*, 70-77.
6. Shing, T.K.M.; Tam, E.K.W.; Tai, V.W.-F.; Chung, I.H.F.; Jiang, Q. *Chem. Eur. J.* **1996**, *2*, 50-57.
7. Yip, W.-P.; Yu, W.-Y.; Zhu, N.; Che, C.-M. *J. Am. Chem. Soc.* **2005**, *127*. 14239-14249.
8. Zimmer, R.; Collas, M.; Czerwonka, R.; Hain, U.; Reissig, H. *Synthesis* **2008**, *2*, 237-244.
9. Taylor, J.E. *Can. J. Chem*. **1984**, *62*, 2641-2645.
10. de Boer, J.W.; Browne, W.R.; Harutyunyan, S.R.; Bine, L.; Tiemersma-Wegman, T.D.; Alsters, P.L.; Hage, R.; Feringa, B.L. *Chem. Commun.* **2008**, 3747-3749.
11. Chow, T. W.-S.; Liu, Y.; Che, C.-M. *Chem. Commun.* **2011**, *47*, 11204-11206.
12. Bruijnincx, P.C.A.; van Koten, G.; Klein Gebbink, R.J.M. *Chem. Soc. Rev*. **2008**, *37*, 2716-2744.
13. Costas, M.; Mehn, M.P.; Jensen, M.P.; Que, L. Jr. *Chem. Rev*. **2004**, *104*, 939-986.
14. Hegg, E.L.; Que, L. Jr. *Eur. J. Biochem*. **1997**, *250*, 625-629.
15. Chen, K.; Que, L. Jr. *Angew. Chem. Int. Ed.* **1999**, *38*, 2227-2229.
16. Oldenburg, P.D.; Shteinman, A.A.; Que, L. Jr. *J. Am. Chem. Soc.* **2005**, *127*, 15672-15673.
17. Suzuki, K.; Oldenburg, P.D.; Que, L. Jr. *Angew. Chem. Int. Ed.* **2008**, *47*, 1887-1889.
18. a) Bukowski, M.R.; Comba, P.; Lienke, A.; Limberg, C.; de Laorden, C.L.; Mas-Ballesté, R.; Merz, M.; Que, L., Jr. *Angew. Chem. Int. Ed.* **2006**, *45*, 3446-3449. b) Chow, T.W.-S.; Wong, E.L.-M.; Guo, Z.; Liu, Y.; Huang, J.-S.; Che C.-M. *J. Am. Chem. Soc.*, **2010**, *132*, 13229-13239.
19. a) Rodriguez, M.-C.; Morgenstern-Badarau, I.; Cesario, M.; Guilhem, J.; Keita, B.; Nadjo, L. *Inorg. Chem.* **1996**, *35*, 78047810. b) Beck, A.; Weibert, B.; Burzlaff, N. *Eur. J. Inorg. Chem.* **2001**, 521-527. c) Beck, A.; Barth, A.; Hübner, E.; Burzlaff, N. *Inorg. Chem.* **2003**, *42*, 7182−7188.
20. a) Dungan, V.J.; Wong, S.M.; Barry, S.M.; Rutledge, P.J. *Tetrahedron* **2012**, *68*, 3231-3236; b) Paria, S.; Halder, P.; Paine, T.K. *Inorg. Chem.* **2010**, *49*, 4518–4523.
21. Jones, M.W.; Baldwin, J.E.; Cowley, A.R.; Dilworth, J.R.; Karpov, A.; Smiljanic, N.; Thompson, A.L.; Adlington, R.M. *Dalton Trans.* **2012**, *41*, 14068-14086.
22. Bruijnincx, P.C.A.; Lutz, M.; Spek, Hagen, W.R.; Weckhuysen, B.M.; van Koten, G.; Klein Gebbink, R.J.M. *J. Am. Chem. Soc.* **2007**, *129*, 2275-2286.
23. Bruijnincx, P.C.A.; Buurmans, I.L.C.; Gosiewska, S.; Moelands, M.A.H.; Lutz, M.; Spek, A.L.; van Koten, G.; Klein Gebbink, R.J.M. *Chem. Eur. J*. **2008**, *14*, 1228-1237.
24. Other studies using this ligand family were reported by Burzlaff and Holland and co-workers. See: a) Peters, L.; Hübner, E.; Burzlaff, N. *J. Organomet. Chem.* **2005**, *690*, 2009-2016; b) Rocks, S.S.; Brennessel, W.W.; Machonkin, T.E.; Holland, P.L. *Inorg. Chim. Acta* **2009**, *362*, 1387-1390.
25. Bruijnincx, P.C.A.; Lutz, M.; Spek, A.L.; van Faassen, E.E.; Weckhuysen, B.M.; van Koten, G.; Klein Gebbink, R.J.M. *Eur. J. Inorg. Chem.* **2005**, 779-787.
26. Braussaud, N.; Rüther, T.; Cavell, K.J.; Skelton, B.W.; White, A.H. *Synthesis,* **2001**, *4*, 626-632.
27. Lucas, P.; El Mehdi, N.; Ho, H.A.; Belanger, D.; Breau, L. *Synthesis* **2000**, *3*, 1253-1258.

28. Elgafi, S.; Field, L.D.; Messerle, B.A.; Turner, P.; Hambley, T.W. *J. Organomet. Chem.* **1999**, *588*, 69-77.
29. Suijkerbuijk, B.M.J.M.; Slagt, M.Q.; Klein Gebbink, R.J.M.; Lutz, M.; Spek, A.L.; van Koten, G. *Tetrahedron Letters*, **2002**, *43*, 6565-6568.
30. Bruijnincx, P.C.A.; Lutz, M.; Spek, A.L.; Hagen, W.R.; Weckhuysen, B.M.; van Koten, G.; Klein Gebbink, R.J.M. *J. Am. Chem. Soc.* **2007**, *129*, 2275-2286.
31. Hagen, K.S. *Inorg. Chem.* **2000**, *39*, 5867-5869.
32. Bergström, P.Å.; French, R. *J. Phys. Chem.* **1995**, *99*, 12603-12611.
33. Bénisvy, L.; Chottard, J.; Marrot, J.; Li, Y. *Eur. J. Inorg. Chem*. **2005**, 999-1002.
34. Bénisvy, L.; Halut, S.; Donnadieu, B.; Tuchagues, J.; Chottard, J.; Li, Y. *Inorg. Chem.* **2006**, *45*, 2403-2405.
35. Robinson, K.; Gibbs, G.V.; Ribbe, P.H. *Science* **1971**, *172*, 567-570.
36. A recent example features a dinuclear Fe(II) complex in which on of the iron centers is found to be either 6- or 7-coordinated within the crystal as the result of a coordination shift of an exogenous carboxylate ligand. See: Burger, B.; Dechert, S.; Große, C.; Demeshko, S.; Meyer, F. *Chem. Commun.* **2011**, *47*, 10428–10430.
37. Britovsek, G.J.P.; Gibson, V.C.; Spitzmesser, S.K.; Tellmann, K.P.; White, A.J.P.; Williams, D.J. *J. Chem. Soc., Dalton Trans.* **2002**, 1159-1171.
38. Evans, D.F. *J. Chem. Soc.* **1959**, 2003-2005.
39. Oldenburg, P.D.; Feng, Y.; Pryjomska-Ray, I.; Ness, D.; Que, L. Jr. *J. Am. Chem. Soc.* **2010**, *132*, 17713-17723.
40. Oldenburg, P.D.; Ke, C-Y.; Tipton, A.; Shteinman, A.A.; Que, L. Jr. *Angew. Chem. Int. Ed.* **2006**, *45*, 7975-7978.
41. Company, A.; Gómez, L.; Fontrodona, X.; Ribas, X.; Costas, M. *Chem. Eur. J.* **2008**, *14*, 5727-5731.
42. Duisenberg, A.J.M.; Kroon-Batenburg, L.M.J.; Schreurs, A.M.M. J. Appl. Cryst. **2003**, *36*, 220-229.
43. Schreurs, A.M.M.; Xian, X.; Kroon-Batenburg, L.M.J. *J. Appl. Cryst.* **2010**, *43*, 70-82.
44. Otwinowski, Z.; Minor, W.; *Methods in Enzymology, Volume 276* (C.W. Carter, Jr. & R.M. Sweet, Eds.) Academic Press (1997) 307-326.
45. Sheldrick, G.M. SADABS: Area-Detector Absorption Correction, v2.10, Universität Göttingen, Germany (1999).
46. Blessing, R.H. *Acta Cryst.* **1995**, *A51*, 33-38.
47. Sheldrick, G.M. *Acta Cryst.* **2008**, *A64*, 112-122.
48. Altomare, A.; Burla, M.C.; Camalli, M.; Cascarano, G.L.; Giacovazzo, C.; Guagliardi, A.; Moliterni, A.G.G.; Polidori G.; Spagna, R. *J. Appl. Cryst.* **1999**, *32*, 115-119.
49. Spek, A.L. *Acta Cryst.* **2009**, *D65*, 148-155.
50. Flack, H.D. *Acta Cryst.* **1983**, *A39*, 876-881.
51. (a) Ahlrichs, R.; Bär, M.; Baron, H.-P.; Bauernschmitt, R.; Böcker, S.; Ehrig, M.; Eichkorn, K.; Elliott, S.; Furche, F.; Haase, F.; Häser, M.; Hättig, C.; Horn, H.; Huber, C.; Huniar, U.; Kattannek, M.; Köhn, A.; Kölmel, C.; Kollwitz, M.; May, K.; Ochsenfeld, C.; Öhm, H.; Schäfer, A.; Schneider, U.; Treutler, O.; Tsereteli, K.; Unterreiner, B.; von Arnim, M.; Weigend, F.; Weis, P.; Weiss, H. Turbomole Version 5.8, January 2002. Theoretical Chemistry Group, University of Karlsruhe; (b) Treutler, O.; Ahlrichs, R. *J. Chem. Phys.* **1995**, *102*, 346-354; (c) Turbomole basis set library, Turbomole Version 5.8, see a; (d) Schäfer, A.; Horn, H.; Ahlrichs, R. *J. Chem. Phys.* **1992**, *97*, 2571-2577; (e) Andrae, D.; Haeussermann, U.; Dolg, M.; Stoll, H.; Preuss, H. *Theor. Chim. Acta* **1990**, *77*, 123-141; (f) Schäfer, A.; Huber, C.; Ahlrichs, R. *J. Chem. Phys.* **1994**, *100*, 5829-5835; (g) Ahlrichs, R.; May, K. *Phys. Chem. Chem. Phys.* **2000**, *2*, 943-945.
52. (a) PQS version 2.4, 2001, Parallel Quantum Solutions, Fayetteville, Arkansas, USA (the Baker optimizer is available separately from PQS upon request); (b) Baker, J. *J. Comput. Chem.* **1986**, *7*, 385-395.

53. (a) Becke, A. D. *Phys. Rev. A* **1988**, *38*, 3098-3100; (b) Perdew, J. P. *Phys. Rev. B* **1986**, *33*, 8822-8824.
54. (a) Lee, C.; Yang, W.; Parr, R. G. *Phys. Rev. B* **1988**, *37*, 785-789; (b) Becke, A. D. *J. Chem. Phys.* **1993**, *98*, 1372-1377; (c) Becke, A. D. *J. Chem. Phys.* **1993**, *98*, 5648-5652; (d) Calculations were performed using the Turbomole functional 'b3-lyp', which is not identical to the Gaussian 'B3LYP' functional.

Appendix 1

Iron chloride and bromide complexes derived from the BMIP^{nPr} ligand: observation of a short-lived oxidized intermediate

This Chapter describes work the synthesis of two iron halide complexes based on the N,N,O ligand BMIP^{nPr}. Chloride complex **1** comprises a 1:1 Fe:ligand complex with a tetrahedral geometry around iron and in which the ester moiety does not coordinate to iron. Bromide complex **2** is likely to combine two of the ligands and a bromide ion with iron. The bromide complex was found to react with H_2O_2 to form a transient green species. This intermediate is tentatively assigned as an iron(IV) oxo species, only on the basis of it absorption feature.

Introduction

In previous work by our group[1] (chapter 6) the coordination behavior of different N,N,O ligands based on the 2-his-1-carboxylate facial triad towards iron as well as the catalytic activity of the resulting complexes in oxidation reactions were investigated. Figure 1 shows the benchmark **BMIP^{nPr}** ligand used in these studies and the overall structure of the corresponding bis-ligand Fe(II) dication formed in combination with non-coordinating counter ions such as triflate (OTf). The ligands in this complex coordinate in a facial manner towards iron providing a six-coordinated iron complex with an overall octahedral geometry; accordingly, the iron center is coordinatively saturated in this complex. Opening up of the coordination sphere around iron would be of interest in order to enhance the catalytic activity of the resulting complexes. The coordination behavior of the **BMIP^{nPr}** ligand toward different iron sources, including iron chlorides and iron bromides, was therefore studied. This chapter presents the structure of the molecular complexes that were isolated and reports on their catalytic activity in the epoxidation of cyclooctene. In addition, the unexpected formation of what seems to be a discrete iron-oxo complex that contains a halide ion as a co-ligand is reported.

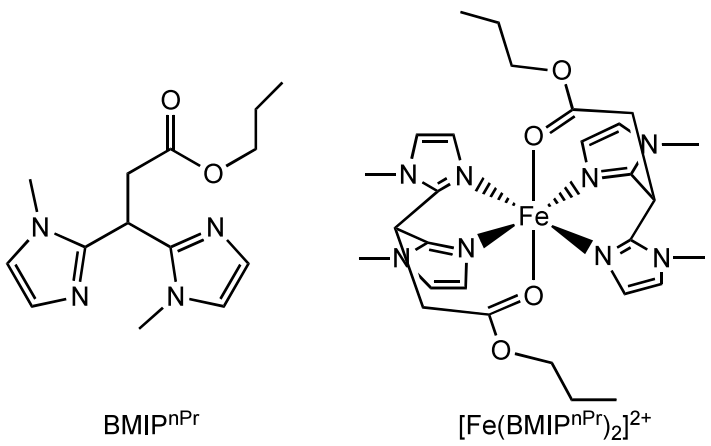

Figure 1. Structure of the benchmark **BMIP^{nPr}** ligand and its corresponding iron(II) complex.

Results

Synthesis of iron chloride and iron bromide complexes

For the preparation of complexes of the type [Fe(**BMIP^{nPr}**)$_2$](OTf)$_2$ a metal to ligand ratio of 1:2 was used. In order to investigate the possible formation of mono-ligand complexes, we decided to investigate the coordination of **BMIP^{nPr}** to iron halides using both a 1:2 and a 1:1 metal to ligand ratio. For the preparation of the chloride complex, $FeCl_2$ was redacted with an equimolar amount of the ligand in methanol for 1 h. After recrystallization from acetonitrile/diethyl ether the chloride complex

$FeCl_2$(**BMIP^{nPr}**) (**1**) was isolated as an yellowish crystalline solid in 85% yield. For the preparation of the bromide complex, a metal to ligand ratio of 1:2 was used. Bromide complex **2** was isolated as a brownish powder in a quantitative yield after the reaction of ligand **BMIP^{nPr}** with $FeBr_2$ in methanol, followed by recrystallization from an acetonitrile/diethyl ether mixture.

ESI-MS analysis showed mono-cations as the parent peak for both complexes; for complex **1** $[Fe(\mathbf{BMIP^{nPr}})(Cl)]^+$ was observed at m/z = 367.055, while complex **2** $[Fe(\mathbf{BMIP^{nPr}})_2(Br)]^+$ was observed at a m/z = 687.171. With IR spectroscopy the carbonyl vibration in **1** was found at 1727 cm^{-1}, which is at the exact same energy as the vibration observed in the free ligand. This indicates that the carbonyl group is non-coordinating in complex **1** and suggests that the ligand is only coordinated via its nitrogen donor atoms towards the iron center in this case. IR spectroscopy on **2** showed a carbonyl vibration at 1724 cm^{-1}, this is again close to the value of the vibration of the free ligand. From this observation it seems likely that also in this complex the two **BMIP^{nPr}** ligands only coordinate via their nitrogen donors to iron and that the carbonyl groups are non-coordinated. It is not clear from the IR spectrum whether both bromide ions are coordinated to the metal or not, or whether only one is coordinated as was observed by ESI-MS. Magnetic susceptibility measurements in CH_3CN solution using Evans' method[2,3] indicate μ_{eff} values of 5.2 μ_B for complex **1** and 5.0 μ_B for complex **2**. While these values are slightly higher than the theoretical value of 4.92 for an S = 2 system, these do indicate a high spin configuration for both the iron(II) chloride and iron(II) bromide complex. An overview of the analytical data of complexes **1** and **2** is shown in Table 1.

Table 1. Properties of the prepared complexes **1** and **2**.

complex	ν(C=O) (cm^{-1})	Δν(C=O) (cm^{-1})	μ_{eff} (μ_B)	spin state	ESI-MS (m/z)
1	1727	0	5.2	HS	367.055 ($[Fe(\mathbf{BMIP^{nPr}})(Cl)]^+$)
2	1724	3	5.0	HS	687.171 ($[Fe(\mathbf{BMIP^{nPr}})_2(Br)]^+$)

Structural features of the iron chloride complex in the solid state (X-ray crystal structure)

Crystals of **1** suitable for single crystal X-ray diffraction were obtained by slow vapor-diffusion of diethyl ether into a solution of **1** in acetonitrile. The molecular structure shows that the **BMIP^{nPr}** ligand coordinates to the iron center with its nitrogen donors only and that indeed the ester carbonyl group does not coordinate (Figure 2). The propyl tail points away from the iron center and the two chloride ions coordinate to

iron and complete its coordination environment, giving rise to a four-coordinated metal center. Selected bond lengths and angles are depicted in Table 2.

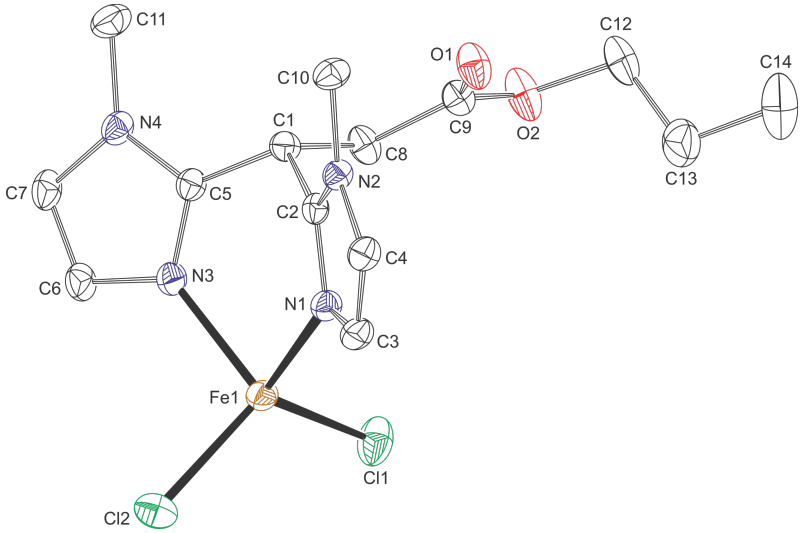

Figure 2. Molecular structure of $FeCl_2(BMIP^{nPr})$ (**1**). Displacement ellipsoid plot (50% probability); all hydrogen atoms are omitted for clarity.

Table 2. Selected bond lengths (Å) and angles (°) for **1**.

	Bond length		Angle		Angle
Fe1-Cl1	2.2586(4)	Cl1-Fe1-Cl2	117.743(15)	N3-Fe1-Cl1	116.84(3)
Fe1-Cl2	2.2654(4)	N1-Fe1-N3	88.13(4)	N3-Fe1-Cl2	103.59(3)
Fe1-N1	2.0755(10)	N1-Fe1-Cl1	109.82(3)		
Fe1-N3	2.0779(11)	N1-Fe1-Cl2	117.10(3)		

The bond angles in **1** are far from the ideal tetrahedral angle of 109°. Correspondingly, the angular variance is 134.22 deg^2.[4] Especially the N1-Fe1-N3 angle of 88.13(4)° is small which seems to originate from the 'bite angle' of the ligand as was observed in other structures containing BAIP ligands (BAIP = bis(alkylimidazole)propionate)[1,5] The lengths of the bonds to iron (2.07-2.26) are in agreement with a high spin iron center. Iron(II) complexes, as d^6 systems, have a strong tendency to adopt a octahedral geometry, however some examples of tetrahedral iron(II) complexes with N,N,Cl,Cl-donors are found in literature. These examples include bidentate imidazole-phosphinimine ligands,[6] tBuBox ligands[7] (tBuBox = 2,2-bis[2-[4(*S'*)-(R')-1,3-oxazolinyl]propane) and bis(1-R-imidazol-2-yl)disulfide and diselenide ligands.[8] The first of these complexes was found to be active in the oligomerization catalysis of ethylene.[6] More recently the group of Betley reported on a four coordinated iron(II) complex that is able to functionalize a broad range of aliphatic C-H bonds to form saturated, cyclic amine products.[9]

Unfortunately, crystals of complex **2** suitable for X-ray diffraction have not been obtained so far.

Catalysis

Next, both complexes were tested in the catalytic oxidation reaction of cyclooctene in order to compare their activity against the corresponding triflate complexes[1] (chapter 6). Like before, the catalytic reactions were carried out in acetonitrile with hydrogen peroxide as the oxidant at room temperature. Two different catalyst:oxidant:substrate ratio's of 1:20:1000 and 1:100:1000 were used in these reactions. Complex **2** proved not to give any substrate turn-over under these conditions. Complex **1** predominately gave epoxide products, while only trace amounts of diol could be detected. The activity towards the epoxide product is comparable with that the benchmark [Fe(**BMIP^{nPr}**)$_2$](OTf)$_2$ after 1 night; i.e. turn over numbers of 3.1 (20 equiv.) and 8.2 (100 equiv.) were found.

Table 3. Catalytic oxidation of cyclooctene by **1**.

complex	equiv. H_2O_2	equiv. substrate	Epoxide[a]			Diol[a]		
			1h	3h	1night	1h	3h	1night
1	20	1000	2.5	2.2	2.2	0.1	0.1	-
	100	1000	4.8	5.9	7.9	-	-	0.1

[a] Yields expressed as turnover numbers (TON = mol product/mol catalyst.

Oxidation of 2 with H_2O_2

While **2** turned out not to be active in the oxidation of cyclooctene, an interesting observation was made when treating it with H_2O_2. Immediately after the introduction of the oxidant a clear green solution formed, which persisted for some minutes after which the green color disappeared and the solution turned yellow/orange like for reaction mixtures with **1**. To get some insight in the formation of this 'green species', a UV-Vis titration was carried with hydrogen peroxide to investigate its formation (Figure 3). Hydrogen peroxide was introduced in portions of 0.2 equiv. after which the solution was allowed to equilibrate before the next addition. After the addition of 2 equiv. of hydrogen peroxide to the solution of complex **2**, the solution turned green and a band at 670 nm (ε = 438 M^{-1} cm^{-1}) formed. Gradually the band disappeared in time and the solution turned yellow/orange in color. Between 2.0 and 2.2 equiv. of hydrogen peroxide the band at 670 nm was the most intense.

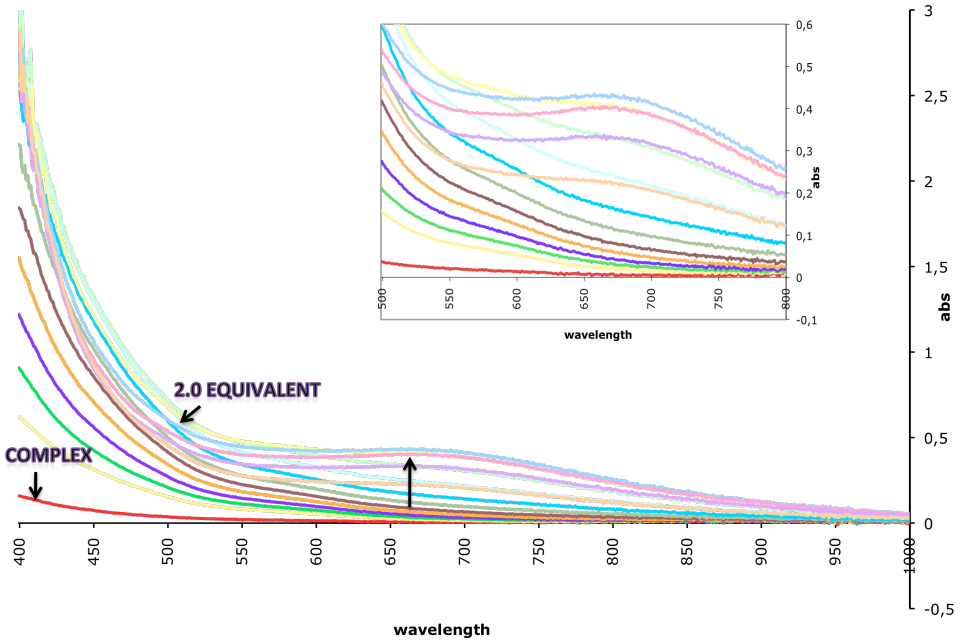

Figure 3. UV-Vis Spectra changes upon the portion wise addition of H_2O_2 to complex **2** in acetonitrile at ambient temperature.

Because the green color disappeared relatively fast at room temperature, the persistence of the green color was investigated at different temperatures. Figure 4 shows the change in absorption intensity at 670 nm at three different temperatures, i.e. room temperature, 0 °C, and –20 °C. The time of addition of H_2O_2 (2.0 equiv.) was taken as t = 0.

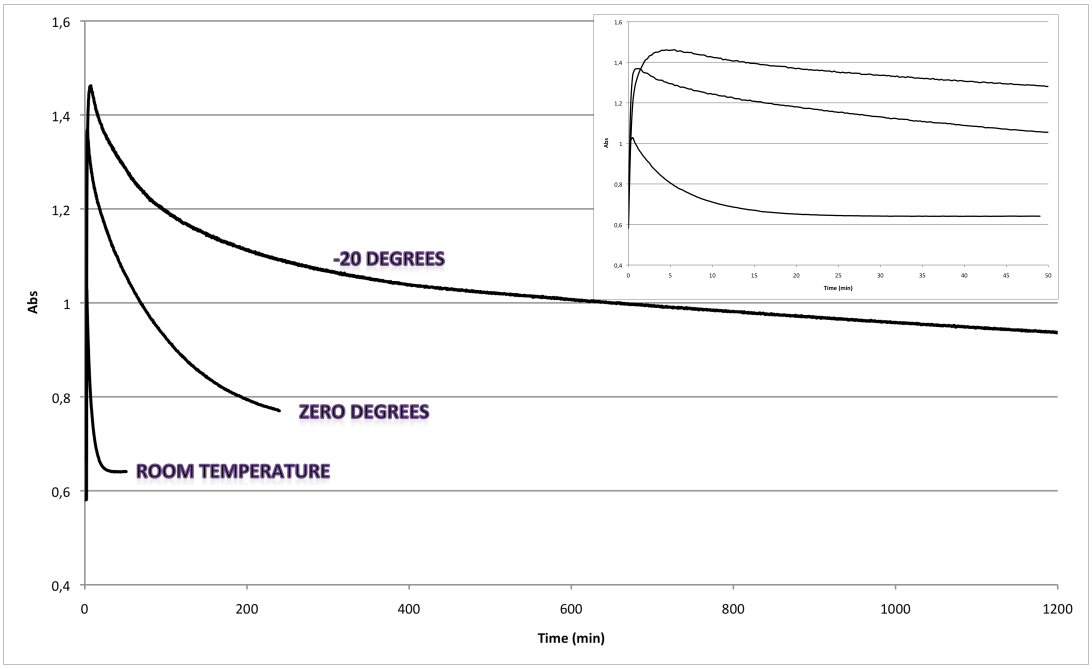

Figure 4. Stability of the green intermediate at different temperatures.

These experiments show that not only the lifetime of the green intermediate but also the extent of its formation (maximum absorption at 670 nm) is temperature dependent. When the intermediate is formed at room temperature the green color is gone within a few minutes, accompanied by a fast decay of the absorption at 670 nm. At 0 °C it takes more then 45 minutes before the green color has vanished, while at –20 °C it takes several hours before the green color is completely gone. The inset in Figure 4 shows that also the rate of formation of the green species is temperature dependent.
The concentration decay of the intermediate could not be fitted a first order kinetic equation. In addition to the absence of a discrete isosbestic point in Figure 3, it therefore seems that both the formation and the decay of the intermediate involve multiple reactants and or involve a number of reaction steps.
Next the reactivity of the intermediate was examined through a UV-Vis experiment. This was carried out by first preparing the green intermediate from **2** by the addition of H_2O_2 (2 equiv.) at 0 °C in acetonitrile, after which cyclooctene (1 equiv.) was added. It was found that the green intermediate persists under these conditions and that only thermal decomposition takes place (Figure 5). After some time PPh_3 (1 equiv.) was added and the green color of the solution was immediately quenched to give a yellow/orange solution. This experiment shows that the formed intermediate is not reactive towards cyclooctene but that is reacts readily with PPh_3.

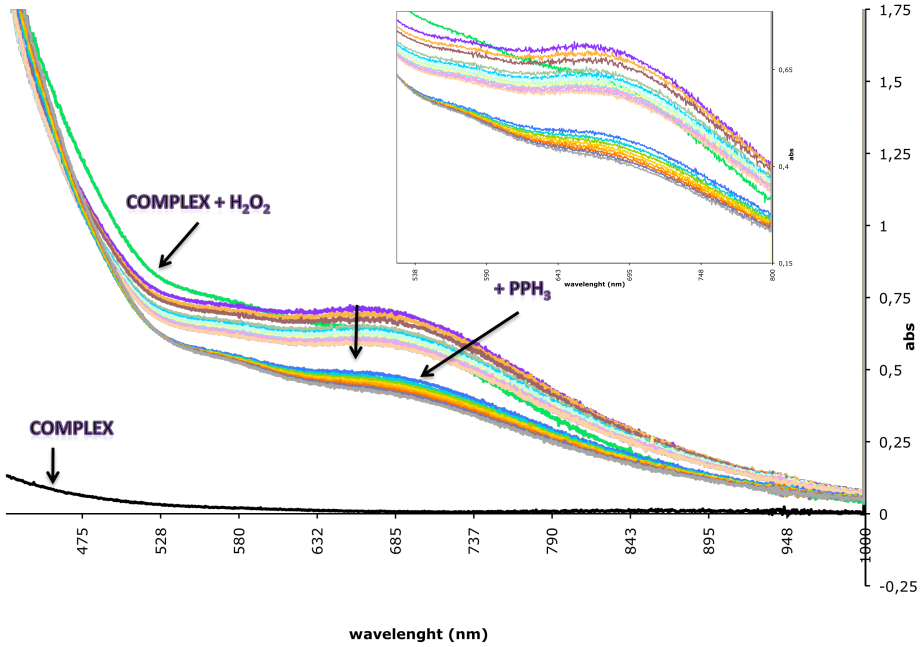

Figure 5. Reactivity of the formed green intermediate towards cyclooctene and PPh_3.

Discussion

In this chapter two newly synthesized iron complexes based on the previously used ligand **BMIP^{nPr}** have been investigated. Instead of the weakly coordinating triflate

anions, the two complexes were made with either chloride or bromide counter ions. The most interesting observation in the experiments described in this chapter is the formation of a short lived green intermediate upon the reaction of bromide complex **2** with H_2O_2.

The appearance of a green color upon addition of an oxidant to a low valent iron compound has been reported on several occasions in the literature. In many cases, these experiments involve the reaction with a non-heme iron(II) coordination compound, typically bearing an all N-ligand and less regularly bearing a mixed N,O ligand to form a green high-valent iron(IV)-oxo species. Such species are believed to be the active oxidants in both enzymatic and synthetic non-heme iron systems. Different research groups have reported on the formation and isolation of different types of these iron(IV)-oxo species. Que and co-workers[10] were the first to report on a synthetic mononuclear non-heme iron(IV)-oxo complex in 2003. The iron(IV)-oxo species was prepared from the iron complex [Fe^{II}(TMC)$(OTf)_2$] (TMC = 1,4,8,11-tetramethyl-1,4,8,11-tetraazacyclotetradecane) by the addition of 1 equiv. of iodosylbenzene (PhIO) in a acetonitrile solution at –40 ºC. The structure of the octahedral iron-oxo complex [Fe^{IV}(O)(TMC)(CH_3CN)]$(OTf)_2$ was determined by X-ray crystallography and showed the Fe^{IV}=O moiety with a corresponding short Fe–O bond length of 1.646(3)Å This complex has a absorption band at 820 nm and is stable for at least one moth at –40 ºC. There are nowadays more than 40 different iron(IV)-oxo species reported in literature, which all have a characteristic low intensity, near-IR absorption in the UV-Vis spectrum. The reported absorption bands are found in the range between 676 and 866 nm, with an average of 780 nm.[11] The short-lived intermediate reported here has an absorption band around 670 nm, which seems a rather high energy for an Fe(IV)-oxo species. The reported iron(IV)-oxo species in literature with an absorption band at 676 nm is the [Fe^{IV}(O)(cyclam-acetate)]$^+$ complex reported by the group of Wieghardt *et al.*.[12] The group of Nam reported on an iron(IV)-oxo complex [Fe^{IV}(O)$(N_4Py)(ClO_4)$]$^+$ which has its absorption around 680 nm.[13] The group of Que recently reported on a Iron-oxo species derived from the N_4Py ligand in which two of the pyridine donors are replaced by carboxylates [Fe^{IV}(O)(^{n}Bu-P2DA)] this ligand represents the closest structural mimic of oxoiron(IV) intermediate ('J') found in TauD with a near-IR absorption band at 770 nm.[14]

The observed lifetimes of the isolated iron(IV)-oxo species differ a lot and are strongly temperature dependent. For example, the reported stabilities vary from a few minutes at 25 ºC to a stability of at least one month at –40 ºC.[10] The green intermediate that was formed during our investigations has a comparable lifetime as was illustrated in Figure 4. At room temperature the green color disappears in a few minutes, while at –20 ºC the color lasts for a few hours.

The reactivity of these synthetic Fe(IV)-oxo complexes has been studied quite extensively and has been proven to include alcohol oxidation, P-oxidation, aromatic

hydroxylation and aliphatic hydroxylation.[15] Yet, they were also found to differ in their reactivity in the sense that some act as nucleophilic and others act as electrophilic oxidants.

The green intermediate isolated from complex **2** showed no reactivity towards cyclooctene. However, the complex turned out to be very reactive towards PPh_3. When 1 equiv. of PPh_3 was added to the green intermediate, the green color of the solution was immediately quenched to give a yellow/orange solution (Figure 5). Based on this reactivity profile the intermediate behaves in an electrophilic manner. The intermediate turned out not to be suitable for alkene oxidation reactions, while it may turn out to be capable of other types of oxidation reactions. More research needs to be done towards the identity of the formed intermediate and its reactivity.

Concluding remarks

Two Fe(II) halide complexes were prepared from the $BMIP^{nPr}$ ligand. Chloride complex **1** was formed with a 1 to 1 ratio between the ligand and iron and comprises a four-coordinated, tetrahedral iron center to which the ester moiety of the ligand is not coordinated. Bromide complex **2** was prepared using a 2 to 1 ratio between the ligand and iron. Although no discrete structural information was obtained for **2**, an ion of the composition $[Fe(L)_2Br]^+$ was observed by ESI-MS. Complex **2** was found to react with H_2O_2 to effort a transient green intermediate. The absorption features, temperature dependent lifetime, and reaction profile lead to the tentative conclusion that the intermediate is a non-heme Fe(IV)-oxo species. Further studies will have to corroborate this assignment. It is therefore of further interest to investigate its overall structure and that of its precursor **2**. The ligand surrounding is most likely to include the imidazoles of either one or two **$BMIP^{nPr}$** ligands, a bromide as suggested by ESI-MS, and may be complemented by the additional coordination of an ester moiety. Similarly, an in-depth study into the reactivity of the intermediate is of interest. An aspect that is of particular interest to be further investigated is the potential of the putative iron(IV)-oxo species to halogenate substrates,[16] in a similar manner as the Pseudomonas putida[17] and Curvularia inaequalis[18] enzymes, with have a typical non-heme iron center related to compounds **1** and **2**.

Experimental section

General. Air-sensitive reactions were carried out under an inert, N_2 atmosphere using standard Schlenk techniques. The used solvents were dried and distilled before use. The chemicals were either commercially obtained and used as received or reproduced from literature. Infrared spectra were recorded with a Perkin-Elmer Spectrum One FT-IR instrument. ESI-MS was measured on a Waters LCT Premier XE. Solution magnetic moments were determined by the Evans' NMR method in acetone-d_6/cyclohexane (95/5 *v*/*v*) or in acetonitrile-d_3/cyclohexane (95/5 *v*/*v*) at 25 °C.[2,3] UV-

Vis spectra were recorded on a Cary 50 Varian spectrometer equipped with a Helma emersion probe for in situ measurements. GC analyses were performed on a Perkin-Elmer Clarus 500 GC (30 m, Econo-Cap EC-5) with FID detector. propyl 3,3-bis(1-methyl(benz)imidazol-2-yl)propionate (**BMIP^{nPr}**)[5] was prepared according to published procedures.

FeCl$_2$(BMIP^{nPr}) (1): $FeCl_2$ (131 mg, 1.03 mmol) in methanol (7 mL) was added to a stirring solution of **BMIP^{nPr}** (288 mg, 1.04 mmol) in methanol (7 mL) and the reaction mixture was stirred for 1 hour at RT. The solvent was evaporated *in vacuo* and the remaining yellow solid was recrystallized from an acetonitrile/diethyl ether mixture at -30 °C. The product was obtained as a slightly yellowish crystalline solid (354 mg, 85%). Crystals suitable for X-ray diffraction were obtained by slow vapor-diffusion of diethyl ether into a solution of **1** in acetonitrile. IR (solid) ν (cm^{-1}): 3121.8, 2964.6, 1727.2, 1628.1, 1547.8, 1503.3, 1467.5, 1396.9, 1364.1, 1279.0, 1196.3, 1180.4, 1159.5, 1140.3, 982.9, 969.4, 765.7, 741.0. Solution magnetic moment (Evans' method): μ_{eff} = 5.2 μ_B. ESI-MS: m/z = 367.055 ($[M-Cl]^+$, calc. 367.063).

Iron bromide complex (2): $FeBr_2$ (100 mg, 0.46 mmol) in MeOH (7 mL) was added to a stirring mixture of **BMIP^{nPr}** (259 mg, 0.94 mmol) in MeOH (7 mL) and the reaction mixture was stirred for 1 hour at room temperature. The solvent was evaporated *in vacuo* and the remaining oily substance was recrystallized twice from an acetonitrile/diethyl ether mixture yielding a brownish powder (360 mg, 100%). IR (solid) ν (cm^{-1}): 3382.8, 3117.5, 2967.5, 1724.3, 1627.2, 1541.3, 1500.3, 1462.4, 1281.2, 1192.1, 1134.9, 1058.7, 958.8, 940.7, 762.0, 735.6. Solution magnetic moment (Evans' method): μ_{eff} = 5.0 μ_B. ESI-MS: m/z = 687.171 ($[M-Br]^+$, calc. 687.171).

Catalysis protocol: To a solution of catalyst (3 μmol) in acetonitrile (2 mL) was added cyclooctene (1000 equiv.) and acetonitrile (to bring the total volume to 2.5 mL). 1,2-dibromobenzene (10 μL) was added as internal standard and subsequently, 0.5 mL of oxidant solution (20 or 100 equiv., diluted from 35% aqueous H_2O_2 with acetonitrile) was added drop wise over 20 min. The reaction mixture was stirred at room temperature and after 1h the first sample was taken. Diethyl ether was added to the sample to precipitate the iron complex after which it was analyzed by GC.

X-ray crystal structure determination of $FeCl_2$(**BMIP^{nPr}**) (**1**): $C_{14}H_{20}Cl_2FeN_4O_2$, Fw = 403.09, pale yellow plate, 0.36 × 0.36 × 0.15 mm^3, monoclinic, $P2_1/c$ (no. 14), a = 10.05732(12), b = 15.8041(3), c = 14.8005(3) Å, β = 129.172(2) °, V = 1823.78(8) $Å^3$, Z = 4, D_x = 1.468 g/cm^3, μ = 1.13 mm^{-1}. 34899 Reflections were measured on a Nonius KappaCCD diffractometer with rotating anode and graphite monochromator

(λ = 0.71073 Å) at a temperature of 150(2) K up to a resolution of $(\sin\theta/\lambda)_{max}$ = 0.65 $Å^{-1}$. Intensity data were integrated with the Eval14 software.[19] Absorption correction and scaling was performed with SADABS[20] (correction range 0.63-0.85). 4182 Reflections were unique (R_{int} = 0.016), of which 3841 were observed [$I>2\sigma(I)$]. The structure was solved with the program SHELXS-97.[21] Least-squares refinement was performed with SHELXL-97[21] against F^2 of all reflections. Non-hydrogen atoms were refined freely with anisotropic displacement parameters. Hydrogen atoms were located in difference Fourier maps and refined with a riding model. The H-atoms of the methyl group at C11 were refined with two conformations. 212 Parameters were refined with no restraints. R1/wR2 [$I > 2\sigma(I)$]: 0.0225 / 0.0574. R1/wR2 [all refl.]: 0.0259 / 0.0594. S = 1.029. Residual electron density between -0.24 and 0.37 e/$Å^3$. Geometry calculations and checking for higher symmetry was performed with the PLATON program.[22]

References

1. Moelands, M.A.H.; Nijsse, S.; Folkertsma, E.; de Bruin, B.: Lutz, M.; Spek, A.L.; Klein Gebbink R.J.M. *Inorg. Chem.* **2013**, *52*, 7394−7410.
2. Britovsek, G.J.P.; Gibson, V.C.; Spitzmesser, S.K.; Tellmann, K.P.; White, A.J.P.; Williams, D.J. *J. Chem. Soc., Dalton Trans.* **2002**, 1159-1171.
3. Evans, D.F. *J. Chem. Soc.* **1959**, 2003-2005.
4. Robinson, K.; Gibbs, G.V.; Ribbe, P.H. *Science* **1971**, *172*, 567-570.
5. Bruijnincx, P.C.A.; Buurmans, I.L.C.; Gosiewska, S.; Moelands, M.A.H.; Lutz, M.; Spek, A.L.; van Koten, G.; Klein Gebbink, R.J.M. *Chem. Eur. J.* **2008**, *14*, 1228-1237.
6. Spencer, L.P.; Altwer, R.; Wei, P.; Gelmini, l.; Gauld, J.; Stephan, D.W. *Organometallics* **2003**, *22*, 3841-3854.
7. Bart, S.C.; Hawrelak, E.J.; Schmisseur, A.K.; Lobkovsky, E.; Chirik, P.J. *Organometallics* **2004**, *23*, 237-246.
8. Figueroa, J.S.; Yurkerwich, K.; Melnick, J.; Buccella, D.; Parkin, G. *Inorg. Chem.* **2007**, *46*, 9234-9244.
9. Betley, T.A.; Hennessy, E.T. *Science* **2013**, *340*, 591-595.
10. Rohde, J.U.; In, J.H.; Lim, M.H.; Brennessel, W.W.; Bukowski, M.R.; Stubna, A.; Münck, E.; Nam, W.; Que, L. Jr. *Science* **2003**, *299*, 1037-1039.
11. McDonald, A.R.; Que, L. Jr. *Coord. Chem. Rev.* **2013**, *257*, 414-428.
12. Grapperhaus, C.; Mienert, B.; Bill, E.; Weyhermüller, T.; Wieghardt, K. *Inorg. Chem.* **2000**, *39*, 5306-5317.
13. Sastri, C.; Seo, M.; Park, M.; Kim, K.; Nam, W. *Chem. Commun.* **2005**, 1405-1407.
14. McDonald, A.R.; Guo, Y.; Vu, V.V.; Bominaar, E.L.; Münck, E.; Que, L. Jr. *Chem. Sci.* **2012**, *3*, 1680-1693.
15. Nam, W. *Acc. Chem. Res.* **2007**, *40*, 522-531.
16. Vaillancourt, F.H.; Yeh, E.; Vosburg, D.A.; Garneau-Tsodikova, S.; Walsh, C.T. *Chem. Rev.* **2006**, *106*, 3364-3378.
17. Itoh, N.; Morinaga, N.; Kouzai, T. *Biochim. Biophys. Acta* **1994**, *1207,* 208-216.
18. Liu, T.N.; M'Timkulu, T.; Geigert, J.; Wolf, B.; Neidleman, S.L.; Silva, D.; Hunter-Cevera, J.C. *Biochem. Biophys. Res. Commun.* **1987**, *142*, 329-333.
19 Duisenberg, A.J.M.; Kroon-Batenburg, L.M.J.; Schreurs, A.M.M. *J. Appl. Cryst.* **2003.** *36*, 220-229.
20 Sheldrick, G. M. (**1999**). SADABS: Area-Detector Absorption Correction, Universität Göttingen, Germany.

21 Sheldrick, G.M. *Acta Cryst.* **2008**, *A64*, 112-122.
22 Spek, A.L. *J. Appl. Cryst.* **2003**, *36*, 7–13.

Appendix 2

catena-Poly[[bis(acetonitrile-κ*N*)-manganese(II)]-bis(*μ*-trifluoromethanesulfonato- κ^2O:O')]

The title compound, $[Mn(CF_3SO_3)_2(CH_3CN)_2]_n$, has an Mn^{II} cation on an inversion center in an octahedral environment. The trifluoromethanesulfonate anions act as bridging ligands and form a one-dimensional coordination polymer in the direction of the *a* axis. The F atoms of the trifluoromethanesulfonate anions form layers parallel to the *ab* plane, but despite short intermolecular distances, no stabilizing F---F interactions are detected. The Mn-N and C-C bonds of the acetonitrile ligand are analyzed according to the Hirshfeld rigid-bond test. Renninger effects in the reflection data are considered, explored and discussed.

Based on: Lutz, M.; Schreurs, A.M.M.; Spek, A.L.; Moelands, M.A.H.; Klein Gebbink, R.J.M. *Acta. Cryst. C.* **2010**, *C66*, m9-m12.

Comment

The title compound, (**1**), was prepared as a starting material for complexation reactions with biomimetic ligands. In the literature, the stoichiometry of the compound is given as $Mn(SO_3CF_3)_2.CH_3CN$,[1] but also contains indications of a variable composition.

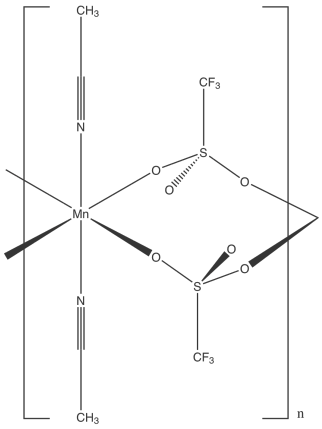

The present crystal structure determination proves the presence of two coordinated acetonitrile molecules and thus the composition $[Mn(SO_3CF_3)_2{\cdot}2CH_3CN]_n$, with the manganese in a 2+ oxidation state (Figure 1, Table 1).

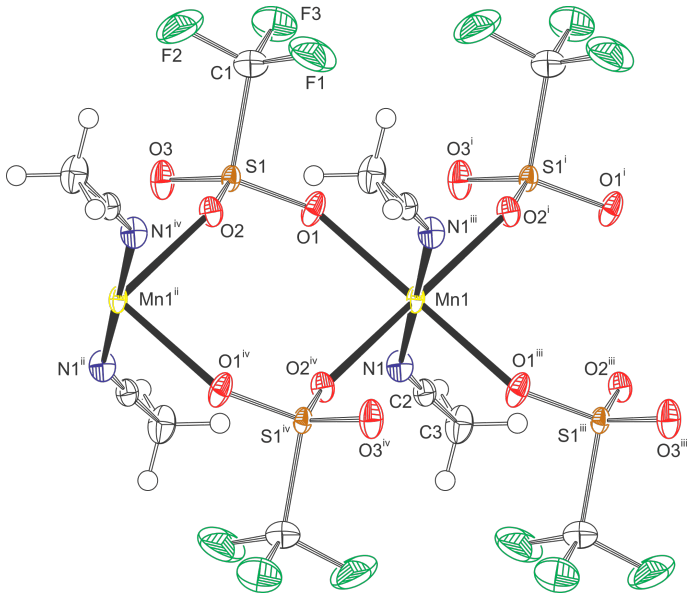

Figure 1. The coordination environment of Mn1 in (**1**), showing the atom numbering scheme. Displacement ellipsoids are drawn at the 50% probability level and H atoms are shown as small spheres of arbitrary radii. [Symmetry codes: (i) x−1, y, z; (ii) x+1, y, z; (iii) 1−x, 1−y, 1−z; (iv) 2−x, 1−y, 1−z.].

Table 1. Selected geometric parameters (Å, °).

Mn1−O1	2.1688 (8)	S1−O3	1.4283 (9)
Mn1−O2^{i}	2.1734 (8)	S1−O1	1.4534 (8)
Mn1−N1	2.2106 (10)	S1−O2	1.4564 (8)
O1−Mn1−O2^{i}	89.59 (3)	C2−N1−Mn1	153.27 (9)
O1−Mn1−N1	91.38 (4)		
O3−S1−C1−F2	58.46 (12)	O2−S1−C1−F1	56.36 (12)
O2−S1−C1−F2	−63.53 (11)	O3−S1−C1−F3	−60.98 (11)
O1−S1−C1−F1	−61.11 (12)	O1−S1−C1−F3	59.57 (11)

Symmetry code: (i) x –1, y, z.

The Mn^{II} ion in (**1**) is located on an inversion center and surrounded by six donor atoms in a slightly distorted octahedral geometry. The equatorial plane is formed by four O atoms of the trifluoromethanesulfonate anions, with Mn-O distances in the expected range for Mn^{II}. The axial positions are occupied by acetonitrile ligands, with similar Mn-N distances to those observed in the $[Mn(CH_3CN)_6]^{2+}$ cation.[2] Due to the inversion symmetry, the equatorial plane is exactly planar and the axial donor atoms are exactly *trans*. Consequently, the angular variance is very small ($0.75°^2$).[3] The slight octahedral distortion can be seen in the small difference between Mn-O and Mn-N distances.

The trifluoromethanesulfonate anions, which are located on general positions, act as bridging ligands between the Mn^{II} cations. Bridging trifluoromethanesulfonate anions occur mainly in copper and silver complexes. In fact, there is only one previously known Mn complex with a bridging trifluoromethanesulfonate anion,[4] but there the bridging is supported by an additional bridging isopropoxide linker, resulting in a discrete binuclear complex. In (**1**), the Mn^{II} cations are connected only by trifluoromethanesulfonate anions. In this way, a one-dimensional chain is formed in the direction of the crystallographic *a* axis. The distance between the Mn^{II} ions in the chain therefore corresponds to the length of the *a* axis [5.13763 (8) Å]. The S-O distances of the coordinated O atoms are about 0.03 Å longer than that of the non-coordinated O atom. The CF_3 group adopts a staggered conformation with respect to the SO_3 group.

While in most transition metal complexes of acetonitrile the coordination is approximately linear, (**1**) deviates significantly from linearity by 26.73 (9)° at the N atom. Previous cases of such a bent coordination mode have been ascribed to crystal

packing effects or steric hindrance with neighboring groups.[5] Indeed, the crystal structure of (**1**) has a packing index of 69.0%,[6] indicating an efficient arrangement of the molecules.[7] The C2---O3(2−x, −y, 1−z) distance is 3.1612 (15) Å, which is approximately the sum of the van der Waals radii (3.22 Å),[8] and this prevents linearization of the acetonitrile coordination (Figure 2). Other close contacts are C2---O3(x−1, y, z) of 3.3374 (15) Å and C2---F1(1−x, 1−y, 1−z) of 3.2299 (15) Å .

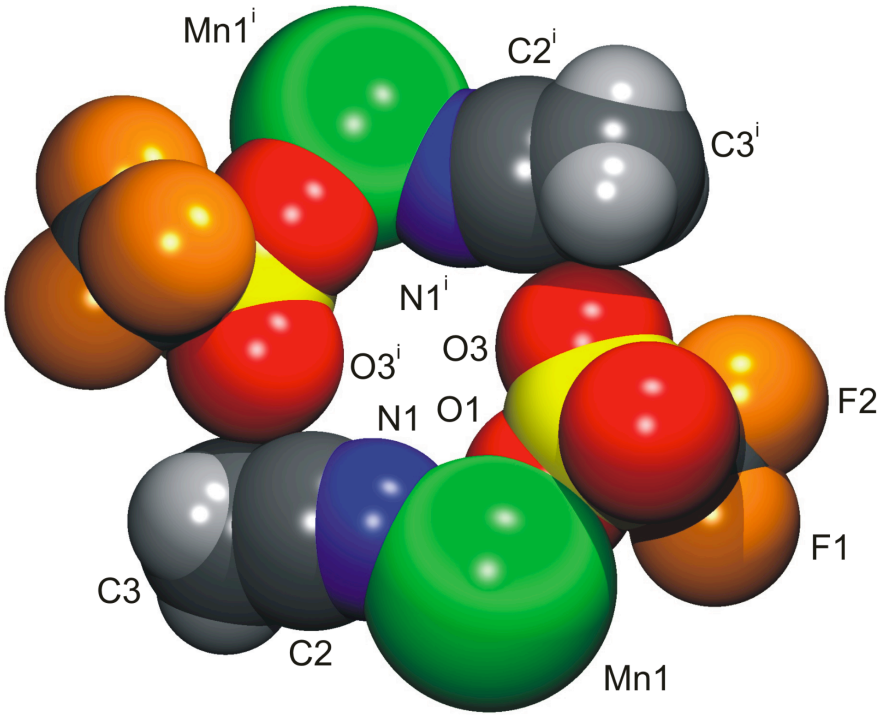

Figure 2. Space-filling plot of (**1**), showing the close intermolecular contacts between atoms O3 and C2^i, which prevent a linear coordination of the acetonitrile ligands. [Symmetry code: (i) 2−x, −y, 1−z.]

The Mn-N and C-C bonds of the acetonitrile fail the rigid-bond test,[9] with Δm.s.d.a./σ of values 8.11 and 5.24, respectively (Δm.s.d.a./σ is the difference of mean square displacement amplitudes and its standard uncertainty). The reason is obviously the non-spherical electron distribution of the triple bond, which cannot be adequately modeled with spherical scattering factors. A similar situation is well known from metal–carbonyl complexes.[10] It should be noted that the absolute magnitudes for the Δm.s.d.a. values of the Mn-N and C-C bonds in (**1**) of 0.0041 (5) and 0.0042 (8) Å^2, respectively, are still small and well below 0.01 Å^2. A comparison with acetonitrile structures from the literature shows that the Δm.s.d.a. values of (**1**) are within the expected range (Table 2).

Table 2. Hirshfeld rigid-bond tests[9] of metal-coordinated acetonitrile. Comparison of (**1**) with structures extracted from *Acta Crystallographica Section C*.

CSD refcode	T (K)	Max sin (θ/λ) (Å^{-1})	M	Δm.s.d.a. (M---N) (Å^2)	Δm.s.d.a. (N—C) (Å^2)	Δm.s.d.a. (C—C) (Å^2)
(**1**)	110 (2)	0.65	Mn	0.0041 (5)#	0.0021 (7)	0.0042 (8)#
AHIFUS	150 (2)	0.91	Rh	0.0024 (4)#	0.0007 (6)	0.0021 (9)
DIKQIY	296	0.66	Ru	0.0092 (27)	0.0021 (43)	0.0064 (57)
GUGTEH	158 (2)	0.63	Co	0.0059 (27)	0.0017 (40)	0.0038 (42)
GUGWIO	180 (2)	0.67	Cu	0.0122 (14)#	0.0060 (23)	0.0056 (33)
IHEJUA	193 (2)	0.66	Cu	0.0009 (18)	0.0080 (26)	0.0109 (33)
JESQAA	193 (2)	0.65	Zn	0.0068 (8)#	0.0019 (11)	0.0032 (15)
LIYXUM	150 (2)	0.60	Ru	0.0008 (30)	0.0171 (50)	0.0087 (67)
MATMOJ	100.0 (10)	0.62	Ru	0.0083 (13)#	0.0041 (20)	0.0029 (27)
MEVRAG	293 (2)	0.64	Cu	0.0043 (15)	0.0047 (22)	0.0041 (23)
NAQMUN01	156 (2)	0.76	Cu	0.0025(17)	0.0025 (24)	0.0059 (26)
OLIYEN	120 (2)	0.65	Cu	0.0033 (20)	0.0004 (28)	0.0000 (42)
PAJKER	110 (2)	0.63	Ag	0.0035 (18)	0.0073 (26)	0.0071 (28)
QANGAO	571 (2)	0.60	Cu	0.0033 (30)	0.0054 (42)	0.0074 (55)
QILXOY	150 (2)	0.63	Cu	0.0060 (8)#	0.0041 (13)	0.0051 (19)
SETPOX	296	0.62	Ru	0.0093 (27)	0.0034 (45)	0.0006 (73)
WIZDOZ	298 (2)	0.60	Cu	0.0006 (57)	0.0037 (80)	0.0053 (83)
XORVIJ	150 (2)	0.65	Cu	0.0091 (13)#	0.0012 (19)	0.0039 (22)
YOJJIQ	298 (2)	0.62	Ru	0.0065 (13)	0.0023 (21)	0.0046 (31)

The structures are identified by their refcode in the Cambridge Structural Database.[11] Structures with Δm.s.d.a./σ > 5 are marked with a hash sign (#). Only one acetonitrile is considered if the structure contains several coordinated acetonitriles (refcodes LIYXUM, NAQMUN01, PAJKER, QILXOY and YOJJIQ).

Besides the coordination chains in the *a* direction, the crystal structure of (**1**) contains layers of F atoms in the *ab* plane (Figure 3). The shortest F---F distance is F1---F1^{iii} of 2.7796 (15) Å [symmetry code: (iii) 1−x, 1−y, 2−z], which is shorter than the sum of the van der Waals radii (2.94 Å). According to Ramasubbu *et al.* [12] and Reichenbächer *et al.* ,[13] F---F interactions with two equal C-F---F angles
are caused by close packing (Type I), and stabilizing F---F interactions are characterized by C-F---F angles of 180° on one side and 90° on the other (Type II).

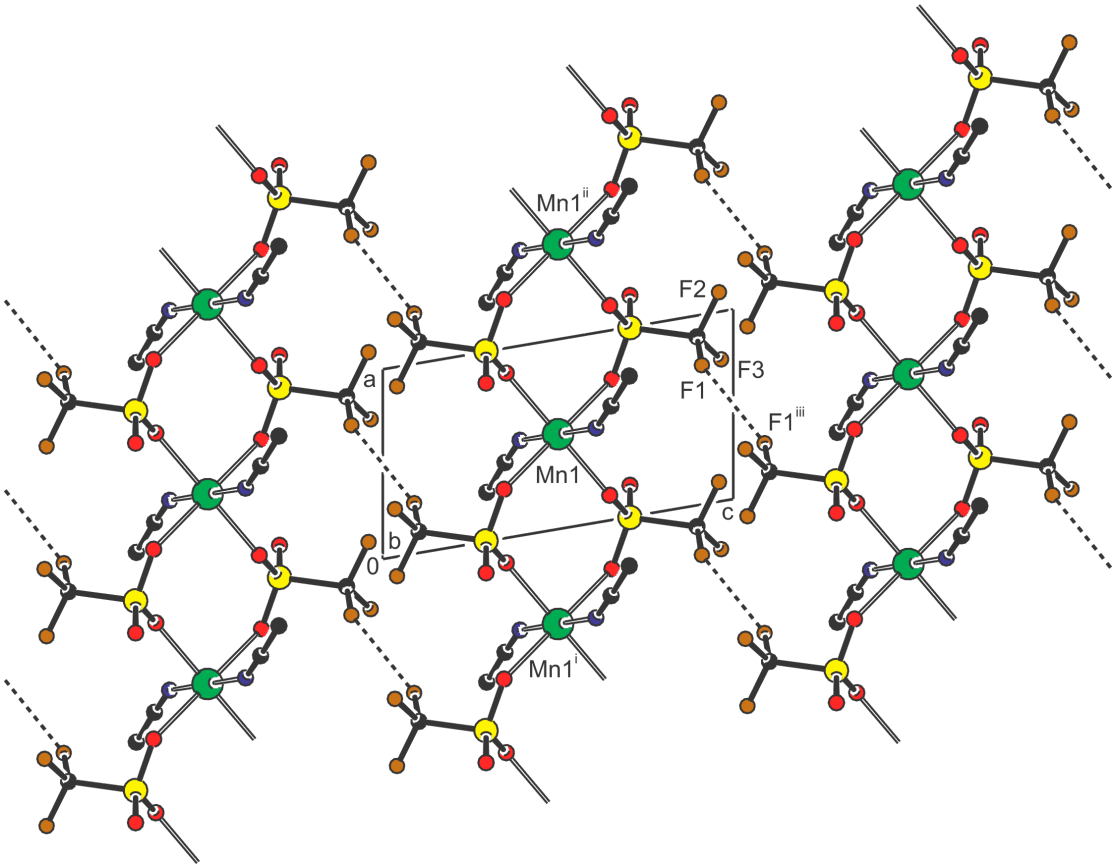

Figure 3. The packing of (**1**) in the crystal structure, viewed along the b axis, showing the one-dimensional coordination chains in the *a* direction and the fluorine layers in the *ab* plane. Short F---F interactions are shown as dashed lines. [Symmetry codes: (i) x–1, y, z; (ii) x + 1, y, z; (iii) 1–x, 1–y, 2–z.]

The above-mentioned short F---F interaction in (**1**) is located on an inversion center and consequently has two equal angles [137.69 (9)°]. The interaction is thus not stabilizing. Nevertheless, it is interesting to note that the crystals have the shape of plates with (001) as the smallest dimension, which is parallel to the fluorine layers. Integration of the raw diffractometer images was performed using the program *EVAL15*,[14] using an accurate description of the diffraction experiment for the prediction of the reflection profiles. A relatively large isotropic mosaicity of 1.3° was used as part of this description, indicating severe defects in the crystal. Nevertheless, some equivalents of weak reflections had significant intensities, which we could interpret as Renninger effects[15] (Table 3). It has been known for a long time that Renninger effects can be present in imperfect crystals[16] and examples involving organic salts can also be found in the literature.[17,18] In the examples in Table 3, the intensity of one of the measurements of the 41$\bar{1}$ reflection (reflA) is caused by the strong 20$\bar{1}$ reflection (reflB), with F^2_{calc} = 3565.42, and for the (reflB – reflA) reflection $\bar{2}10$, F^2_{calc} = 1400.59. In the case of the 512 reflection, the interfering reflection is again 20$\bar{1}$. Here, for the (reflB – reflA) reflection $\bar{3}13$, F^2_{calc} = 2387.81.

Table 3. Examples of weak reflections influenced by Renninger effects.

hkl	F^2_{calc}	F^2_{meas}	$\sigma(F^2_{meas})$	I/σ	Renninger score
41-1	0.33	17.36	0.57	30.46	1253.46
41-1	0.33	1.30	0.25	5.20	0.00
41-1	0.33	0.51	0.20	2.55	0.00
41-1	0.33	1.15	0.25	4.60	0.00
41-1	0.33	0.50	0.19	2.63	0.00
−5−1−2	0.36	0.80	0.32	2.50	0.00
512	0.36	0.71	0.24	2.96	0.00
512	0.36	8.90	0.52	17.12	1368.45
512	0.36	0.22	0.29	0.76	0.00
512	0.36	0.62	0.27	2.30	0.00
512	0.36	0.19	0.28	0.68	0.00

F^2_{meas} and $\sigma(F^2_{meas})$ are taken from the raw data after integration using EVAL15[14] and before the application of SADABS.[15] For a definition of the Renninger score, see the Comment.

Based on these observations, we calculated Renninger scores for all reflections. In the first instance, it is checked if the geometric condition of two reflections being simultaneously in the reflecting position is satisfied, or, in other words, $\overline{512}$ whether the corresponding reciprocal lattice points are both on the Ewald sphere. This condition is fulfilled if the lengths of both reflected beam vectors are equal to the radius of the Ewald sphere within a chosen tolerance of 0.12%. A second condition is the intensity condition, meaning that (reflB) and (reflB – reflA) must both be strong. We consider a reflection as strong if the intensity is larger than $0.02F(000)^2_{calc}$. If both conditions are fulfilled, the Renninger score is calculated as intensity(reflB) x intensity(reflB – reflA)/[$F(000)^2_{calc}$ x sinth], where sinth = sin(θ)/λ. We did not try to correct the affected intensities for multiple diffraction,[19] but omitted all reflections with a Renninger score larger than 500 from the final data set. This omission corresponds to 3.8% of all reflections. Due to the redundant measurement this still resulted in a complete data set of unique reflections.

Experimental section

Compound (**1**) was synthesized according to the a literature procedure.[1] Single crystals suitable for X-ray diffraction were obtained by vapor diffusion of diethyl ether into an acetonitrile solution of (**1**). IR (ν, cm^{-1}): 3458.5, 2950.7, 2309.5 (CH_3CN), 2280.1 (CH_3CN), 1666.5, 1632.7, 1365.7, 1302.7 (SO_3, *as*), 1228.8 (SO_3, *as*), 1210.5 (CF_3, *s*), 1184.2 (CF_3, *as*), 1031.4 (SO_3, *s*), 938.6, 799.4, 769.1.

Crystal data:

$[Mn(CF_3O_3S)_2(C_2H_3N)_2]$	γ= 76.025 (1)º
*M*r = 435.19	V = 372.35 (1) Å^3
Triclinic, $P\bar{1}$	Z = 1
a = 5.13763 (8) Å	Mo *Kα* radiation
b = 8.11880 (12) Å	μ = 1.26 mm^{-1}
c = 9.75293 (10) Å	*T* = 110 K
α = 73.126 (1)º	0.36 x 0.33 x 0.09 mm
β= 76.885 (1)º	

Data collection:

Nonius KappaCCD area-detector	12368 measured reflections
Diffractometer	1710 independent reflections
Absorption correction: multi-scan[20]	1661 reflections with I > 2σ(I)
T_{min} = 0.626, T_{max} = 0.746	R_{int} = 0.017

Refinement:

R[F^2 > 2σ(F^2)] = 0.018	118 parameters
*w*R(F^2) = 0.048	All H-atom parameters refined
S = 1.06	$\Delta\rho_{max}$ = 0.46 e Å^{-3}
1710 reflections	$\Delta\rho_{min}$ = –0.34 e Å^{-3}

H atoms were located in difference Fourier maps and refined freely with isotropic displacement parameters [C—H = 0.90 (3)– 0.94 (3) Å].

Data collection: COLLECT;[21] cell refinement: PEAKREF;[22] data reduction: EVAL15[14] and SADABS;[15] program(s) used to solve structure: SHELXS97;[23] program(s) used to refine structure: SHELXL97;[23] molecular graphics: PLATON;[24] software used to prepare material for publication: SHELXL97.

References

1. Bryan, P.S.; Dabrowiak, J.C. *Inorg. Chem*. **1975**, *14*, 296–299.
2. Weller, F.; Mai, H.-J.; Dehnicke, K. *Z. Naturforsch. B* **1996**, *51*, 298–300.
3. Robinson, K.; Gibbs, G.V.; Ribbe, P.H. *Science* **1971**, *172*, 567–570.
4. Berben, L.A.; Peters, J.C. *Inorg. Chem.* **2008**, *47*, 11669–11679.
5. Murthy, N.N.; Mahroof-Tahir, M.; Karlin, K.D. *Inorg. Chem.* **2001**, *40*, 628–635.
6. Kitajgorodskij, A.I. *In Molecular Crystals and Molecules* **1973**, New York: Academic Press.
7. Dunitz, J.D. **1995**, X-ray Analysis and the Structure of Organic Molecules, 2nd Corrected Reprint, pp. 106–111. Basel: Helvetica Chimica Acta.
8. Bondi, A. *J. Phys. Chem.* **1964**, *68*, 441–451.
9. Hirshfeld, F.L. *Acta Cryst.* **1976**, *A32*, 239–244.
10. Braga, D.; Koetzle, T.F. *Acta Cryst.* **1988**, *B44*, 151–156.

11. Allen, F.H. *Acta Cryst.* **2002**, *B58*, 380–388.
12. Ramasubbu, N.; Parthasarathy, R.; Murray-Rust, P. *J. Am. Chem. Soc.* **1986**, *108*, 4308–4314.
13. Reichenbächer, K.; Süss, H. I.; Hulliger, J. *Chem. Soc. Rev.* **2005**, *34*, 22–30.
14. Schreurs, A.M.M.; Xian, X.; Kroon-Batenburg, L.M.J. *J. Appl. Cryst.* **2010**, *43*. In the press. doi:10.1107/S0021889809043234.
15. Renninger, M. *Z. Phys.* **1937**, *106*, 141–176.
16. Zachariasen, W.H. *Acta Cryst*. **1965**, *18*, 705–710.
17. Speakman, J.C. *Acta Cryst.* **1965**, *18*, 570–571.
18. Grochowski, J.; Hupe, A.; Krane, H.-G.; Rossmanith, E.; Schmidt, H.; Serda, P. **2000**, HASYLAB Jahresber. http://www1.uni-hamburg.de/mpi/rossmanith/Reprints/hasy_00a.pdf
19. Hauback, B.C.; Mo, F.; Thorkildsen, G. *Aust. J. Phys.* **1990**, *43*, 77–91.
20. Sheldrick, G.M. **2008a**, SADABS. University of Göttingen, Germany.
21. Noniu **1999**, COLLECT. Nonius BV, Delft, The Netherlands.
22. Schreurs, A.M.M. **2005**, PEAKREF. Utrecht University, The Netherlands.
23. Sheldrick, G.M. *Acta Cryst.* **2008b**, *A64*, 112–122.
24. Spek, A.L. *Acta Cryst.* **2009**, *D65*, 148–155.

Summary

This Thesis describes the synthesis and structural analysis of bio-inspired iron and manganese complexes used for the catalytic oxidation reactions of olefin substrates. The development of catalytic systems for oxidation chemistry that are based on first row transition metals and that apply a green oxidant like hydrogen peroxide is an ongoing research topic in the fields of homogeneous catalysis, bioinorganic chemistry, and green chemistry. For the inspiration in the design of such systems, biological oxidation reactions that involve a metallo-enzyme are used as the starting point. The initial design of the ligand used in the catalytic system is based on the active site structure of one particular or of a family of metallo-enzymes. Further catalyst development and optimization is then carried out by ligand variation and reaction parameter optimization. This bio-inspired approach in catalyst design may on the one hand lead to discrete structural analogues of the active site of a metallo-enzyme (structural modeling) and may on the other hand lead to the development of efficient transition metal catalysts that are of use to organic synthesis (functional modeling).

The first part of this thesis is dedicated to a study on manganese complexes derived from mixed N,O ligands, while the second part focuses on iron complexes based on related, yet different mixed N,O ligands. The interest in the use of mixed N,O ligands in the development of bio-inspired oxidation catalysts stems from the structure and activity of a class of mono-nuclear non-heme iron enzymes that feature a so-called 2-His-1-carboxylate facial triad in their active site. In this triad, the iron center is coordinated in a facial manner by only three endogenous donor ligands, i.e. two histidines and one glutamate or aspartate. This particular structural features leads to a uniquely diverse reactivity of enzymes that contain this active site. Efforts to model the structural and reactivity aspects of the facial triad enzymes have mainly focused on the use of all-nitrogen ligands and have to a much lesser extent made use of mixed N,O ligand donor sets. Figure 1 provides a general overview of the ligand types used in this thesis for the development of bio-inspired iron and manganese oxidation catalysts.

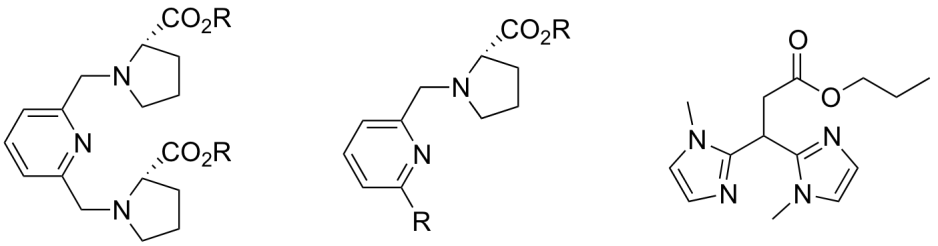

Figure 1. General structures of the **Py(ProR)$_2$** (left), **RPyProR** (middle), and **BMIP^{nPr}** (right) ligands used in this thesis.

Chapter 1 provides an overview of typical bio-inspired iron and manganese complexes that have been applied as catalyst in the oxidation reaction of olefin substrates. This overview also discusses the characteristics of enzymes featuring the 2-His-1-carboxylate facial triad and describes the bio-inspired complexes in terms of structural and functional mimicry of the enzymes.

In **Chapter 2** the synthesis of manganese(II) triflate complexes based on the Py(ProR)$_2$ ligand framework is reported. This ligand type comprises a central pyridine group flanked by two chiral proline-based moieties that each provide an N,O donor set next to the pyridine N-donor. Using ligands containing either two proline methylester moieties or two prolinol moieties, leads to the formation of seven-coordinated Mn-complexes with distorted pentagonal bipyramidal geometries (Figure 2, left). The organic ligand in these complexes coordinates in the meridional plane around manganese via the pyridine group, the proline nitrogen atoms, and via the additional coordination of the carbonyl oxygen atoms of the proline moiety. The two triflate counter ions coordinate in the axial positions around the manganese center.

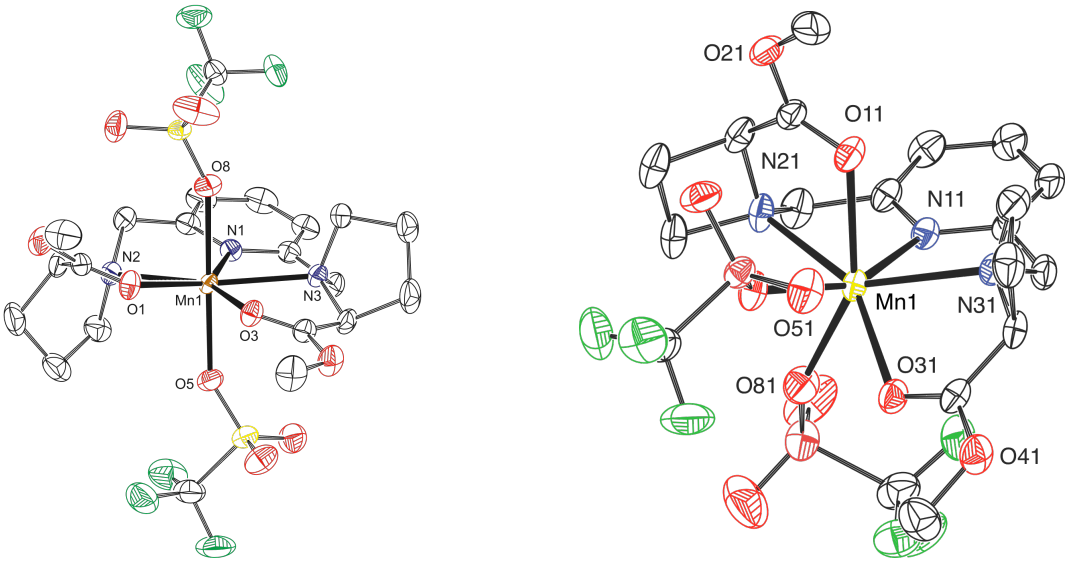

Figure 2. Molecular structures of the seven-coordinated Mn(II) complexes reported in Chapter 2 (left) and of the analogous azetidine complex described in Chapter 4 (right).

The epoxidation of cyclooctene with hydrogen peroxide was used as a benchmark reaction to evaluate the catalytic properties of these complexes. It turned out that the catalytic reactions are best carried out in acetone at room temperature and with a slow, drop-wise addition of 500 equivalent of H_2O_2 compared to the catalyst. In addition, the addition of 5 equiv. of 4-methylimidazole was found to be essential for catalytic activity. After this initial screening the complexes were tested in the epoxidation of other substrates, in which turnover numbers (TON) up to 94 per Mn (oxidant limiting conditions), substrate conversions up to 45% (for cyclooctene under substrate limiting conditions), and *ee*'s up to 35% (for *trans*-beta-methylstyrene) were obtained.

In **Chapter 3** the effect of the additive 4-methylimidazole (4-MeIm) on the catalytic epoxidation reactions is further investigated. Through a combination of spectroscopic techniques (^{19}F-NMR, IR, EPR, and ESI-MS) the coordination of 4-MeIm to the Mn-complexes is studied. From this study it turned out that 4-MeIm interacts with the manganese complex and forms an 'activated' intermediate. In the formation of this intermediate different coordination equilibrium involving the possible donor atoms (4-MeIm, triflate and the carbonyl groups) take part. The investigations point at a relative weak interaction between 4-MeIm and [Mn(**Py(ProMe)$_2$**)(OTf)$_2$], leading to the formation of a catalytically active bis-imidazole adduct and ultimately to catalytically inert oligo-imidazole adducts such as a hexakis 4-MeIm Mn(II) complex. Binding of 2 equiv. of 4-MeIm to [Mn(**Py(ProMe)$_2$**)(OTf)$_2$] was found to lead to a decrease in the intra-molecular coordination of the ester carbonyl groups and to their fluxional coordination behavior. It is proposed that non-coordinated carbonyl groups may aid the activation of H_2O_2 by means of hydrogen-bonding interactions. Catalytic experiments, in which the amount of 4-MeIm was systematically varied, showed an optimum in catalytic activity between 5-8 equiv. of 4-MeIm.

Chapter 4 continues on the work described in Chapter 2 through the synthesis of a small library of ONN'NO ligands, in which the proline moieties are systematically varied. This library consists of ligands with different and more bulky proline esters, and of ligands in which the five-membered pyrrolidine ring is replaced by a six-membered piperidine or a four-membered azetidine ring (Figure 3).

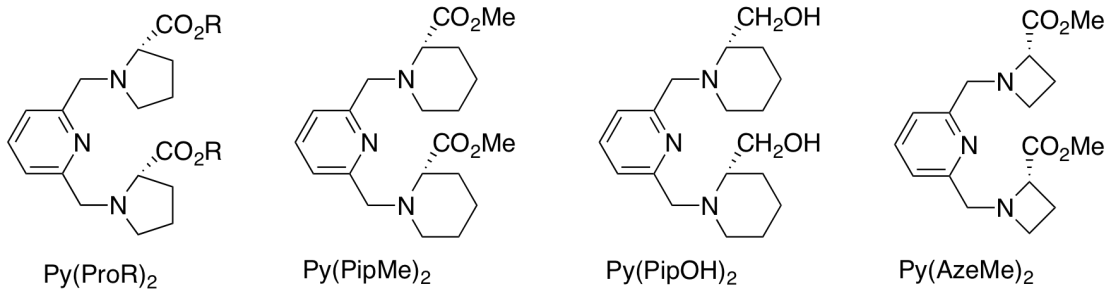

Figure 3. Examples from the small library of ligands studied in chapter 4.

The coordination behavior towards Mn(II) of most of these ligands is the same as for the parent complex from Chapter 2 (Figure 2, left). The exception to this trend is the complex derived from the azetidine-based ligand. In this case, the seven-coordinated Mn-complex shows the coordination of the two triflate groups in *cis*-positions (Figure 2, right). Not only has this coordination behavior not earlier been described with these types of complexes, this structurally distinct complex also turns out to be the most active in catalysis of the complexes described in this chapter. In the epoxidation of cyclooctene substrate conversions of 75% and 120 TONs per Mn are reached, and for *trans*-beta-methylstyrene an enantioselectivity of 40% was reached at a 74% product formation. This is one of the few uses of the azetidine moiety in the design of ligands for transition metal catalysis.

In the second part of this thesis, iron coordination complexes are studied. **Chapter 5** describes how the omission of one of the proline moieties from the ligands studied in chapters 2-4 provides access to ligands with an NN'O binding motive. The iron coordination chemistry of such ligands has been studied to address their potential to mimic the active site structure in non-heme iron enzymes with a 2-His-1-carboxylate facial triad, through a rigorous single crystal X-ray crystallography study. Starting from Fe(II) triflate, homoleptic bis-ligand complexes $[FeL_2](OTf)_2$ are formed that comprise an octahedral and coordinatively saturate iron center (Figure 4, top). The use of $FeCl_2$ on the other leads to 5-coordinated complexes $[Fe(L)(Cl)_2]$ with a meridionally bound N,N',O ligand (Figure 4, bottom left). Crystallization of these complexes from a coordinating solvent leads to the formation of 6-coordinated $[Fe(L)(solv)(Cl)_2]$ complexes (solv = methanol or acetonitrile; Figure 4, bottom right). Interestingly, solvent coordination induces a change in the N,N',O ligand coordination mode from meridional to facial. Introduction of an additional 6-Me substituent on the

pyridine ring prevents solvent coordination, most likely because of steric constrains that do not allow for the change of ligand coordination mode, and allow for the isolation of 5-coordinated iron complexes. The chloride complexes were found to act as catalysts for the epoxidation of styrene substrates (styrene and *trans*-beta-methylstyrene). In the best case, a 65% productive consumption of hydrogen peroxide toward epoxide and benzaldehyde products was obtained.

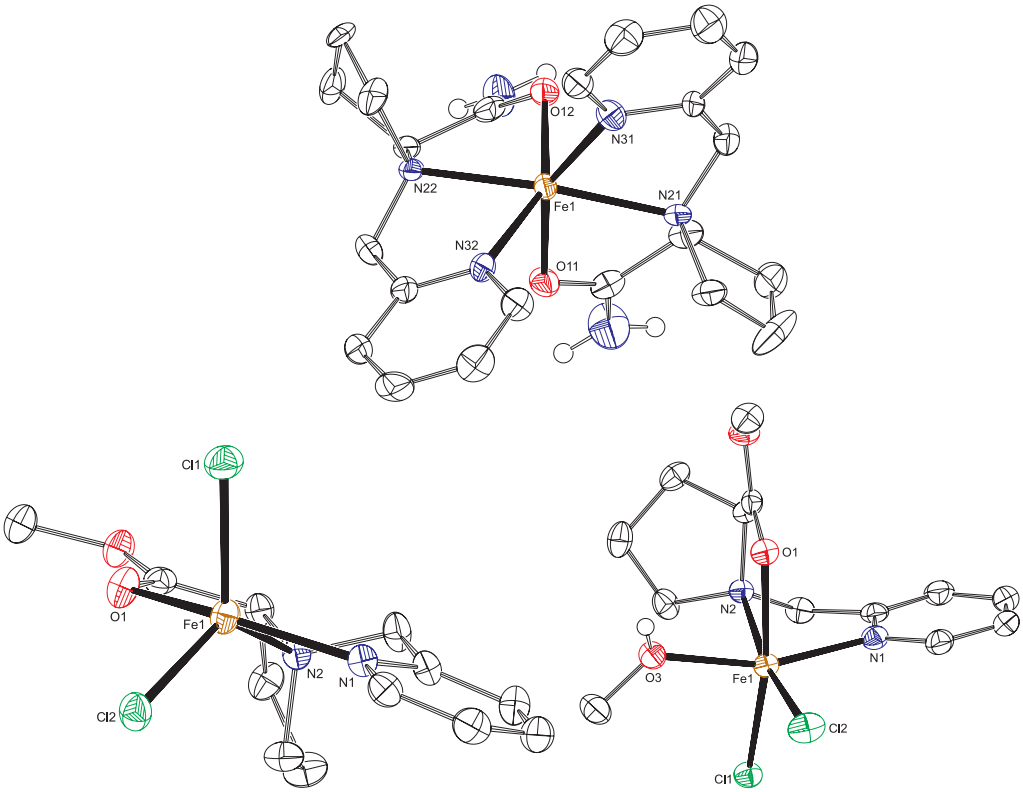

Figure 4. Iron triflate complex [Fe(**PyProNH$_2$)$_2$**](OTf)$_2$ (top) and iron chloride complexes [Fe(Cl)$_2$(**PyProMe**)] crystallized from dichloromethane (bottom left) and from methanol (bottom right).

Chapter 6 describes the iron coordination chemistry of a set of biomimetic facial N,N,O ligands that closely resemble the 2-His-1-carboxylate facial triad in non-heme iron enzymes. Previous studies had shown that Fe(II) complexes derived from these bis(alkylimidazol-2-yl)proprionate ester (**BAIP^R**) ligands are capable of catalyzing the *cis*-dihydroxylation of olefins. This chapter elaborates on this work through the synthesis of a small library of BAIP^R ligands in which *i*) different ester groups, *ii*) the use of a methylbenzimidazole backbone instead of a methylimidazole backbone, and *iii*) the use of a 1-ethyl-4-isopropylimidazole backbone are explored. For all of the ligands the structural properties of the [FeL$_2$](OTf)$_2$ complexes have been examined through single crystal X-ray crystallography (Figure 5). The general structure of the resulting complexes comprises two facially capping ligands around a coordinatively

saturated octahedral Fe(II) center, with either a *transoid* or *cisoid* orientation of the N,N,O donor manifold depending on the combined steric and electronic demand of the ligands. In case of the sterically most encumbered ligand, a 4-coordinated all N-coordinated complex is formed as well, which co-crystallizes with the 6-coordinated complex.

The complexes were also tested as oxidation catalyst in the epoxidation/*cis*-dihydroxylation of cyclooctene. All tested complexes are able to oxidize cyclooctene albeit with rather low TON's and low productive H_2O_2 consumption. The productive H_2O_2 conversion varies between 5-25% after one night of reaction time, which corresponds to a range of 0-10 turn-overs per iron. Although these studies have so far not lead to the development of improved olefin *cis*-dihydroxylation catalyst, they do provide designer tools for the further development of bio-mimetic mono-nuclear non-heme iron complexes and for steering the reactivity of such complexes in catalysis.

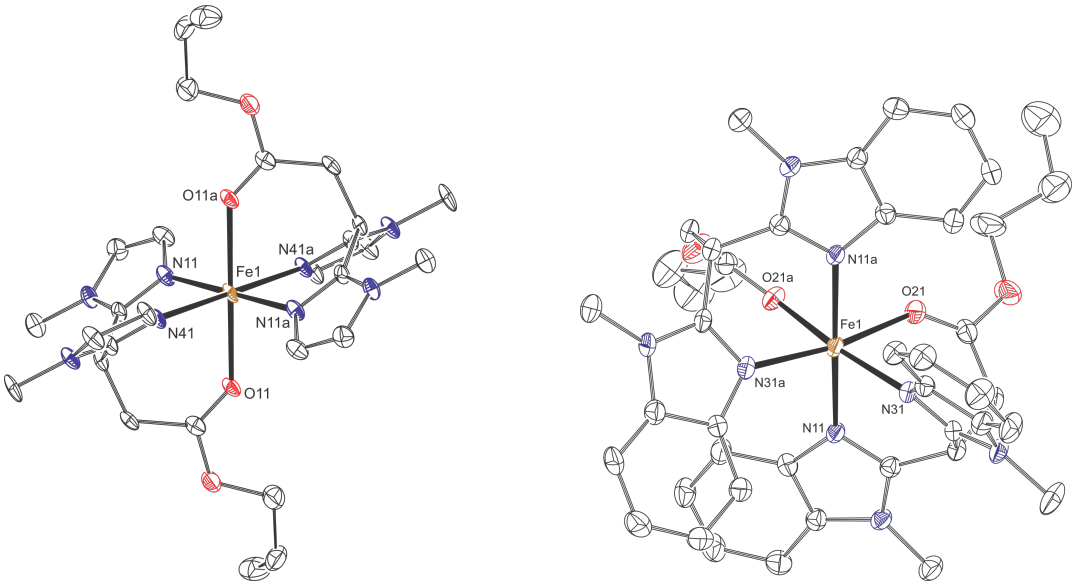

Figure 5. Example of *transoid* complex [Fe(**BMIP^{nPr}**)$_2$](OTf)$_2$ (left) and *cisoid* complex [Fe(**BMBIP^{nPr}**)$_2$](OTf)$_2$ (right).

In the **appendix** of this thesis the synthesis of two iron halide complex derived from the **BMIP^{nPr}** ligand is described. The mono-ligand chloride complex [Fe(Cl)$_2$(**BMIP^{nPr}**)] adopts a tetrahedral geometry around iron in the solid state, while ESI-MS analysis of the bromide complex formed using two equivalents of the ligand showed the formation of bis-ligand complexes. Most interestingly, treatment of the bromide complex with H_2O_2 results in the formation of a transient green intermediate. Based on its UV-Vis spectral features the intermediate is tentatively characterized as an iron(IV) oxo species. Further studies will have to corroborate this assignment and have to clarify the overall structure of the intermediate.

During the research described in this thesis a library of bio-inspired iron and manganese complexes was synthesized and structurally analyzed. The mixed N,O ligand systems are good structural and functional mimic of their biological counterparts. The complexes were all tested in the catalytic oxidation reactions of olefin substrates, showing a diversity of activities. The information obtained by studying these synthesized ligands and their complexes can be used as a lead for the further development of bio-inspired iron and manganese complexes for the oxidation of olefins and other substrates.

Samenvatting

Dit proefschrift beschrijft de synthese en de structurele analyse van bio-geïnspireerde ijzer- en mangaancomplexen die gebruikt worden in de katalytische oxidatie van alkenen. Het ontwikkelen van oxidatiekatalysatoren die gebaseerd zijn op eerste-rij-overgangsmetalen is een relevant onderzoeksonderwerp binnen de homogene katalyse, de bio-anorganische chemie en de groene chemie. Biologische oxidatiereacties waarin metallo-enzymen een belangrijke rol spelen dienen als inspiratiebron voor de ontwikkeling van vele van deze katalysatoren. Als uitgangspunt voor het eerste ontwerp van de organische liganden in dergelijke biomimetische katalysatoren wordt specifiek gekeken naar het actieve deel van zulke metallo-enzymen. Na de synthese van het eerste ligand en de evaluatie van de overeenkomstige katalysator volgen typisch een aantal optimalisatieslagen door verschillende analoga van het ligand te synthetiseren en door de katalytische reactie-omstandigheden te optimaliseren. De strekking van het onderzoek naar biomimetische metaalcomplexen is tweeledig. Enerzijds kunnen de complexen de structurele aspecten van de actieve centra van de metallo-enzymen waarvan zij zijn afgeleid nabootsen (structurele modellen), en anderzijds kunnen deze complexen soortgelijke reactiviteit als de biologische systemen vertonen (functionele modellen).

Het eerste deel van dit proefschrift beschrijft het onderzoek naar mangaancomplexen die gebaseerd zijn op samengestelde N,O liganden, terwijl het tweede deel van dit proefschrift zich richt op soortgelijke ijzercomplexen met N,O liganden. De belangstelling en interesses naar de ontwikkeling van dergelijke samengestelde N,O liganden voor katalytische toepassingen in oxidatiereacties komt voort uit de structuur en reactiviteit van een bepaalde klasse van niet-heem ijzer-enzymen met een 2-His-1-carboxylaat faciale triade in het actieve centrum. In deze triade is het ijzeratoom op een faciale manier gecoördineerd aan twee histidine en een glutamaat- of aspartaam-residu. Enzymen met een dergelijk actief centrum zijn betrokken bij een diversiteit aan oxidatiereacties. Pogingen om het structurele en functionele aspect van deze faciale triade enzymen na te bootsen hebben zich tot nu toe met name gericht op liganden die enkel stikstofdonoratomen bevatten. Tot op heden is er weinig aandacht besteed aan de ontwikkeling van samengestelde N,O liganden, die de faciale triade in niet-heem ijzer-enzymen meer realistisch zouden nabootsen. Figuur 1 geeft een algemeen overzicht van de verschillende typen liganden die in dit proefschrift aan bod komen in het onderzoek naar biogeïnspireerde ijzer- en mangaankatalysatoren voor oxidatiereacties.

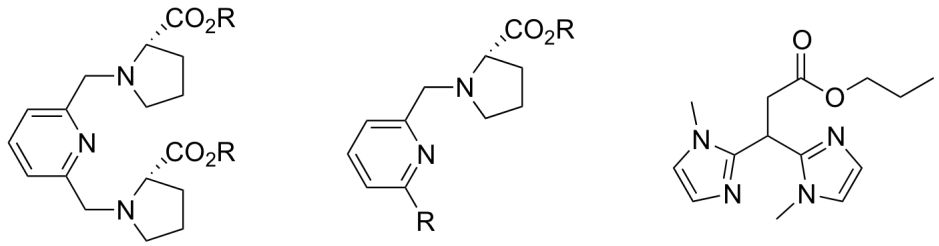

Figuur 1. Algemene structuren van de **Py(ProR)$_2$** (links), **RPyProR** (midden), and **BMIP^{nPr}** (rechts) liganden die gebruikt worden in dit proefschrift.

Hoofdstuk 1 geeft een overzicht van typische bio-geïnspireerde ijzer- en mangaancomplexen die gebruikt worden in de katalytische oxidatie van alkenen. Dit overzicht bespreekt ook de karakteristieke eigenschappen van enzymen die een 2-His-1-carboxylaat faciale triade bevatten in hun actieve centra. Er is zowel aandacht voor de structurele als voor de functionele modellen die ontwikkeld zijn voor deze enzymen.

In **hoofdstuk 2** wordt de synthese van mangaan(II) triflaat complexen beschreven die gebaseerd zijn op het **Py(ProR)$_2$** ligand. Dit type ligand bestaat uit een centrale pyridinegroep met aan weerszijde een chiraal prolinederivaat. Elk van deze chirale derivaten zorgt voor een N,O coördinatiemogelijkheid naast de N-donor die afkomstig is van de pyridinegroep. De synthese van mangaancomplexen gebaseerd op liganden met twee prolinemethylester-groepen of twee prolinolgroepen leidt tot de vorming van zeven-gecoördineerde mangaancomplexen met een verstoorde, pentagonale bipyramidale geometrie (Figuur 2, links). Het organische ligand in deze complexen coördineert daarbij in het meridionale vlak rond mangaan via de pyridinegroep, de stikstofatomen en de carbonyl- of alcoholgroepen van de prolinederivaten. De twee triflaat-tegenionen coördineren in de axiale posities.

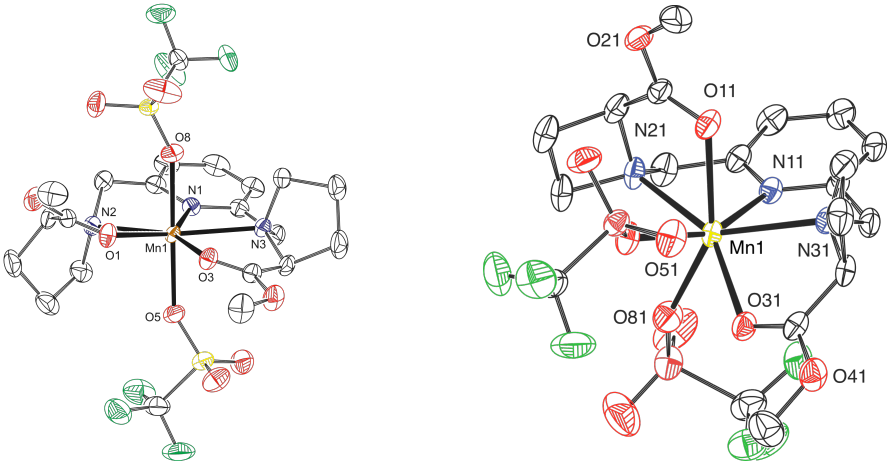

Figuur 2. Moleculaire structuren van de zeven-gecoördineerde mangaan(II) complex dat beschreven is in hoofdstuk 2 (links) en dat van het analoge azetidinecomplex dat beschreven staat in hoofdstuk 4 (rechts).

Om de katalytische eigenschappen van deze complexen in de oxidatiereacties met waterstofperoxide te onderzoeken zijn de reacties in eerste instantie getest met cycloocteen als substraat. Uit deze testen bleek dat de katalytische reacties het beste uitgevoerd kunnen worden in aceton bij kamertemperatuur, waarbij het waterstofperoxide geleidelijk wordt toegedruppeld. Verder bleek het voor de katalytische activiteit essentieel te zijn om 5 equiv. 4-methylimidazool toe te voegen. Na deze initiële testen werden de complexen getest in de epoxidatie van andere substraten. Hierbij werden activiteiten van 94 omzettingen per mangaan behaald (bij een ondermaat oxidant), substraatomzettingen van 45% (bij een ondermaat substraat) en *ee*-waardes tot 35% (voor *trans*-beta-methylstyreen).

In **Hoofdstuk 3** wordt het effect van het additief 4-methylimidazool (4-MeIm) op de katalytische epoxidatiereacties verder onderzocht. Hierbij werd gebruik gemaakt van verschillende spectroscopische technieken (^{19}F-NMR, IR, EPR, en ESI-MS). Uit deze studies komt naar voren dat 4-MeIm bindt aan het mangaancomplex en daarbij een geactiveerd intermediair vormt. De vorming van dit intermediair is onderhevig aan een aantal coördinatietevenwichten tussen het mangaancentrum en de verschillende aanwezig donorgroepen (4-MeIm, triflaat en de carbonylgroepen). Het onderzoek wijst op een relatieve zwakke interactie tussen 4-MeIm en het complex [Mn(**Py(ProMe)$_2$**)(OTf)$_2$]. Deze interactie leidt tot de vorming van het katalytisch actieve bis-imidazool intermediair. In aanwezigheid van een overmaat 4-MeIm ontstaat uiteindelijk een katalytisch inert hexakis-imidazool mangaancomplex. De binding van ten minste twee equiv. 4-MeIm aan [Mn(**Py(ProMe)$_2$**)(OTf)$_2$] leidt tot een verminderde coördinatie van de carbonylgroepen. Er wordt daarbij verondersteld dat de niet-gecoördineerde carbonylgroepen kunnen bijdragen aan de activering van waterstofperoxide door de vorming van waterstofbruggen. Katalytische experimenten

tonen verder aan dat de hoogste katalytische activiteit verkregen wordt door het toevoegen van 5 tot 8 equiv. 4-MeIm.

Hoofdstuk 4 borduurt voort op het werk dat beschreven staat in hoofdstuk 2 door middel van de synthese van een serie van ONN'NO liganden, waarbij de prolinegroepen systematisch zijn gevarieerd. Deze serie van liganden bestaat uit liganden met grotere proline esters en uit liganden waarbij de pyrrolidine 5-ring veranderd is in een piperidine 6-ring of een azetidine 4-ring (Figuur 3).

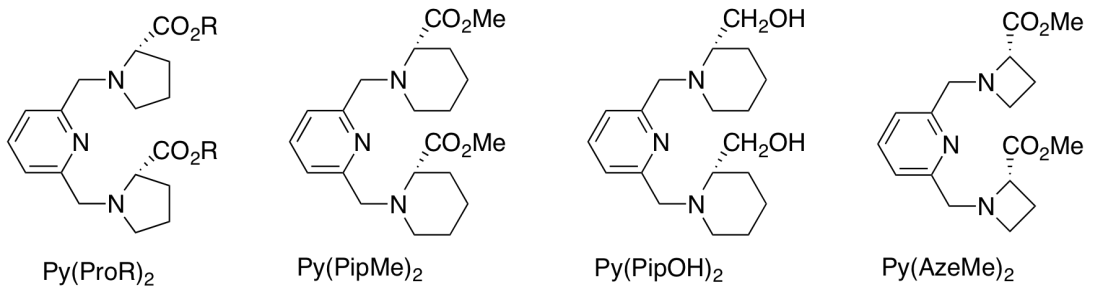

Figuur 3. Voorbeelden uit de serie van liganden die onderzocht wordt in hoofdstuk 4.

Het coördinatiegedrag van deze liganden ten opzichte van mangaan(II) is hetzelfde als die van de complexen die beschreven staan in hoofdstuk 2. Een uitzondering op deze regel is het complex dat gebaseerd is op het van azetidine afgeleidde ligand **Py(AzeMe)$_2$**. In dit geval bevinden de twee triflaatgroepen in het zeven-gecoördineerde mangaancomplex zich niet in een *trans*-positie, maar in een *cis*-positie (Figuur 2, rechts). Dit coördinatiegedrag is niet eerder beschreven voor dit type liganden. Bovendien vertoont dit uitzonderlijke complex een goede katalytische reactiviteit in de epoxidatie van alkenen en is daarmee het meest actieve complex binnen de serie. In de epoxidatie van cycloocteen is een substraatconversie van 75% bereikt met 120 omzettingen per mangaan. Tevens is er in de oxidatie van *trans*-beta-methylstyreen een *ee* behaald van 40% bij een productvorming van 74%. Dit is een van de weinige voorbeelden van het gebruik van op azetidine-gebaseerde liganden in de ontwikkeling van katalytische reacties met overgangsmetalen.

In het tweede deel van het proefschrift worden ijzercomplexen bestudeerd. **Hoofdstuk 5** beschrijft hoe het verwijderen van één van de prolinegroepen van de liganden die bestudeerd zijn in de hoofdstukken 2 t/m 4 toegang geeft tot nieuwe liganden met een NN'O donorset. De ijzer-coördinatiechemie van deze liganden is bestudeerd ter modellering van het actieve centrum van niet-heem ijzer-enzymen met de 2-His-1-carboxylaat faciale triade, waarbij met name van kristalgrafische studies aan enkelkristallen gebruik gemaakt is. Uit de reactie van ijzer(II)triflaat en twee equivalenten van het ligand worden bis-ligand complexen gevormd met een

octaëdrische geometrie en een coördinatief verzadigd ijzercentrum ($[FeL_2](OTf)_2$) (Figuur 4, boven). Het gebruik van $FeCl_2$ als ijzerbron geeft 5-gecoördineerde complexen $[Fe(L)(Cl)_2]$ met een meridionaal gebonden N,N',O ligand (Figuur 4, onder links). De kristallisatie van deze complexen uit een coördinerend oplosmiddel leidt tot 6-gecoördineerde complexen $[Fe(L)(opl)(Cl)_2]$ (opl = methanol of acetonitril; Figuur 4, onder rechts). Opvallend hierbij is dat de coördinatie van een oplosmiddelmolecuul aan het metaalcentrum leidt tot een verandering in het coördinatiegedrag van het N,N',O ligand van meridionaal naar facial. De introductie van een additionele 6-Me substituent op de pyridinering voorkomt de coördinatie van oplosmiddelmoleculen. Dit wordt waarschijnlijk veroorzaakt doordat de substituent door sterische hinder voorkomt dat het coördinatiegedrag van het ligand verandert. Hierdoor is het mogelijk om 5-gecoördineerde ijzer-complexen te isoleren. De chloride-complexen zijn actief in de epoxidatie van styreensubstraten (styreen en *trans*-beta-methylstyreen). In het beste geval wordt een productieve consumptie van waterstofperoxide van 65% bereikt, leidend tot epoxide- en bezaldehydeproducten.

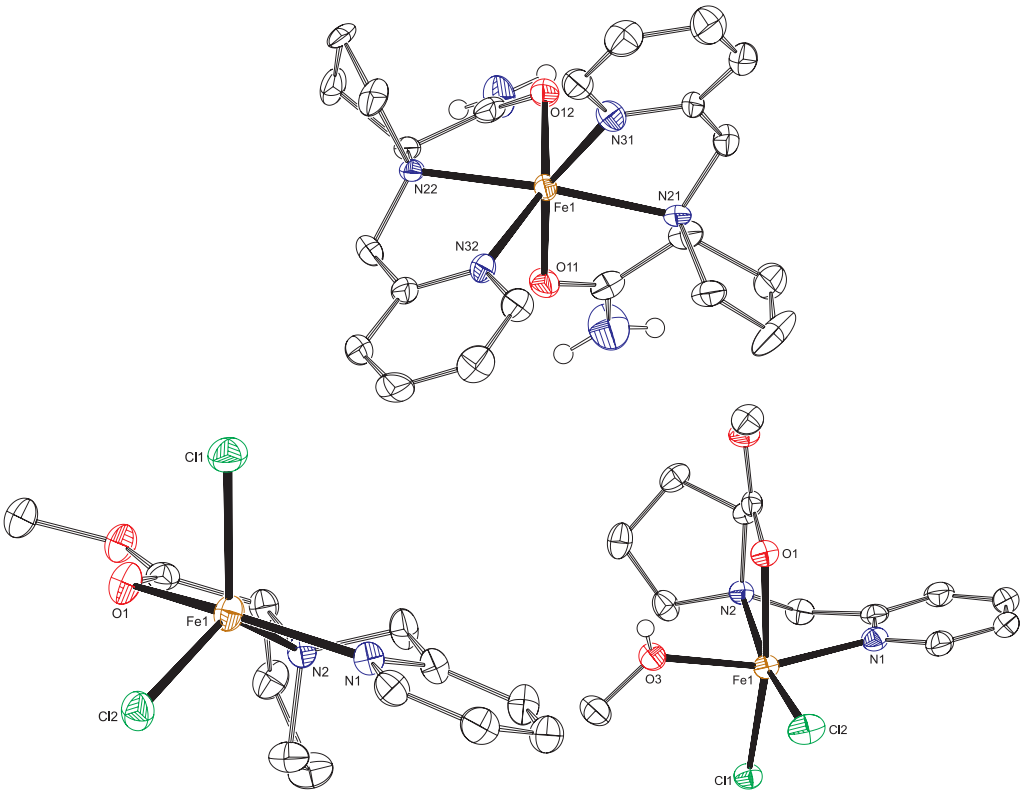

Figuur 4. IJzertriflaat complex $[Fe(\mathbf{PyProNH_2})_2](OTf)_2$ (boven) en het ijzerchloride complex $[Fe(Cl)_2(\mathbf{PyProMe})]$ gekristalliseerd uit dichloormethaan (onder links) en uit methanol (onder rechts).

Hoofdstuk 6 beschrijft de coördinatiechemie van een serie van biomimetische faciale N,N,O liganden die grote gelijkenis vertonen met de 2-His-1-carboxylaat faciale

triade aanwezig in niet-heem enzymen. Eerdere studies hebben al aangetoond dat ijzer(II)complexen die gebaseerd zijn op de di(alkylimidazol-2-yl)propionaat ester (**BAIP^{R}**) in staat zijn om alkenen te *cis*-dihydroxyleren. Dit hoofdstuk borduurt voort op deze studies door een serie van nieuwe BAIP^{R} liganden te synthetiseren. In deze studie worden de liganden op de volgende punten gevarieerd: (1) verschillende estergroepen, (2) het gebruik van methylbenzimidazool in plaats van methylimidazool, en (3) het gebruik van 1-ethyl-4-isopropylimidazool. Opnieuw zijn met behulp van kristallografie de structurele eigenschappen van de $[FeL_2](OTf)_2$ complexen algeleid van de verschillende liganden onderzocht (Figuur 5). De algemene structuur van de complexen bestaat uit een ijzercentrum dat faciaal wordt omringd door twee liganden, waarbij een verzadigd octaëdrisch ijzer(II)complex ontstaat. Afhankelijk van de sterische eigenschappen van de liganden zijn de N,N,O liganden *trans* of *cis* georiënteerd rondom ijzer. In het geval van het meest sterisch gehinderde ligand wordt een tetrakis-imidazool gecoördineerd ijzercomplex gevormd, dat met het meer gebruikelijke 6-gecoördineerde complex voorkomt in een enkele kristalvorm. De serie complexen is getest in de katalytische epoxidatie/*cis*-dihydroxylering van cycloocteen. Hoewel alle complexen in staat zijn om cycloocteen te oxideren, is de algehele activiteit laag, waarbij een productieve consumptie van waterstofperoxide tussen 5 en 25% wordt waargenomen. Dit komt overeen met een omzetting van 0-10 moleculen substraat per ijzercomplex. Hoewel deze studie niet heeft geleid tot de ontwikkeling van een verbeterde *cis*-dihydroxyleringskatalysator, heeft het nieuwe inzichten opgeleverd voor de verdere ontwikkeling van biogeïnspireerde niet-heem ijzercomplexen met interessante katalytische eigenschappen.

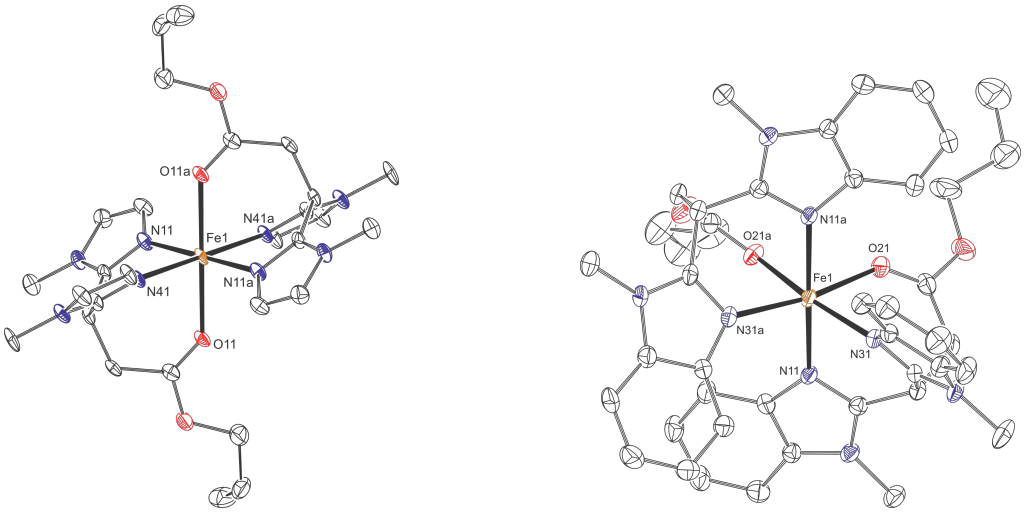

Figuur 5. Voorbeeld van het *trans*-complex [Fe(**BMIP^{nPr})$_2$**](OTf)$_2$ (links) en het *cis*-complex [Fe(**BMBIP^{nPr})$_2$**](OTf)$_2$ (rechts).

In de **appendix** van dit proefschrift komt de synthese van twee ijzerhalidecomplexen gebaseerd op het $BMIP^{nPr}$ ligand aanbod. Het mono-ligand ijzerchloridecomplex $[Fe(Cl)_2(\mathbf{BMIP^{nPr}})]$ neemt in de vaste toestand een tetragonale geometrie aan rond ijzer, terwijl met behulp van twee equivalenten van het ligand een bis-ligand ijzerbromidecomplex wordt verkregen. Het meest in het oog springende resultaat is de vorming van een groen intermediair tijdens de reactie van het bromidecomplex met waterstofperoxide. UV-VIS metingen wijzen vooralsnog op de vorming van een ijzer(IV)oxo intermediair in deze reactie. Verdere studies moeten uitwijzen of deze toekenning terecht is en dienen de structuur van het intermediair op te helderen.

Tijdens het onderzoek dat beschreven staat in dit proefschrift is een scala aan verschillende biogeïnspireerde ijzer- en mangaancomplexen gesynthetiseerd en bestudeerd. De samengestelde N,O ligandsystemen die gebruikt worden in deze complexen modelleren de faciale triade aanwezig in mononucleaire niet-heem ijzerenzymen. De complexen zijn getest in de katalytische oxidatie van alkenen, waarbij een diversiteit aan reactiviteiten is waargenomen. De informatie die verkregen is tijdens dit onderzoek aan samengestelde N,O liganden en de overeenkomstige metaalcomplexen kan gebruikt worden als leidraad voor de verdere ontwikkeling van biogeïnspireerde ijzer- en mangaancomplexen voor de oxidatie van alkenen en andere substraten.

Graphical abstract

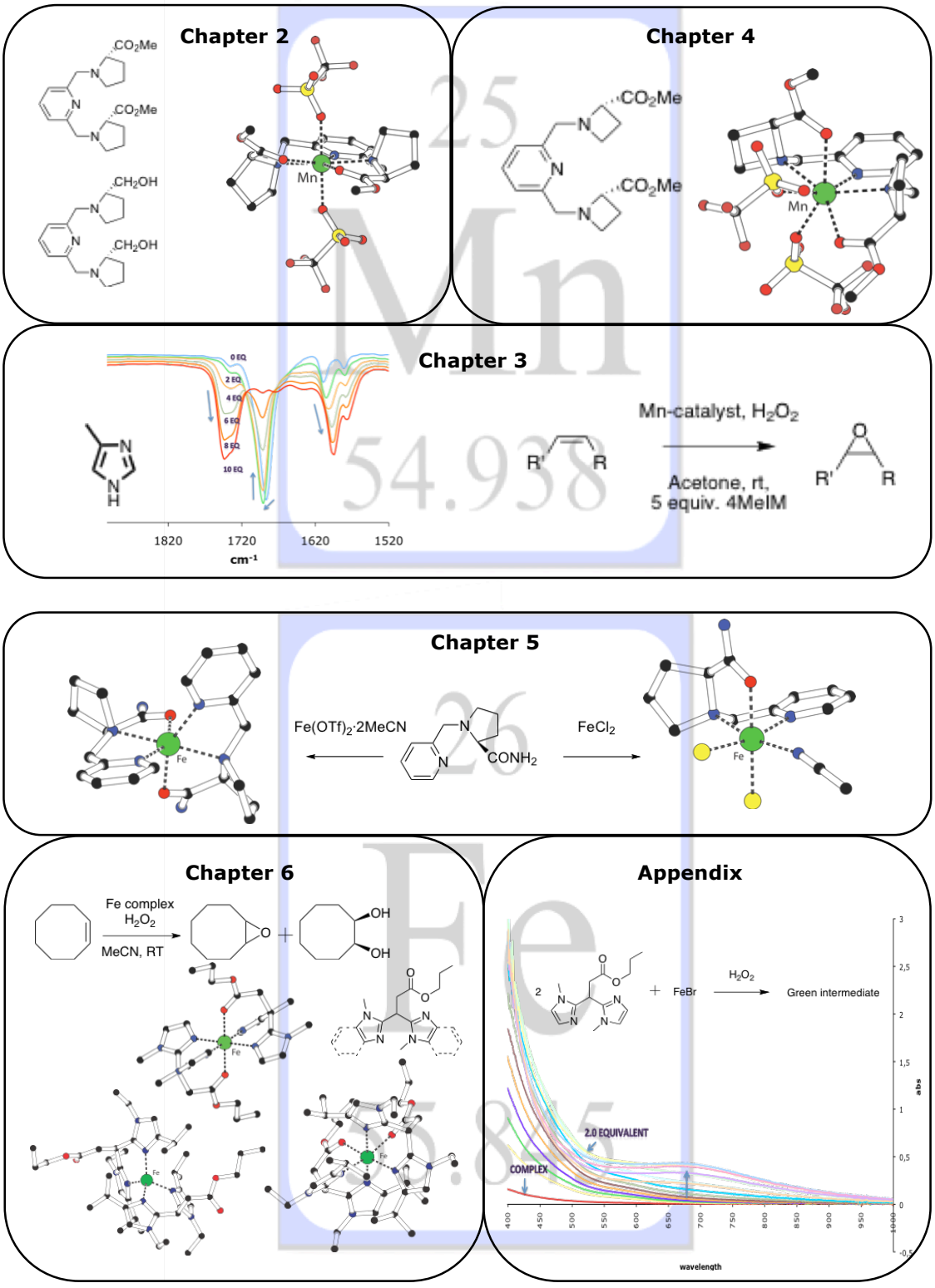

Dankwoord

Het is zover. Na een aantal jaren hard werken is het proefschrift klaar en kan het laatste onderdeel: het dankwoord, geschreven worden. Promoveren doe je niet alleen en om die reden wil ik graag een aantal mensen dat heeft bijgedragen aan het tot stand komen van dit proefschrift, bedanken.

Als eerste wil ik mijn promoter prof. dr. Bert Klein Gebbink bedanken voor de geboden mogelijkheid om in zijn groep mijn promotieonderzoek te doen. Bert, aan het einde van mijn industriële stage bij Organon in Oss ter afsluiting van mijn doctoraalstudie scheikunde in Nijmegen, kwam ik via Rob Abbenhuis in contact met je. Na een gesprek en het geven van een presentatie belde je nog dezelfde middag terug met het aanbod om mijn promotieonderzoek te komen doen in jouw groep. Ik hoefde er dan ook niet lang over na te denken en nam het aanbod graag aan. Na een vakantie van twee weken naar het zonnige Aruba, begon ik op 1 februari aan mijn nieuwe uitdaging. De vrijheid die ik tijdens mijn onderzoek had om eigen plannen en ideeën te onderzoeken, vond ik prettig. Bovendien stond je deur altijd open voor verdere ideeën en suggesties voor het onderzoek. Nadat al het experimentele werk gedaan was, brak de laatste fase aan van het beschrijven van het onderzoek en het werk dat gedaan was tijdens de daaraan voorafgaande vier jaar. Een fase waarin je me met raad en daad bijgestaan hebt. Ik wil je ook zeer bedanken voor het lezen en het corrigeren van al mijn manuscripten.

Ik wil ook graag andere personen bedanken die mijn promotieperiode tot een succes hebben gemaakt. Niet alleen de mensen op het lab, maar ook personen daarbuiten.
Ik denk daarbij als eerste aan Wilbert Buijs, mijn scheikundedocent op het Liemers College te Zevenaar. In zijn lessen is de liefde voor het vak scheikunde ontstaan. Zonder dit begin was ik nooit scheikunde gaan studeren.
Aansluitend wil ik een aantal stafleden van de Organische Chemie en Katalyse groep (OCC) bedanken. Als eerste dr. Johann Jastrzebski voor het oplossen van allerlei praktische problemen. Je stond altijd voor me klaar om eventuele computerproblemen op te lossen. Voor het doen van onderzoek zijn chemicaliën van essentieel belang. Een belangrijke steun voor mij was Henk Kleijn. Henk bedankt voor alle chemicaliën die je tijdens de vier jaar hebt besteld. Je stond ook altijd voor me klaar wanneer een apparaat weer eens kuren kreeg en niet wilde doen waarvoor hij gemaakt was. Tot slot wil ik ook graag Milka Westbeek bedanken. Milka heel erg bedankt voor alle secretariële ondersteuning tijdens mijn periode in Utrecht. Als er een administratief probleem was, wist je die elke keer weer goed en snel op te lossen.

Een belangrijk deel van dit proefschrift is mede tot stand gekomen door de collega's van de vakgroep Kristallografie. In bijzonder wil ik graag prof. dr. Ton Spek en dr. Martin Lutz hartelijk danken voor al de kristalstructuren die zij voor mij hebben weten te bepalen. Ik had het geluk dat onze vakgroep en de vakgroep Kristallografie op dezelfde verdieping zaten. Als ik weer eens kristallen van een van de gemaakte complexen had, was het maar een korte wandeling naar Martin. Na een kritische inspectie konden de kristallen gemeten worden. Dit heeft er mede voor gezorgd dat in dit proefschrift in totaal 27 kristalstructuren opgenomen zijn. Door al deze structuren was het mogelijk om een duidelijk beeld te krijgen van het coördinatiegedrag van de gesynthetiseerde complexen.

Ook wil ik Bas de Bruin van de Universiteit van Amsterdam bedanken voor de DFT-berekeningen die hij voor mij gedaan heeft. Mede met zijn hulp kon ik de resultaten na kristallisatie verklaren.

Ik mag zeker niet de studenten vergeten die aan mijn promotieonderzoek een bijdrage hebben geleverd, soms in de vorm van een afstudeerstage, soms in de vorm van een bachelorstage. Hun inspanningen hebben mij erg geholpen. Resultaten van hun werk staan dan ook in het proefschrift vermeld. Ik zou in dit kader graag Daniel Schamhart willen noemen. Daniel graag dank ik je voor het vele werk dat je voor me hebt gedaan. Ik moet wel opmerken dat als het niet ging zoals je zelf wilde, dat te horen was in de labzaal. Ik vind het erg jammer dat je je stage nooit afgemaakt hebt. Je hebt erg veel mooi werk gedaan, waar je zelf niet altijd van overtuigd was. Je ijverige en harde werk vind je terug in het merendeel van hoofdstuk 5. De tweede master student die ik noem is Sjoerd Nijsse. Sjoerd je bent een harde werker en je was altijd heel zelfstandig aan het werk. Je hebt heel veel werk gedaan voor hoofdstuk 6 en appendix 1. Door je ontdekking van het 'groene deeltje' is appendix 1 ontstaan. Ik heb altijd met veel plezier met je samengewerkt. Ik vind het dan ook leuk dat je een van mijn paranimfen wilt zijn.

Ik wil ook graag mijn bachelorstudent Bas Reijers bedanken voor zijn inzet. Ondanks je inzet wilde het project niet worden wat we er van gehoopt hadden en deden de moleculen andere dingen dan we verwachtten en hoopten. Ook wil ik Maha Jemal bedanken die bij mij een HBO afstudeerstage gedaan heeft. Maha een deel van je onderzoek vind je terug in hoofdstuk 4.

Naast de studenten die hebben bijgedragen aan mijn proefschrift wil ik natuurlijk ook alle aio's, post-docs en andere studenten van de vakgroep Organische Chemie & Katalyse bedanken. Als eerste mijn kamergenoten van het eerste uur: Monica, Aiden en Sylvester van Z809. Dank dat jullie mij zo hartelijk ontvangen hebben tijdens mijn begin in Utrecht. Mede dankzij jullie voelde ik me vanaf het begin thuis. Daarnaast wil ik Silvia en Pieter bedanken voor hun introductie in de mooie wereld van de oxidatiechemie met ijzercomplexen. Door jullie werk kon mijn project voortvarend van start gaan.

Als promovendus breng je een groot deel van de tijd door op het lab. Ik wil dan ook mijn collega's van Zuid I, waar ik vier jaar heb doorgebracht, danken voor de gezellige tijd die we op het lab hadden. Sipke, Pieter, Morgane, Henk, Dennis, Kees, Sohail, Mandy en Ties hartelijk bedankt voor de mooie tijd. Ook bedank ik graag de collega's van onze vakgroep: Harm, Monica, Aiden, Sylvester, Bart, Erwin, Guido, Birgit, Elena, Maaike, Jie, Niels, Yves, Vital, Nesibe en Peter. Dat geldt ook voor Layo en Jacco van de Fysische Organische Chemiegroep. Daarnaast is er in de vier jaar een constante stroom van studenten aanwezig geweest op onze vakgroep, sommigen vergeet je snel en anderen zul je niet snel vergeten. Emma, Kimberly, Bart, Inge, Matthijs en Nicole, ook jullie bedankt voor de gezellige tijd.
Emma jou wil ik danken dat je naast Sjoerd mijn tweede paranimf wilt zijn. Je bent inmiddels zelf ook aan het promoveren. Mede door jouw inbreng is hoofdstuk 6 geaccepteerd.
Tot slot wil ik Ties bedanken. Ik vind het jammer dat je niet aanwezig kunt zijn bij de verdediging. Ik wil je bedanken voor je hulp bij de opmaak van de voorkant van mijn proefschrift.

Een speciale dank gaat ook uit naar mijn familie en vrienden die mij hebben bijgestaan tijdens mijn promotieperiode. Voor een aantal van jullie was het vaak lastig om te begrijpen waar mijn werk in Utrecht betrekking op had. Gelukkig was er naast de tijd voor onderzoek op het lab en het schrijven van het proefschrift ook nog ruimte voor een leven zonder chemie. En daaraan hebben jullie een grote invulling gegeven. Ik dank iedereen van de vriendengroep: Ursula, Sander, Bianca, Jorma, Natasja, Arjan en Miranda voor de gezellige avonden tijdens de verjaardagen, de kermis en de verschillende feesten. Deze zorgden altijd voor de nodige ontspanning. Voor mij waren ook de wekelijkse judotrainingen belangrijk. Het judo gaf mij een goede manier van ontspanning. Ik kon alle agressie van niet-werkende reacties van mij afschudden. Judo Groessen bedankt voor het broodnodige gooi en smijtwerk.

Natuurlijk wil ik ook mijn familie en schoonfamilie bedanken voor de getoonde belangstelling en de gezellige momenten, en dan speciaal mijn ouders. Pap en mam, zonder jullie steun in al die jaren zou ik nooit zover gekomen zijn. Ik ben jullie daar dan ook zeer dankbaar voor.

Ik wil zeker ook mijn volkswagen Polo met het mooie kenteken 44-GH-GH bedanken voor de vier jaar trouwe dienst. Elke dag bracht hij me van Duiven/Zevenaar naar Utrecht. Geen enkele dag liet hij me in de steek. Samen hebben we in deze vier jaar ongeveer 130.000 kilometer gereden en hebben we menig uurtje doorgebracht op de snelweg. Natuurlijk wil ik ook mijn hond Russel, een zwarte labrador, danken voor zijn altijd aanwezige enthousiasme als ik na een dag schrijven weer naar beneden

kwam. Bovendien zorgde hij tijdens het schrijven op tijd voor de benodigde frisse lucht. Hij moest immers uitgelaten worden.

Als laatste blijft er nog een belangrijk iemand over om te bedanken. Natuurlijk wil ik en mag ik deze persoon niet vergeten. Zoals vaak gebruikelijk zijn de laatste regels van het dankwoord gereserveerd voor jou. Lieve Marjolein, je zult wel blij zijn dat na al deze jaren het proefschrift af is. Bedankt voor al je steun en begrip voor de momenten dat ik weer eens boven zat om het proefschrift verder af te schrijven. Ik kan me voorstellen dat ik niet altijd even gezellig was wanneer ik toch nog even snel iets wilde afmaken. Maar mede dankzij jouw steun en geduld is het proefschrift nu klaar. Ik dank je voor alles.

Marcel

Curriculum Vitae

The author of this thesis was born on March 27, in Uden, the Netherlands. After graduating from high school at the Liemers College in 2000, he went on to study Chemistry at the Radboud University Nijmegen that same year. After a minor in industrial chemistry (Organon, Oss, prof. dr. F.P.J.T. Rutjes and dr. M. Ostendorf) and a major in organic chemistry (prof. dr. F.P.J.T. Rutjes) his MSc degree was obtained in 2005.

From February 2006 until February 2010 the author worked as a PhD student in the Organic Chemistry & Catalysis group under the supervision of prof. dr. R.J.M. Klein Gebbink on the research described in this thesis. The research project was financially supported by the National Research School Combination-Catalysis (NRSC-C). Parts of the research described in this thesis were presented at several national and international meetings, including the Netherlands' Chemistry and Catalysis Conference (NCCC), the 10th International Symposium on Activation of Dioxygen and Homogeneous Catalytic Oxidation (ADHOC 10, Venice, Italy), Young COST D40-III meeting (Bratislava, Slovakia), COST D40-III meeting (Turku, Finland) and the 6th World Congress on Oxidation Catalysis (WCOC 6, Lille, France). Afterwards the author of this thesis worked temporarily as a technical education assistant at Het Rhedens in Dieren/Rozendaal and subsequently obtained his first degree in chemistry teaching at the Radboud University Nijmegen. He then started as a NaSK (combined physics/chemistry) and Physics teacher at Gymnasium Apeldoorn and at Veluws College Apeldoorn. Currently he is working fulltime as a NaSK and Physics teacher at Veluws College Apeldoorn.

Curriculum Vitea

De schrijver van dit proefschrift werd geboren op 27 maart 1981 te Uden. Na het behalen van het VWO diploma in 2000 aan het Liemers College, begon hij datzelfde jaar met de studie Scheikunde aan de Radboud Universiteit Nijmegen. Na een bijvak industriële chemie (Organon, Oss, prof. dr. F.P.J.T. Rutjes en dr. M. Ostendorf) en een hoofdvak Organische chemie (prof. dr. F.P.J.T. Rutjes) werd het doctoraal examen afgelegd in 2005.

Van februari 2006 tot februari 2010 verrichtte de schrijver het in dit proefschrift beschreven onderzoek als Assistent in Opleiding in de vakgroep Organische Chemie & Katalyse onder de supervisie van prof. dr. R.J.M. Klein Gebbink. Het onderzoek werd financieel ondersteund door de toponderzoeksschool NRSC-C. Delen van het onderzoek hier beschreven werden gepresenteerd op verschillende nationale en internationale bijeenkomsten, zoals de 'Netherlands' Chemistry and Catalysis Conference' (NCCC), het 10^{e} International Symposium on Activation of Dioxygen and Homogeneous Catalytic Oxidation (ADHOC 10, Venetië, Italië), Young COST D40-III meeting (Bratislava, Slowakije), COST D40-III meeting (Turku, Finland) en het 6^{e} World Congress on Oxidation Catalysis (WCOC 6, Lille, Frankrijk). Na zijn promotie werkte de schrijver van dit proefschrift tijdelijk als technisch onderwijs-assistent op Het Rhedens in Dieren/Rozendaal, waarna hij aan de Radboud Universiteit Nijmegen zijn eerste graads bevoegdheid tot scheikunde docent heeft behaald. Vervolgens was hij werkzaam als docent NaSk en Natuurkunde aan het Gymnasium Apeldoorn en het Veluws College in Apeldoorn. Op dit moment werkt hij voltijd als docent NaSk en Natuurkunde aan het Veluws College in Apeldoorn.

List of publications

Bio-inspired non-heme iron complexes derived from an extended series of N,N,O-ligated BAIP ligands
Moelands, M.A.H.; Nijsse, S.; Folkertsma, E.; de Bruin, B.; Lutz, M.; Spek, A.L.; Klein Gebbink. R.J.M. *Inorg. Chem.* **2013**, *52*, 7394−7410.

Catena-Poly[[bis(acetonitrile-κN)-manganese(II)]-bis(μ-trifluoromethanesulfonato-κ^2O;O')]
Lutz, M.; Schreurs, A.M.M.; Spek, A.L.; Moelands, M.A.H.; Klein Gebbink, R.J.M. *Acta. Cryst. C.* **2010**, *C66*, m9-m12.

Iron(II) Complexes with Bio-Inspired N,N,O Ligands as oxidation Catalyst: Olefin Epoxidation and cis-Dihydroxylation
Bruijnincx, P.C.A.; Buurmans, I.L.C.; Gosiewska, S.; Moelands, M.A.H.; Lutz, M.; Spek, A. L.; van Koten, G.; Klein Gebbink, R.J.M. *Chem. Eur. J.* **2008**, *14*, 1228-1237.

A Ring-Closing Metathesis Approach to Cyclic α,β-Dehydroamino Acids
Hekking, K.F.W.; Waalboer, D.C.J.; Moelands, M.A.H.; Van Delft, F.L.; Rutjes, F.P.J.T. *Adv. Synth. Catal*. **2008**, *350*, 95-106.

An In-Depth Study on Ring-closing metathesis of Carbohydrate-Derived α-Alkoxyacrylates: Efficient Synthesis of DAH, KDO, and 2-Deoxy-β-KDO
Hekking, K.F.W.; Moelands, M.A.H.; Van Delft, F.L.; Rutjes, F.P.J.T. *J. Org. Chem*. **2006**, *71*, 6444-6450.

Lipase-Promoted Dynamic Kinetic Resolution of Racemic β-Hydroxyalkyl Sulfones
Kielbasinski, P.; Rachwalski, M.; Mikolajczyk, M.; Moelands, M.A.H.; Zwanenburg, B.; Rutjes, F.P.J.T. *Tetrahedron Asymmetry* **2005**, *16*, 2157-2160.